Hochschule Neubrandenburg
University of Applied Sciences

Department of Landscape Architecture, Geoinformatics,
Geodesy and Civil Engineering
Course of studies Geodesy

GFZ
Helmholtz Centre
POTSDAM

# GPS-based earthquake parameter reconstruction within the German Indonesian Tsunami Early Warning System

---

Thesis

to graduate as

Dipl.-Ing. (FH)

---

submitted by

**Manuela Schönrock**
born on 11 September 1983

Supervisor:
Prof. Dr. rer. nat. habil. Gerd Teschke
Assessor:
Dipl.-Phys. Andreas Höchner

Neubrandenburg, January 2009

urn:nbn:de:gbv:519-thesis2008-0074-2

*"Mathematics is the language in which God has written the universe."*

- Galileo Galilei -

## Affidavit

Hereby I assure that the following thesis has been written only by the undersigned without any assistance from third parties only with the specified sources and aids.
This thesis, in same or similar form, has not been available to any audit authority yet.

Neubrandenburg, January 2009

## Acknowledgement

I would like to express my gratitude to Prof. Dr. rer. nat. habil. Gerd Teschke for his excellent mentoring throughout the entire thesis as well as for his encouragement and not least for his friendship.

Furthermore, I thank Andreas Höchner and Dr. Andrey Babeyko for their expertise and guiding.

I want to thank Odile Haydari for her linguistic help.

I also owe thanks to my Professors, my fellow students and to all the people who have accompanied me during my studies at the University of Applied Sciences Neubrandenburg.

I must particularly thank my family and friends for their emotional support.

## Abstract

This work is concerned with the linear ill-posed inverse problem of GPS-based earthquake parameter reconstruction in the context of the German Indonesian Tsunami Early Warning System (GITEWS). Inversion of three-dimensional near field GPS observations, regarding slip distribution at the Sunda subduction interface, is performed by using a GREEN's function approach. The inverse approach which has been published by HOECHNER et al. (2008), employs a GREEN's function approach and minimisation of the misfit between "observed" (still synthetic) and modelled GPS data using a simplex algorithm from the MATLAB Optimization Toolbox. The task of this thesis is to perform a sensitivity analysis considering noise on the GPS data. In addition, it will be dealt with two other inverse approaches which are QR decomposition and an iterative approach by surrogate functionals.

**Keywords:** German Indonesian Tsunami Early Warning System (GITEWS), GPS inversion, earthquake parameter, GREEN's function, Rupture Generator (RuptGen), near field GPS, subfault array

Diese Arbeit befasst sich mit dem linearen inversen schlecht gestellten Problem der GPS-basierten Erdbebenparameterrekonstruktion im Rahmen des Deutsch-Indonesischen Tsunami-Frühwarnsystems (GITEWS). Die Inversion von dreidimensionalen near field GPS-Beobachtungen, hinsichtlich der Slip-Verteilung an der Sunda-Subduktionszone, wird mittels GREENscher Funktionen durchgeführt. Das inverse Verfahren, welches von HOECHNER et al. (2008) publiziert wurde, wendet einen GREENschen Funktionsansatz sowie Minimierung der Residuen zwischen "beobachteten" (bis dato synthetischen) und modellierten GPS-Daten mit Hilfe eines Simplex-Verfahrens aus der MATLAB Optimization Toolbox an. Im Rahmen dieser Diplomarbeit wird eine Sensitivitätsanalyse bezüglich Rauschen auf den GPS-Daten durchgeführt. Zusätzlich wird sich mit zwei weiteren inversen Lösungsansätzen, der QR-Zerlegung und ein iteratives Verfahren mit Ersatzfunktionen, befasst.

**Schlagwörter:** Deutsch-Indonesisches Tsunami-Frühwarnsystem (GITEWS), GPS-Inversion, Erdbebenparameter, GREENsche Funktion, Rupture Generator (RuptGen), near field GPS, subfault array

# Contents

# 1 Problem

Some regions of the Indonesian coast are in high danger of being struck by the next giant tsunami that could be generated by an earthquake within decades or even years. The probably next large submarine earthquake and the subsequent tsunami similar to the Great Sumatra-Andaman event, is expected close to the capital of West Sumatra, Padang, see Pollitz et al. (2006).

Due to the presence of the Mentawai Islands, resulting tsunami wave height in Padang is very sensitive to the rupture location perpendicular to the trench. The Mentawai Islands protect the mainland efficiently. Hence, shallow ruptures western or under the Siberut Island which is the largest of the Mentawai Islands do not produce large tsunamis in Padang. In contrast, rupturing of deep locked subfaults between Siberut and Padang results in devastating tsunami with short arrival times even for smaller earthquakes because tsunami energy might be trapped between the Mentawai Islands and the Sumatran coast.[4]

Furthermore, for a reliable Tsunami Early Warning System, the local geomorphological setting of the Indonesian coast has to be taken into account: the trench is located closely to the coast and the bathymetry is very complex.[20]

For near field tsunamis off Sumatra, size of the rupture is comparable to distance to the coast and even larger. Therefore, an earthquake can not be treated as a point-event but rather described as a chain of smaller point source earthquakes, each of these with its own epicentre and magnitude. Every member of this chain is as important for tsunami prediction as the starting point itself. Hence, knowledge of epicentre and magnitude only, is absolutely not enough for reliable local tsunami prediction. More detailed information on fault position and slip distribution is needed. Additionally, short arrival times require a priori incorporation of as much as possible data on local tectonics in order to minimise real time uncertainty of rupture parameters.

Finite fault parameters can be derived from seismology, ocean wave measurements or even online tracking of GPS vectors. Ocean wave measurements like buoys, work perfectly if the buoy constellation is dense enough (about 100km) which is in turn hardly achievable due to economical reasons. If these conditions were given, approximately 10 minutes would be necessary at early warning. Online tracking of GPS vectors has a great advantage compared to seismology: the deformation field is measured directly. Thus, very fast and precise

inversion of finite fault parameters is allowed.[4] Rapid knowledge of slip distribution which could be achieved by using real time GPS arrays is crucial. One of the main issues in GPS inversion is the lack of exactitude of the solution due to arbitrary weighting coefficients in the below-mentioned cost function. As the number of model parameters is larger than the number of observations, the inversion problem becomes an optimisation problem.

Because of this background, the main aim of this thesis is to verify the inversion technique which has been published by the GFZ German Research Centre for Geosciences Potsdam in the context of the German Indonesian Tsunami Early Warning System (GITEWS), see Hoechner et al. (2008). Within a sensitivity analysis considering noise on the GPS data, the grade of quality of earthquake parameter reconstruction by using the mentioned GPS inversion technique should be shown, and the basic case of slip distribution (single rupture scenarios and dip slip only) should be adopted.
Furthermore, other approaches might be given to solve this ill-posed inverse problem to be able to reconstruct rupture parameters reliably.

## 2 Motivation and Introduction

The catastrophic consequences of the submarine Great Sumatra-Andaman earthquake and in its wake, the devastating tsunami offshore Sumatra, Indonesia in December 2004 (see figure no. 1) has strongly emphasised the need for the development of reliable Tsunami Early Warning Systems (TEWS).


Figure 1: Banda Aceh (Indonesia) before and after tsunami of December, 2004 [28]

The proximity of Sumatra to a subduction zone and its closeness to the "Pacific Ring of Fire" makes Indonesia the most endangered region of the Indian Ocean when earthquakes occur.

The goal of the complex German Indonesian Tsunami Early Warning System (GITEWS) is to provide reliable early tsunami warnings for the Indian Ocean coast of Indonesia to the population at risk.[31] Therefore, it is necessary to obtain reliable information about

an earthquake event (expected arrival times, wave heights and inundation) as quickly as possible.

The greatest challenge of GITEWS is detecting tsunamis within 5 minutes as is claimed by the Intergovernmental Oceanographic Commission (IOC).[13] This requirement is indispensable to prevent hundreds of thousands from loosing their lives, like in 2004.

GITEWS contains a local Tsunami Early Warning System which is based on observational networks. The project is led by the German Research Centre for Geosciences, Potsdam.[16] The German conception of the establishment of a TEWS for the Indian Ocean relies on different kinds of sensor systems. The concept aims at achieving indicators of a tsunami and its dimension by analysing different measurements at a very early stage.

While a tsunami wave spreads out with a speed up to circa 800 km/h in the wideness of the sea, a period of about 20 minutes elapses between wave's generation and the first contact with the Indonesian mainland. In this time frame, sensors that are installed at different locations inside the considered propagation areas, are able to detect deviations from normality (anomalies) rapidly. The sensor network of the Tsunami Early Warning System comprises seismometers, tide gauges, buoys and ocean bottom pressure sensors as well as GPS instruments, compare with following figure.

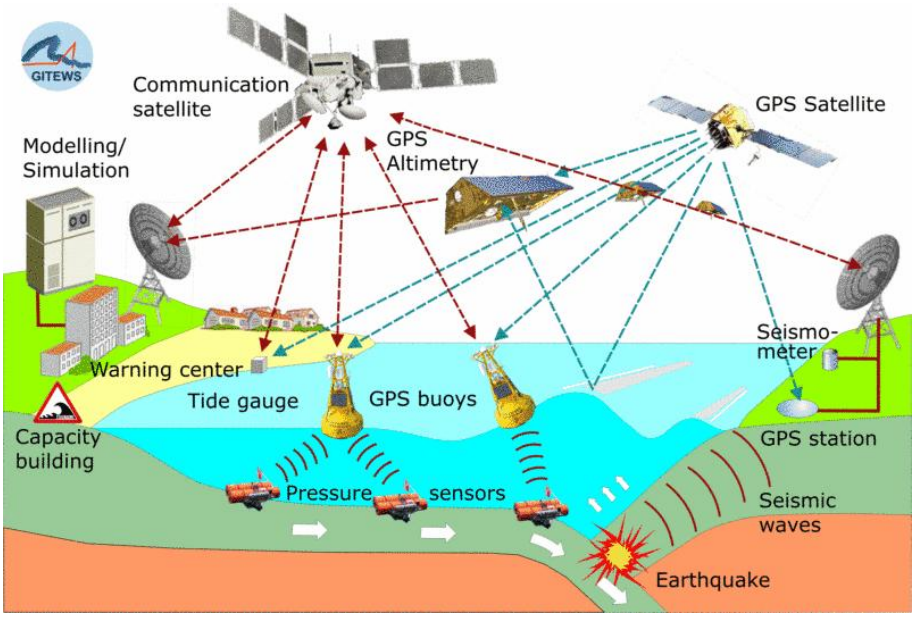


Figure 2: GITEWS components [16]

This compact measuring network shortens time for the seismic wave to reach the measuring instruments. However, it is extremely difficult to register and to evaluate the signals of strong earthquakes in the near field. Therefore, new measuring and evaluation procedures have been developed for GITEWS.

During the catastrophic event of 2004, horizontal and vertical displacements of several decimetres to metres were evident. Even at a distance of some hundred kilometres from the quake, displacements of millimetres were recorded. The direction of this resulting shift is a good indication for the mechanism of the earthquake and thus for the possible tsunami potential and the expected hazard.

Not every earthquake generates a tsunami. For this reason, it must be determined at sea whether or not an earthquake has actually triggered the deadly wave. In order to determine vertical and horizontal displacements immediately, all tide gauges within GITEWS have been additionally equipped with GPS receivers. GPS antennas on buoys are already used to determine sea motion and sea levels as well as to detect tsunami waves. Innovative measuring and filter procedures allow the normal sea motion data to be removed. So, a centimetre-exact determination of the rise in the sea level remains and herewith also the early detection of a tsunami wave.

Additionally, the buoys are equipped with ocean bottom units where a pressure gauge is employed to record a tsunami passing above. Data are sent to the buoys via acoustic modem and passed on from there to a central warning centre via satellite communication. In a central warning centre in Indonesia, sensor data are compared to a multitude of pre-taylored tsunami simulations immediately in order to derive and deliver reliable warnings. Simulations are needed for the synthesis of an overall picture of the situation because the sensor network supplies data only at a few points. In this way, with the help of a computer model for the ascertainment of arrival times and wave heights as well as information on the habitants and infrastructure, fast risk estimations can be reached, that in turn support the decision to issue a warning.

Detection and prediction of tsunamis are only one part of work of the system. The ability to warn the population of the areas that will be affected is of equal importance.[15]

GITEWS is a project of the German Government at the reconstruction of the tsunami-prone region of the Indian Ocean. It is coordinated by the Intergovernmental Oceanographic Commission (IOC) of the United Nations Educational, Scientific and Cultural Organisation (UNESCO) and instructed by the United Nations (UN). The German Indonesian Tsunami Early Warning System is achieved by a consortium of nine German institutions: Helmholtz Centre Potsdam - German Research Centre for Geosciences (GFZ), Alfred Wegener Institute for Polar and Marine Research (AWI), Federal Institute for Geosciences and Natural Resources (BGR), German Aerospace Centre (DLR), GKSS Forschungszentrum Geesthacht, Deutsche Gesellschaft für Technische Zusammenarbeit (GTZ), Konsortium Deutsche Meeresforschung (KDM), Leibniz Institute of Marine Sciences (IFM-GEOMAR) and the United Nations University Institute for Environment and Human Security (UNU-EHS).[16]

On 11 November 2008, GITEWS started its operation and entered a further two-year development and optimisation phase. The system will be handed over to Indonesia completely in 2010.[29]

# 3 Basics

## 3.1 Geophysical Basics

### 3.1.1 Plate tectonics

Plate tectonics is a geological theory that has been developed to explain the evidence of large scale motions of the Earth's lithosphere.

The outermost part of the Earth's interior is made up of two layers: above is the lithosphere, comprising the crust and the rigid uppermost part of the mantle. Below the lithosphere lies the asthenosphere that has relatively low viscosity and shear strength. The deeper mantle below the asthenosphere is more rigid. This is not because of cooler temperatures but because of high pressure.

The lithosphere is divided into tectonic plates, see figure no. 3. In the case of the Earth, there are seven major and many minor plates. The lithospheric plates ride on the asthenosphere. These plates move in relation to one another at one of three types of plate boundaries: convergent or collision boundaries, divergent or spreading boundaries and transform boundaries. Earthquakes, volcanic activity, mountain-building and oceanic trench formation occur along plate boundaries. The average speed of the lateral movement of the plates (continental drift) is about 5-10cm/year.[59]

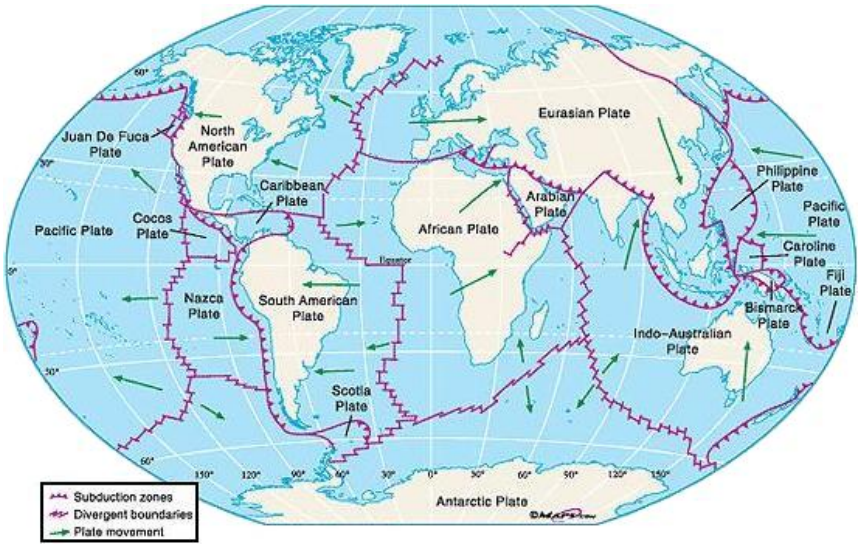


Figure 3: Earth's tectonic plates [26]

### 3.1.2 Earthquake

Earthquakes originate from dynamic processes of the Earth. An earthquake is the result of a sudden release of energy in the Earth's crust that creates seismic waves. Earthquakes with a magnitude of 3 or lower on the moment magnitude scale (logarithmical classification), which is a successor of the RICHTER scale, are mostly imperceptible. However, magnitude 7 causes serious damage over large areas.

An earthquake's point of initial rupture is called hypocentre. The term epicentre refers to the point at ground level directly above the hypocentre.[52] When a large earthquake happens offshore (submarine earthquake), the sea floor sometimes suffers sufficient displacement to cause a tsunami. Note that the epicentre does not necessarily coincide with the position of slip maximum. Slip heterogeneities play an important role for near field and the magnitude of large earthquakes is often underestimated.[20]

The tremors of earthquakes can also trigger landslides and occasionally volcanic activity. Earthquakes are caused mostly by rupture of geological faults, huge amounts of gas migration, mainly methane deep within the Earth, but also by volcanic activity, landslides, mine blasts and nuclear experiments. Particularly, at plate boundaries where adjacent plates move in different directions, it comes to increasing stress within the rock. If the shearing resistance of rock is exceeded, stresses are discharged by sudden movements of the Earth's crust, and it comes to a tectonic quake. Tectonic earthquakes will occur anywhere within the Earth where there is sufficient stored elastic strain energy to drive fracture propagation along a fault plane.

Shaking and ground rupture are the main effects created by earthquakes, principally resulting in more or less severe damage to buildings or other rigid structures. The severity of local effects depends on the complex combination of earthquake magnitude, distance from epicentre, and local geological and geomorphological conditions which may amplify or reduce wave propagation.[52]

Large tsunamigenic earthquakes with magnitude greater than 8 have large spatial dimensions ($>$ 200-300km). For instance, the Great Sumatra-Andaman earthquake with a magnitude of 9.3 ruptured an approximately 1300km-long segment.[3]

### 3.1.3 Tsunami

A tsunami (jap. harbour wave) is a water wave that is generated by an abrupt displacement of huge volumes of water. In the majority of cases, this displacement is caused by a vertical deformation of ocean floor during a submarine earthquake. Landslides, volcanic eruptions and meteorite impacts as well are possible factors that generate tsunamis. All of this mechanisms have in common that they can generate seismic waves that travel through the Earth with a velocity of several kilometres per second. Contrarily, tsunami waves reach only velocities of several 100 kilometres per hour. After an earthquake at the Sunda Trench off the coast of Indonesia, seismic waves usually arrive at the shore in approximately 30 to 40 seconds, whereas tsunami waves would reach the coast soonest after about 20 to 30 minutes.[16]

Following conditions cause tsunamis:

- minimum magnitude of about 7
- hypocentre is close (at least 50km) to the Earth's surface on the ocean's floor
- vertical deformation of ocean bed

Basically, a water wave does not represent a movement of water but a movement of energy caused by water (kinetic energy). On physical view, a wave propagation assumes that a displacement of the balance condition, which is due to a against directed restoring force, is given. In this case, it means rising and lowering of water level. The restoring force is the gravity that wants the surface of the water area to be horizontal.
Tsunamis are shallow water waves because their wave lengths are much greater than the depth of the ocean. Thereby, an enormous water amount is carried. Typical wave lengths of tsunamis are 100 to 500km.

Tsunamis are described by:

- total energy
- period of wave

During propagation of tsunamis, the whole water column is stimulated and mechanical energy as well as the period of the wave remain approximately constant. The velocity of

phase and the wave length depend on the depth of the ocean; the shallower the depth is, the slower and shorter the wave is. Thus, the energy of tsunami waves is more concentrated before it strikes the coast. Mostly in the wideness of the sea, the amplitude is not greater than a few decimetres. Therefore, it is difficult to identify tsunamis optically offshore. Degradations of energy by friction are insignificant because of great wave lengths. The loss of energy which occurs is only caused by geometrical propagation. So, tsunamis can circle the terrestrial globe several times.[64]
A tsunami is a natural disaster which can not be prevented nor precisely predicted. Hence, reliable Tsunami Early Warning Systems are essential to contain fatal damages.

### 3.1.4 Earth model - IASP91

Seismological earth models give in return changes of propagation velocites of seismic waves in the Earth's body according to the depth layers. The velocity distribution is based on analysis of the terms of seismic waves in different measuring points on the Earth. The term describes the duration needed by a seismic wave from its place of origin (hypocentre) up to a measuring station. The distance to the epicentre can be calculated from the term difference between seismic waves, which are the quicker P-waves (primary longitudinal waves) and the slower S-waves (secondary transversal waves).
IASP91 (also: IASPEI model) describes a common reference model for seismic velocities in the interior of the Earth, see figure no. 4. It was published by Kennett and Engdahl (1991) and is applied as a standard earth model of the International Association of Seismology and Physics of the Earth's Interior (IASPEI). The IASP91 model is a 1D-parameterised velocity model which shows a summary of global term-characteristics for an average earth radius of 6371km. It expresses S- and P-wave velocities (grey and black lines in figure 4) in the Earth's interior.[53]

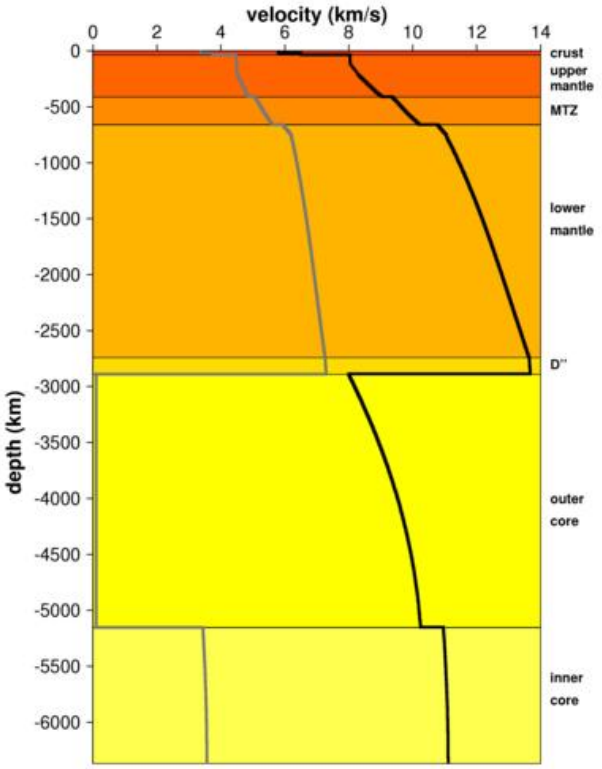


Figure 4: IASP91 Earth reference model [53]

### 3.1.5 Sunda Arc and Sunda Trench

The Sunda Arc is a volcanic arc that has originated the islands of Sumatra and Java as well as the Sunda Strait and the Lesser Sunda Islands. The arc marks an active convergent boundary between the Eurasian Plate and the Indo-Australian Plate. The Sunda and the Burma Plate as parts of the Eurasian Plate lies under Indonesia. The Indo-Australian Plate is drifting North-East at an average of 6cm/year and is subducting the Eurasian Plate along the Sunda Trench.[60] The Sunda Trench has a maximum depth of 7725 metres and is therewith the second deepest trench of the Indian Ocean.[55]

Adjoining tectonic plates can remain locked for decades or centuries, while slip-deficit of up to tens of metres accumulates, which is suddenly released during an earthquake. Deformation at the Sunda subduction zone caused for instance the Great Sumatra-Andaman earthquake of December 2004.


Figure 5: Tectonic setting of the North-East Indian Ocean [44]

## 3.2 Geodetical Basics

### 3.2.1 GPS Technologies

In comparison to existing Tsunami Early Warning Systems, GITEWS uses Differential Global Positioning System (DGPS) to quantify displacements of tectonic movements.[16] References to the procedure of GPS can be found in suitable technical literature (e.g. *Satellite Geodesy* from Seeber).

GPS land stations are being installed at the coastline of the Indonesian mainland and at the islands off Sumatra like the Mentawai Islands. GPS receivers record surface deformations continuously. Along with equivalent reference stations on the mainland, GPS provides detailed information on lateral movements and on the lifting and sinking rates of the surface.[31]

The main task of the GPS land stations is detection of horizontal and vertical deformations

of the Earth's surface due to a strong earthquake. This can be done in a very short time and with an accuracy of a few centimetres. Also buoys and tide gauges are equipped with GPS instruments which monitor their particular location and shifting, regarding position and altitude. Furthermore, new technologies like GPS reflectometry are considered as to their application in tsunami early warning issues.[16]

## 3.3 Mathematical Basics

### 3.3.1 Numerical analysis

Numerical analysis is the study of algorithms for problems of continuous mathematics. There are two different types of methods: direct methods compute the solution to a problem in a finite number of steps. These methods would give a precise answer if they were performed in infinite precision arithmetic. Examples include Gaussian elimination, QR decomposition and simplex method of linear programming. In practice, finite precision is used and the result is an approximation of the true solution, assuming stability.
In contrast to direct methods, iterative methods are not expected to terminate in a number of steps. Starting from an initial guess, iterative methods form successive approximations that converge to the exact solution only in the limit. A convergence criterion is specified in order to decide if a sufficiently accurate solution has been found. Even in infinite precision arithmetic, these methods would generally not reach the solution in finite many steps. Examples include Newton's method, bisection method, and Jacobi iteration. In computational matrix algebra, iterative methods are generally needed for large problems. Some methods are direct in principle but are usually used as though they were not, e.g. generalised minimal residual method (GMRES) and the conjugate gradient method. For these methods, the number of steps which are needed to obtain the exact solution is so large that an approximation is accepted in the same manner as for an iterative method.[58]

### 3.3.2 Curve fitting and Least squares method

Curve fitting is a mathematical optimisation method. The aim is that the final model or function adapts itself to a series of data points and possibly other constraints and its inevitable small contradictions in the best way possible.[50]
The method of least squares is used to model numerical data obtained from observations

by adjusting parameters of a model so as to get an optimal fit of data. The best fit is when the sum of squared residuals of the model has its least value. A residual is the difference between an observed value and the value given by the model. Big divergences of the model function of data are much stronger punished than small ones. Small improvements are attached to observations and the square sum of improvements should be the minimum.[56]

### 3.3.3 Lagrange multipliers

In mathematical optimisation, the method of LAGRANGE multipliers is a method to reformulate optimisation problems with constraints. The task of an optimisation problem subject to constraints, is to find a local extremum of a function in several variables with one or several constraints. The constraints are defined while putting functions on given values. This method introduces a new unknown scalar variable for every constraint, the LAGRANGE multipliers, and defines a linear combination which integrates the multipliers as coefficients. This can reduce the constrained problem to a problem without constraints.[62]

### 3.3.4 Simplex algorithm - Nelder-Mead method

In mathematical optimisation theory, the simplex algorithm is a popular algorithm for numerical solution of a linear programming problem. An unrelated, but similarly named method is the NELDER-MEAD method also referred to as the downhill simplex method due to NELDER and MEAD (1965) and is a commonly used numerical method for optimising multidimensional unconstrained problems, belonging to the more general class of search algorithms. The method uses the concept of a simplex which is a polytope of $n+1$ vertices in $n$ dimensions (a line segment on a line, a triangle on a plane, a tetrahedron in three-dimensional space and so forth).

The NELDER-MEAD method approximately finds a locally optimal solution to a problem with $n$ variables when the objective function varies smoothly. As a specific feature, this simplex algorithm gets by without derivations of the function, which are not computable with defensible expenditure in the case of some problems. The trend of the values and the gradient is approximated by sensible comparisons of the function values of several points in the parameter space in the direction of optimum. That means concretely that at each step of the search, a new point in or near the current simplex is generated. The function value at the new point is compared with the function's values at the vertices of the simplex

and, usually, one of the vertices is replaced by the new point, giving a new simplex. This step is repeated until the diameter of the simplex is less than a specified tolerance.
The procedure does not converge extremely fast but it is a simple and relatively robust optimisation method.[51] The Nelder-Mead method is also used for curve fitting.

### 3.3.5 Inverse problem

A mathematical problem is called an inverse problem if its task is to infer the causes that are underlying to the effect (physical properties) from observed effects of a system, see Louis (1989) and Rieder (2003). Inverse problems can be formulated as a transformation from data to model parameters. The transformation is a result of the interaction of a physical system, for example the Earth. Inverse problems are mostly very difficult or not at all solvable.[54]
One distinguishes well-posed and ill-posed inverse problems. But the most of inverse problems are ill-posed. That means that little varied effects (measurement errors) result in great variations regarding the causes (increasing data errors). Hence, contrary to well-posed problems, ill-posed problems do not meet the three conditions that are suggested by Hadamard [25]:

1. A solution exists (existence)
2. The solution is unique (uniqueness)
3. The solution depends continuously on the data, in some reasonable topology (stability of solution)

In the case of inverse problems, the condition of stability is most often violated. If an ill-posed inverse problem does exist, it needs to be re-formulated for numerical treatment. Typically, this involves including additional assumptions, such as smoothness of solution. This process is known as regularisation and the Tikhonov regularisation is one of the most commonly used for regularisation of linear ill-posed problems.[65]
Inverse problems can be found in many branches of science and mathematics where values of model parameters must be obtained from observed data.

### 3.3.6 QR decomposition

The QR decomposition belongs to the most stable algorithms in numerical linear algebra because orthogonal transformations entail no error amplification. The QR decomposition, also known as QR factorisation, is a linear algebra operation that factors a matrix into an orthogonal component $Q$ which is the basis for the row space of a matrix, and a triangular component $R$ (also called right triangular matrix). The QR decomposition of a $m \times n$ matrix $A$ with $m \geq n$ is a pair of matrices $A = Q \cdot R$ where the unitary matrix $Q$ is of size $m \times m$ and the upper triangular matrix $R$ is of size $m \times n$.[47]

### 3.3.7 Green's function

Green's function is a type of function used to solve inhomogeneous differential equations subject to boundary conditions.[61] Thus, it is an alternative method to the Fourier transform or Laplace transform, applicable to many of the same problems. The Green's function method takes a fundamental solution and assigns a weight at each point of the boundary according to the value of the given boundary conditions.[41]
The Green's function approach is derived from the standard elastic half-space model by Okada (1985, 1992). This conventional homogeneous model is used in most of the case studies. It derives the expressions for the coseismic (permanent) displacement at the Earth's surface. The standard Okada model defines the relation between the earthquake source parameters and the geodetic measurements of surface deformation.[24]

### 3.3.8 Mathematical model and Computer model

A mathematical model uses mathematical language to describe a system. It is used particularly in natural sciences and engineering disciplines to be controlled or optimised. In analysis, it can build a descriptive model of the system as a hypothesis as to how the system could work, or try to estimate how an unforeseeable event could affect the system. Similarly, in control of a system, different control approaches can be tried out in simulations.[57]
A computer model is a mathematical model that can only be analysed by computer because of its complexity. Analysis means an approximate solution using numerical analysis.[49] Computer models are highly beneficial, e.g. tsunami arrivals can be predicted (as TsunAWI).

# 4 Scenario modelling

## 4.1 Forward scenario modelling

### 4.1.1 Subfault array

The plate interface between the subducting Indo-Australian Plate and the upper Sunda Plate is discretised in its seismogenic part, which extends from the trench (0km) to 60km depth, into a regular mesh of rectangular patches, a so-called subfault array of the zone with maximal potential of earthquakes (WADATI-BENIOFF zone).

The mesh follows very accurately the geometry of the plate interface as derived from the regionalised upper mantle (RUM) seismic model by GUDMUNDSSON and SAMBRIDGE (1998). Detailed representation of the subduction zone geometry allows better localisation of slip. The mesh consists of 15 × 150 patches (altogether 2250 patches) and equates an area of about 300km × 6000km, see figure no. 6.

Each patch, also referred to as subfault, represents a rectangular fault plane of known geometry (amongst others: width, length) and position (longitude, latitude and depth). All patches have an individual size (at an average of 40km × 20km) and orientation, see figure no. 7.

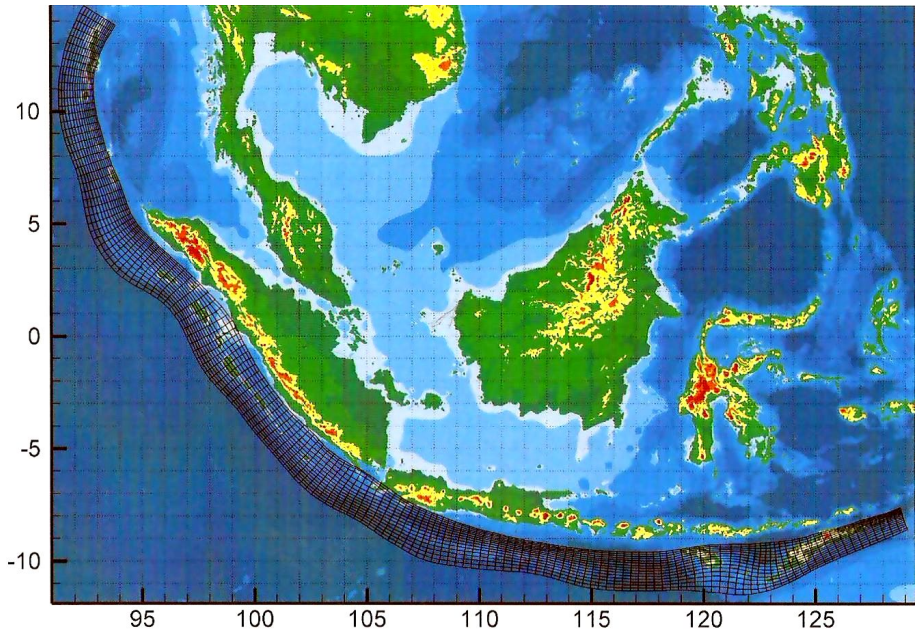


Figure 6: Discretisation of the plate interface off Sumatra [2]

Orientation of each subfault can be described by strike angle and dip angle. Strike represents the intersection of subfaults with the horizontal (azimuth). Strike is measured clockwise (0-360°) from North. Here, the average strike angle is about 300°. Dip describes the steepness of fault surface and can be defined as the angle below the horizontal of subfaults (0-90°). Dip varies in our case between 7° and 32°.

Slip indicates relative movement of material on the two sides of a subfault. Slip is represented as a vector and consists of two components: dip slip and strike slip.

Faults can be categorised into three groups based on the geometry of faulting. A fault where the main direction of movement on the fault plane is vertical, is known as a dip slip fault. Dip slip faults can be classified into normal fault and reverse or thrust fault. A normal fault occurs when the crust is extended. Then, the hanging wall moves downward, relative to the footwall. A thrust fault is the opposite of a normal fault, for example in the case of the Sunda Trench. Reverse faulting is the result of compressional forces. The largest earthquakes are generally low-angle (shallow dipping) reverse faults, like the Great Sumatra-Andaman earthquake.

Where the main direction of slip is horizontal, the fault is known as a strike slip fault. Here, the fault surface is usually almost vertical and the footwall moves either left or right or laterally with very little vertical motion. A fault which has a significant component of dip slip and strike slip is termed an oblique slip fault.

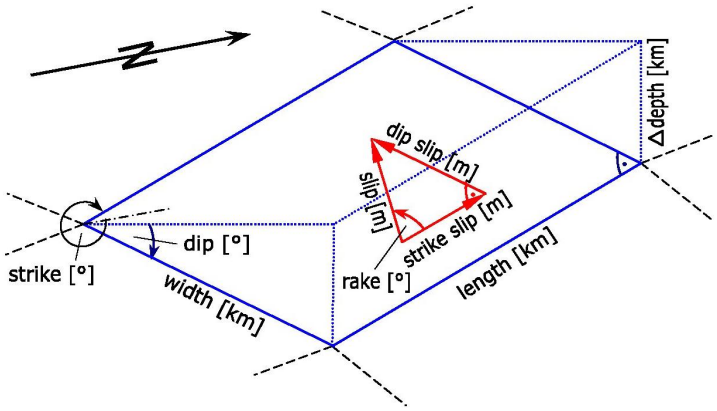


Figure 7: Definition of a single subfault and its slip components

Rake angle is defined by the slip vector and runs anticlockwise (0-360°) and is the direction in which the hanging wall moves in relation to the footwall. For example: if the hanging wall moves to the right (left-lateral fault), rake is 0°; if it moves up, rake is 90° (reverse or thrust fault); if it moves to the left (right-lateral fault), rake is 180°; and if it moves down (normal fault), rake is 270°.[43]
Following the definitions, the slip vector can be described by dip slip and strike slip or by rake angle and the length of the slip vector. Slip distribution of each subfault is recorded by GPS arrays.

### 4.1.2 Near field GPS arrays

The proposal made by Sobolev et al. (2007), is to implement a specially aligned array of one high rate (1-10Hz), real time GPS station (master station) and several slave stations, all equipped with precise geodetic dual-frequency receivers. The array master station receives high rate GPS observations from its slave stations and calculates coordinate differences for each single measurement epoch in real time, as suggested by Bock, Y. et al. (2000, 2004).

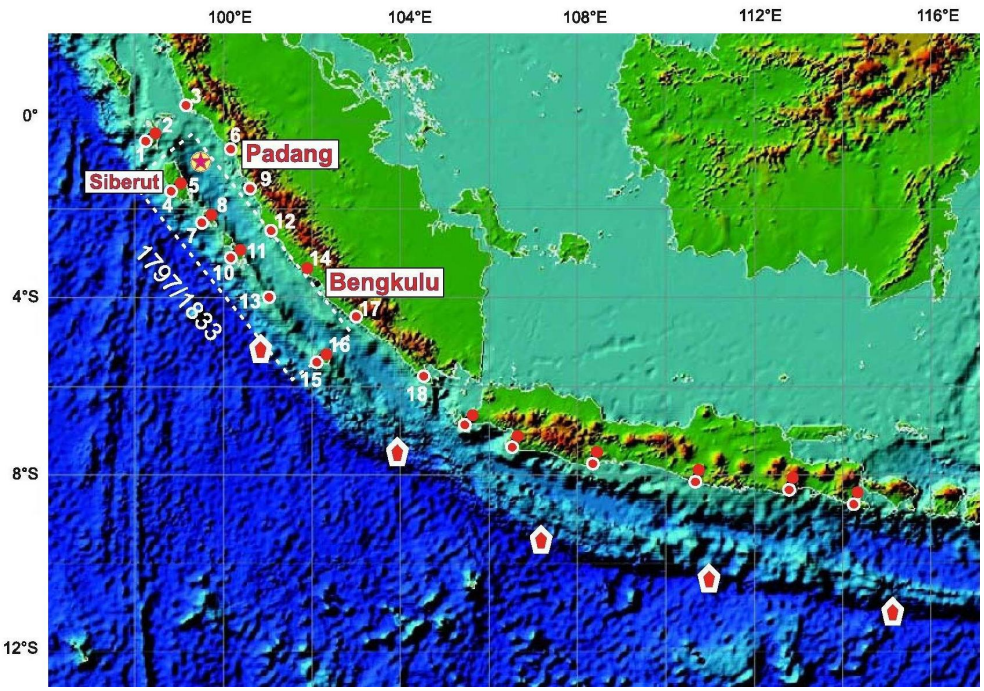


Figure 8: Distribution of conceptual GPS shield system [40]

The so-called GPS shield should be located close to the source as it is on the Mentawai Islands, about 150km offshore Sumatra, and at the Sumatran coast (compare with figure no. 8). The stations on the islands (two or more) should be closely located (10-20km) and aligned perpendicularly to the trench thus parallel to the expected gradient of surface coseismic displacement. Such array will exploit large displacements and their trench-perpendicular gradients in the near field.

The array measures surface deformations of each subfault using instantaneous GPS positioning techniques, see Bock, H. et al. (2000). So, for a single epoch, 1-Hz displacement measurements achieve a realistic accuracy of more than several centimetres for absolute values of displacements (horizontal: ±2.5cm, vertical: ±5cm) and of a few centimetres for relative values of displacements (horizontal: ±0.5cm, vertical: ±1.5cm) between the closely located stations using differential GPS. That will provide a much improved slip resolution, which is especially important for early tsunami warning for Sumatra.

The real time GPS stations (red circles) should be set along the trench with a distance of 100-200km, a distance that is appropriate to resolve major trench parallel slip heterogeneity. In the case where no islands are located between the trench and Sumatra, the suggestion is to use ocean buoys equipped with GPS devices and bottom pressure sensors (red diamonds). In addition, it is useful to complete some of the GPS stations with broad band seismometers and strong motion recorders (red circles with white rings).

Figure no. 8 also illustrates the zone of the potential giant earthquake which is expected at the site of the past earthquakes in 1797 and 1833 (dashed box). The numbers mark the sites where synthetic seismograms were calculated and which are used for 3D-inversion for rupture parameters.[40]

It is already demonstrated by Banerjee et al. (2005) that slip inversions from GPS data are very sensitive to assumed fault geometry. Therefore, precise mapping of geometry of the seismogenic zone which can be accomplished only with long term observations using broad band seismometers, is essential for the success of the GPS shield concept.[39]

An analysis by Sobolev et al. (2006, 2007) shows that GPS arrays can resolve tsunami rupture parameters very well, provided they are placed above the rupture zone. By moving the array landwards, the resolution decreases but it remains fair until the array is moved away some 50-100km from the surface projection of the rupture zone. Consequently, if arrays are located further from the trench, the resolution strongly decreases and can nei-

ther resolve average slip on the fault nor the depth of maximum slip. But they still allow the estimation of the seismic moment of a giant earthquake with high accuracy, even at a distance of 500km from the trench. The higher the accuracy of measurements at single GPS stations, the larger the distance from the trench at which GPS array can resolve the rupture parameters can be. The best results in predicting tsunami waves within less than 10min can be obtained where GPS stations are located closer than 100km from the seismogenic zone. Therefore, real time GPS measurements may differentiate between less dangerous and more dangerous rupturing off Padang.[39]

Summing up, the resolving power of near field GPS arrays depends on their distance to the trench, furthermore on the accuracy of displacement measurements at the stations and not least on the uncertainty about the knowledge of the fault geometry. In addition to their tsunami warning function, GPS arrays will also allow long-term deformation monitoring in most convergent plate boundaries to provide important data for constraining global geodynamics.[40]


Figure 9: Sumatran GPS Array (SuGAr), as at July 2008 [32]

Note that the Caltech/LIPI Sumatran GPS Array (SuGAr) GPS network has already continuous GPS sites in some of the appropriate places (see figure no. 9) but unfortunately none of those sites are yet equipped to allow real time applications. The Sumatran GPS Array is being designed, constructed and operated by members of the Tectonics Observatory at the California Institute of Technology (Caltech) and the Indonesian Institute of Sciences (LIPI).[35]

### 4.1.3 Rupture Generator

Rupture Generator (RuptGen, version 1.1) developed by Babeyko is a tool of the GITEWS project for generating virtual earthquakes. This programme makes it possible to compute static displacements caused by an earthquake for any constellation of GPS receivers (e.g. a virtual idealised GPS array or the existing Sumatran GPS array (SuGAr)). RuptGen calculates sea floor deformation due to co-seismic slip at the Sunda Trench by using the mathematical forward model of Green's functions. Both, single and multiple rupture scenarios can be easily modelled due to the flexible programme input. Multiple rupture option allows modelling of earthquakes with any slip distribution. The programme performs output for slip and surface deformation in various formats.

Three components concerning surface deformation (longitude, latitude, altitude) due to unit dip and strike are precomputed for each patch and stored on a regular surface grid as a databank of Green's functions. Using this databank of Green's functions, sea floor deformation can be easily calculated for any earthquake scenario with given slip distribution. The mentioned databank is calculated using the 1D layered earth dislocation code by Wang et al. (2003) and seismic velocities from the IASP91 model.[20] The intention is to implement a dislocation model based on 3D Finite Element Method (FEM).[4]

Rupture Generator is controlled by command line arguments as well as by configuration file. The Green's functions of each patch are in a form of Golden Software GRD-files and should be placed in a subdirectory called `gf`. Another necessary component to run RuptGen is the plate interface description that is specified in a file (`pi15150.pi`) whose name should be stated in the configuration file (`ruptgen.cfg`).

The command line takes two forms. The first variant corresponds to a single rupture earthquake with pre-defined slip distribution.

Here, the command line has the following syntax:

*RuptGen.exe* {**-mw** <mw> | **-slip** <slip>} {**-xy** <lon> <lat> | **-ij** <i> <j>} [**-out** <string>] [**-area** <rand>] [**-nodisp**]

Either moment magnitude $M_W$ or value of slip [m] should be specified. Another obligatory parameter is rupture epicentre. It is defined either in geographical coordinates (longitude and latitude) or as patch ij-indices. The indices of patches run from South-East to North-West, as shown in figure no. 10. The i-index runs along the rupture zone of the Sunda Trench (i = 1-150) and the j-index (j= 1-15) runs at right angles to the i-index.
There are three facultative arguments: `-out`, `-area` and `-nodisp`. The specification of the optional argument `-out` can be any combination of letters: `a` for ASCII output, `p` for Tecplot-format output and `g` for Golden Software GRD-format output. The default output has to be specified in the configuration file.

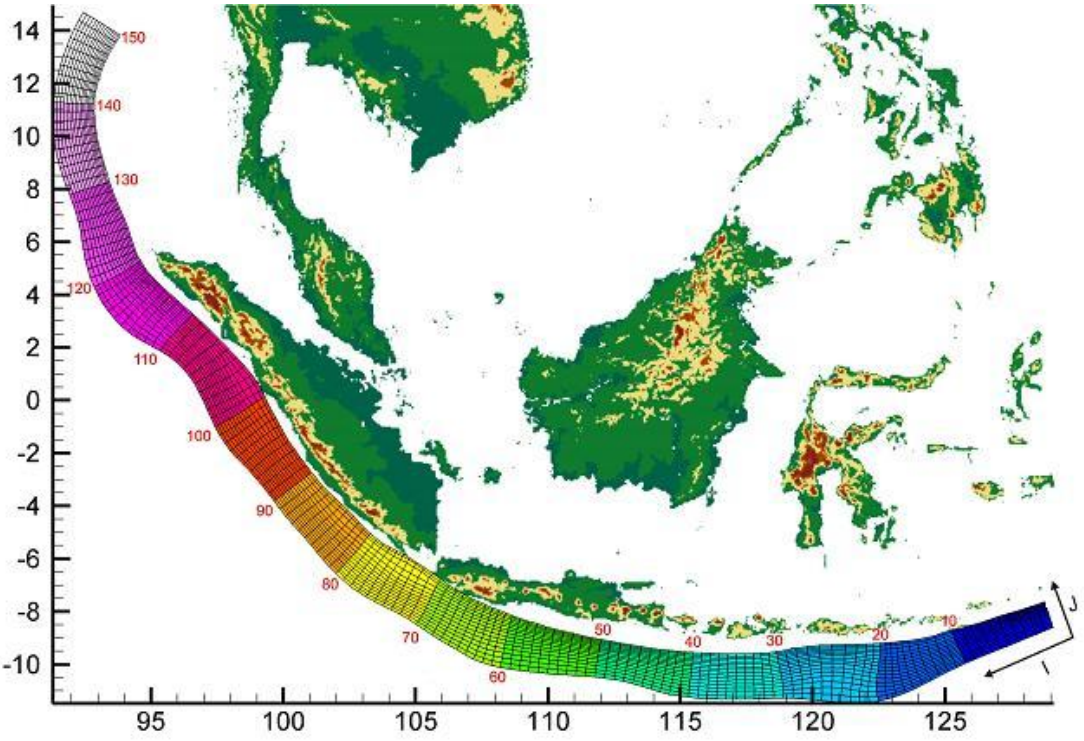


Figure 10: Numbering of patches [1]

Another optional parameter is `-area`. It tells the programme to save time and space and to calculate sea floor displacements on a local grid also defined in the configuration file (`ruptgen.cfg`). The value of this argument corresponds to the boundaries which will be added to the surface projection of the current rupture area.
The third optional parameter `-nodisp` tells the programme to calculate slip distribution only.
The programme behaviour depends on whether moment magnitude $M_W$ or slip is given at the command line. Should the magnitude be given, rupture dimensions will be first calculated by applying the scaling laws by WELLS and COPPERSMITH (1994). The resulting multi-patch rupture will be symmetrically placed around the epicentre. The corresponding effective slip which is calculated from the seismic moment and from the derived rupture dimensions will be distributed along the rupture according to a GAUSSian shape function. Should the slip be given on the command line, epicentral patch will be the only one activated. This option gives more flexibility but should be applied with care in order to avoid incorrect physical scenarios. Note that earthquakes generally follow scaling laws. For this reason e.g., one can hardly expect 10m slip at a single patch surrounded by patches with 0m slip.
Possible commands for given slip distribution or given magnitude:

```
RuptGen.exe -slip 1.0 -ij 95 7
RuptGen.exe -Mw 8.4 -xy 100.0 -2.0
```

In case of modelling ruptures with arbitrary slip distribution or complex earthquakes consisting of several ruptures, the second variant of the programme input is more suitable. Here, the syntax is:

*RuptGen.exe* **-f** <rupture-list-filename> [**-out** <string>] [**-area** <rand>] [**-nodisp**]

For example:

```
RuptGen.exe -f TestScenario.slip
```

The file, whose name was specified at the command line as rupture-list-filename, should contain a list of ruptures in which each rupture is defined on a separate line such as:

```
-slip 1.0 -ij 95 7
-slip 2.0 -ij 95 8
-slip 1.0 -ij 95 9
```

This example describes an earthquake consisting of three single patch ruptures. Another opportunity allows the modelling of earthquakes with arbitrary slip distribution as an event of multi-patch ruptures like:

```
-mw 7.5 -xy 95.0 5.0
-mw 8.0 -ij 100.0 -2.0
```

RuptGen generates following outputs: scenario summary, slip distribution and surface displacement. If TsunAWI node definition file exists, uplift will be projected onto this mesh and stored in TsunAWI input format.[2] The TsunAWI model launched by Alfred Wegener Institute for Polar and Marine Research (AWI) is a computer model based on non-linear shallow water equations particularly suited for simulation of tsunamis (wave propagation).[14] If a GPS stations file exists, displacements will be projected onto the corresponding stations and stored in ASCII and/or Tecplot format. TsunAWI node file and TsunAWI input file as well as an optional GPS stations input file need also to be specified in the configuration file `ruptgen.cfg`.[2]

### 4.1.4 Forward algorithm

The forward algorithm can be described as a matrix vector equation:

$$\mathbf{A} \cdot \vec{\mathbf{x}} = \vec{\mathbf{b}} \tag{1}$$

where

- $\vec{\mathbf{b}} \in \mathbb{R}^{3*\mathbb{k}}$, $\vec{\mathbf{b}} \sim$ GPS measurements (3D surface deformation), $\mathbb{k} \sim$ number of available GPS stations at a specific position.
- $\vec{\mathbf{x}} = \begin{pmatrix} x^1 \\ x^2 \end{pmatrix}$, $x^1 \sim$ dip slip, $x^2 \sim$ strike slip, $x^n \in \mathbb{R}^{750}$ (with $n = 1, 2$) because the subfault array is limited to the region off Padang with 750 subfaults. Each entry of the vectors $x^n$ corresponds to an individual subfault location in the Earth.
  In particular, $(x^n)_l$ corresponds to the $(i, j)$th subfault, where $i = \lfloor \frac{l}{15} \rfloor$ ($i$ runs from 71 to 120), $j = l - 15 \cdot i$ ($j$ runs from 1 to 15) and resulting from this: $l = j + 15 \cdot i$.

- $\mathbf{A} : \mathbb{R}^{2 \cdot 750} \rightarrow \mathbb{R}^{3 \cdot \mathbb{k}}$, $\mathbf{A} = \begin{pmatrix} A^1 & A^2 \end{pmatrix}$, where $A$ is the propagation matrix, whereas $A^1$ describes the GREEN's functions with respect to dip slip and $A^2$ with respect to the strike slip component of each subfault.

Since the surface deformation can be split into three components (respecting longitude, latitude, altitude), it comes to three linear systems:

$$A_1 \cdot \vec{\mathbf{x}} = \vec{b_1} \qquad (longitude) \tag{2}$$

$$A_2 \cdot \vec{\mathbf{x}} = \vec{b_2} \qquad (latitude) \tag{3}$$

$$A_3 \cdot \vec{\mathbf{x}} = \vec{b_3} \qquad (altitude) \tag{4}$$

Combining these, the three systems yield:

$$\mathbf{A} \cdot \vec{\mathbf{x}} = \begin{pmatrix} A_1 \\ A_2 \\ A_3 \end{pmatrix} \cdot \vec{\mathbf{x}} = \begin{pmatrix} A_1^1 & A_1^2 \\ A_2^1 & A_2^2 \\ A_3^1 & A_3^2 \end{pmatrix} \cdot \begin{pmatrix} x^1 \\ x^2 \end{pmatrix} = \begin{pmatrix} b_1 \\ b_2 \\ b_3 \end{pmatrix} = \vec{\mathbf{b}} \tag{5}$$

where

- $A_m^n \in \mathbb{R}^{750}$, $n \sim$ slip component (dip slip, strike slip), $m \sim$ deformation component (longitude, latitude, altitude).

The forward algorithm will be realised by using Rupture Generator that is explained in detail in subsection 4.1.3.

## 4.2 Backward scenario modelling - GPS inversion

### 4.2.1 Inversion algorithm

The system of equations above (5) describes the mathematical initial position very well but the system is instable (ill-posed) because the eigenvalues or rather the singular values of the propagation matrix $A$ are close to zero. Therefore, $A$ is not accurately invertible. So, another method than matrix inversion is required to be able to invert rupture parameters. The present ill-posed inverse problem needs to be re-formulated (regularisation).
This GPS inversion concept is similar to the one which has been already demonstrated by other authors (see e.g. BANERJEE et al. (2005), BLEWITT et al. (2006) and CHLIEH et

al. (2007) but includes some changes in its regularisation as it takes into consideration the physical justification of boundary conditions. Furthermore, displacements at GPS array stations which are computed by Rupture Generator, are altered by adding random noise to mimic real time GPS accuracy.

This inversion algorithm includes besides physically justified boundary conditions penalty terms for slip and rake roughness (gradient). The summation in the penalty terms concerns the three displacement components (longitude, latitude, altitude) at all available GPS stations (penalty term of norm of slip) and all selected subfaults and their respective nearest neighbours (penalty term of azimuth of slip). Additionally, virtual subfault layers are placed at the boundaries for the slip penalty term. These layers are set to zero to avoid physically impossible infinite stress concentration at the fault boundaries.

The inversion employs a simplex algorithm from the MATLAB Optimization Toolbox to find the slip distribution, which minimises squares of differences (residuals) of "observed" (synthetic) and model-predicted GPS displacements on the one hand, and which simultaneously minimises differences of slip magnitudes and rake angles between adjacent subfaults on the other hand. The cost function that has to be minimised has been published by Hoechner et al. (2008) and can be described as follows:

$$J(x^1, x^2) = \Xi(x^1, x^2) + \lambda_1 \cdot \Phi(x^1, x^2) + \lambda_2 \cdot \Psi(x^1, x^2) \tag{6}$$

where

- $x^1$, $x^2$ $\sim$ dip slip and strike slip components concerning each subfault.
- $\Xi(x^1, x^2)$, $\Phi(x^1, x^2)$, $\Psi(x^1, x^2)$ $\sim$ single terms of the cost function, where $\Xi(x^1, x^2)$ minimises distances concerning surface deformation and $\Phi(x^1, x^2)$, $\Psi(x^1, x^2)$ two constraints (penalty terms) that are supposed to be physically as homogeneous as possible (smoothness).
- $\lambda_1$, $\lambda_2$ $\sim$ weighting factors (so-called Lagrange multipliers) of the penalty terms. These Lagrange multipliers can not be used as a routine because they depend on corresponding scenarios. They are calibrated using synthetic scenarios with different types of slip distributions, see Hoechner et al. (2006).[20]

The chi-square reduced term is:

$$\Xi(x^1, x^2) = \frac{1}{3 * \mathbb{k}} \sum_{n=1}^{3*\mathbb{k}} \left( \frac{||A \cdot (\frac{x^1}{x^2}) - b^\epsilon||^2}{\sigma^2} \right)_n \tag{7}$$

where

- $\mathbb{k} \sim$ number of available GPS stations
- $b^\epsilon \in \mathbb{R}^{3*\mathbb{k}}$, $b^\epsilon \sim$ noisy GPS measurements
- $\sigma \in \mathbb{R}^{3*\mathbb{k}}$, $\sigma \sim$ 1-sigma standard deviations of the GPS measurements

The summation for $\Xi(x^1, x^2)$ concerns the displacement components (longitude, latitude, altitude) at all available GPS stations. The value of this term indicates the quality between "observed" (synthetic) and modelled GPS data, basics therefore see subsection 3.3.2.

The penalty term of norm of slip is the first physical constraint:

$$\Phi(x^1, x^2) = \sum_{i=71}^{120} \sum_{j=1}^{15-1} \left( \left( s(x^1_{(i-1)\cdot 15+j+1}, x^2_{(i-1)\cdot 15+j+1}) - s(x^1_{(i-1)\cdot 15+j}, x^2_{(i-1)\cdot 15+j}) \right)^2 \right) \tag{8}$$

$$+ \sum_{i=71}^{120-1} \sum_{j=1}^{15} \left( \left( s(x^1_{i\cdot 15+j}, x^2_{i\cdot 15+j}) - s(x^1_{(i-1)\cdot 15+j}, x^2_{(i-1)\cdot 15+j}) \right)^2 \right) \tag{9}$$

$$+ \sum_{i=71-1} \sum_{j=1}^{15} \left( s(x^1_{(i-1)\cdot 15+j}, x^2_{(i-1)\cdot 15+j}) \right)^2 \tag{10}$$

$$+ \sum_{i=120} \sum_{j=1}^{15} \left( s(x^1_{(i-1)\cdot 15+j}, x^2_{(i-1)\cdot 15+j}) \right)^2 \tag{11}$$

$$+ \sum_{i=71}^{120} \sum_{j=15} \left( s(x^1_{(i-1)\cdot 15+j}, x^2_{(i-1)\cdot 15+j}) \right)^2 \tag{12}$$

$$+ \frac{1}{4} \sum_{i=71}^{120} \sum_{j=1} \left( s(x^1_{(i-1)\cdot 15+j}, x^2_{(i-1)\cdot 15+j}) \right)^2 \tag{13}$$

where

- $i \sim$ index of respective subfaults along the trench
- $j \sim$ index of respective subfaults perpendicular to the trench

- (8) and (9) are the penalty terms towards the $(i, j)$-index
- (10) to (13) include a so-called virtual subfault layer at the boundaries for the eastern (10), western (11), bottom (12) and upper (13) borders to avoid physical impossible infinite stress concentration at the fault boundaries

Dip slip ($x^1$) and strike slip ($x^2$) of each subfault can be combined as:

$$s(x_l^1, x_l^2) := \sqrt{(x_l^1)^2 + (x_l^2)^2} \tag{14}$$

with

- $l = j + 15 \cdot i$, $l \sim$ number of respective subfault

The penalty term of azimuth of slip is the second physical constraint:

$$\Psi(x^1, x^2) = \sum_{i=71}^{120} \sum_{j=1}^{15-1} (y_{i,j+1} - y_{i,j})^2 + \sum_{i=71}^{120-1} \sum_{j=1}^{15} (y_{i+1,j} - y_{i,j})^2 \tag{15}$$

where
the azimuth of slip can be described as the difference of strike angle and projection of rake angle to the horizontal, whereas rake is defined by the slip components (by the quotient of dip slip and strike slip) and needs to be transformed by dip angle, as follows:

$$y_{i,j} = \vartheta_{(i-1)\cdot 15+j} - \arctan\left(\frac{x^1_{(i-1)\cdot 15+j}}{x^2_{(i-1)\cdot 15+j}} \cdot \cos(\delta_{(i-1)\cdot 15+j})\right) \tag{16}$$

with

- $\vartheta \in \mathbb{R}^{750}$, $\vartheta \sim$ strike angle
- $\delta \in \mathbb{R}^{750}$, $\delta \sim$ dip angle

Both, strike angle and dip angle, are predefined by the predetermined geometry of the subfault array.

### 4.2.2 MATLAB's `fminsearch`

To minimise residuals of a regularised inversion problem, the task is to find the minimum of the cost function. Therefore, the MATLAB function `fminsearch` from the MATLAB Optimization Toolbox can be used. `fminsearch` employs the simplex search method of NELDER and MEAD (see subsection 3.3.4) to minimise a function of several variables, starting at an initial estimate.

The syntax is:

```
x = fminsearch(fun,x0,options,P1,P2,...)
```

where
the MATLAB function starts at the point `x0` $\in \mathbb{R}^n$ and finds a local minimum `x` of the function described in `fun` : $\mathbb{R}^n \to \mathbb{R}$ iterative. The initial value `x0` can be scalar, a vector or a matrix. `fminsearch` minimises with the optimisation parameters specified in the structure `options`. These parameters are: level of display, maximum number of function evaluations allowed, maximum number of iterations allowed and termination tolerance on `x`. The structure `options` can be defined using the MATLAB function `optimset`, see MATLAB Documentation. `fminsearch` passes the problem-dependent parameters `P1, P2, etc.` directly to the function `fun`.
The solution this MATLAB function may give, is a scalar local minimum. Applied to the inversion, this means that `fminsearch` yields a local minimum of the cost function.

### 4.2.3 Other inverse approaches

In comparison to the mentioned inverse algorithm, there are other approaches to solve the present ill-posed problem. Note that these two techniques suggested at this point, do not consider physical constraints as it can be found in the inverse algorithm. One of these approaches is QR decomposition (see subsection 3.3.6) of the transposed system.

**QR decomposition of transposed system** If $A \in \mathbb{R}^{m \times n}$ with $m \geq n$ and $rank\ A = n$, it can be factorised as:

$$A = Q \cdot R \tag{17}$$

with

- $Q \in \mathbb{R}^{m \times n}$ that satisfies $Q^{\mathrm{T}} \cdot Q = I$
- $R \in \mathbb{R}^{n \times n}$ as an upper triangular with $r_{ii} > 0$

An under-determined system of equations with $m < n$, as in the case of the propagation matrix $A$ of the forward algorithm (see subsection 4.1.4), can be solved by QR decomposition of the transposed system:

$$A^{\mathrm{T}} = Q \cdot R \tag{18}$$

Thus, QR decomposition of the transposed system is unique because of the dimension $m \geq n$ which is given now.

Transposition of the forward algorithm:

$$(A \cdot \vec{x})^{\mathrm{T}} = \vec{b}^{\mathrm{T}} \tag{19}$$

$$\vec{x}^{\mathrm{T}} \cdot A^{\mathrm{T}} = \vec{b}^{\mathrm{T}} \tag{20}$$

QR decomposition of matrix $A^{\mathrm{T}}$ yields:

$$\vec{x}^{\mathrm{T}} \cdot Q \cdot R = \vec{b}^{\mathrm{T}} \tag{21}$$

Reduce $Q$ and $R$ to $\hat{Q}$ and $\hat{R}$ to save time and memory[47] on the one hand, but primarily to obtain the invertible matrix $\hat{R}$ to reconstruct rupture parameters:

$$Q \cdot R = \begin{pmatrix} \hat{Q} & \tilde{Q} \end{pmatrix} \cdot \begin{pmatrix} \hat{R} \\ 0 \end{pmatrix} \tag{22}$$

$$A^{\mathrm{T}} = \hat{Q} \cdot \hat{R} \tag{23}$$

Reduced QR decomposition of the transposed system:

$$\vec{x}^{\mathrm{T}} \cdot \hat{Q} \cdot \hat{R} = \vec{b}^{\mathrm{T}} \tag{24}$$

Re-transposition yields:

$$\hat{R}^{\mathrm{T}} \cdot \hat{Q}^{\mathrm{T}} \cdot \vec{x} = \vec{b} \tag{25}$$

Invert $\hat{R}^{\mathrm{T}}$ and multiply with $\hat{Q}$:

$$\hat{Q} \cdot \hat{Q}^{\mathrm{T}} \cdot \vec{x} = \hat{Q} \cdot \hat{R}^{\mathrm{T}^{-1}} \cdot \vec{b} \tag{26}$$

As $\hat{Q} \cdot \hat{Q}^{\mathrm{T}} = I$:

$$\vec{x} = \hat{Q} \cdot \hat{R}^{\mathrm{T}^{-1}} \cdot \vec{b} \tag{27}$$

Below, this approach is also referred to as "QR_min".

**Iterative approach by surrogate functionals** Another suggested inverse approach is a technique of optimisation transfer that is named iterative algorithm through surrogate functionals. Here, it is renounced of the derivation of this approach, rather it is referred to Teschke (2007) and Daubechies et al. (2004).

Surrogate functionals that act as penalty terms:

$$\Theta(\vec{x}, \vec{a}) = C \cdot ||\vec{x} - \vec{a}||^2 - ||A \cdot \vec{x} - A \cdot \vec{a}||^2 \tag{28}$$

added to the initial problem of the forward algorithm and the $l_p$-norm yield:

$$\Theta_{forward}(\vec{x}, \vec{a}) = ||A \cdot \vec{x} - \vec{b^{\epsilon}}||^2 + 2 \cdot t \cdot ||\vec{x}||_p^p + C \cdot ||\vec{x} - \vec{a}||^2 - ||A \cdot \vec{x} - A \cdot \vec{a}||^2 \tag{29}$$

where

- $t \sim$ thresh parameter
- $0 \leq p \leq 1$
- $C > ||A^{\mathrm{T}} \cdot A||$, $C \sim$ constant
- $\vec{a} \sim$ auxiliary element

Since $\Theta(\vec{x}, \vec{a})$ is strictly convex in $\vec{x}$, $\Theta_{forward}(\vec{x}, \vec{a})$ is also strictly convex in $\vec{x}$ and has an unique minimiser for any choise of $\vec{a}$. As $\vec{a}$ represents the initial value, the iterative algorithm applied to the present ill-posed problem, for $p = 1$, can be described as follows:

$$\vec{x}_{n+1} = S_{\frac{t}{C}} \cdot \left( A^{\mathrm{T}} \cdot \vec{b^{\epsilon}} + C \cdot \vec{x}_n - A^{\mathrm{T}} \cdot A \cdot \vec{x}_n \right) \tag{30}$$

with

$n = 0, 1, 2, ...$

Below, this approach is also referred to as "sparse", and combined with QR decomposition of the transposed system as "QR_min_sparse".

**Notice** A great number of other inverse approaches that could be applied for ill-posed inverse problems as earthquake parameter reconstruction, are also available but it would go beyond the framework of this work.

# 5 Application

As the region off Padang (longitude: 100.3606°, latitude: -0.9556°) is the most tsunami threatened area, the subfault array is limited to that territory, from the full array $150 \times 15$ to $50 \times 15$ ($i = 71 - 120$, $j = 1 - 15$). In the context of this work, the resolution of the limited subfault array is reduced to $25 \times 5$ (but concerning same i- and j-indices) to save time and memory. The difference of accuracy regarding earthquake parameter reconstruction using the reduced subfault array, in comparison to the full subfault array, is only about $\pm 0.7$cm for an event with a moment magnitude of 7.5. Thus, using the reduced subfault array can be accounted as sufficiently accurate.

Since rupturing of deep locked subfaults between the Mentawai Islands and the Sumatran coast off Padang results in devastating tsunamis with short arrival times even for smaller earthquakes, a subfault of that area ($i = 98$, $j = 10$ that corresponds to longitude: 98.9064°, latitude: -1.0091°) is chosen for this sensitivity analysis to act in the worst cases. The 25 GPS stations that are employed within this analysis, are chosen from the existing Sumatran GPS Array (SuGAr) which has its GPS stations on the mainland of Sumatra and on the Mentawai Islands as well.

Earthquakes with a moment magnitude less than 7.0 can be determined using traditional seismic method. Earthquakes with a magnitude greater than 8.0 have a very large signal to noise ratio in GPS measurements and an accurate distribution of slip can be obtained by using GPS inversion. But earthquakes with $7.0 \leq \mathrm{M}_W \leq 8.0$ which may or may not be tsunamigenic, have a relatively poor signal to noise ratio in GPS.[21] Hence, the magnitude interval which is mainly considered here, runs from 7.0 to 8.0 (increment: 0.1). Note that the moment magnitude scale is logarithmic, so an earthquake one number higher on the scale is approximately thirty times more powerful (e.g. a 7.0 vs. a 8.0).

Scenarios simulated at this point are single events and do not consider strike slip because rake of 90° is chosen. Therefore, slip distribution denoted here contains dip slip only.

Within this analysis, different noise behaviour are simulated. Defined noise levels are: 1cm/3cm, 5cm/10cm, 10cm/20cm and 20cm/40cm (regarding position and elevation separately), where both former noise levels correspond to achievable GPS technique accuracy. Both other noise levels are chosen to show the behaviour between "observed" (synthetic) and reconstructed GPS data in the case of clearly worse signal reception. So, the grade of

quality of earthquake parameter reconstruction considering different noise behaviour can be shown.

The initial position for every GPS inversion approach of the present ill-posed inverse problem is the forward algorithm which is realised by Rupture Generator. So, GPS displacements at the stations of the Sumatran GPS Array are computed by RuptGen and altered by adding noise (according to the mentioned noise levels).

## 5.1 Using MATLAB's fminsearch

After addition of noise levels, RuptGen generated GPS displacements can be regarded as real time GPS measurements with different noise behaviour. The 1-sigma standard deviations of the GPS measurements are in accordance with applied noise levels. The GREEN's function with respect to slip needs to be reduced in order to make dimensions correspond with the reduced subfault array (slip distribution). MATLAB's function `fminsearch` minimises the cost function to a local minimum, see subsection 4.2.1. Following, on the basis of reconstructed slip distribution, surface deformation (in the form of GPS displacements) can be derived by multiplication of the reduced GREEN's function with the reconstructed slip distribution (forward algorithm), see MATLAB code.

Using `fminsearch`, different aspects which are visualised in figures (see below and appendix), are tested. Concretely, surface deformation recorded by GPS stations (circles) are mapped at their geographical positions. Noiseless RuptGen generated GPS displacements (red), noisy GPS displacements (blue) according to the indicated noise level and their reconstructions (black) via `fminsearch` are pictured. It is distinguished graphically between geographical position (continuous line) and elevation (dotted line). As an example, an event of $M_W = 8.0$ and noise level = 5cm/10cm at subfault $i = 98$, $j = 10$ is shown in figure no. 11. For more figures see appendix A.1.1

Furthermore, a target-performance comparison of noiseless RuptGen generated slip distributions (as target slip: "slip") and `fminsearch` reconstructed slip distributions (as actual slip: "slipopt") with respect to different noise levels is carried out. On the one hand, slip distributions are illustrated concerning the subfault array (for $7.0 \leq M_W \leq 8.0$), and on the other hand, slip vectors are shown as a graph (for $6.0 \leq M_W \leq 8.0$). Therefore, see figures no. 12 and no. 13 as well as appendix A.1.2 and A.1.3.

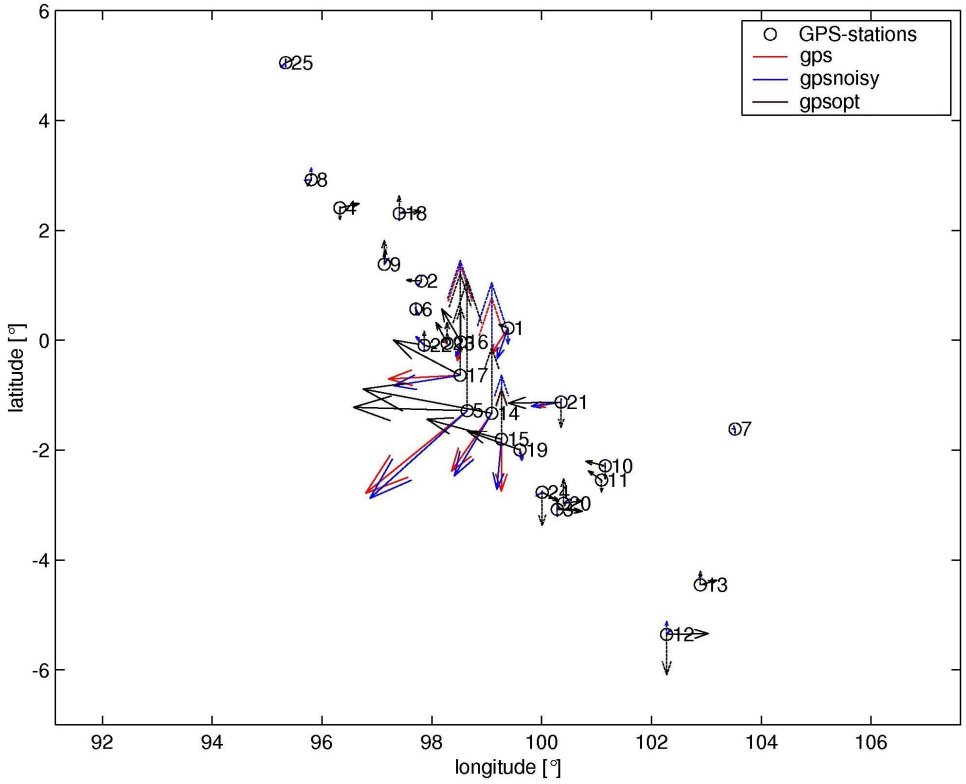


Figure 11: GPS displacements on SuGAr stations for an event of $M_W = 8.0$, noise level = 5cm/10cm

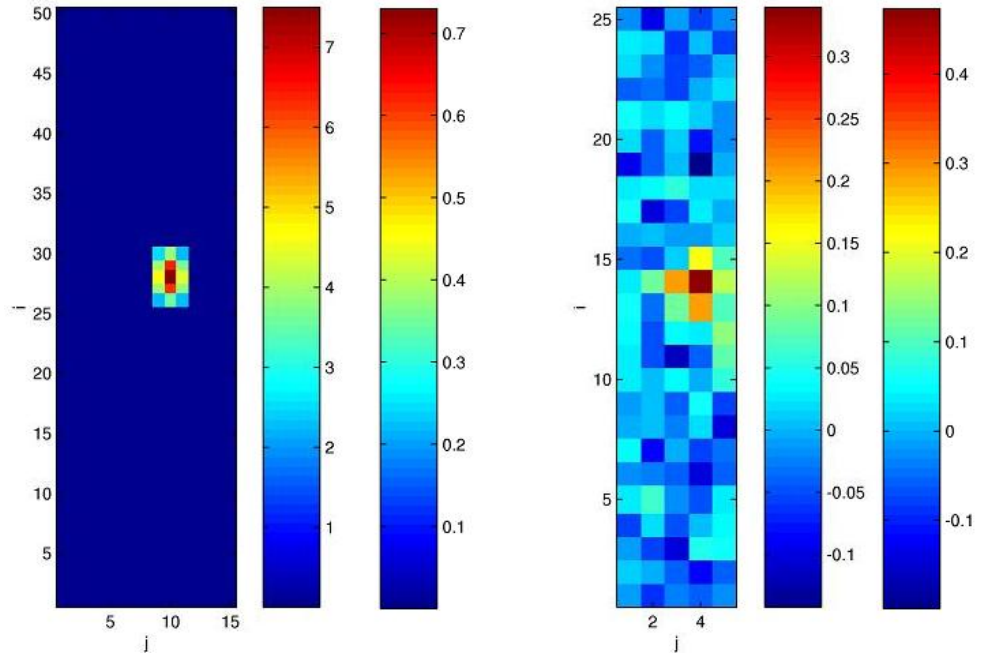


Figure 12: Target-performance comparison at subfault array: target slip (left) and actual slip (right) with original and normalised scale for an event of $M_W = 8.0$, noise level = 5cm/10cm

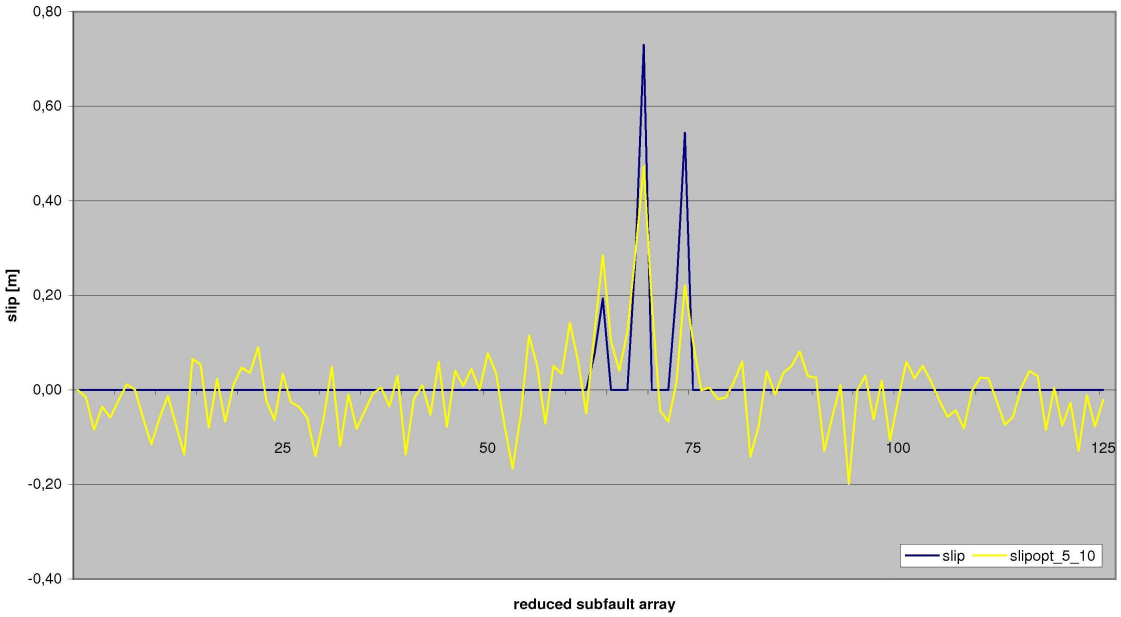


Figure 13: Target-performance comparison as graph: target slip normalised (blue) and actual slip normalised (yellow) for an event of $M_W = 8.0$, noise level = 5cm/10cm

In addition, the initial system (forward algorithm) is stabilised by a scalar factor $\alpha$ that corresponds to the chosen noise behaviour (e.g. noise level = 1cm/3cm, so $\alpha$ = 1cm) for $M_W = 7.0$ to 7.5 and 8.0. Therefore, multiply factor $\alpha$ by the identity matrix $I$ which has the size of $A$ and add this product obtained to the propagation matrix $A$ including the GREEN's function:

$$A_\alpha = A + \alpha \cdot I \tag{31}$$

Thus, the stabilised forward algorithm yields:

$$A_\alpha \cdot \vec{x} = \vec{b} \tag{32}$$

Reconstructed slip distributions of the stabilised initial system are pictured as well. Here, a comparison between reconstructions of non-stabilised and stabilised initial system is drawn. More figures on this can be found in the appendix A.1.2 and A.1.3.

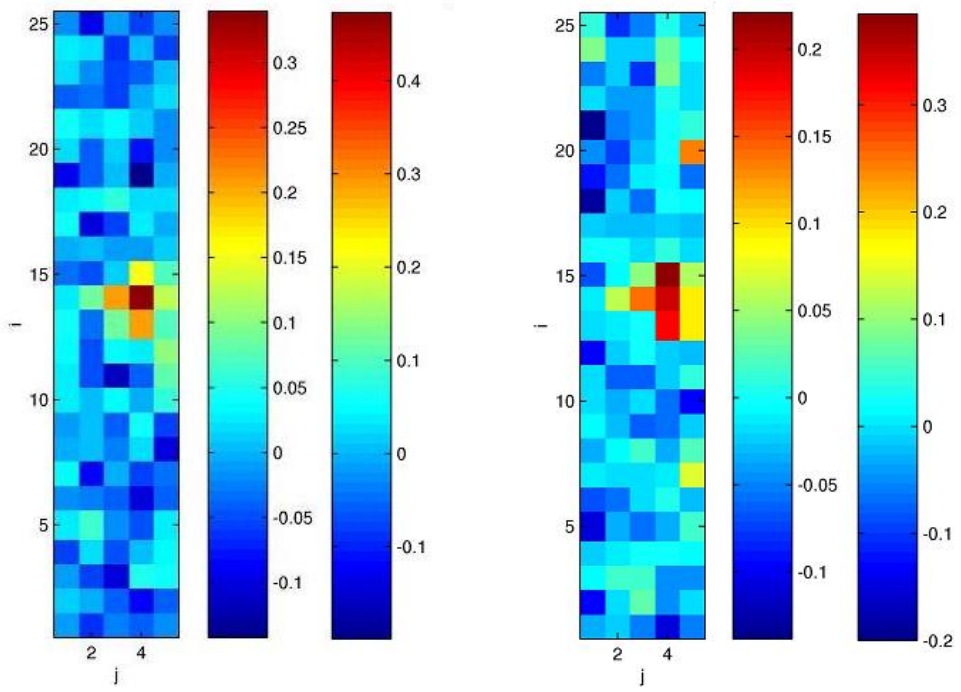


Figure 14: Comparison at subfault array: reconstruction of non-stabilised (left) and stabilised (right) initial system with original and normalised scale for an event of $M_W = 8.0$, noise level = 5cm/10cm

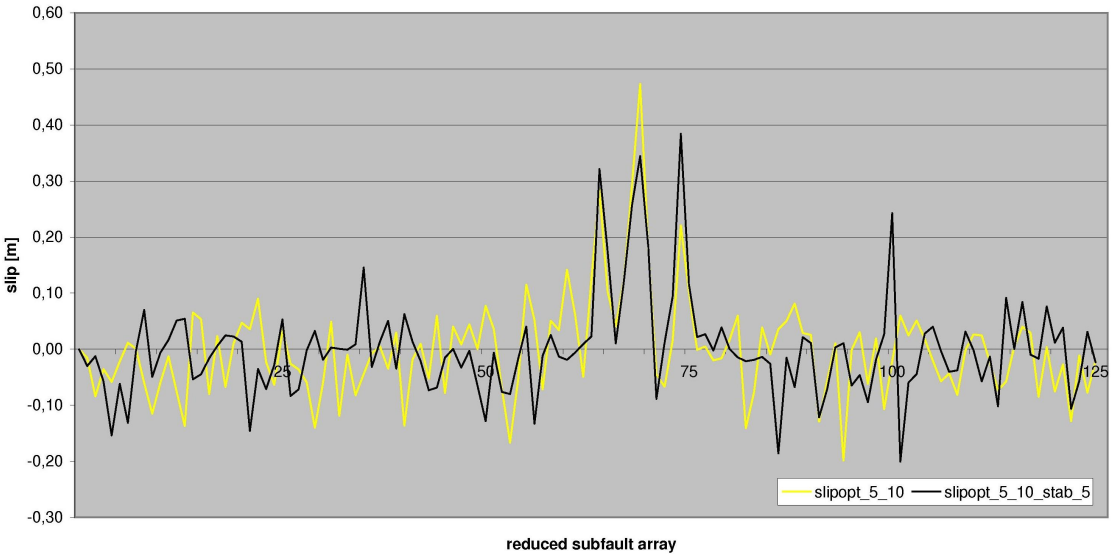


Figure 15: Comparison as graph: normalised reconstruction of non-stabilised (yellow) and stabilised (black) initial system for an event of $M_W = 8.0$, noise level = 5cm/10cm

Further on, maximum values of discrepancies between noiseless RuptGen generated GPS displacements (target) and noisy (see noise level), via MATLAB's `fminsearch` reconstructed GPS displacements (actual) are determined. So, compare figure no. 16 with figures of GPS displacements on SuGAr stations (see above and appendix).
This discrepancies concern the single deformation component (longitude, latitude, altitude) which has the maximum value. For this, see following figure and table.

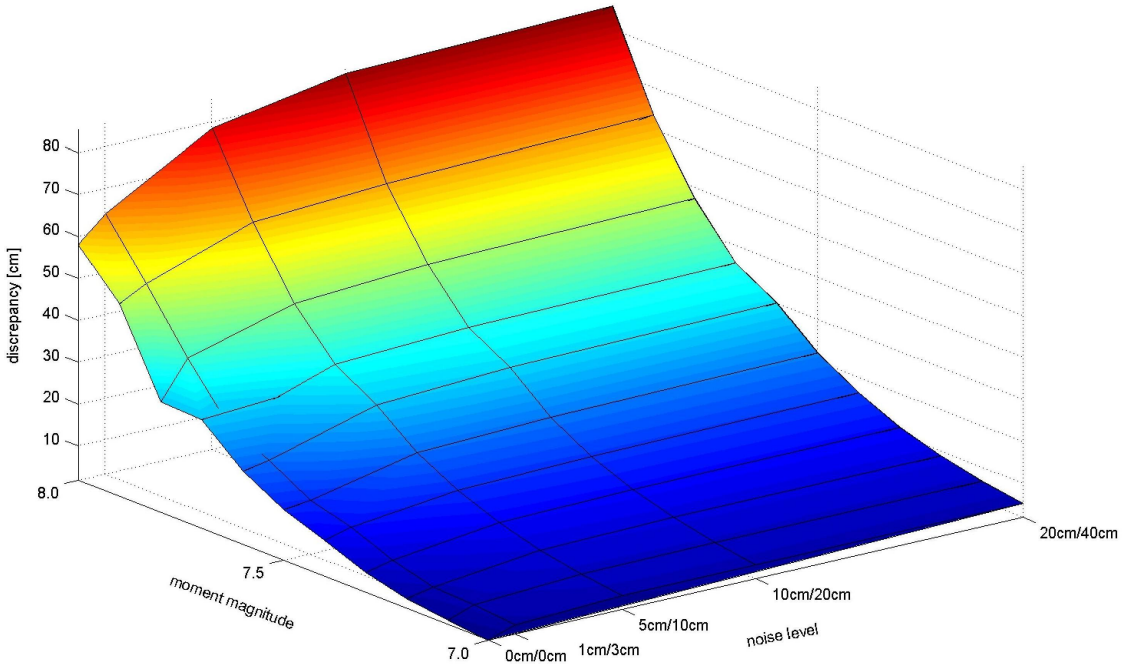


| | 7.0 | 7.1 | 7.2 | 7.3 | 7.4 | 7.5 | 7.6 | 7.7 | 7.8 | 7.9 | 8.0 |
|---|---|---|---|---|---|---|---|---|---|---|---|
| **0cm/0cm** | 1,9 | 2,9 | 4,2 | 6,7 | 10,5 | 14,1 | 19,4 | 27,9 | 28,2 | 47,8 | 58,0 |
| **1cm/3cm** | 4,1 | 5,1 | 5,6 | 8,1 | 12,2 | 14,8 | 20,4 | 25,1 | 37,2 | 51,2 | 64,0 |
| **5cm/10cm** | 5,2 | 6,6 | 8,4 | 11,2 | 15,0 | 20,3 | 27,8 | 33,6 | 44,3 | 60,0 | 78,4 |
| **10cm/20cm** | 5,3 | 6,8 | 8,9 | 11,8 | 15,8 | 21,3 | 29,5 | 35,1 | 46,3 | 61,8 | 84,1 |
| **20cm/40cm** | 5,3 | 6,7 | 9,0 | 12,0 | 16,3 | 22,0 | 30,2 | 35,9 | 47,5 | 63,4 | 85,5 |

Figure 16: Maximum values of discrepancies concerning single deformation component, for events of 7.0 $\leq M_W \leq$ 8.0, noiseless and above defined noise levels

Figure no. 17 shows a trend of described discrepancies for the moment magnitude interval from 6.0 to 8.0. Here, EUCLIDean norm regarding all deformation components is employed. Moreover, this trend splitted into geographical position (longitude, latitude) and altitude, can be found in the appendix A.1.4.

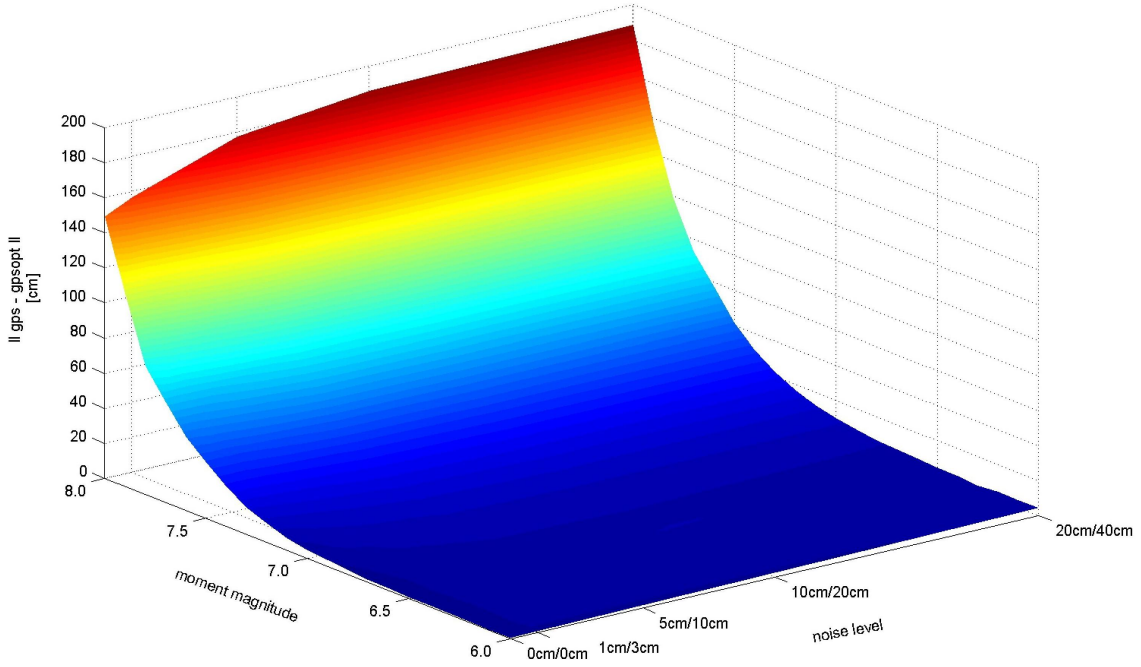


Figure 17: EUCLIDean norm of target (RuptGen generated) and actual (`fminsearch` reconstructed) GPS displacements concerning all deformation components for events of $6.0 \leq M_W \leq 8.0$

## 5.2 Using other inverse approaches

Certainly, the initial position is the same as using MATLAB's `fminsearch`: noise altered RuptGen computed GPS displacements.

The two other inverse approaches that have been already introduced in this work (see subsection 4.2.3), are implemented in MATLAB as well. Reduced QR decomposition of transposed system ("QR_min") and iterative approach by surrogate functionals ("sparse") are employed separately as well as combined ("QR_min_sparse"), see MATLAB code.

Whereas solving the cost function (see equation no. 6) by MATLAB's `fminsearch` uses a limited subfault array, here, the full subfault array can be applied. That is applicable because solving this two approaches is not very time-consuming.

Within this analysis, only selected examples with respect to moment magnitude and noise level are shown. In particular, the mentioned approaches are applied to magnitudes of 7.0, 7.5, 8.0, noiseless cases as well as noise level of 1cm/3cm. A comparison between the approaches "QR_min", "sparse" and "QR_min_sparse" applied to noiseless and noisy (1cm/3cm) events of $M_W = 8.0$ is drawn, as can be found in figures 18 to 20. Other figures on this can be taken from the appendix A.2.1.

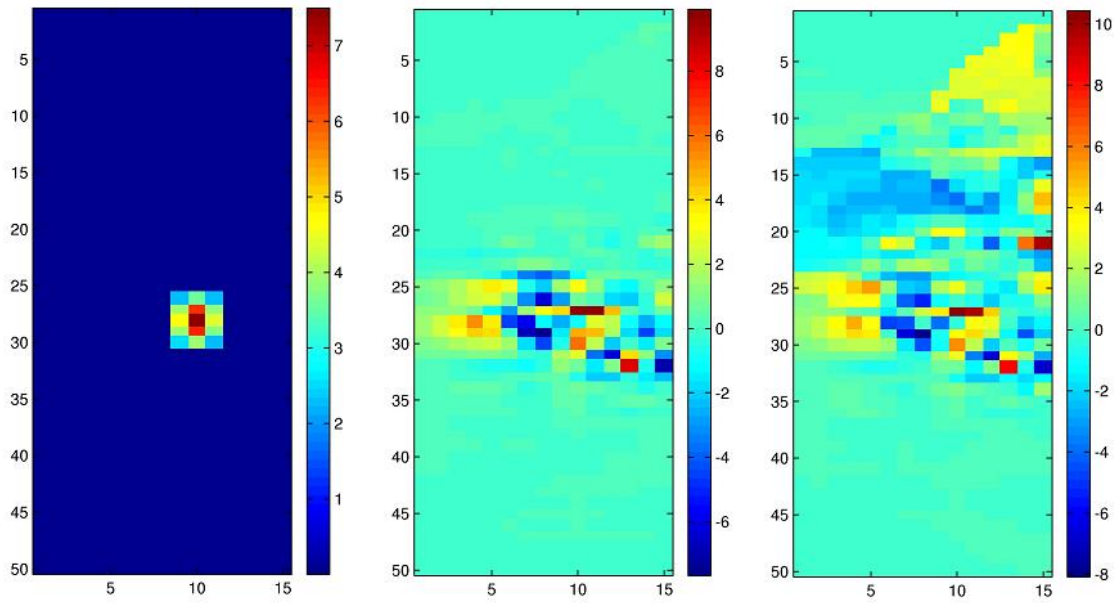


Figure 18: QR decomposition of transposed system "QR_min": target slip (left), noiseless reconstruction (middle) and noisy reconstruction (right)

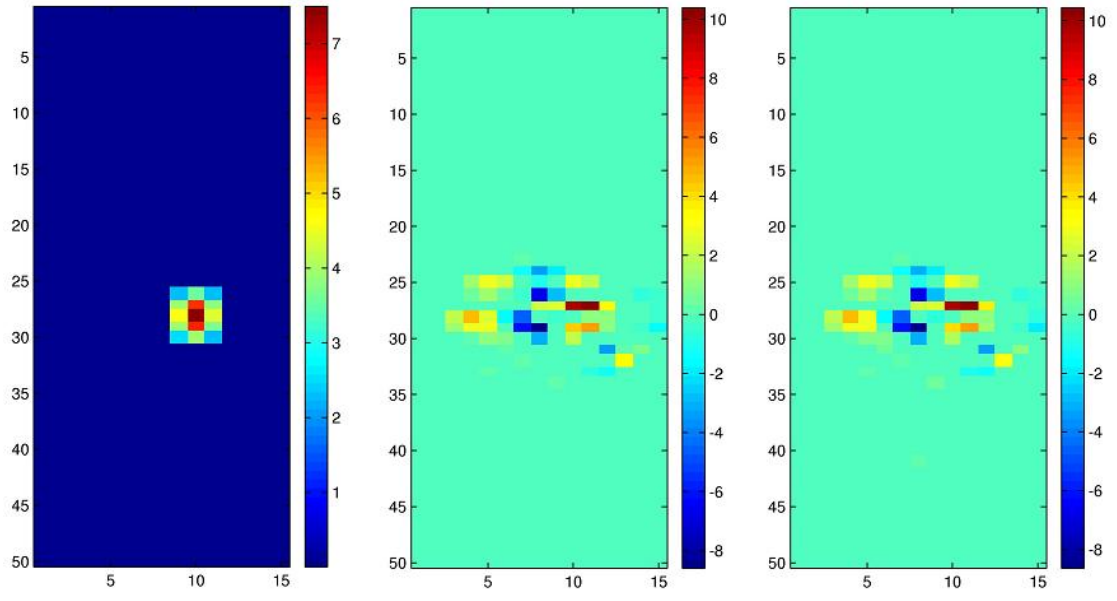


Figure 19: Iterative approach by surrogate functionals "sparse": target slip (left), noiseless reconstruction (middle) and noisy reconstruction (right)

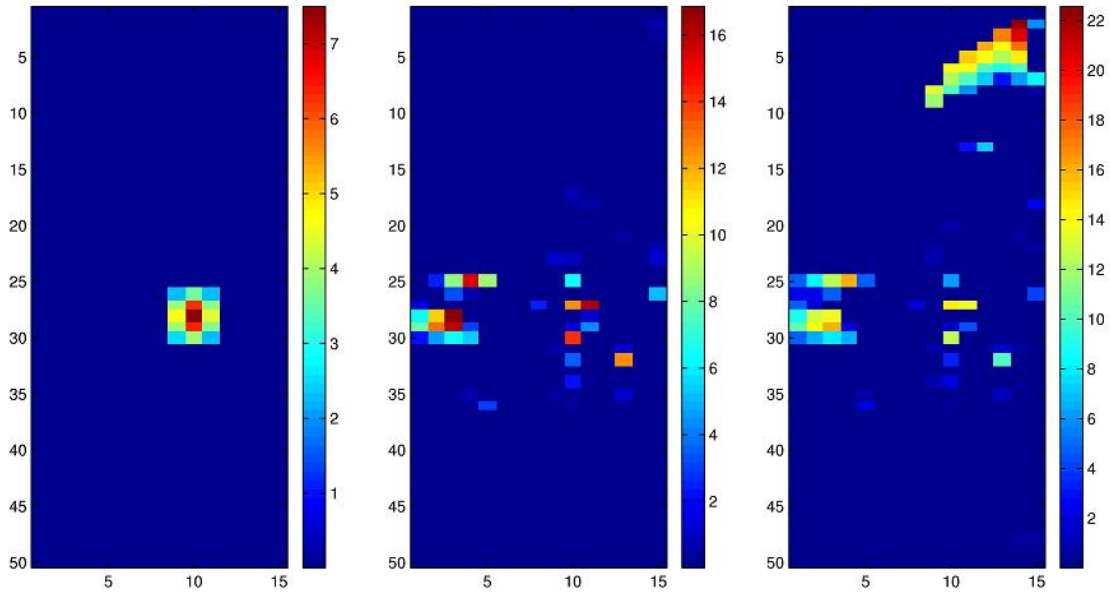


Figure 20: QR decomposition of transposed system combined with iterative approach by surrogate functionals "QR_min_sparse": target slip (left), noiseless reconstruction (middle) and noisy reconstruction (right)

Note, reconstructions which employ iterative approach by surrogate functionals, depend on its chosen parameters $(t, p, C)$, see MATLAB code.

# 6 Results

First of all, it can be asserted that a huge difference of size between the results for the target slip distribution and slip distribution of the inversion algorithm using `fminsearch`, exists. Because of this, slip needs to be normalised to become more comparable.

However, noiseless RuptGen generated slip compared to noisy `fminsearch` reconstructed slip yields: slip distributions of earthquakes with $7.0 \leq M_W \leq 7.2$ are very sensitive regarding noise. Here, the maximum allowable noise level of GPS measurements amounts 1cm/3cm only, to obtain a slip distribution which can be regarded as sufficiently accurate. In case of $M_W = 7.3$, noiseless input is reconstructed at an unexpected location and hence, the noise level that is allowed exclusively, amounts 1cm/3cm. If the moment magnitude is 7.4, a similar behaviour as in the previous case can be found. But in this case, also noise level 5cm/10cm yields allowable slip distribution. If $M_W$ is 7.5, same noise as in the case of 7.4 is acceptable. Furthermore, moment magnitude of 7.6 allows following noise levels on the GPS stations: 1cm/3cm, 5cm/10cm and 10cm/20cm. From $M_W = 7.7$ up to 8.0 which is the greatest event considered here, even noise level 20cm/40cm is allowed. Note that there are noiseless cases ($M_W \geq 7.3$) as well as cases of adding a little noise of 1cm/3cm ($M_W \geq 7.9$), whose reconstructed slip distributions are not sufficiently accurate.

In addition, a group whose slip distributions are highly sensitive ($6.0 \leq M_W \leq 6.9$), is considered. Here, it can be asserted that events of $M_W \leq 6.7$ do not allow any noisy GPS measurements. Only in cases of a moment magnitude of 6.8 and 6.9, slip distributions allow noise level 1cm/3cm.

Moreover, reconstructions of stabilised initial system yield more or less similar results, comparing to reconstructions without stabilisation. Summing up, the larger the magnitude is, the larger the accepted noise is. Therefore, see extensive documentation in appendix.

Regarding surface deformation, it can be asserted that there are cases, in which GPS displacements that are not actually recorded (forward algorithm), are reconstructed on respective SuGAr stations. This reconstruction error is especially noticeable in noiseless cases. Because of adding noise at all GPS stations, independent of actually GPS displacements, reconstruction of noise is simulated.

Further on, discrepancies between RuptGen generated GPS displacements (target) and

their reconstructions (actual) exist. Even in cases in which reconstructed slip distribution is sufficiently accurate, mentioned discrepancies concerning single deformation components are larger than respective noise level. In general, the larger the moment magnitude and noise level are, the larger the discrepancies are. The discrepancies increase according to noise nearly linear and according to moment magnitude as an exponential function. Maximum values of discrepancies can be found on the GPS stations which are next to the epicentre, especially regarding altitude.

Altogether, this sensitivity analysis concerning basic cases of slip distribution shows that the GPS inversion technique which has been published by HOECHNER et al. (2008), is an adequate approach to reconstruct earthquake parameters (slip) with restriction of allowed noise levels.

QR decomposition of the transposed initial system ("QR_min") yields blurred slip distributions, regardless of applied moment magnitude and noise level, because matrix $R$ is bad conditioned (almost singular) and thus not accurately invertible. But the maximum value of slip can be found at expected location concerning noiseless cases. This approach is very sensitive to noise: adding little noise (1cm/3cm) alters the reconstruction significantly.

Iterative approach by surrogate functionals ("sparse") yields reasonable but not convincing results. This approach is relatively robust considering adding noise of 1cm/3cm.

The combination of both shows a result that is not acceptable. Hence, adding noise does not need to be considered.

Beside the grade of quality of reconstruction, calculation period is of equal importance. The calculation period of the mentioned approaches varies highly: while solving the complex cost function (inversion algorithm) is the most time-consuming one, the iterative approach by surrogate functionals ("sparse") needs about a third of that time and the combined approach ("QR_min_sparse") a seventh part. QR decomposition of the transposed initial system ("QR_min") can be considered as solved instantly.

# 7 Conclusions and Outlook

The goal of this thesis set initially, was to upgrade the inversion technique which is presently used, but has been modified for verification, because of the complexity of this ill-posed inverse problem on the one hand and of the available time frame on the other hand.

As conclusion of this work, the inversion technique by HOECHNER et al. (2008) offers sufficiently accurate earthquake parameter reconstructions with restriction of allowed noise levels, but can still be enhanced as well as other adequate approaches can be employed. As seen in the results of this analysis, the present ill-posed inverse problem is not trivial: high sensitivity regarding adding noise on the one hand, and regarding choice of the applied inverse approach on the other hand exists. Following up this sensitivity analysis, more complex scenarios (multi rupture scenarios, including strike slip) can be applied.

Even with a perfectly working warning system, a natural occurrence such as the Great Sumatra-Andaman earthquake and its resulting tsunami of 2004 can not be prevented and such catastrophes will continue to cause victims. However, with an Early Warning System as GITEWS, the impact of such a natural disaster can certainly be minimised.

I hope that I could make a little contribution to the project GITEWS and therefore to tsunami early warning.

# List of Figures

# A Appendix

## A.1 Figures - Using MATLAB's `fminsearch`

### A.1.1 GPS displacements on SuGAr stations

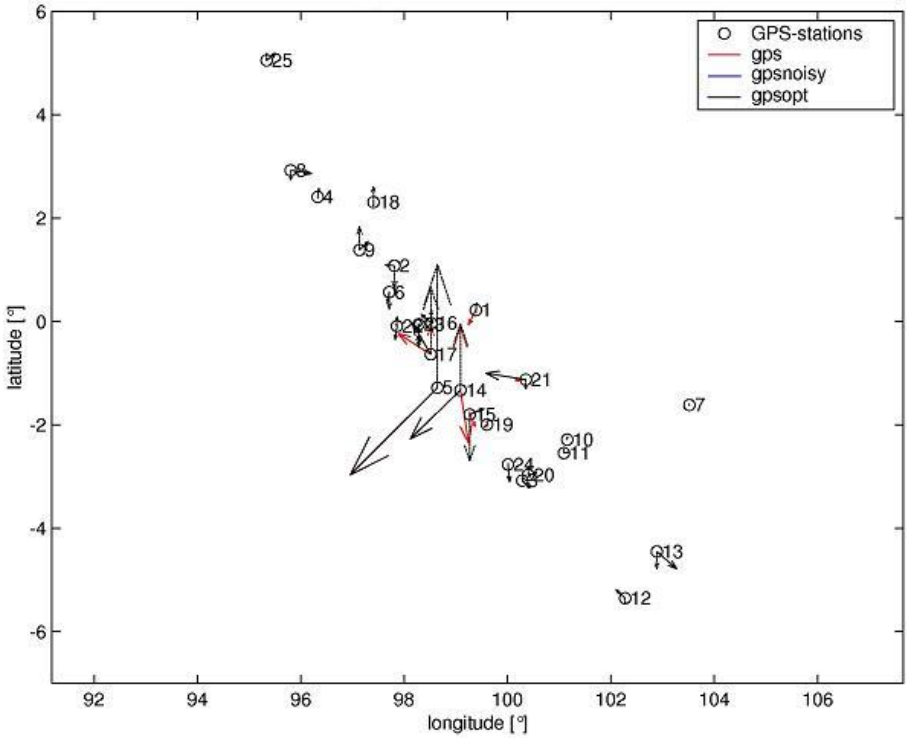


Figure A1: $M_W = 7.0$, noiseless

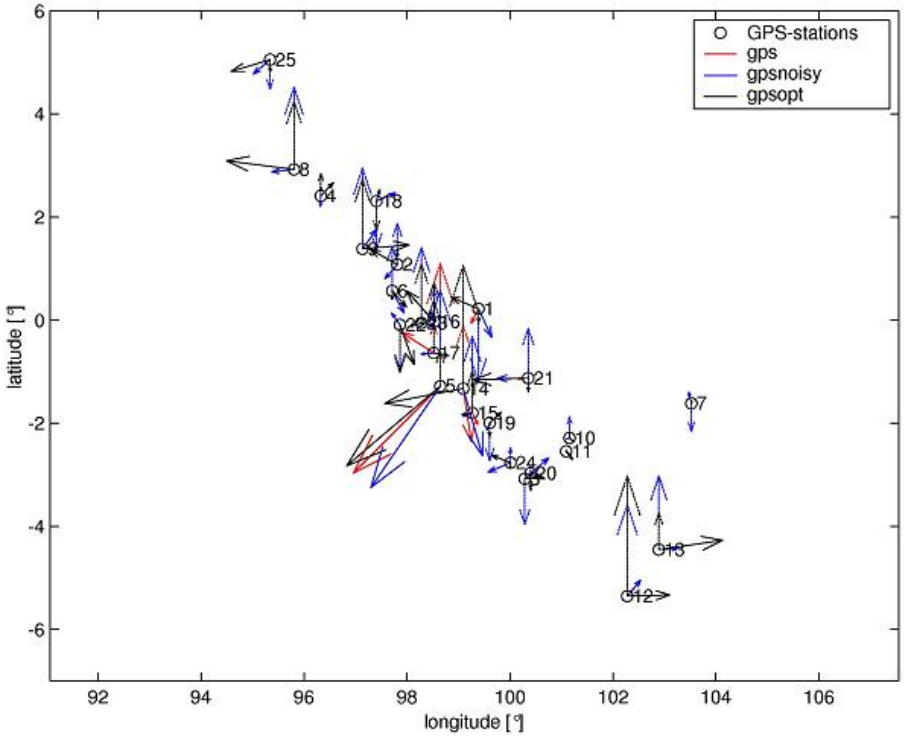


Figure A2: $M_W = 7.0$, noise level: 1cm/3cm

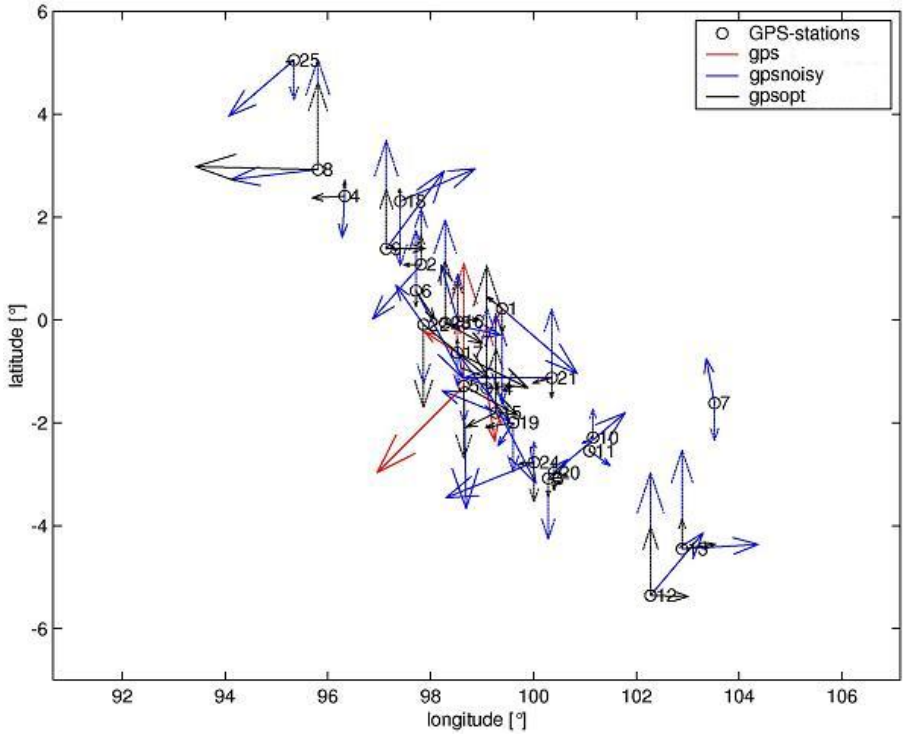


Figure A3: $M_W = 7.0$, noise level: 5cm/10cm

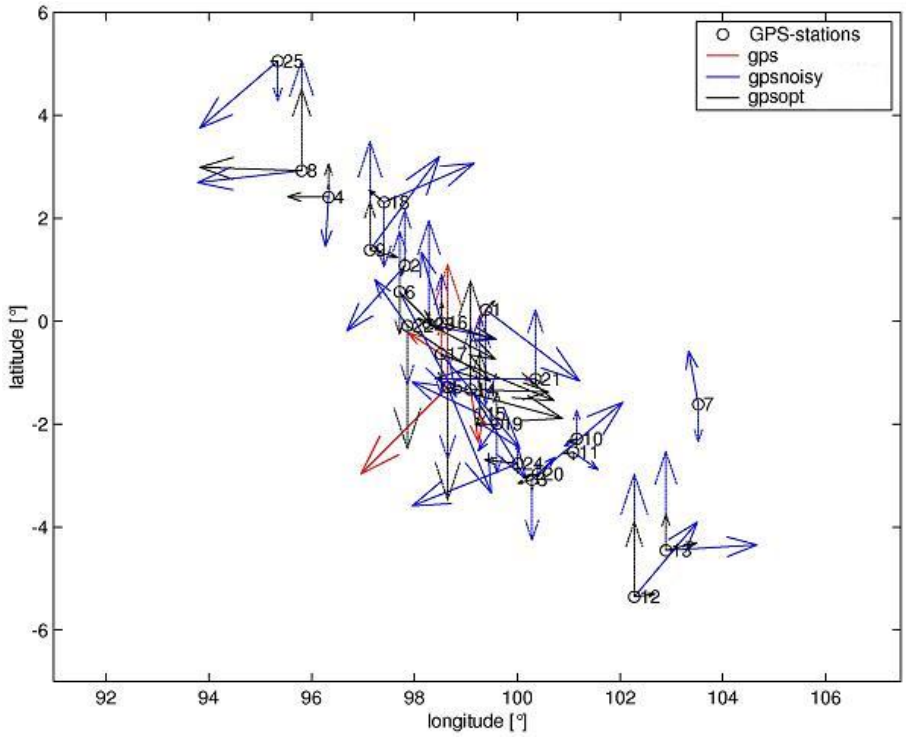


Figure A4: $M_W = 7.0$, noise level: 10cm/20cm

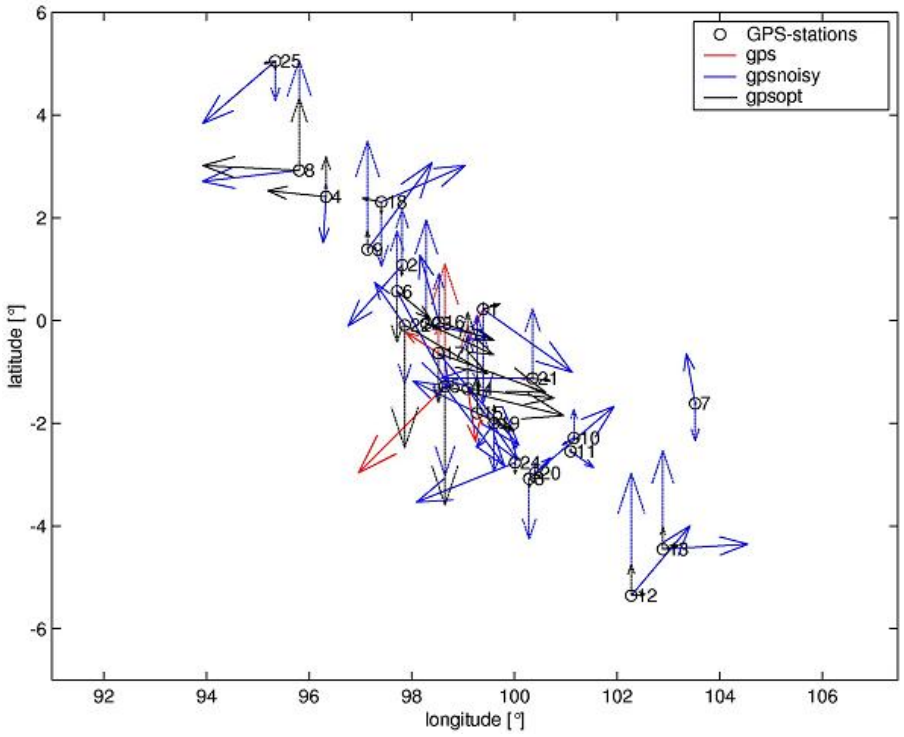


Figure A5: $M_W = 7.0$, noise level: 20cm/40cm

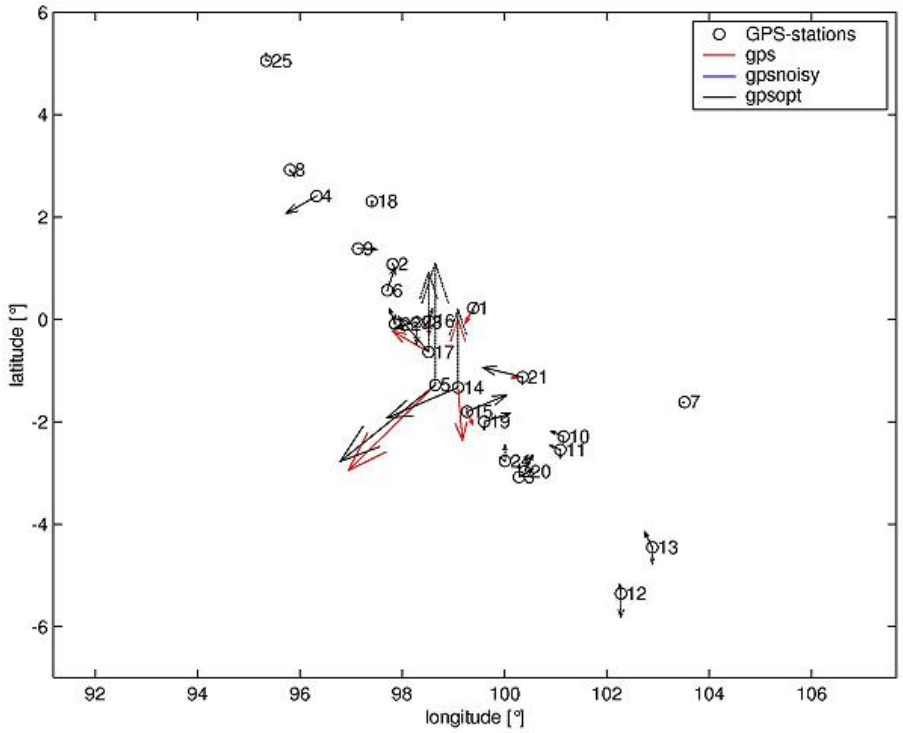


Figure A6: $M_W = 7.1$, noiseless

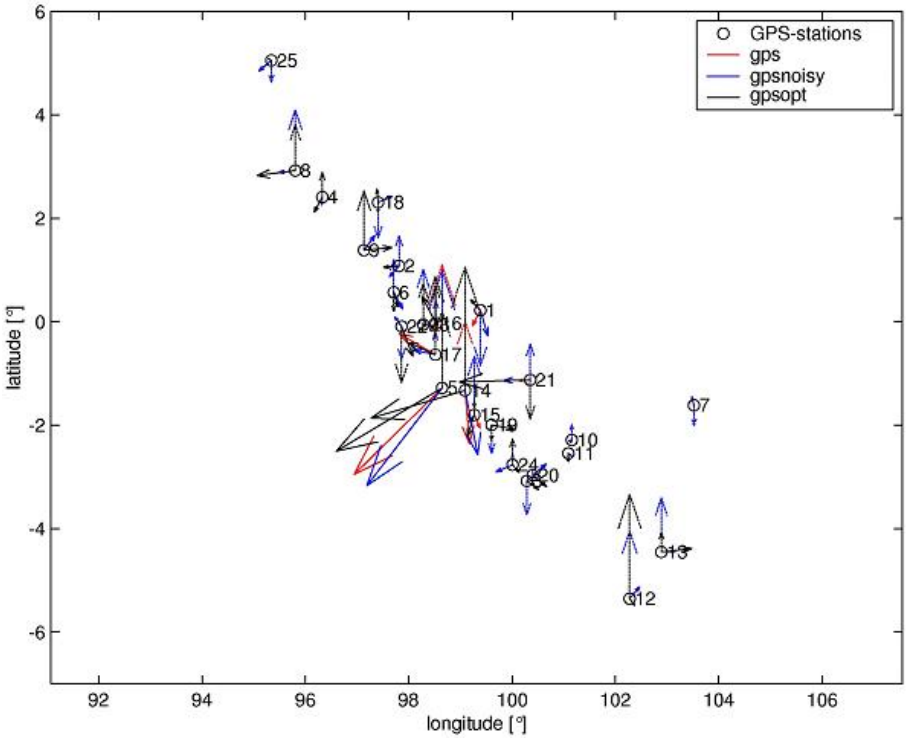


Figure A7: $M_W = 7.1$, noise level: 1cm/3cm

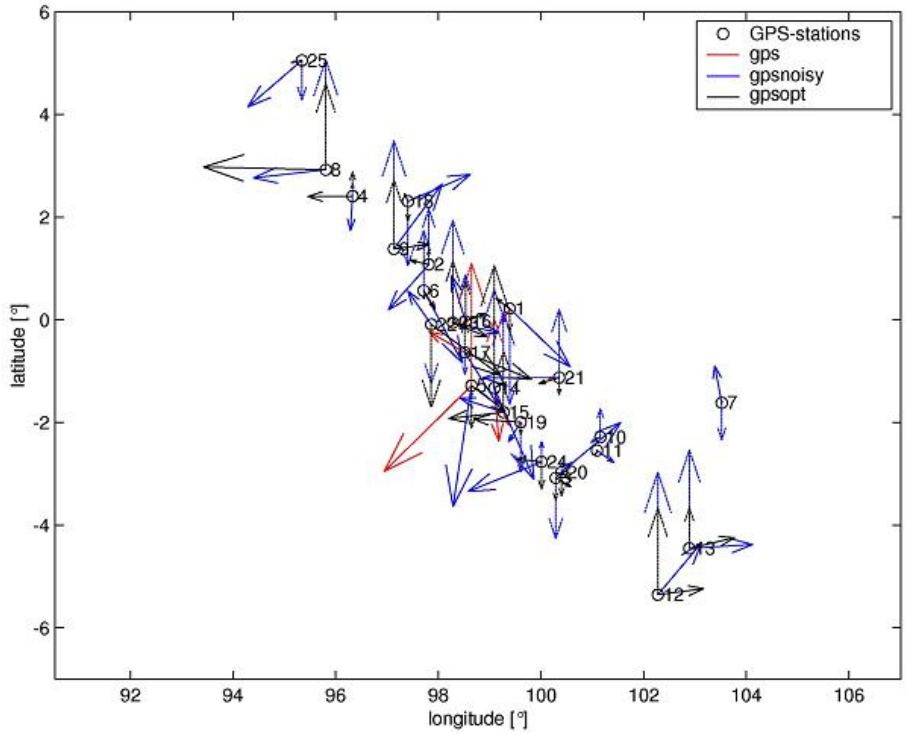


Figure A8: $M_W = 7.1$, noise level: 5cm/10cm

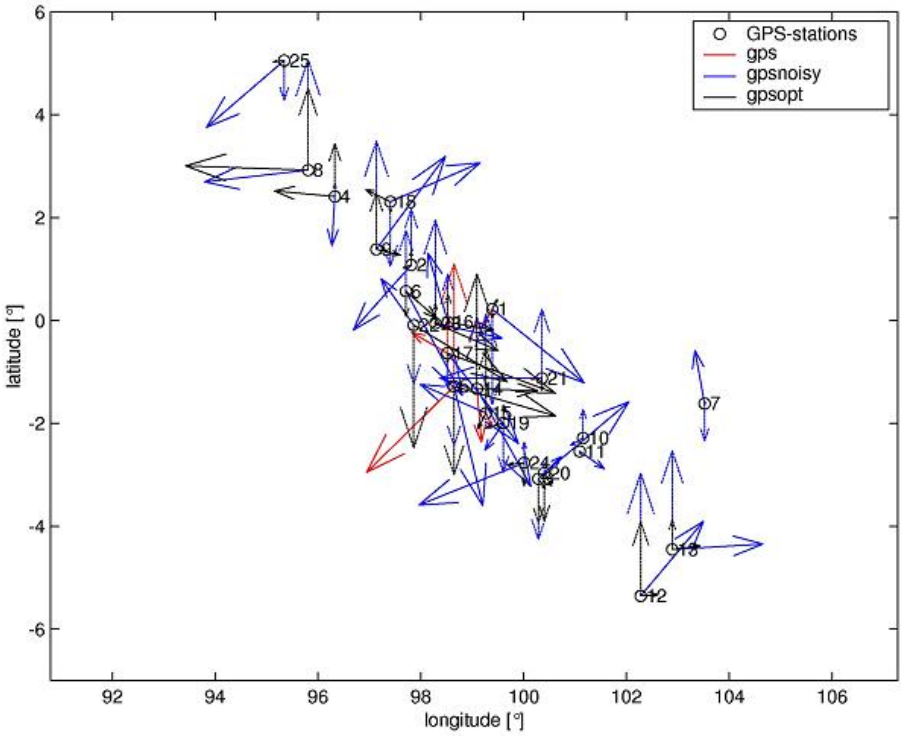


Figure A9: $M_W = 7.1$, noise level: 10cm/20cm

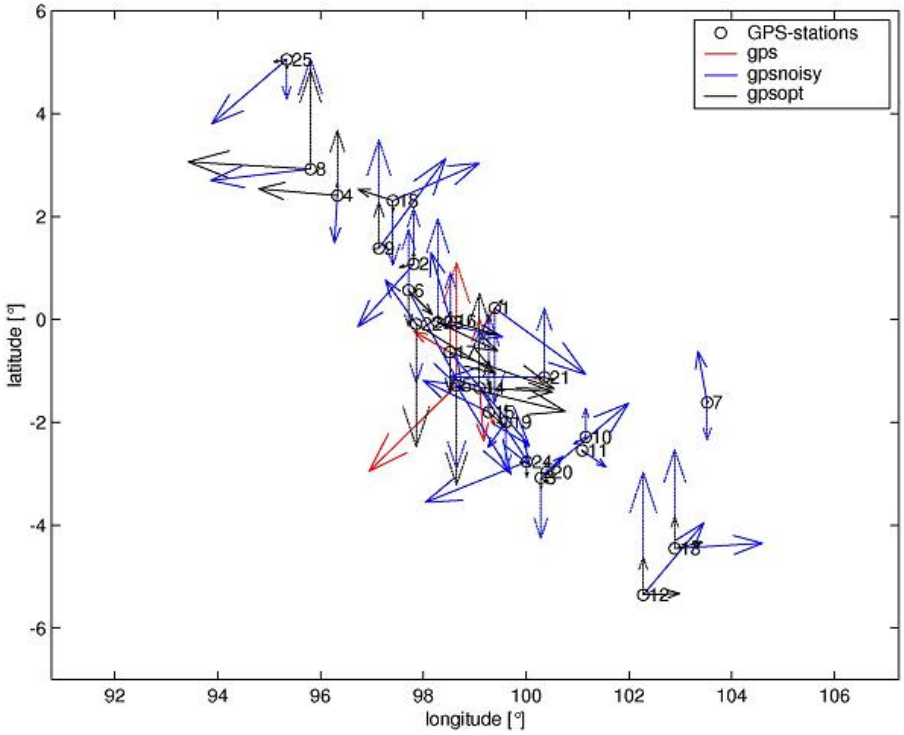


Figure A10: $M_W = 7.1$, noise level: 20cm/40cm

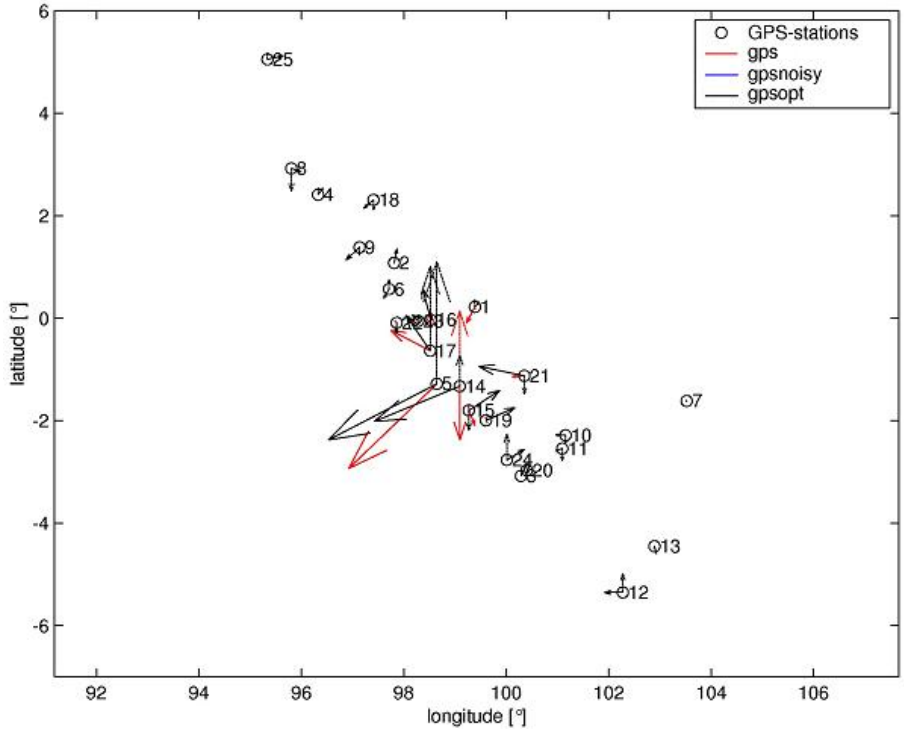


Figure A11: $M_W = 7.2$, noiseless

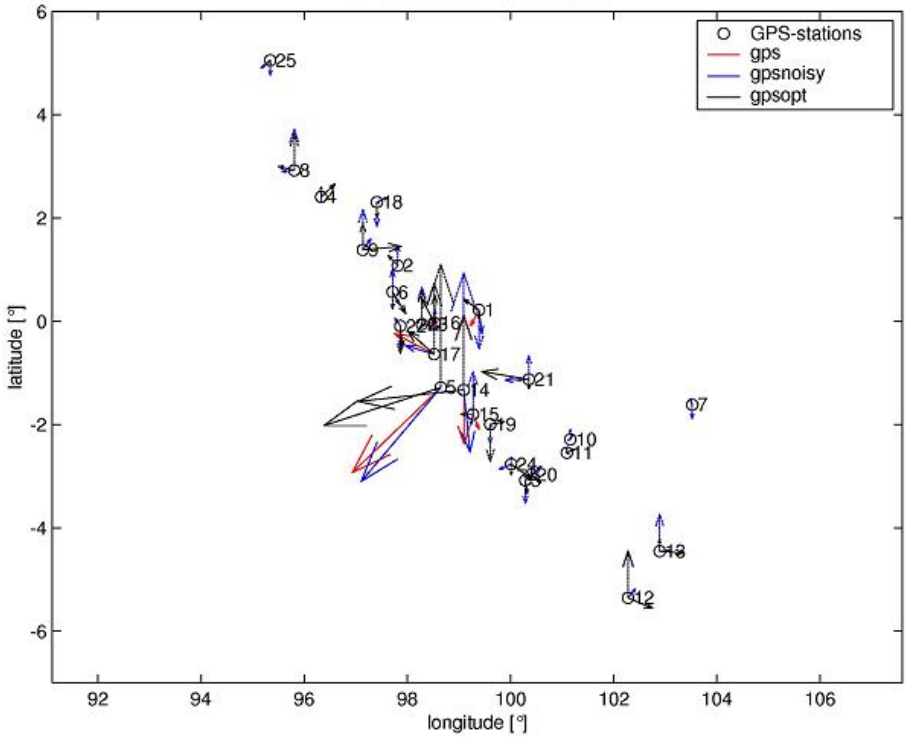


Figure A12: $M_W = 7.2$, noise level: 1cm/3cm

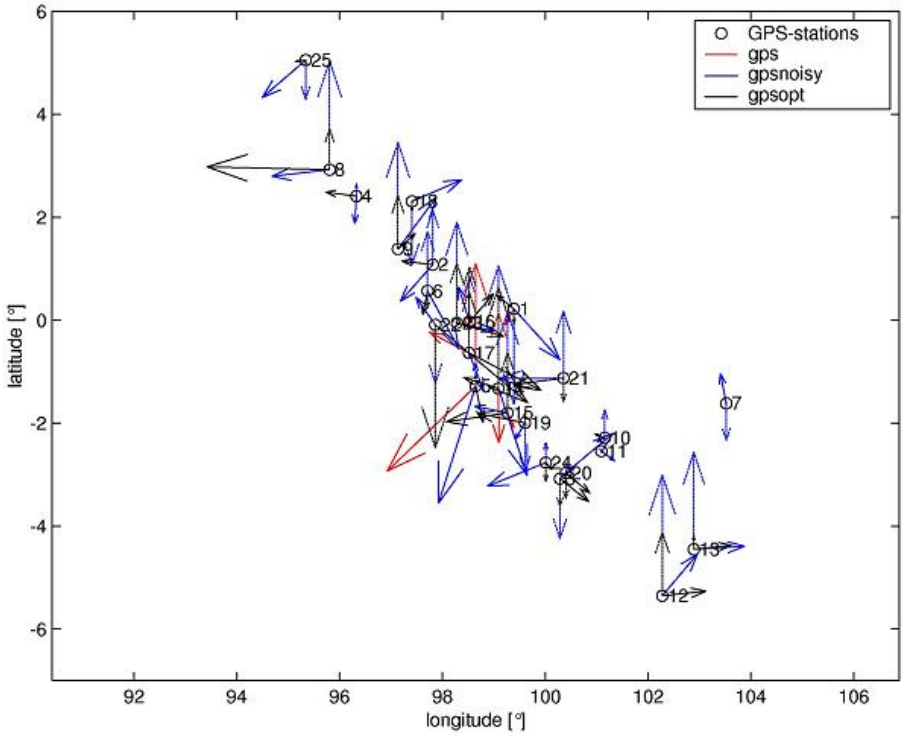


Figure A13: $M_W = 7.2$, noise level: 5cm/10cm

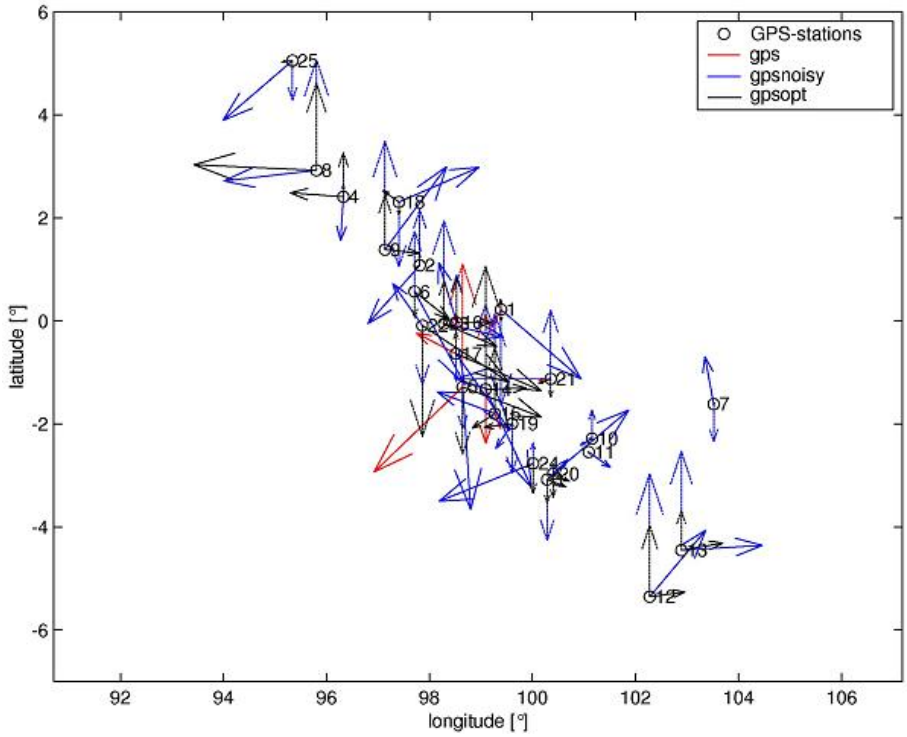


Figure A14: $M_W = 7.2$, noise level: 10cm/20cm

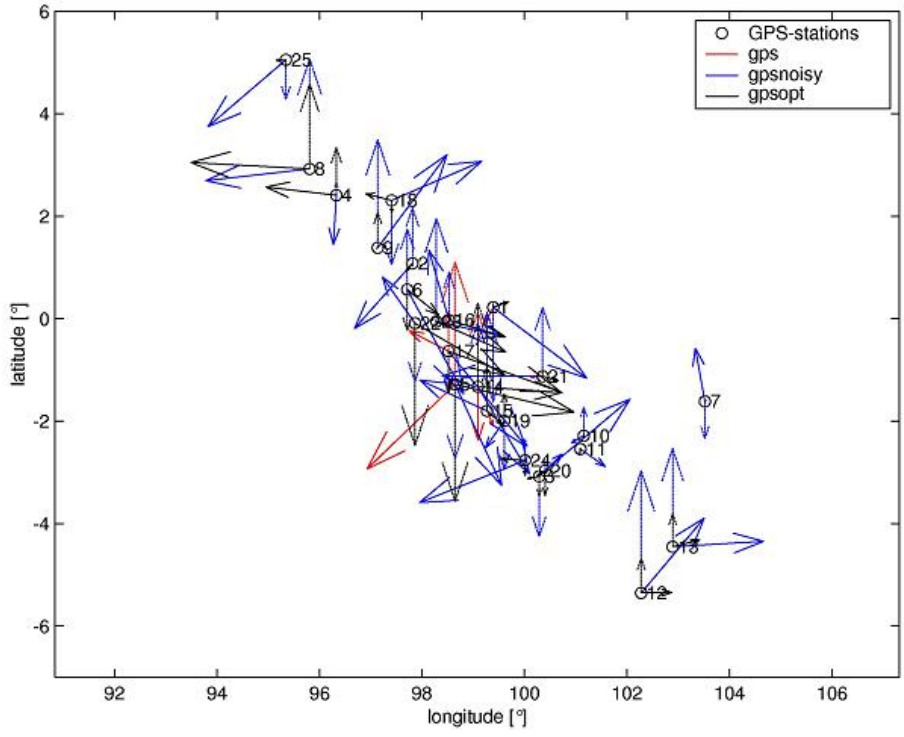


Figure A15: $M_W = 7.2$, noise level: 20cm/40cm

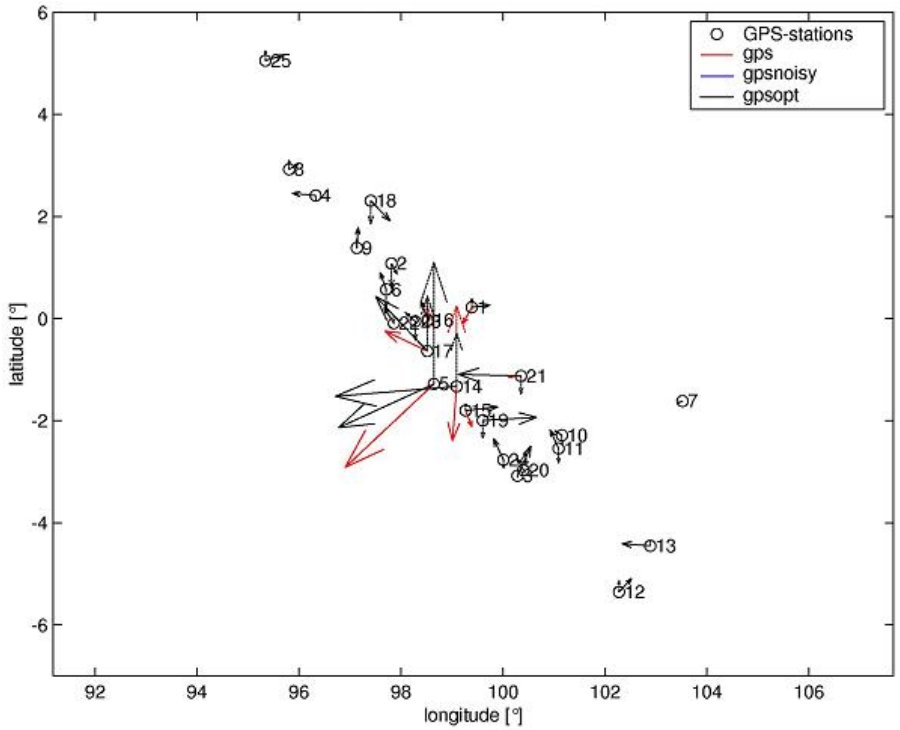


Figure A16: $M_W = 7.3$, noiseless

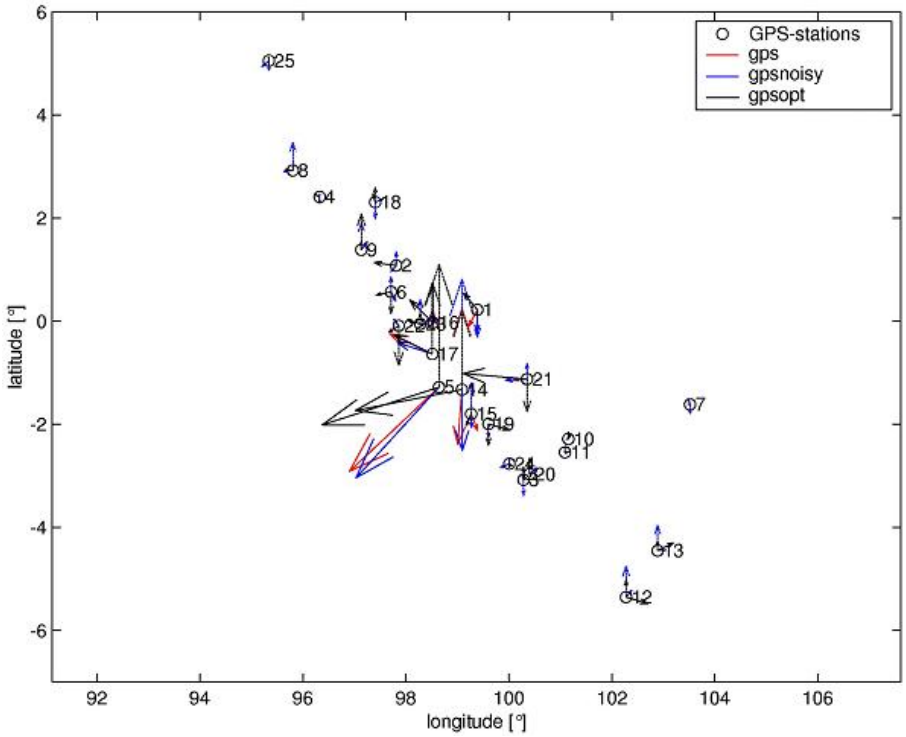


Figure A17: $M_W = 7.3$, noise level: 1cm/3cm

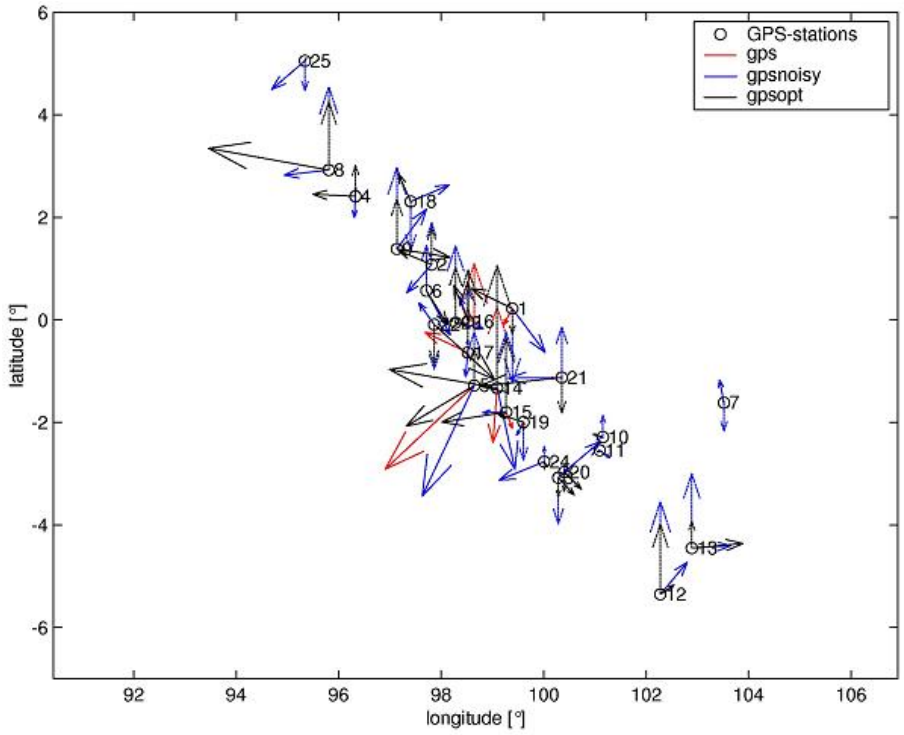


Figure A18: $M_W = 7.3$, noise level: 5cm/10cm

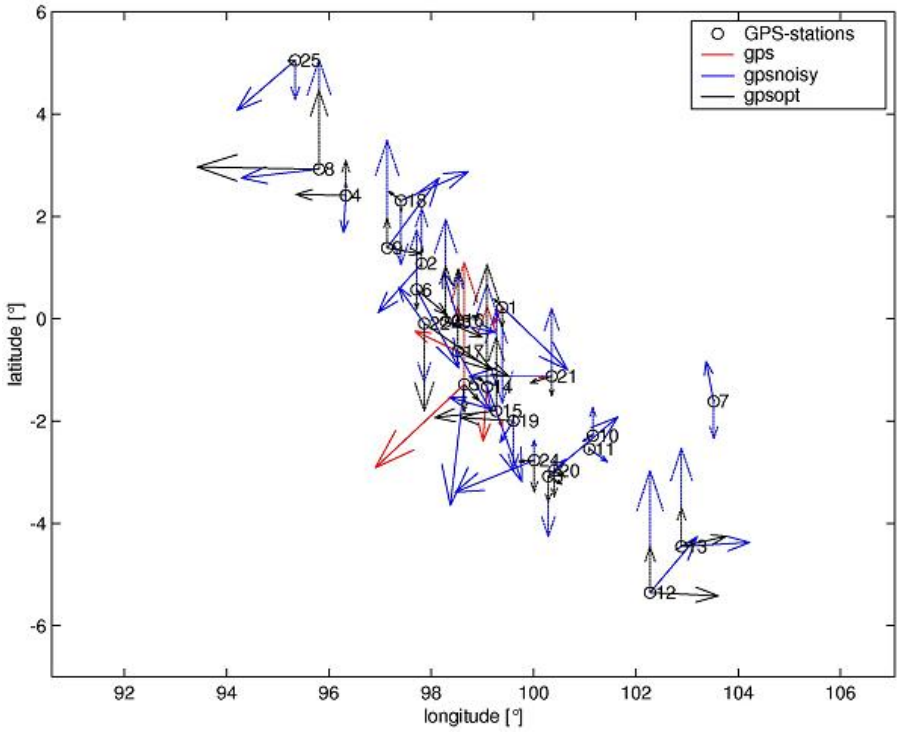


Figure A19: $M_W = 7.3$, noise level: 10cm/20cm

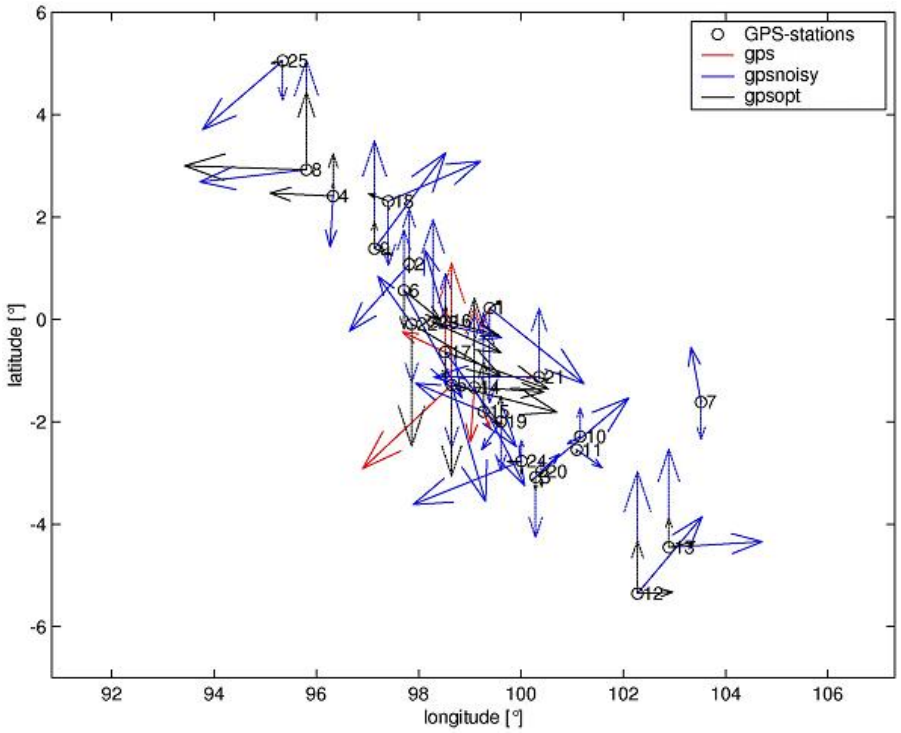


Figure A20: $M_W = 7.3$, noise level: 20cm/40cm

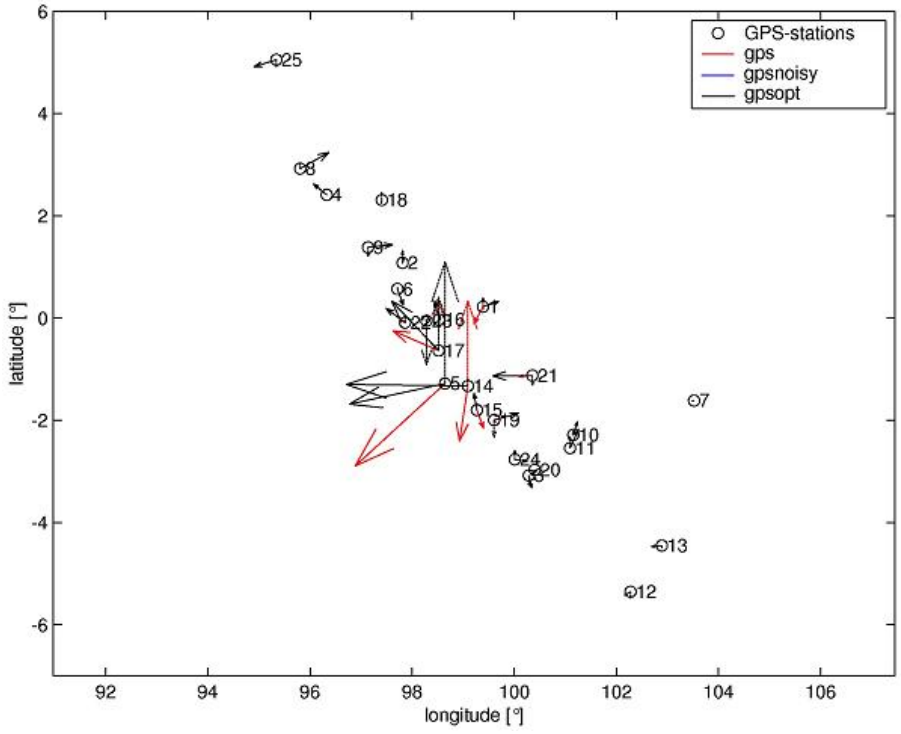


Figure A21: $M_W = 7.4$, noiseless

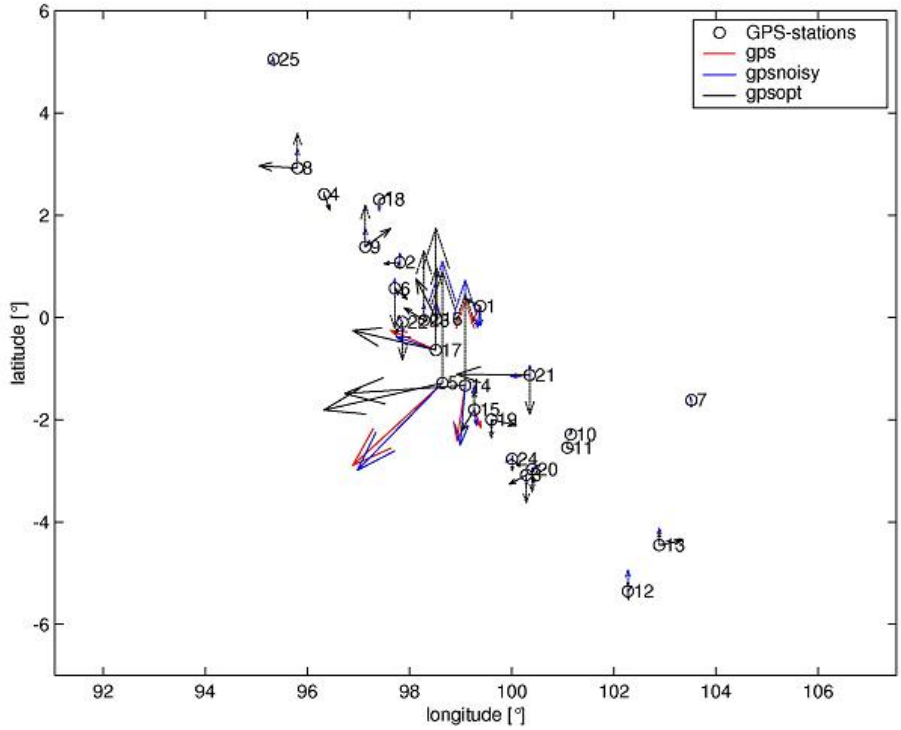


Figure A22: $M_W = 7.4$, noise level: 1cm/3cm

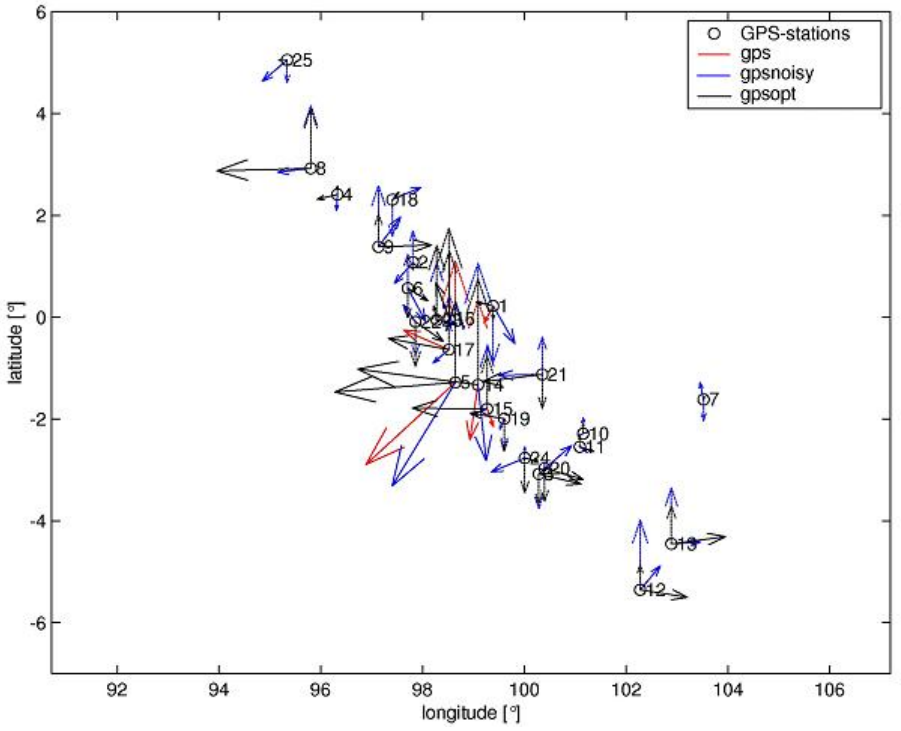


Figure A23: $M_W = 7.4$, noise level: 5cm/10cm

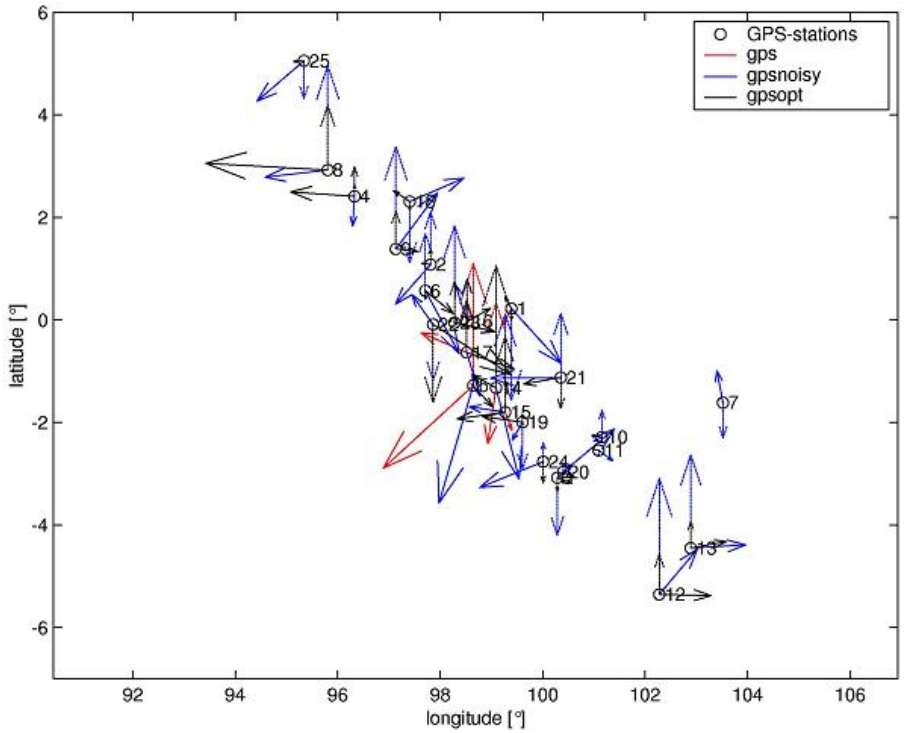


Figure A24: $M_W = 7.4$, noise level: 10cm/20cm

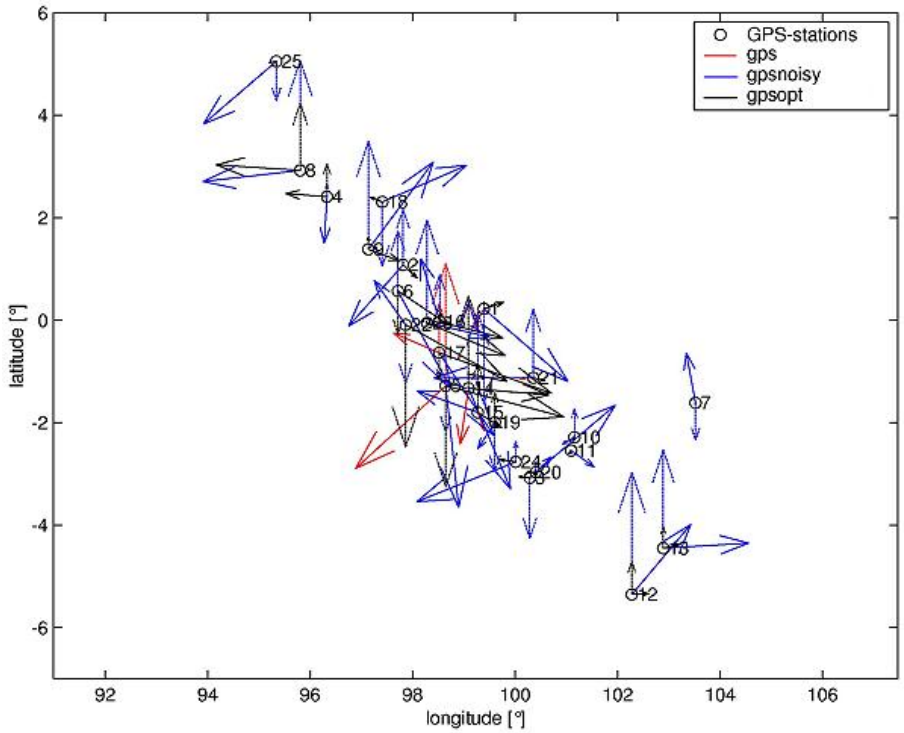


Figure A25: $M_W = 7.4$, noise level: 20cm/40cm

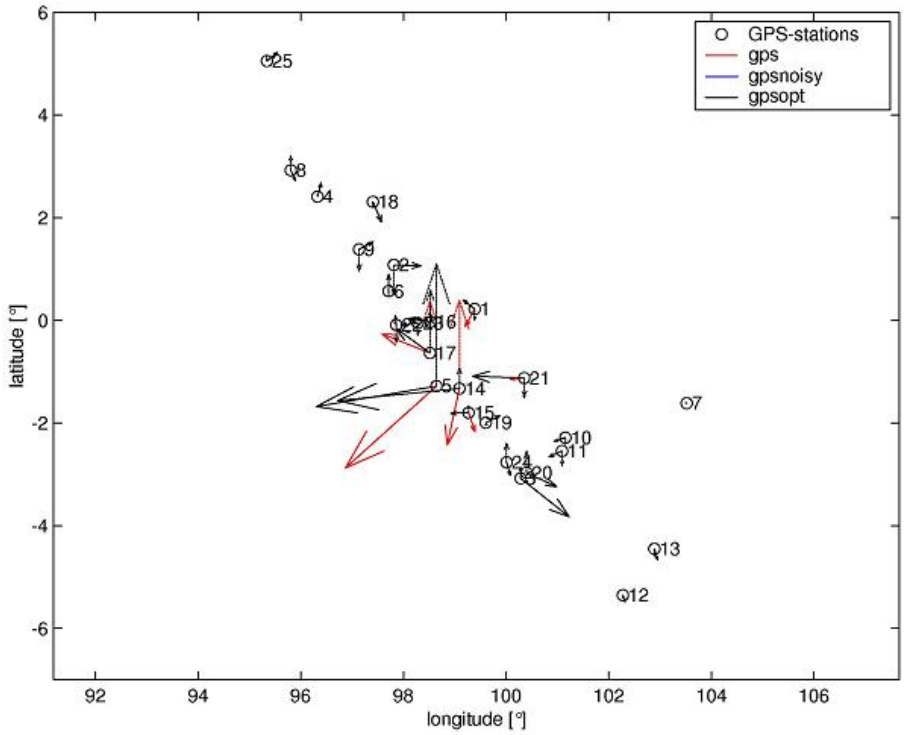


Figure A26: $M_W = 7.5$, noiseless

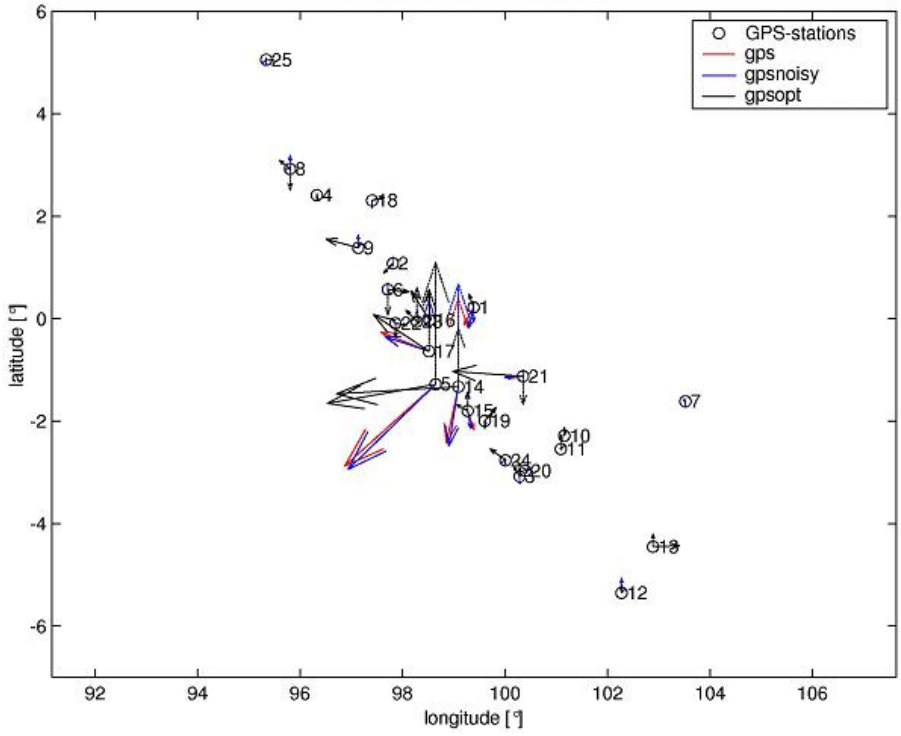


Figure A27: $M_W = 7.5$, noise level: 1cm/3cm

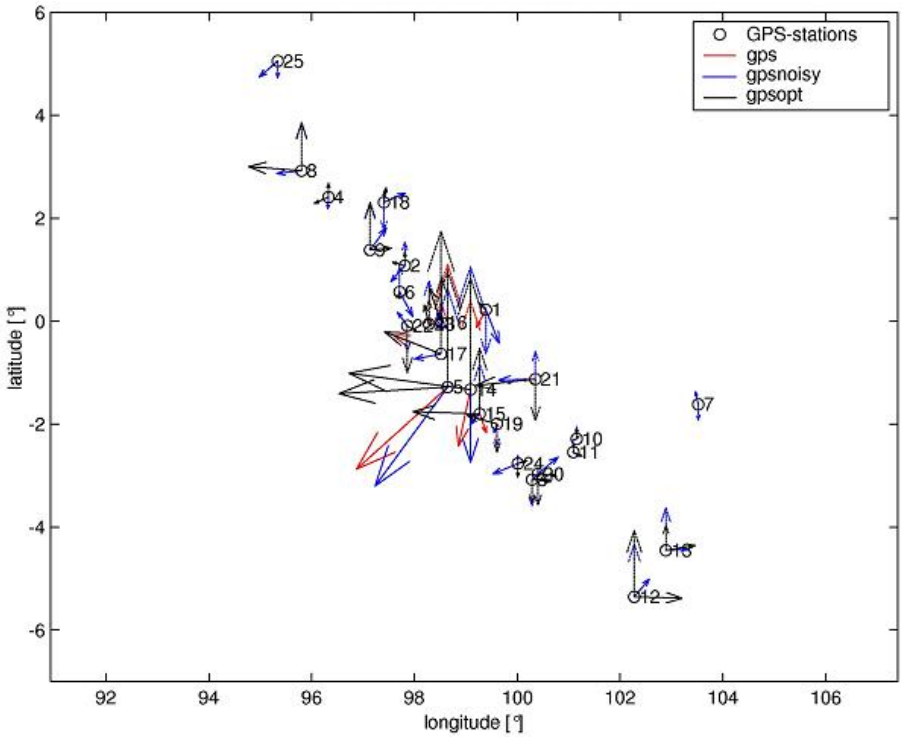


Figure A28: $M_W = 7.5$, noise level: 5cm/10cm

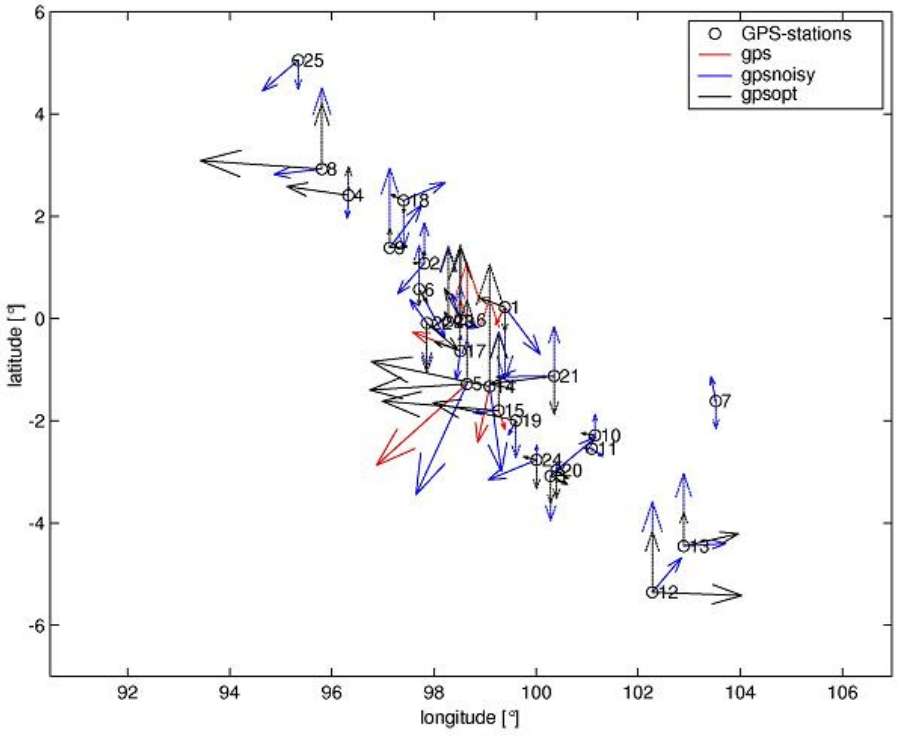


Figure A29: $M_W = 7.5$, noise level: 10cm/20cm

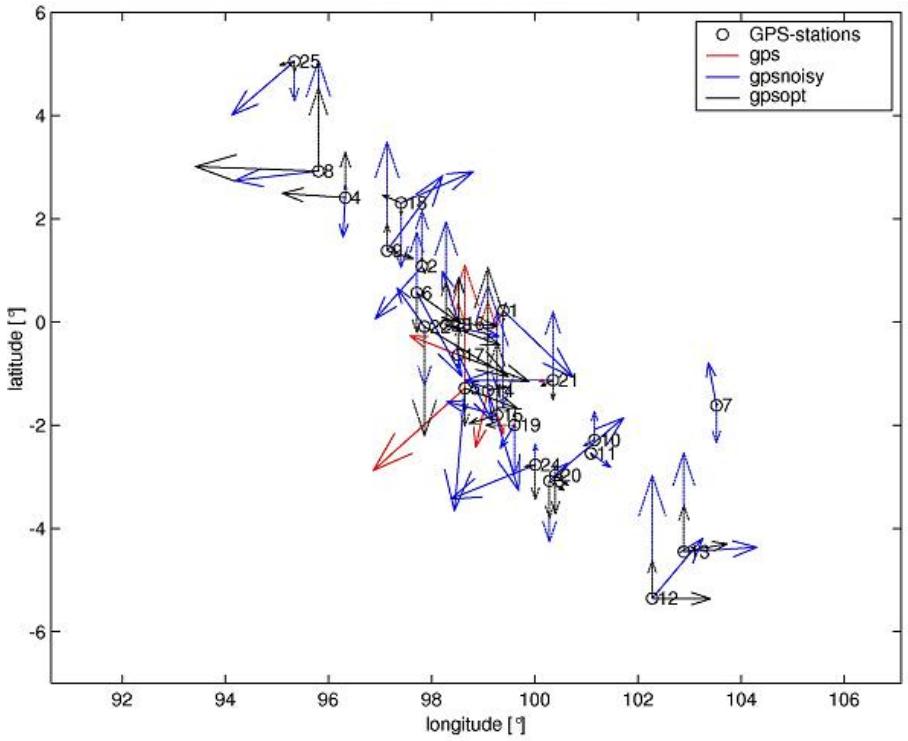


Figure A30: $M_W = 7.5$, noise level: 20cm/40cm

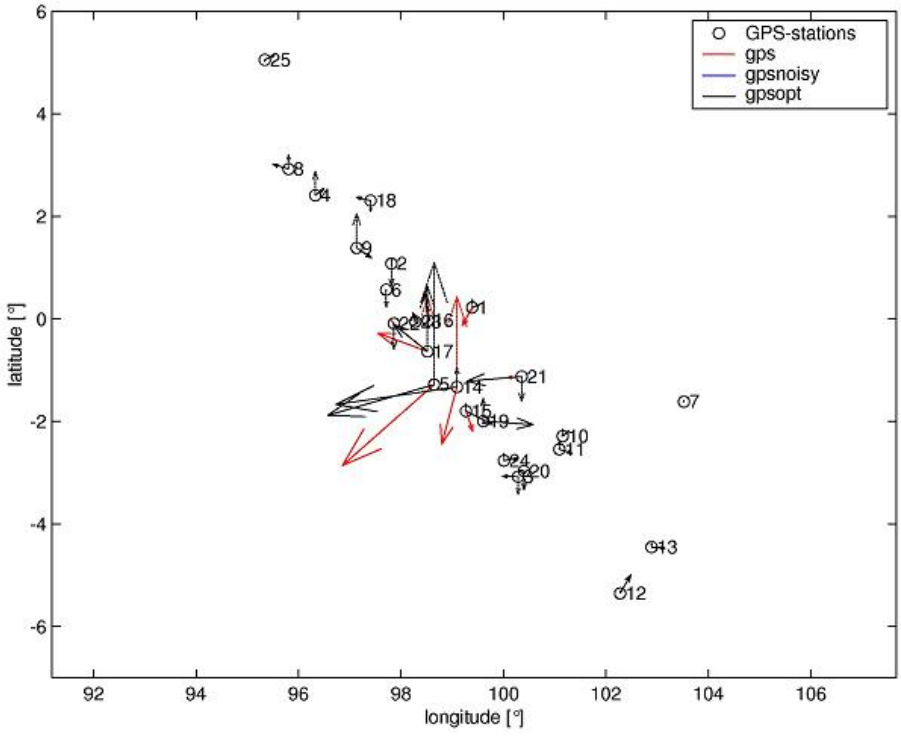


Figure A31: $M_W = 7.6$, noiseless

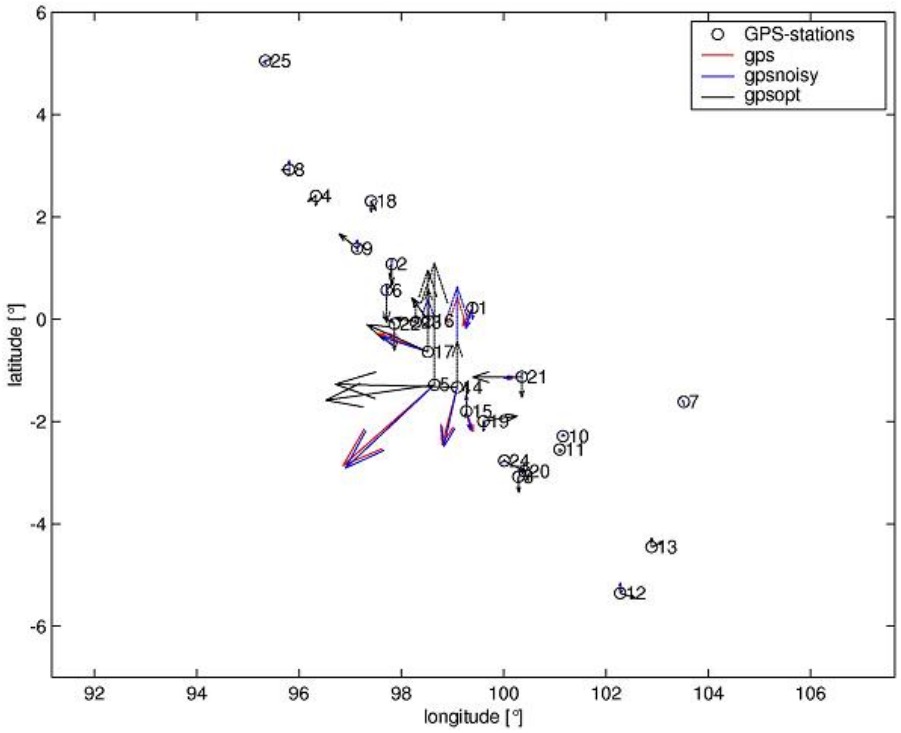


Figure A32: $M_W = 7.6$, noise level: 1cm/3cm

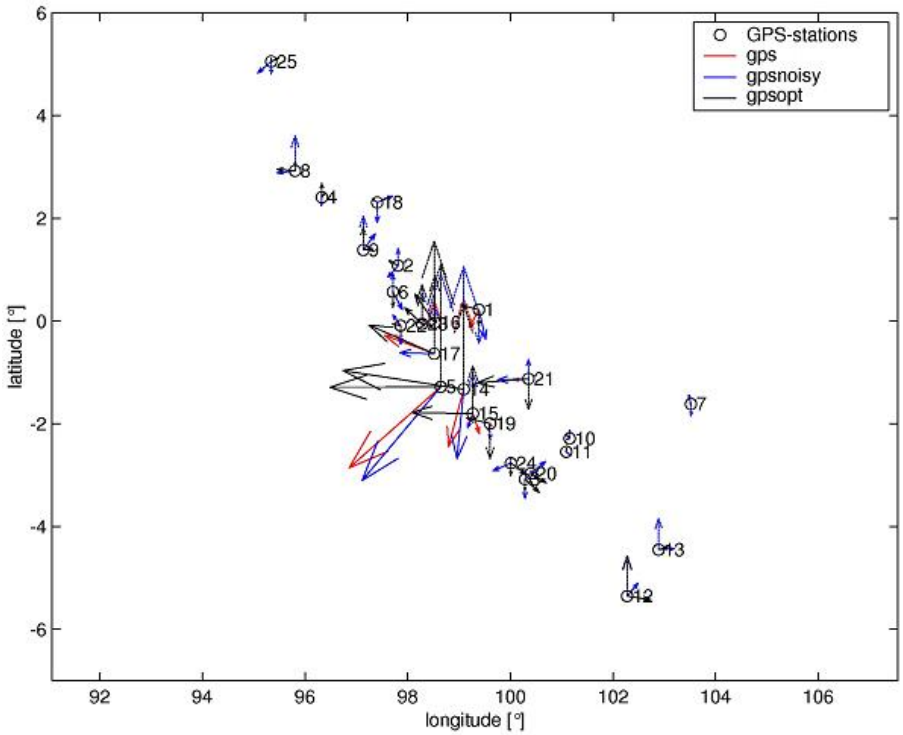


Figure A33: $M_W = 7.6$, noise level: 5cm/10cm

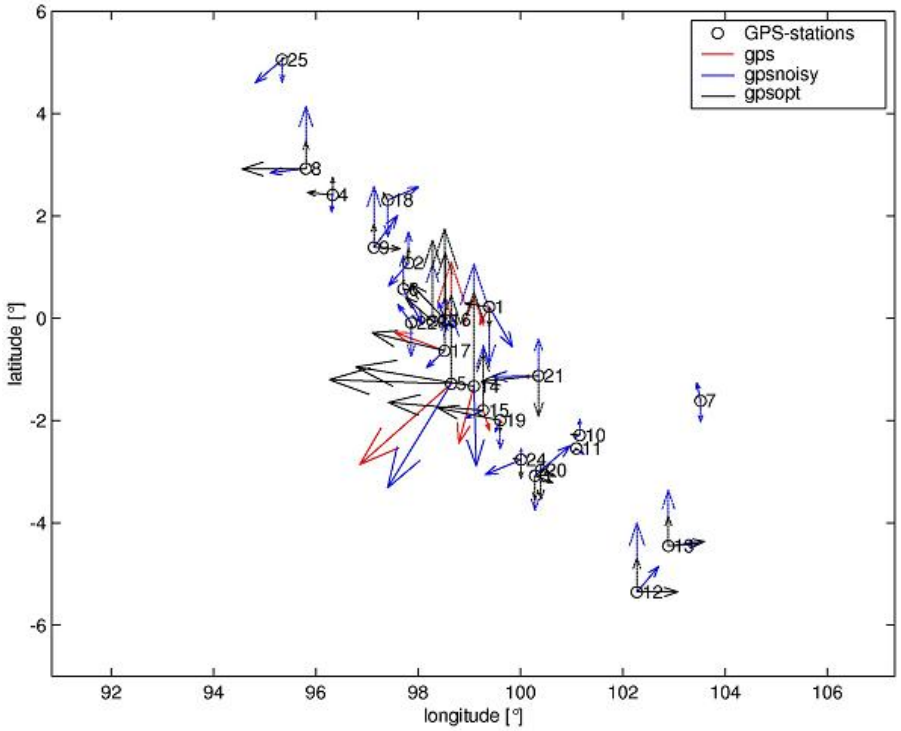


Figure A34: $M_W = 7.6$, noise level: 10cm/20cm

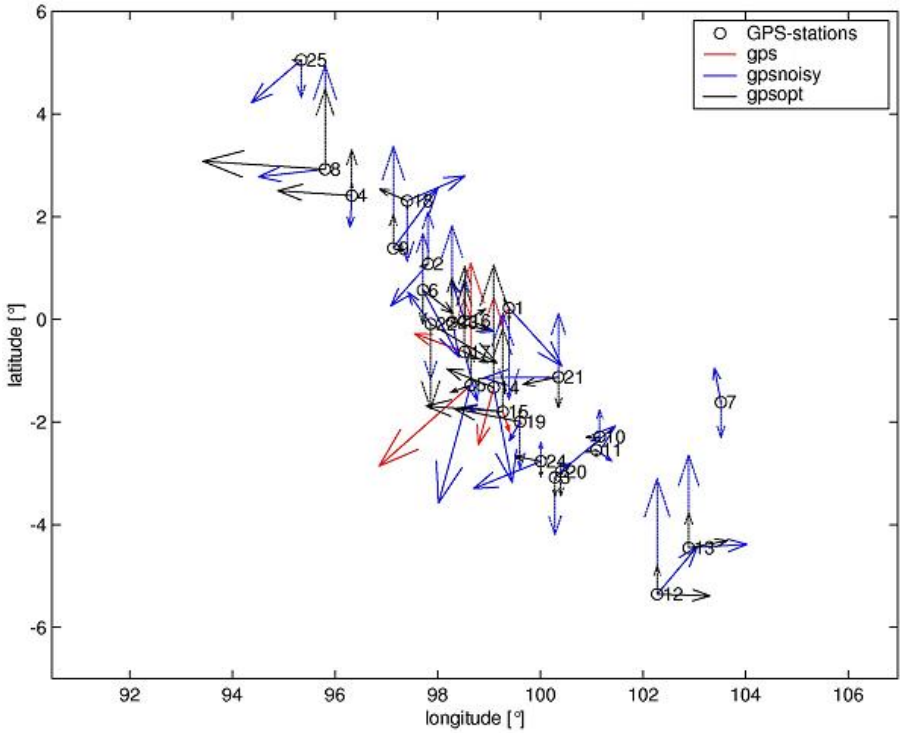


Figure A35: $M_W = 7.6$, noise level: 20cm/40cm

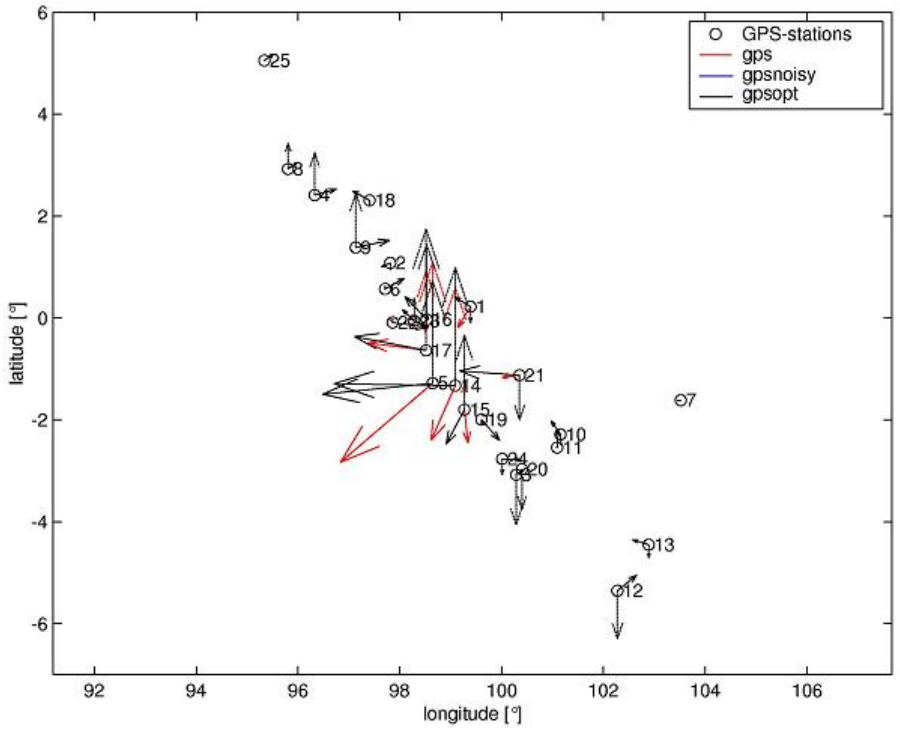


Figure A36: $M_W = 7.7$, noiseless

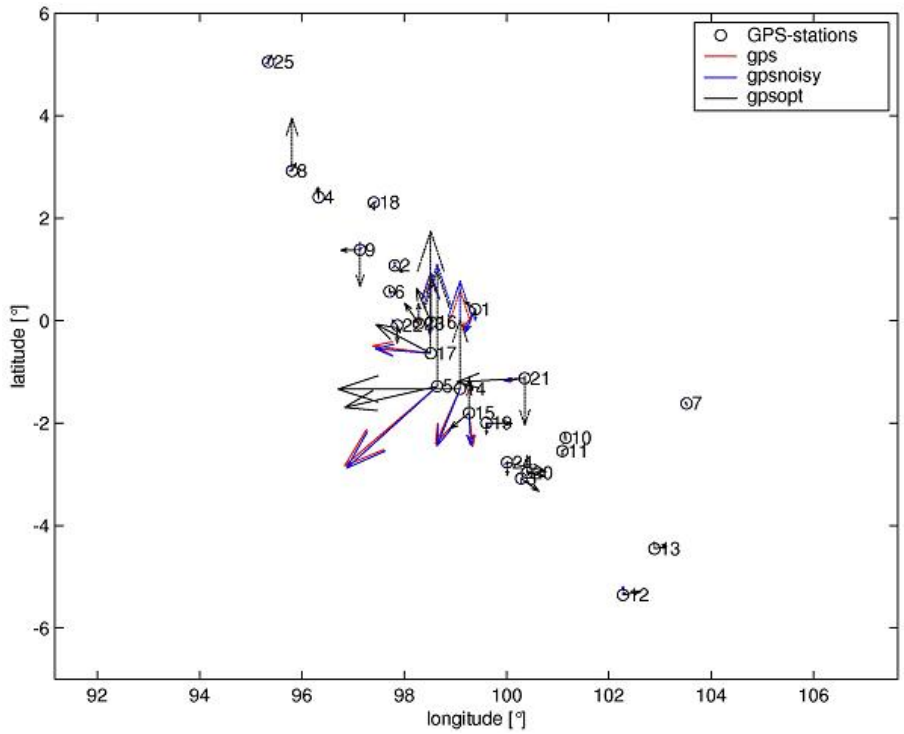


Figure A37: $M_W = 7.7$, noise level: 1cm/3cm

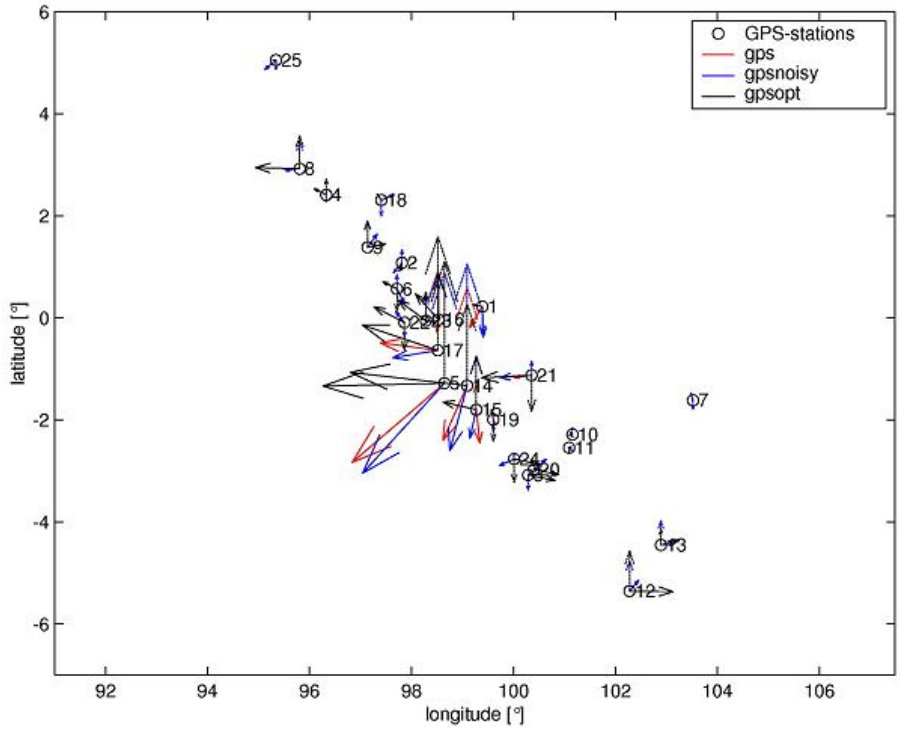


Figure A38: $M_W = 7.7$, noise level: 5cm/10cm

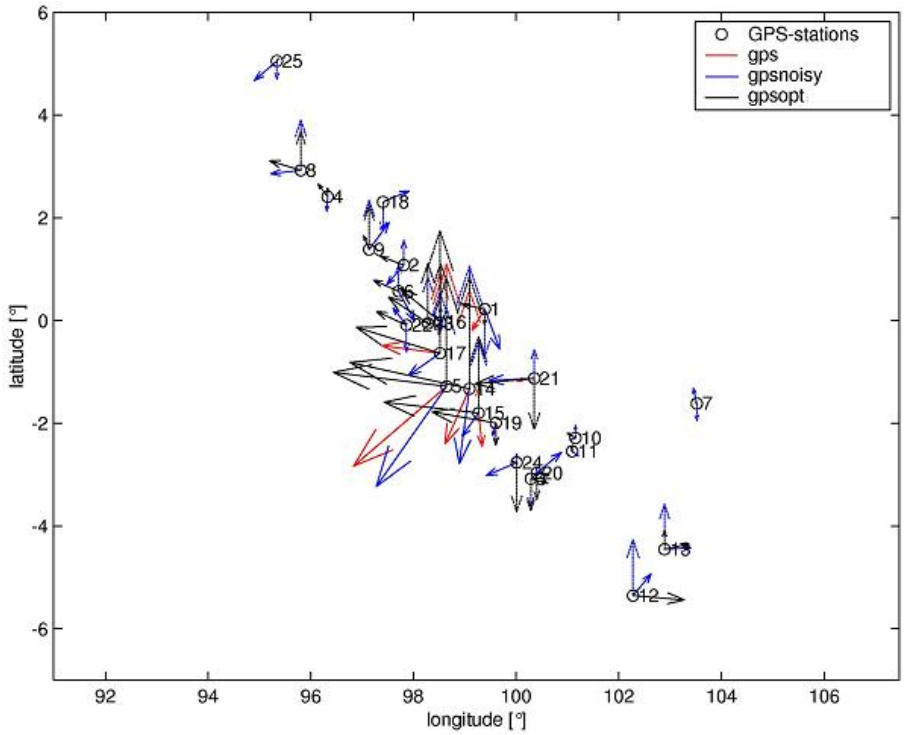


Figure A39: $M_W = 7.7$, noise level: 10cm/20cm

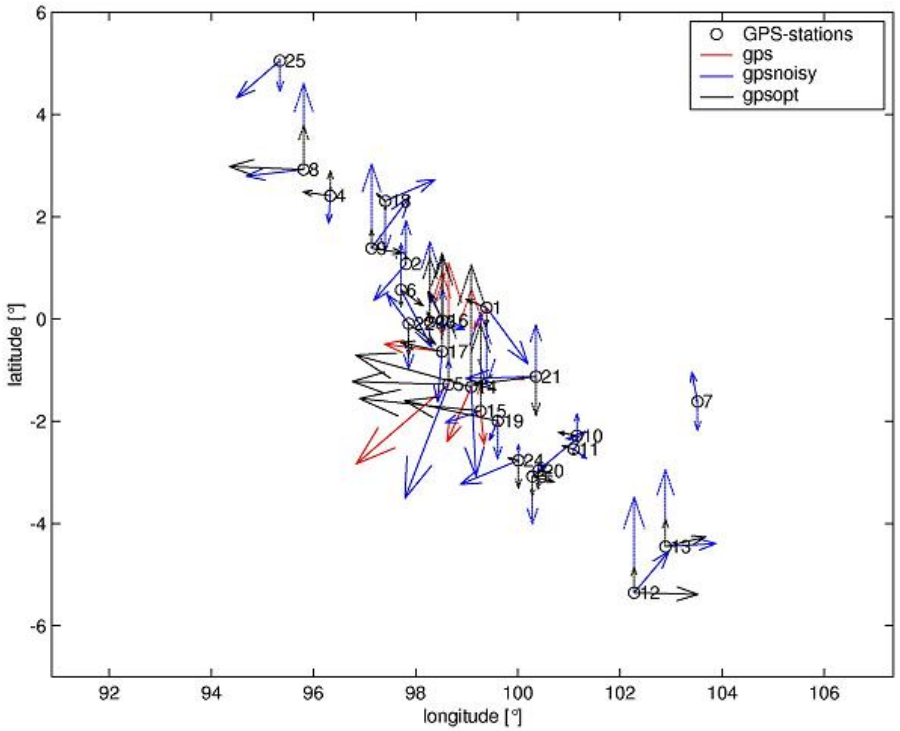


Figure A40: $M_W = 7.7$, noise level: 20cm/40cm

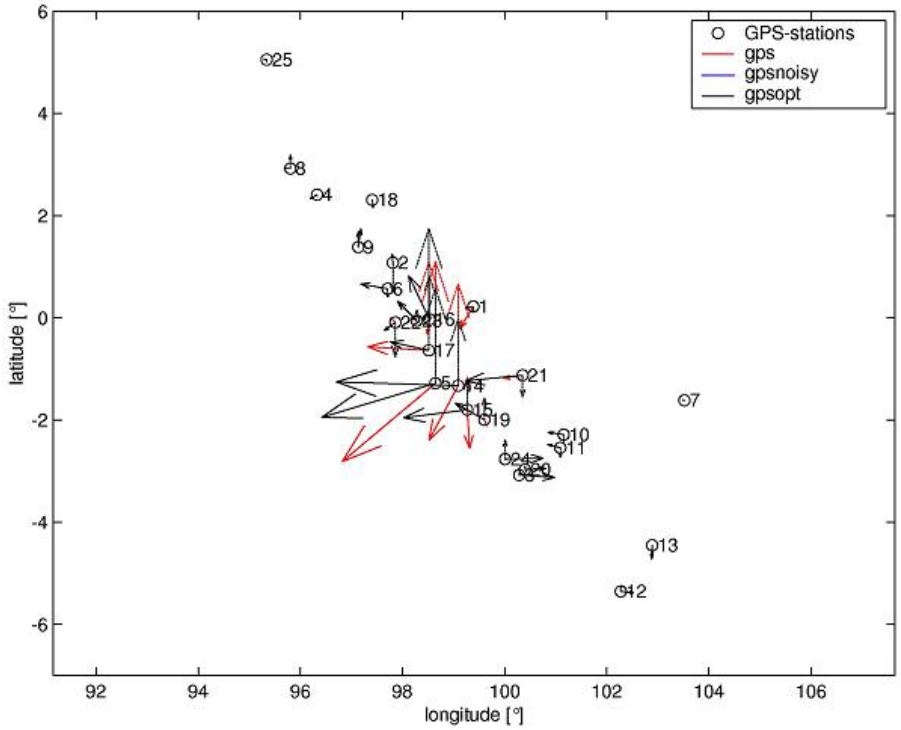


Figure A41: $M_W = 7.8$, noiseless

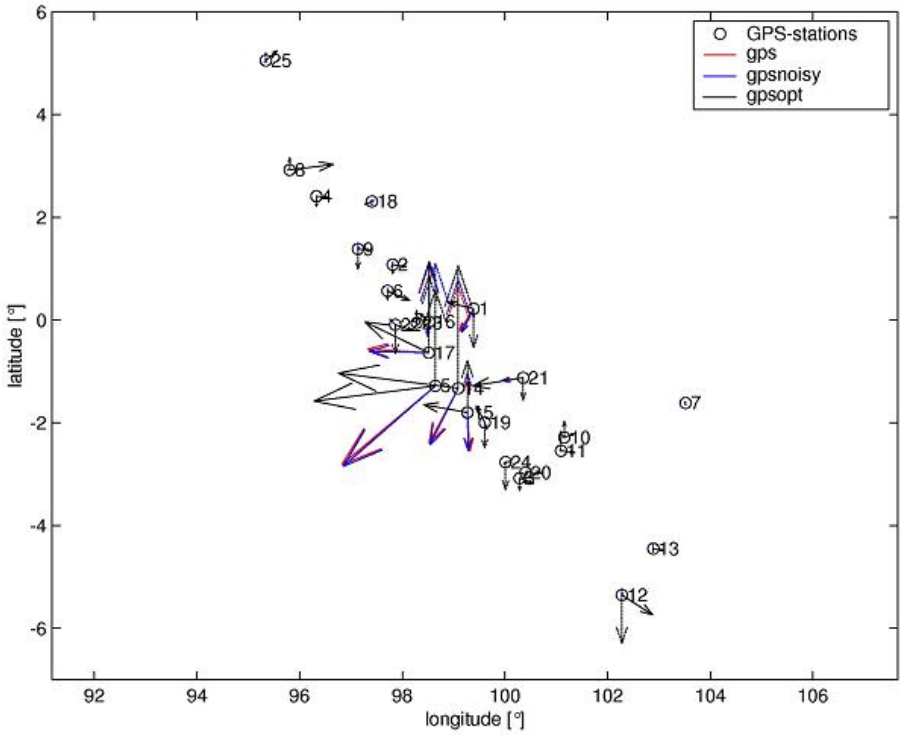


Figure A42: $M_W = 7.8$, noise level: 1cm/3cm

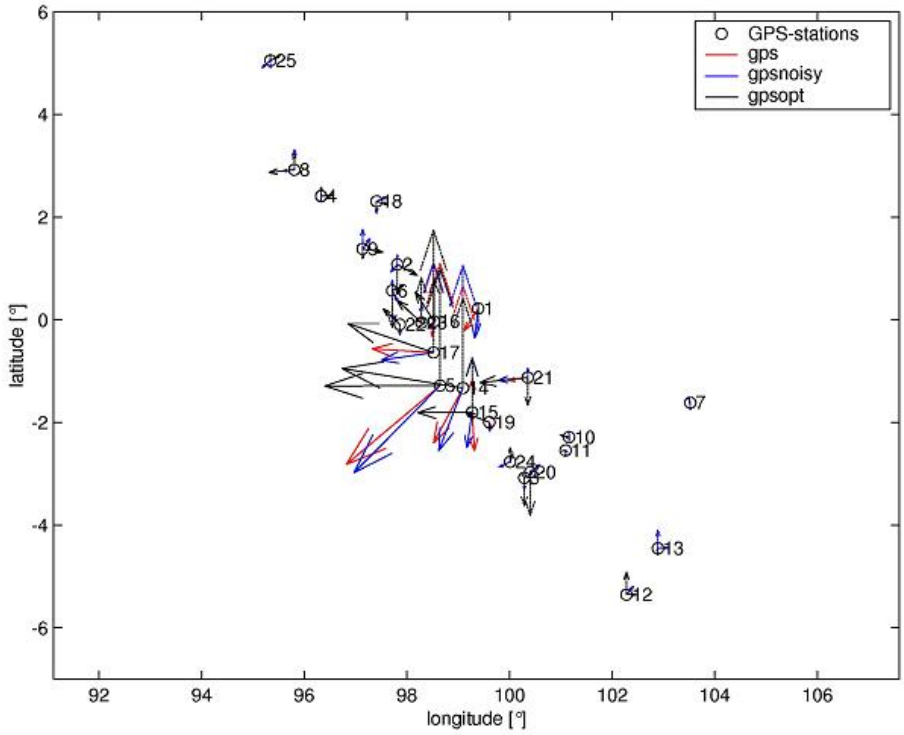


Figure A43: $M_W = 7.8$, noise level: 5cm/10cm

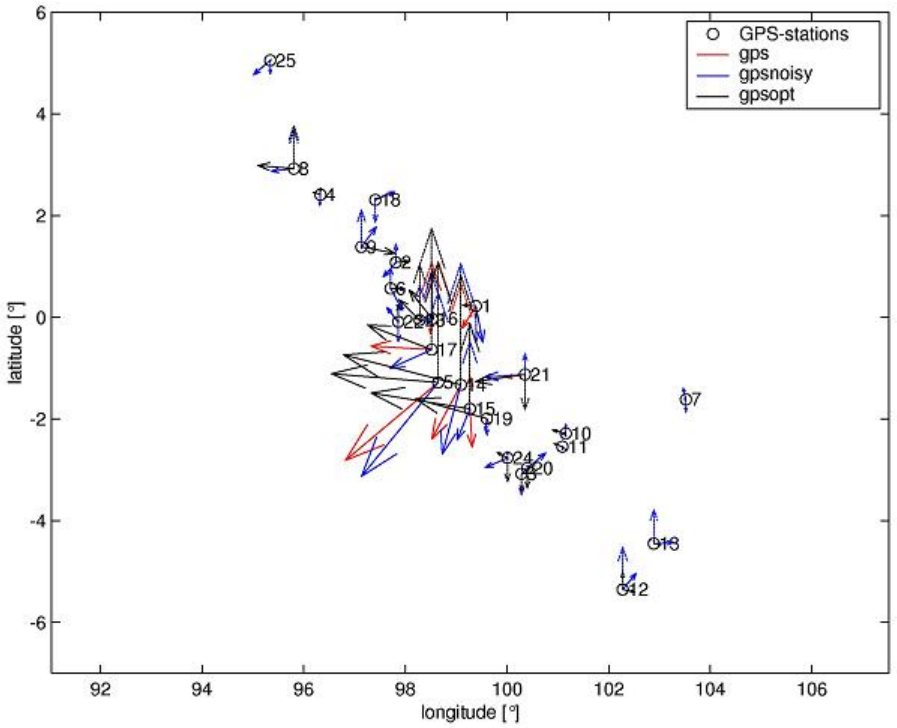


Figure A44: $M_W = 7.8$, noise level: 10cm/20cm

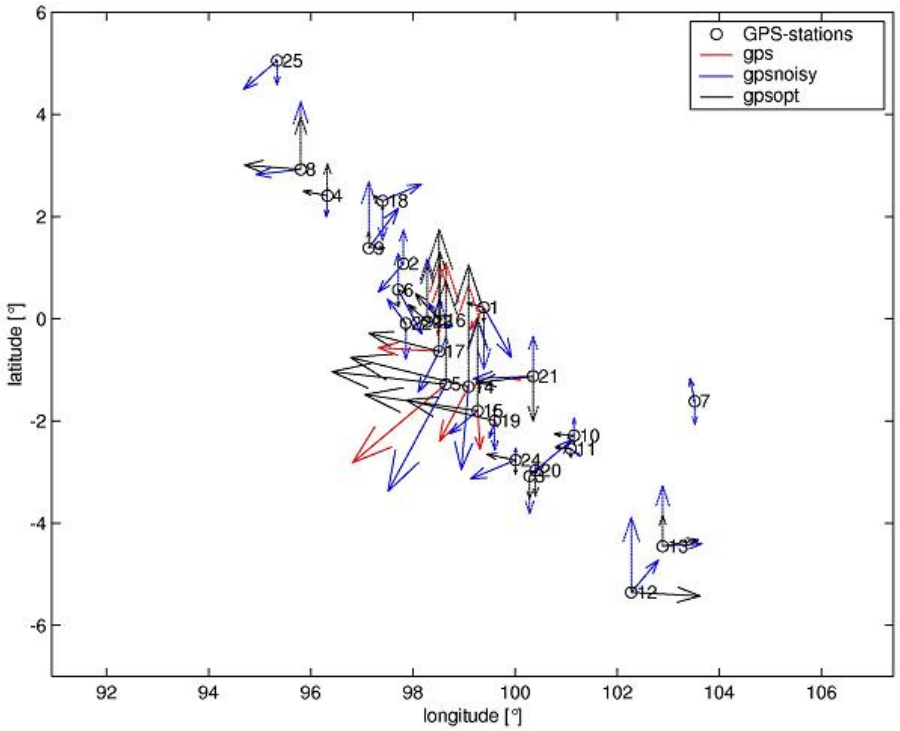


Figure A45: $M_W = 7.8$, noise level: 20cm/40cm

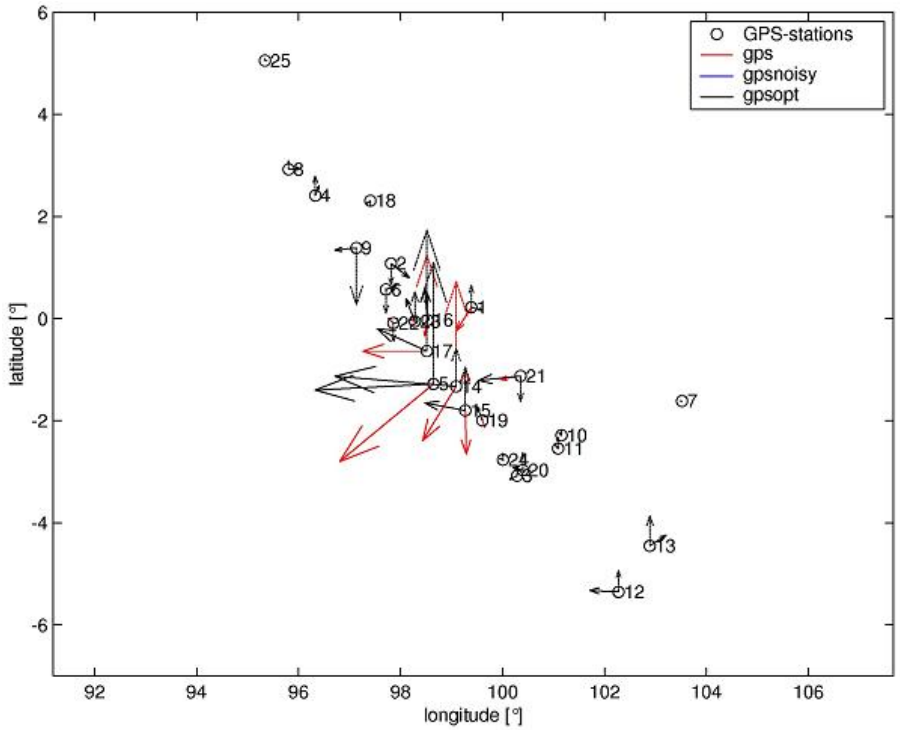


Figure A46: $M_W = 7.9$, noiseless

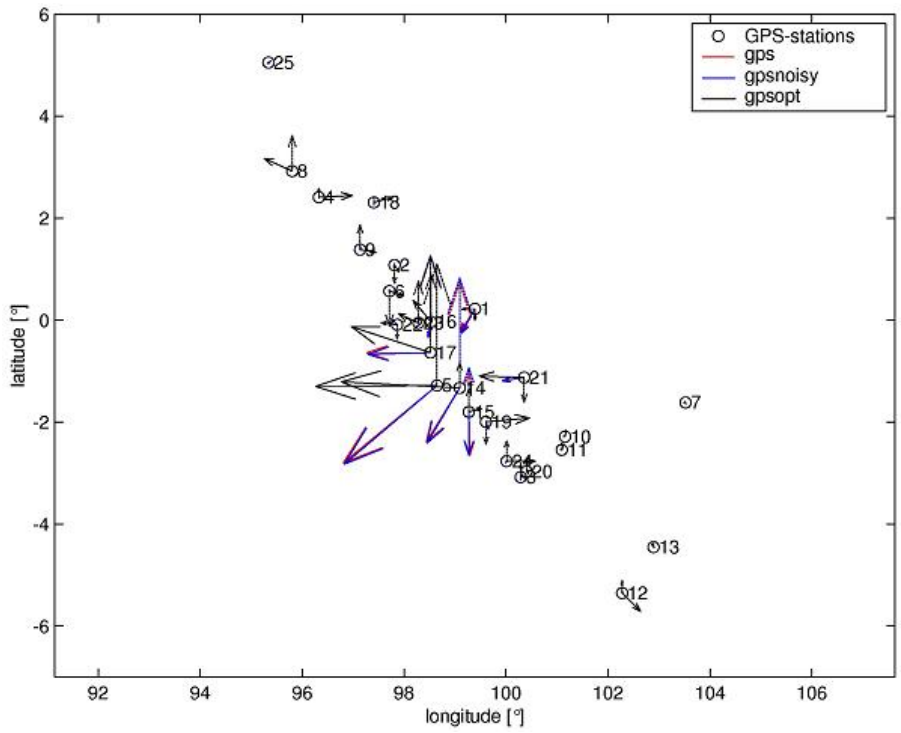


Figure A47: $M_W = 7.9$, noise level: 1cm/3cm

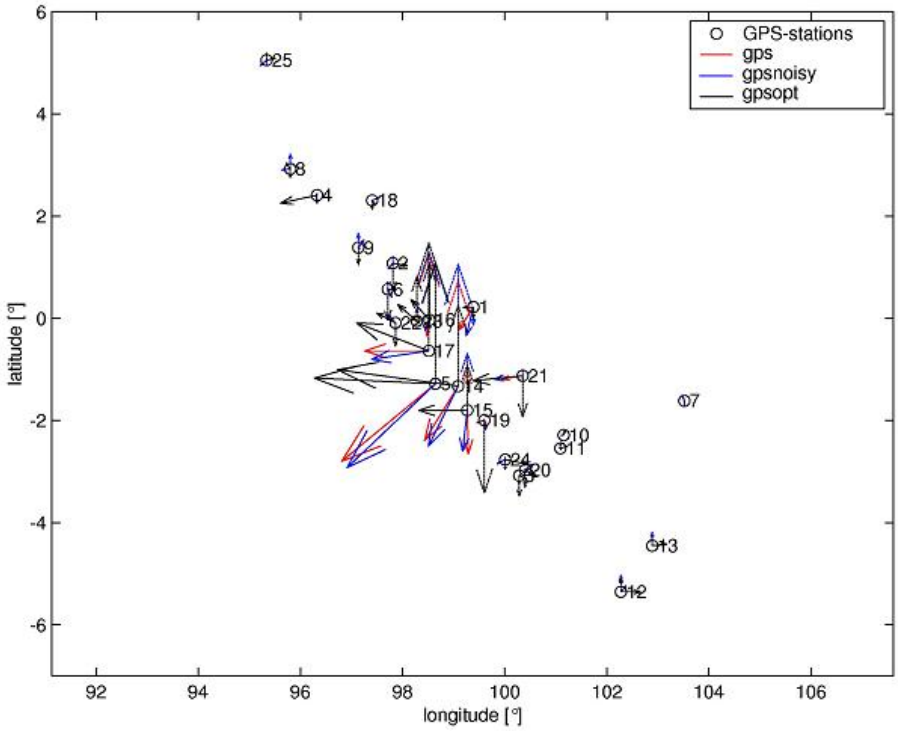


Figure A48: $M_W = 7.9$, noise level: 5cm/10cm

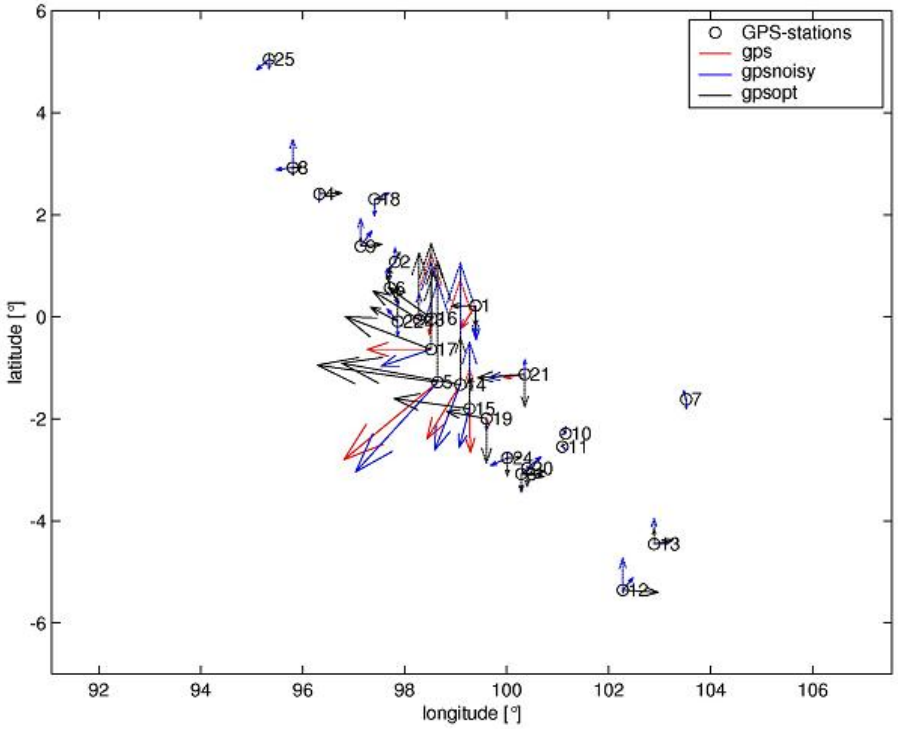


Figure A49: $M_W = 7.9$, noise level: 10cm/20cm

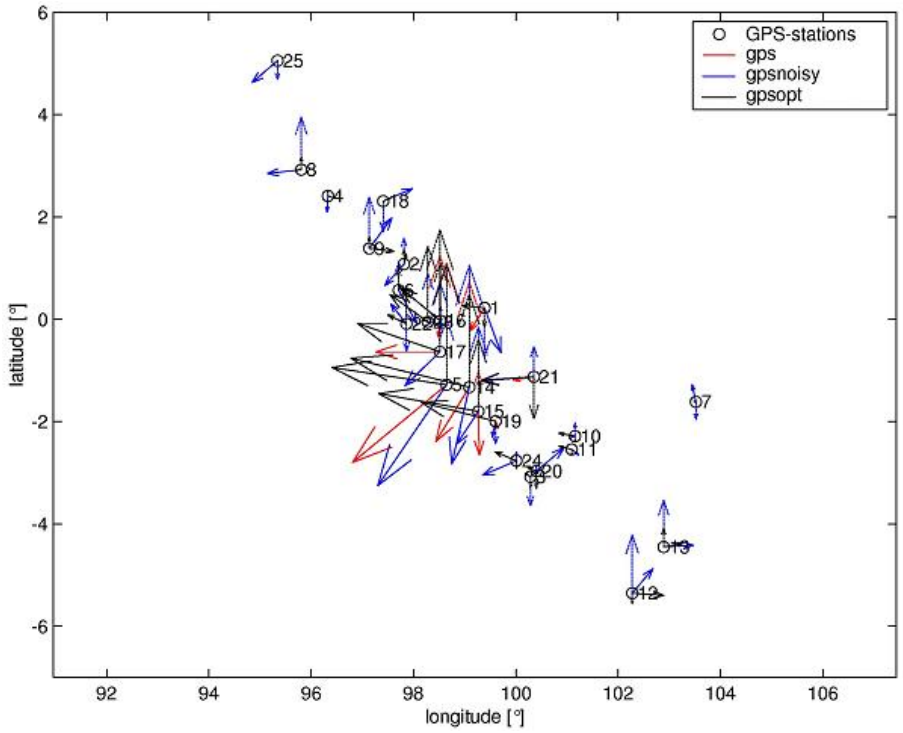


Figure A50: $M_W = 7.9$, noise level: 20cm/40cm

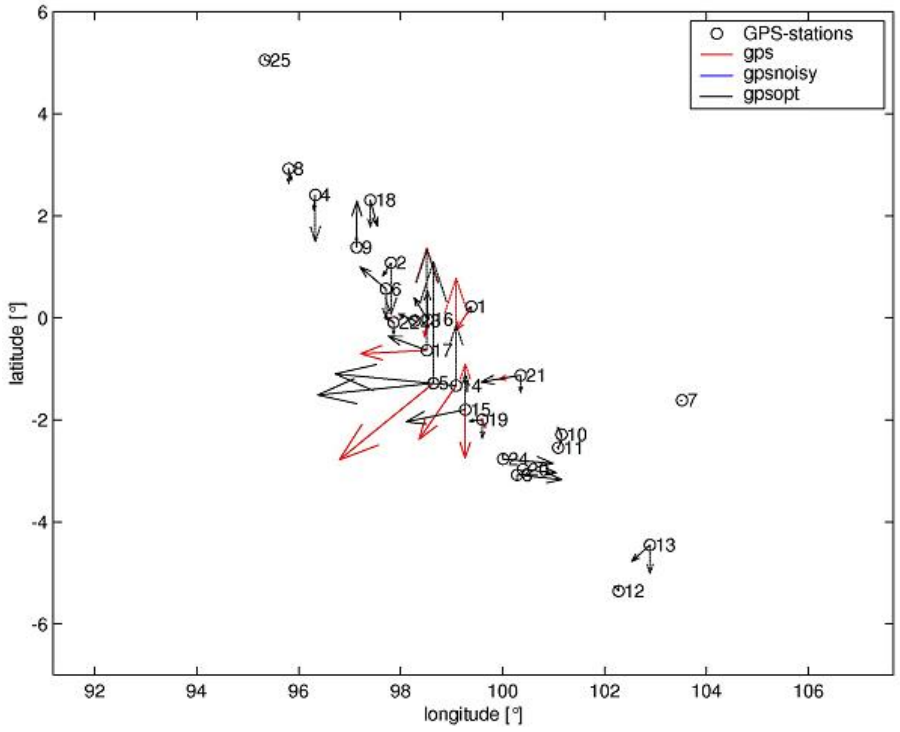


Figure A51: $M_W = 8.0$, noiseless

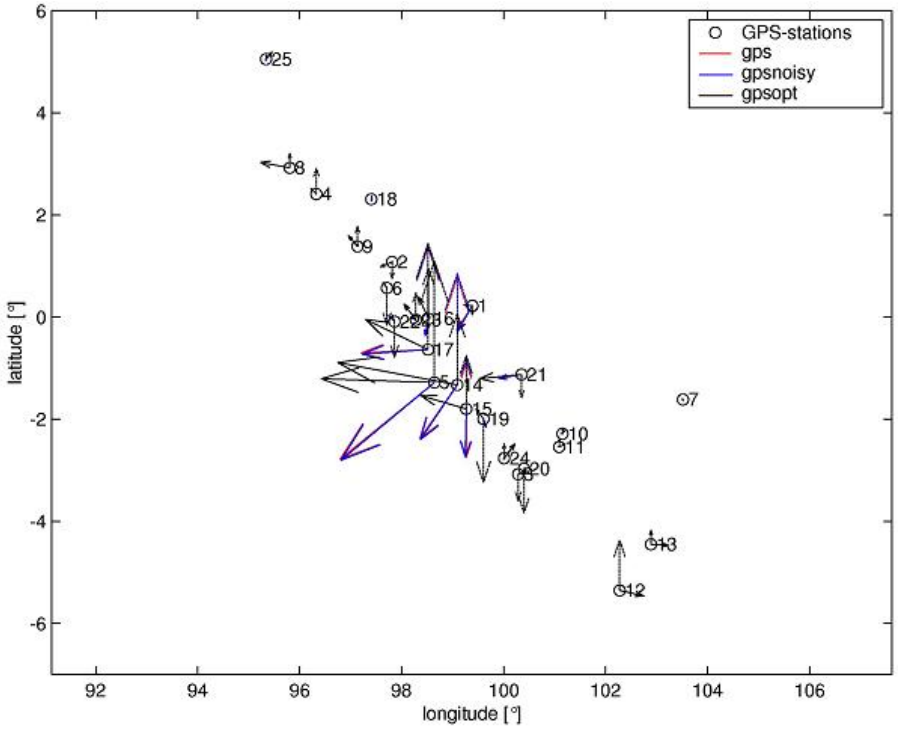


Figure A52: $M_W = 8.0$, noise level: 1cm/3cm

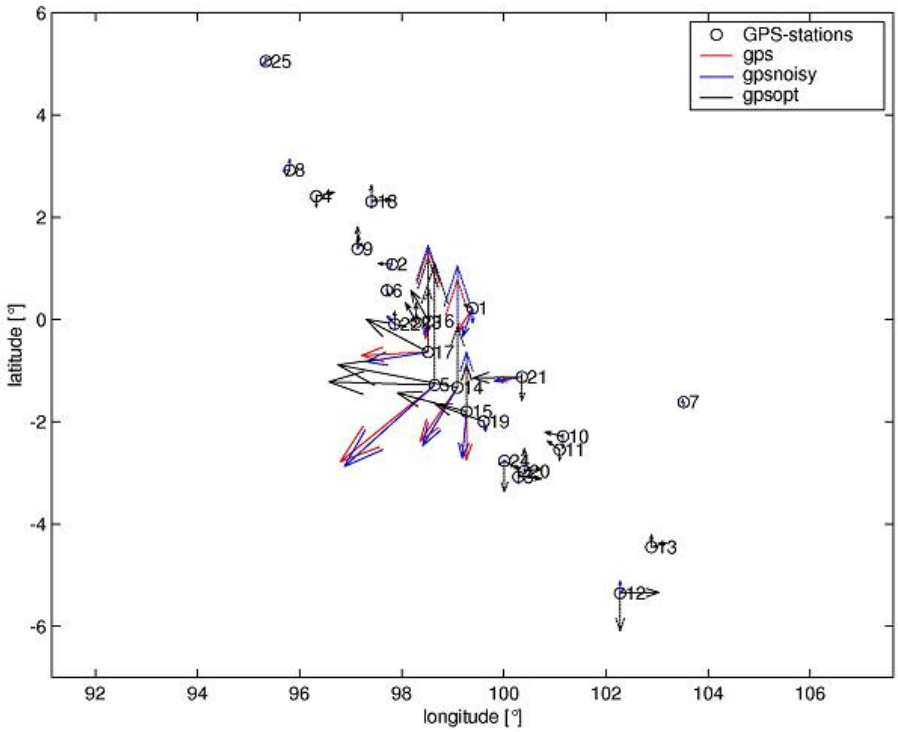


Figure A53: $M_W = 8.0$, noise level: 5cm/10cm

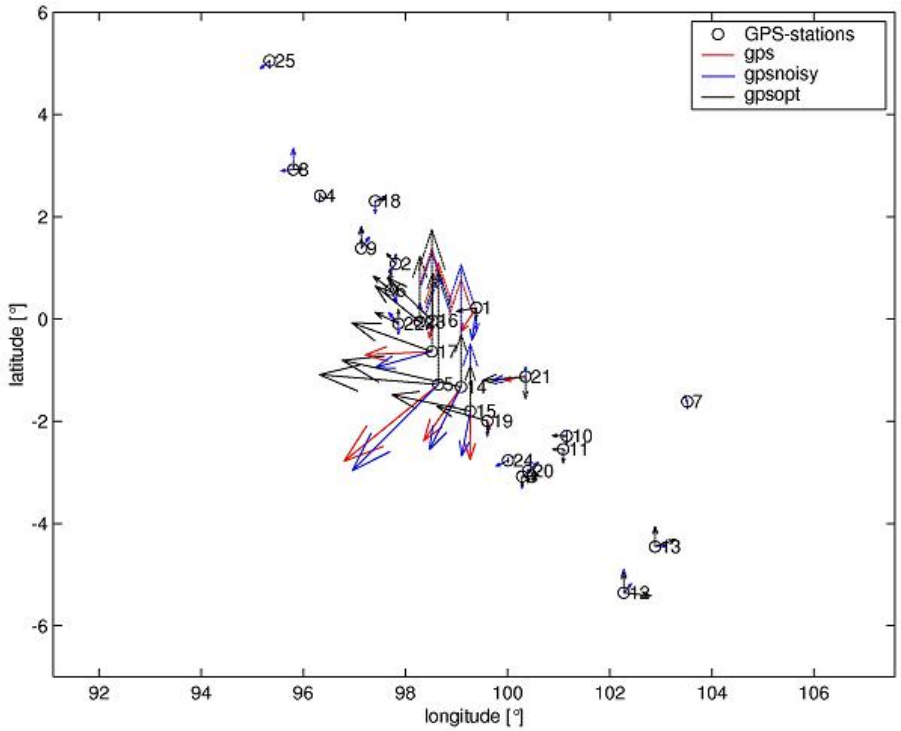


Figure A54: $M_W = 8.0$, noise level: 10cm/20cm

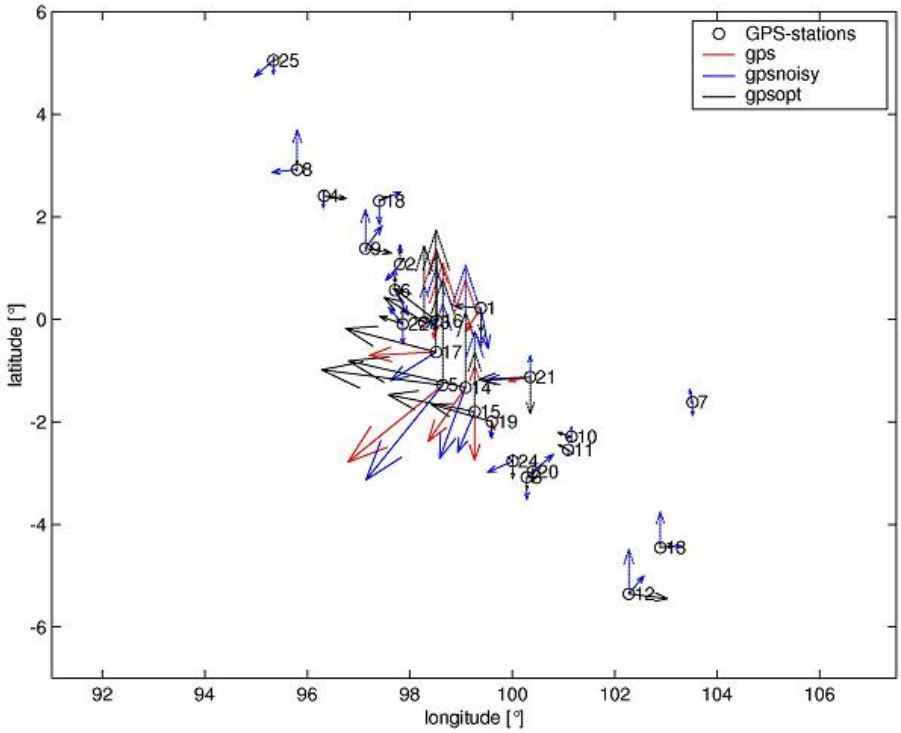


Figure A55: $M_W = 8.0$, noise level: 20cm/40cm

### A.1.2 Slip distributions at subfault array

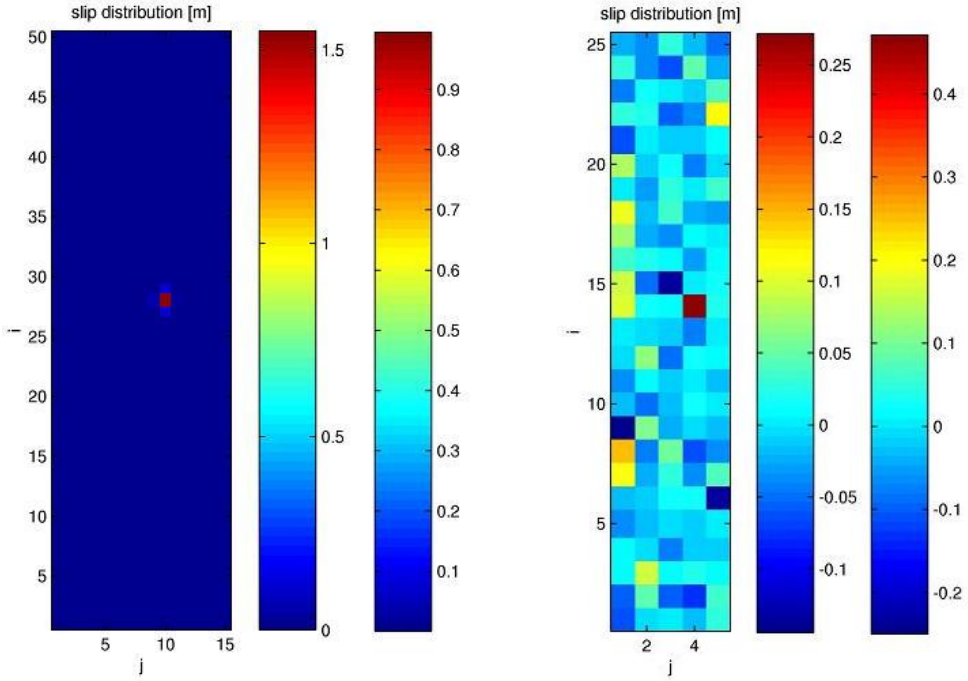


Figure A56: $M_W = 7.0$: target (left) and reconstructed, noiseless(right) slip distribution with original and normalised scale

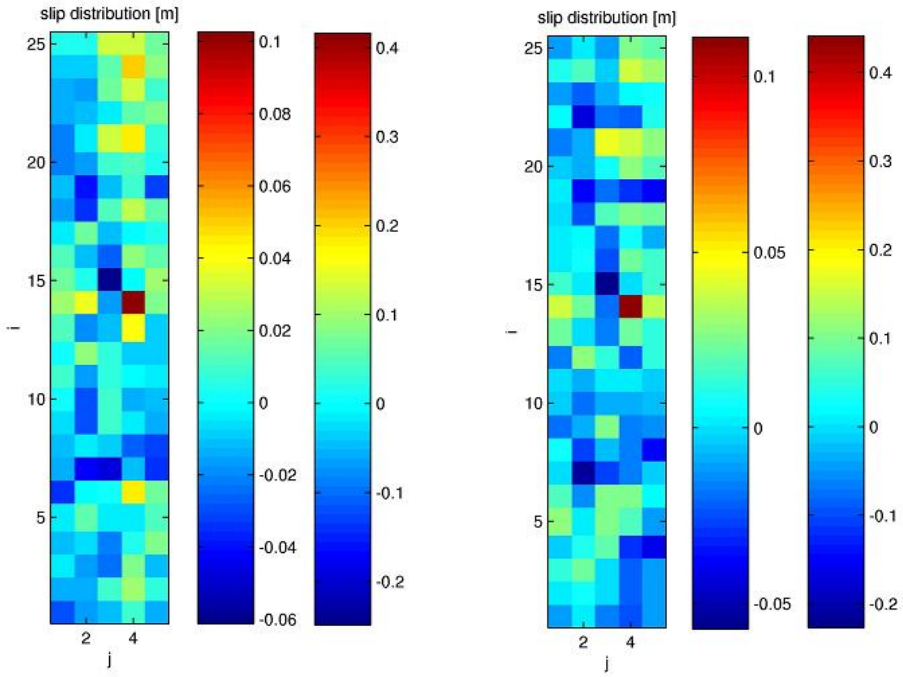


Figure A57: $M_W = 7.0$, noise level 1cm/3cm: non-stabilised (left) and stabilised (right) reconstruction of slip distribution with original and normalised scale

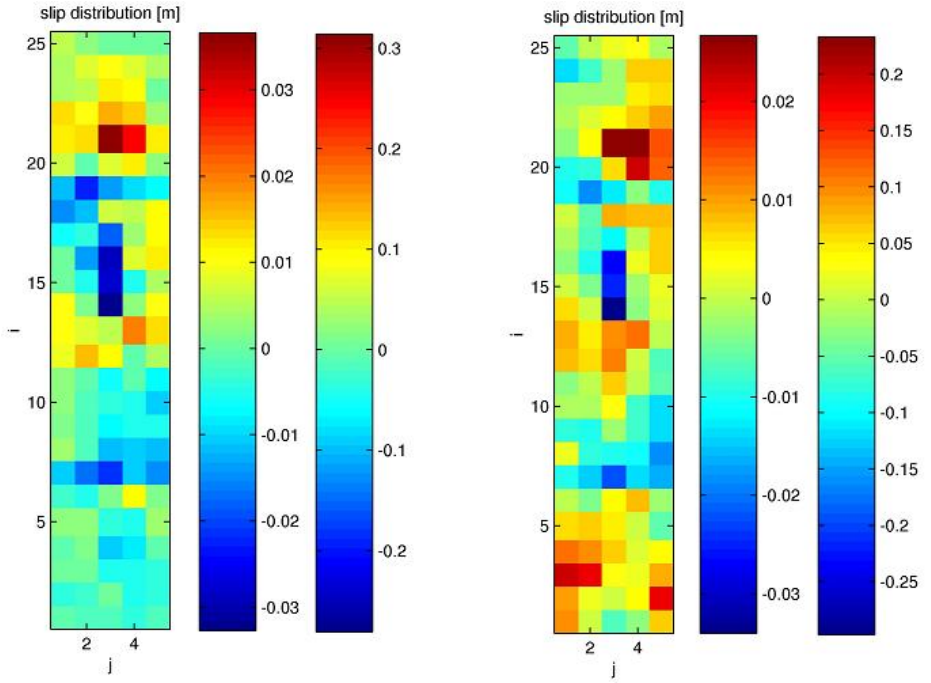


Figure A58: $M_W = 7.0$, noise level 5cm/10cm: non-stabilised (left) and stabilised (right) reconstruction of slip distribution with original and normalised scale

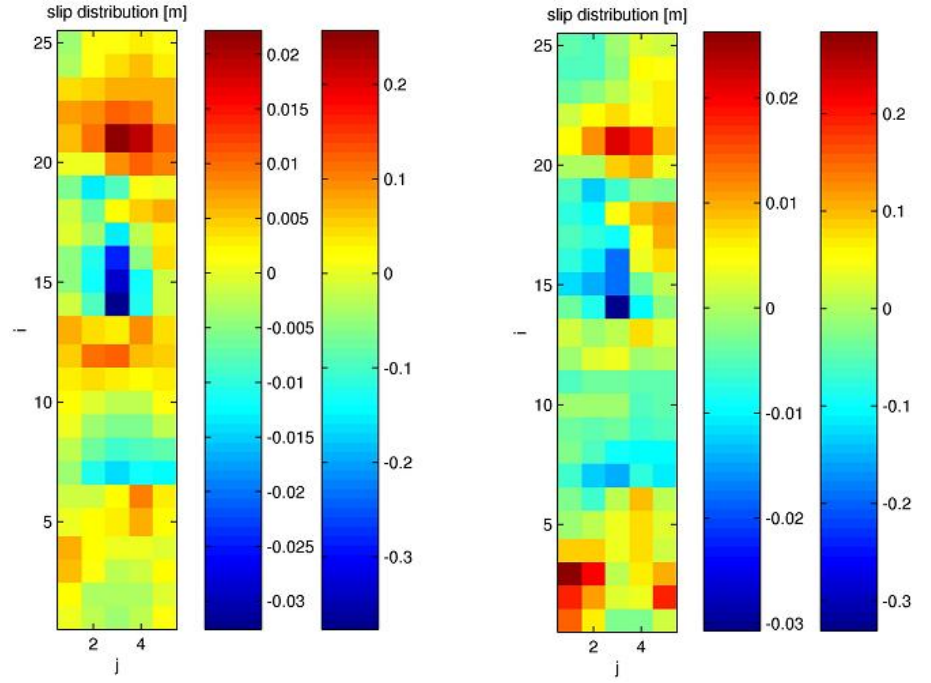


Figure A59: $M_W = 7.0$, noise level 10cm/20cm: non-stabilised (left) and stabilised (right) reconstruction of slip distribution with original and normalised scale

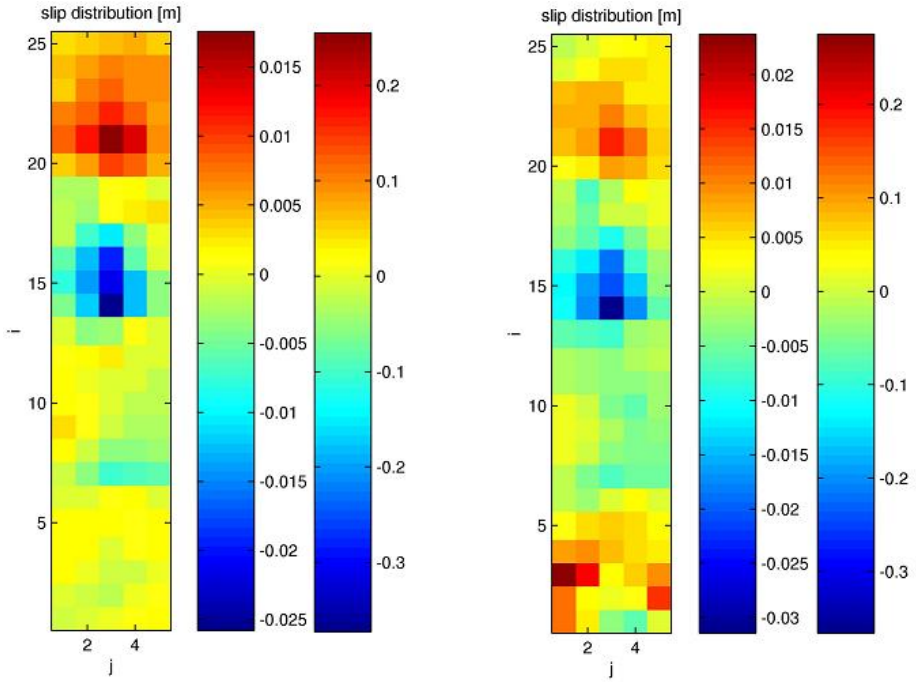


Figure A60: $M_W = 7.0$, noise level 20cm/40cm: non-stabilised (left) and stabilised (right) reconstruction of slip distribution with original and normalised scale

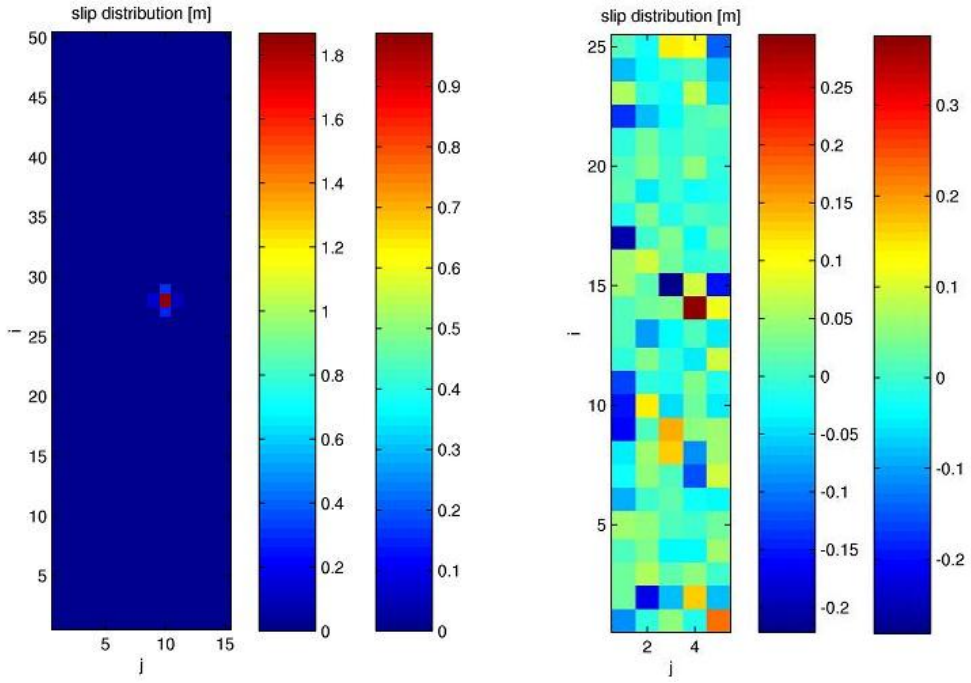


Figure A61: $M_W = 7.1$: target (left) and reconstructed, noiseless(right) slip distribution with original and normalised scale

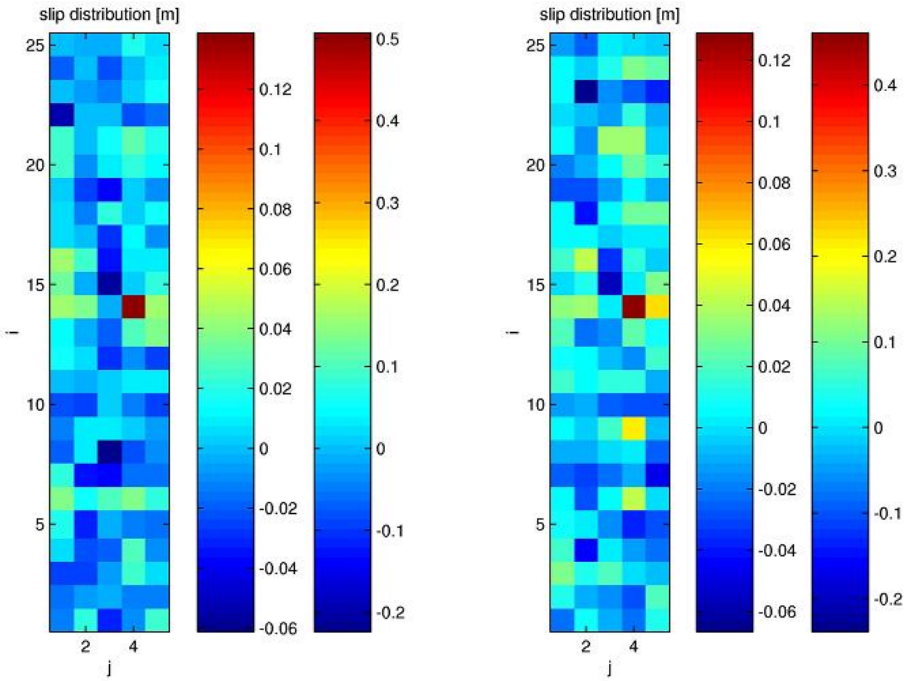


Figure A62: $M_W = 7.1$, noise level 1cm/3cm: non-stabilised (left) and stabilised (right) reconstruction of slip distribution with original and normalised scale

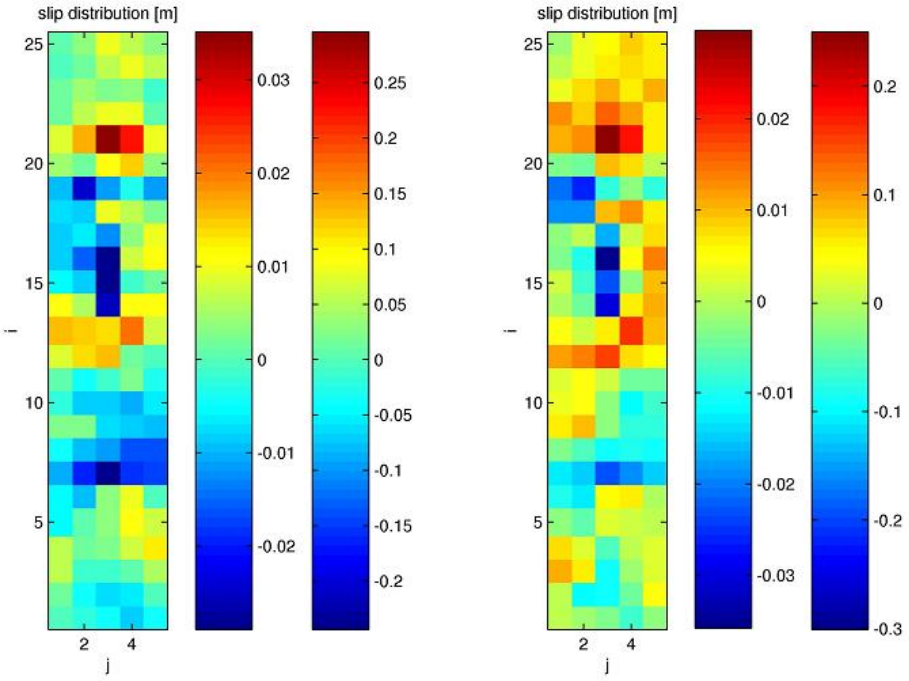


Figure A63: $M_W = 7.1$, noise level 5cm/10cm: non-stabilised (left) and stabilised (right) reconstruction of slip distribution with original and normalised scale

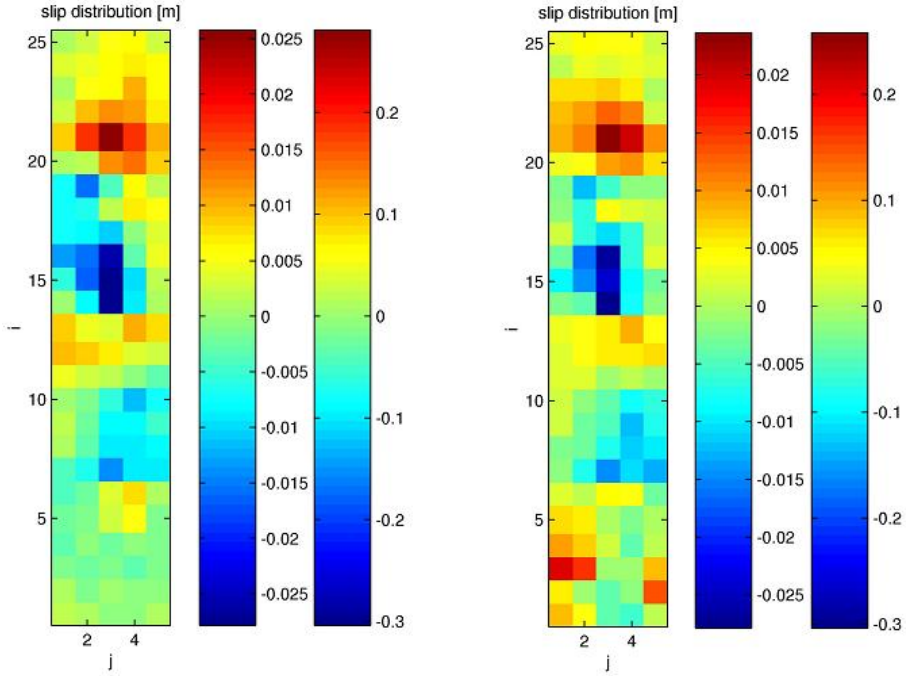


Figure A64: $M_W = 7.1$, noise level 10cm/20cm: non-stabilised (left) and stabilised (right) reconstruction of slip distribution with original and normalised scale

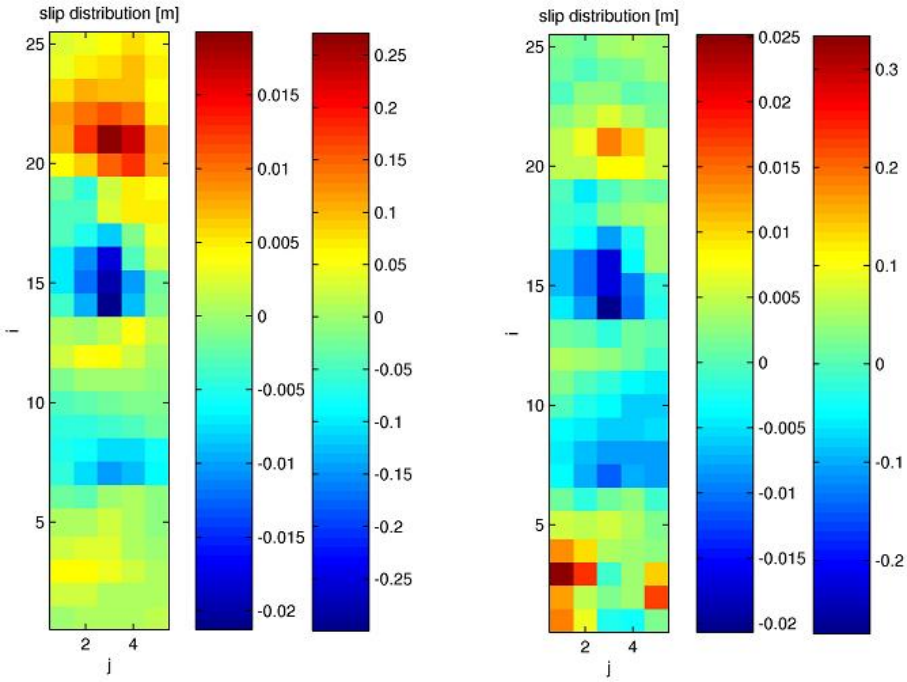


Figure A65: $M_W = 7.1$, noise level 20cm/40cm: non-stabilised (left) and stabilised (right) reconstruction of slip distribution with original and normalised scale

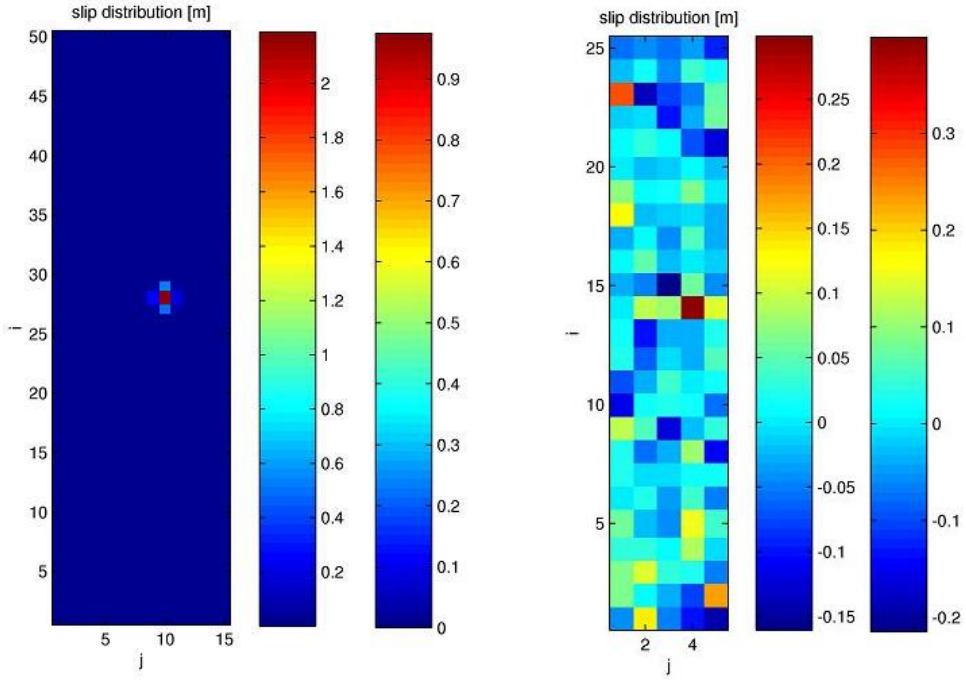


Figure A66: $M_W = 7.2$: target (left) and reconstructed, noiseless(right) slip distribution with original and normalised scale

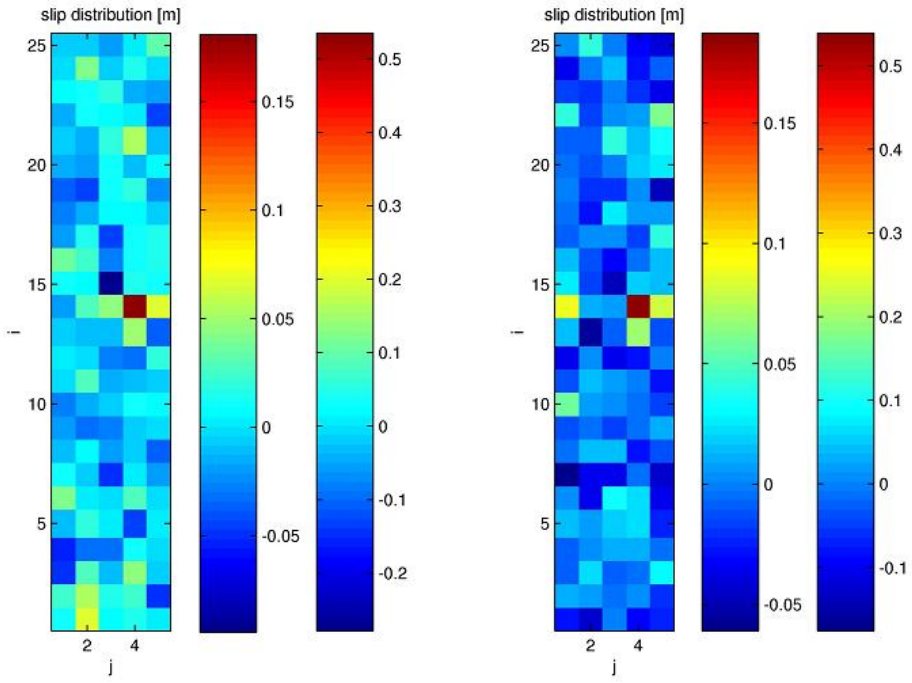


Figure A67: $M_W = 7.2$, noise level 1cm/3cm: non-stabilised (left) and stabilised (right) reconstruction of slip distribution with original and normalised scale

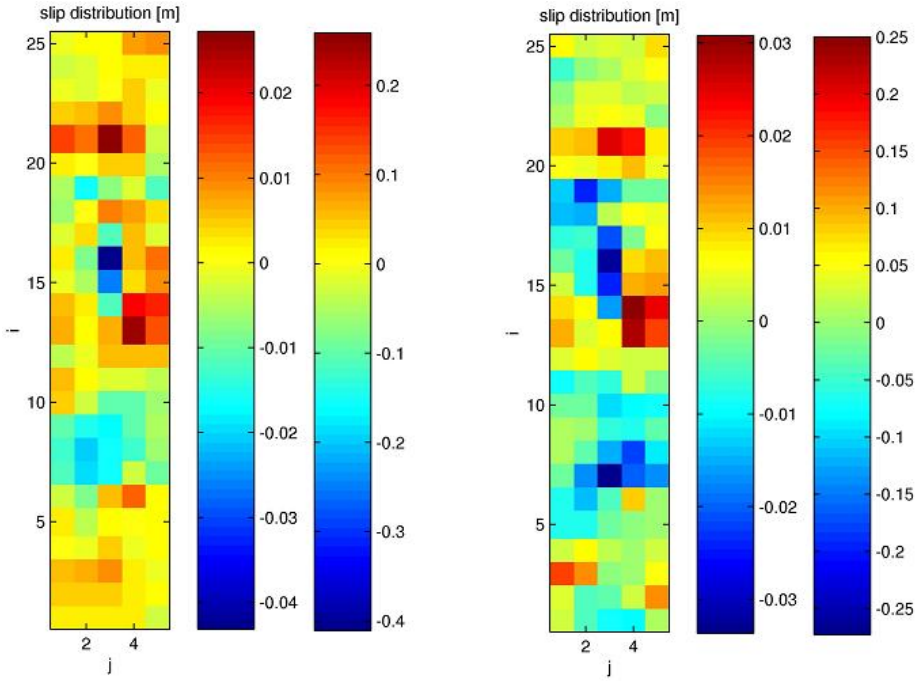


Figure A68: $M_W = 7.2$, noise level 5cm/10cm: non-stabilised (left) and stabilised (right) reconstruction of slip distribution with original and normalised scale

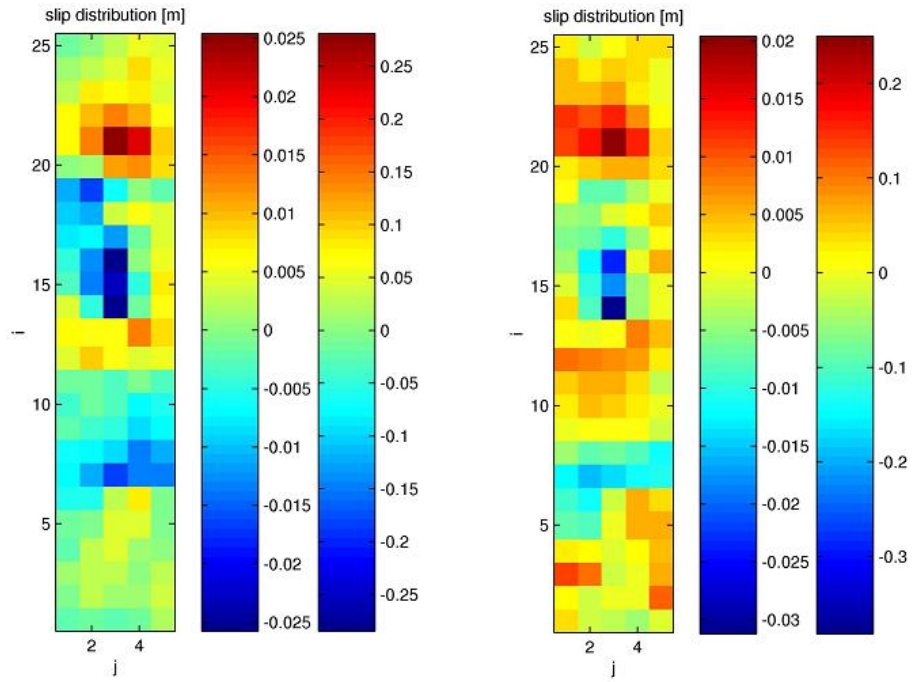


Figure A69: $M_W = 7.2$, noise level 10cm/20cm: non-stabilised (left) and stabilised (right) reconstruction of slip distribution with original and normalised scale

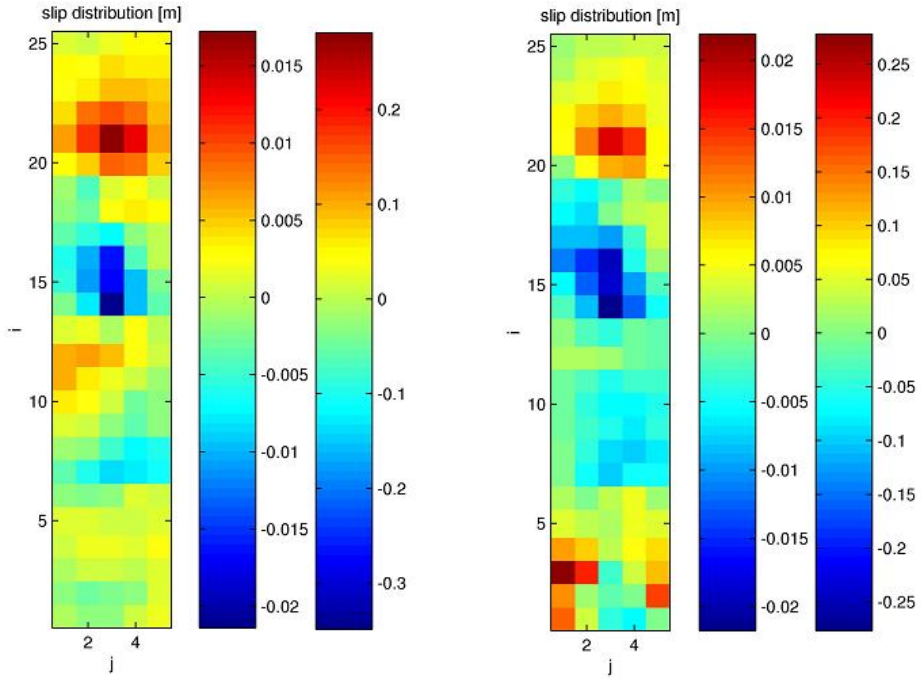


Figure A70: $M_W = 7.2$, noise level 20cm/40cm: non-stabilised (left) and stabilised (right) reconstruction of slip distribution with original and normalised scale

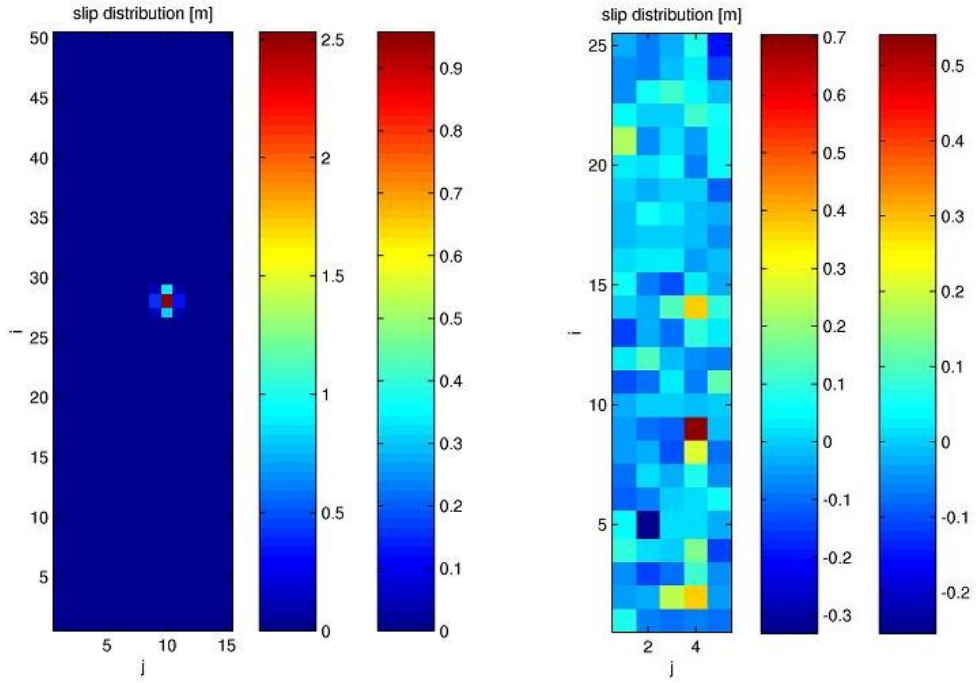


Figure A71: $M_W = 7.3$: target (left) and reconstructed, noiseless(right) slip distribution with original and normalised scale

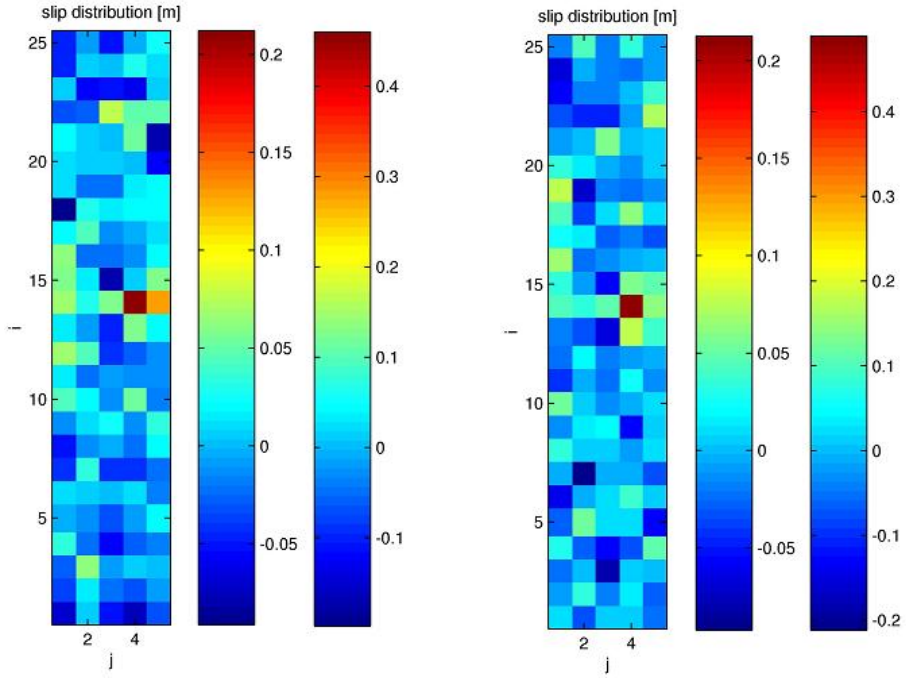


Figure A72: $M_W = 7.3$, noise level 1cm/3cm: non-stabilised (left) and stabilised (right) reconstruction of slip distribution with original and normalised scale

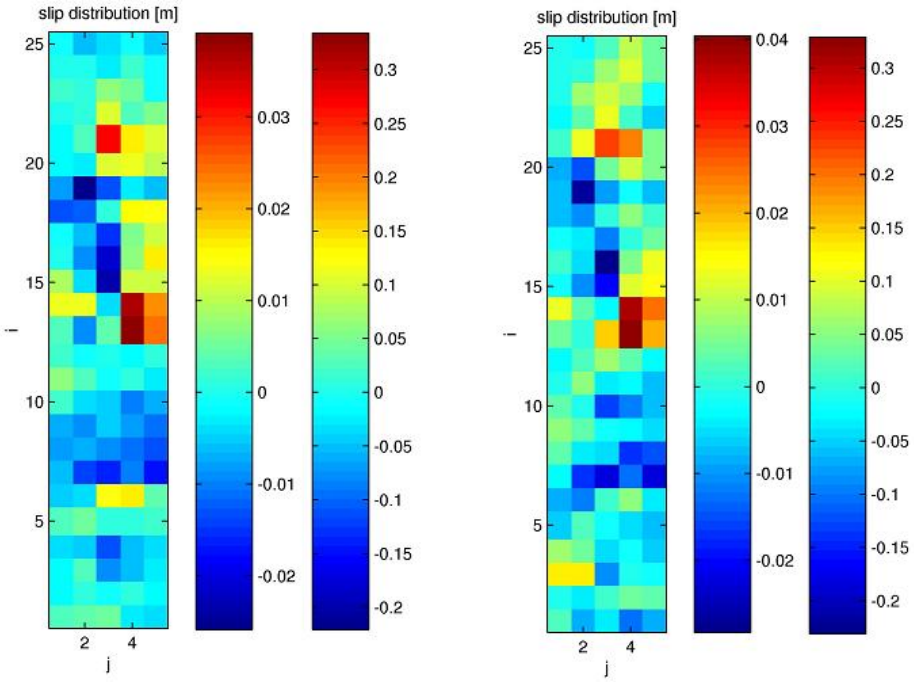


Figure A73: $M_W = 7.3$, noise level 5cm/10cm: non-stabilised (left) and stabilised (right) reconstruction of slip distribution with original and normalised scale

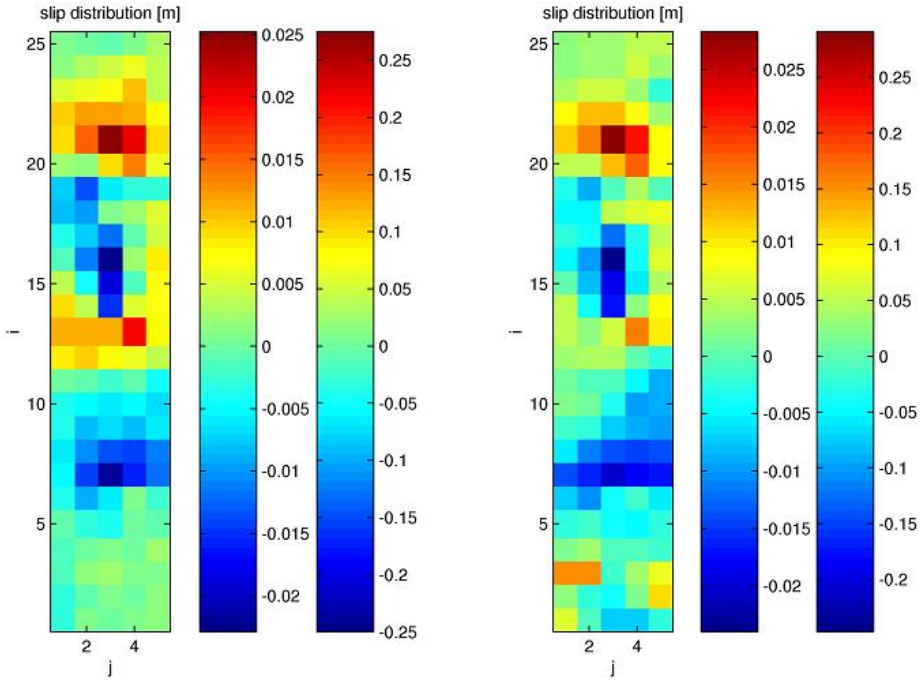


Figure A74: $M_W = 7.3$, noise level 10cm/20cm: non-stabilised (left) and stabilised (right) reconstruction of slip distribution with original and normalised scale

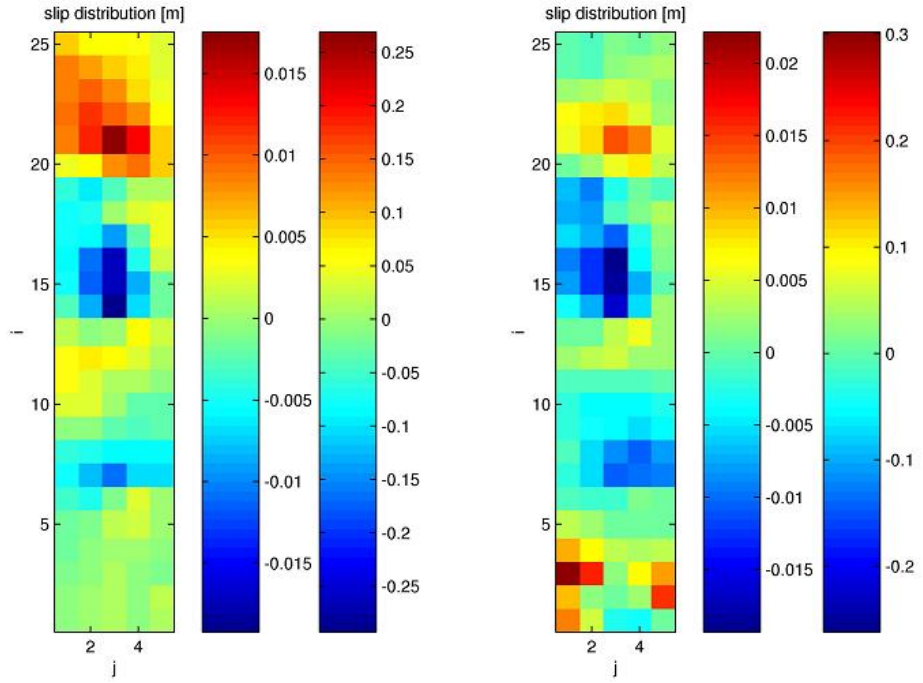


Figure A75: $M_W = 7.3$, noise level 20cm/40cm: non-stabilised (left) and stabilised (right) reconstruction of slip distribution with original and normalised scale

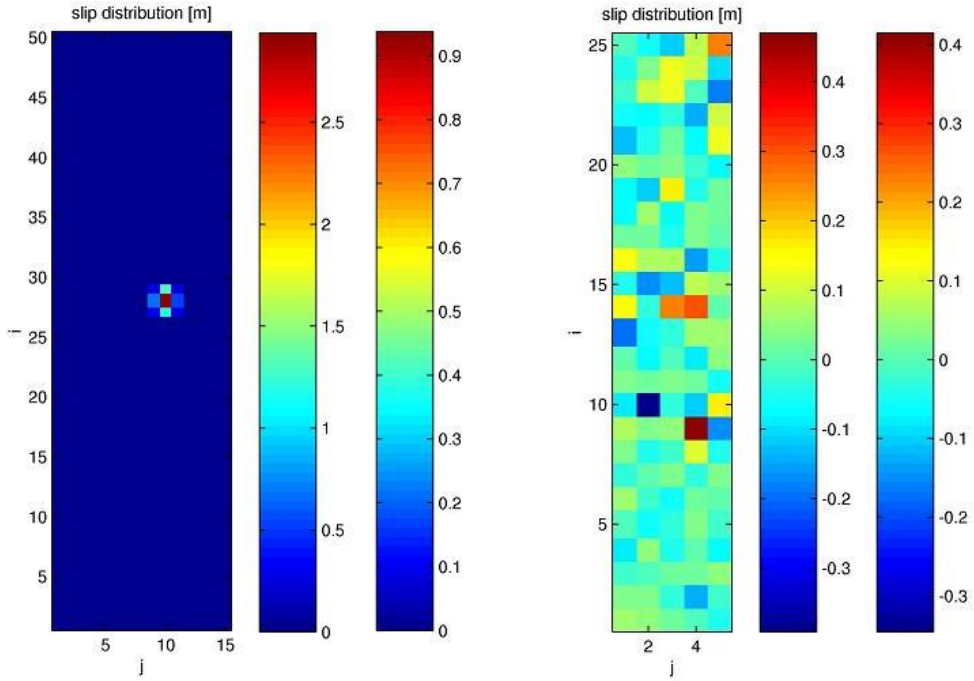


Figure A76: $M_W = 7.4$: target (left) and reconstructed, noiseless(right) slip distribution with original and normalised scale

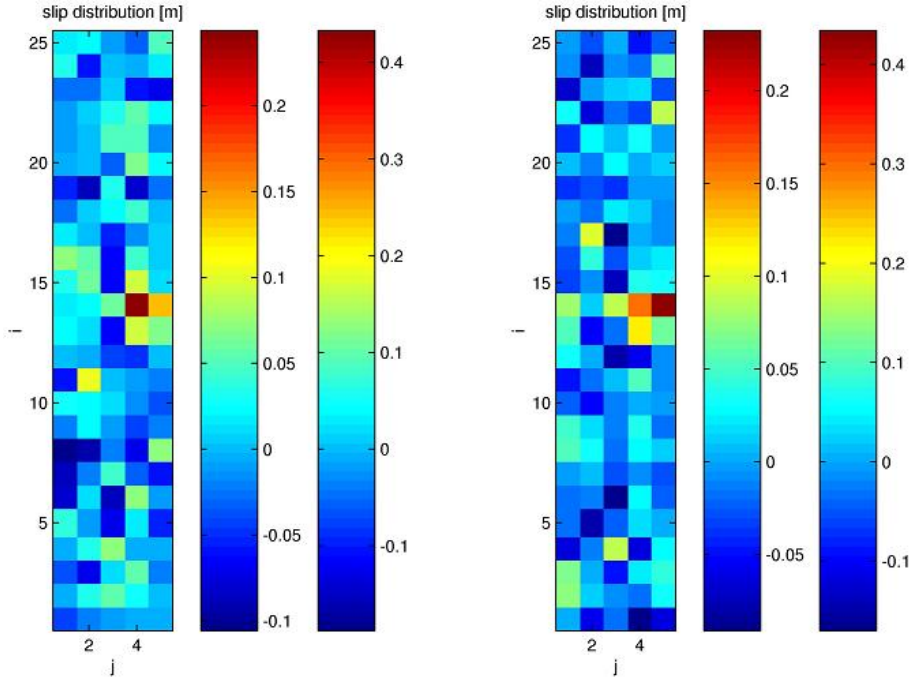


Figure A77: $M_W = 7.4$, noise level 1cm/3cm: non-stabilised (left) and stabilised (right) reconstruction of slip distribution with original and normalised scale

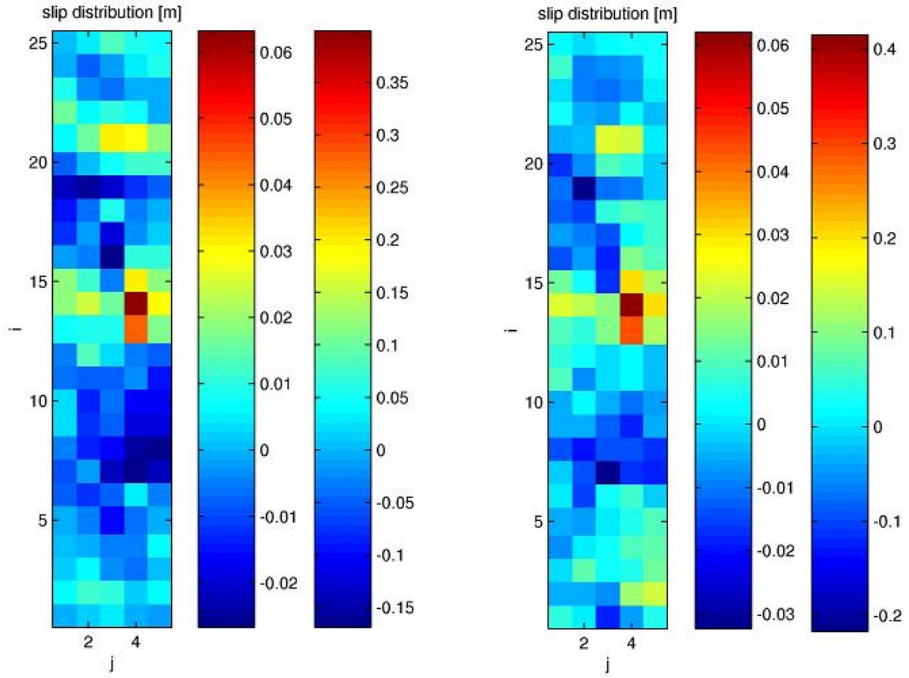


Figure A78: $M_W = 7.4$, noise level 5cm/10cm: non-stabilised (left) and stabilised (right) reconstruction of slip distribution with original and normalised scale

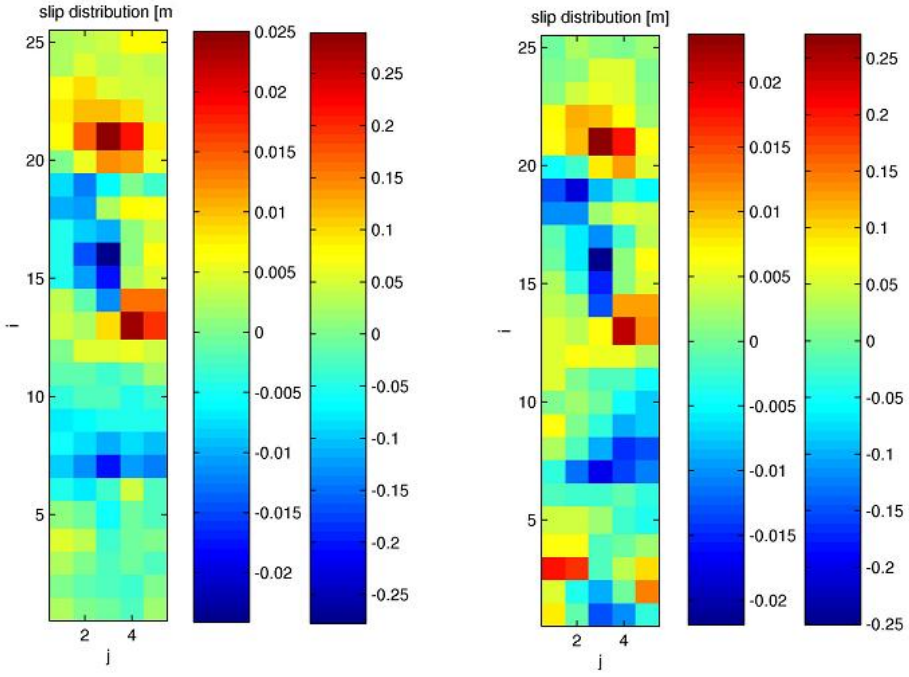


Figure A79: $M_W = 7.4$, noise level 10cm/20cm: non-stabilised (left) and stabilised (right) reconstruction of slip distribution with original and normalised scale

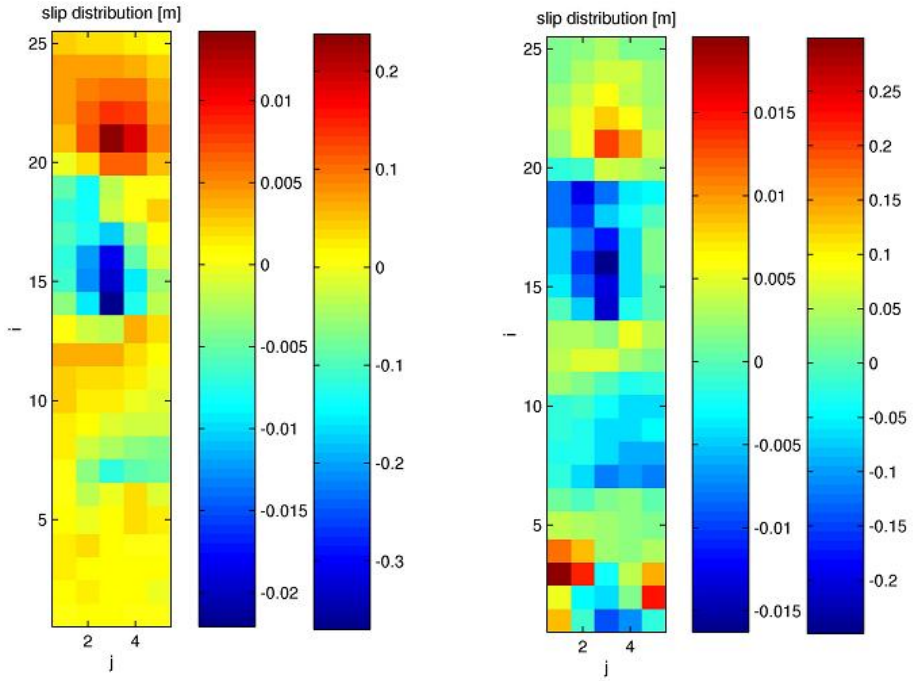


Figure A80: $M_W = 7.4$, noise level 20cm/40cm: non-stabilised (left) and stabilised (right) reconstruction of slip distribution with original and normalised scale

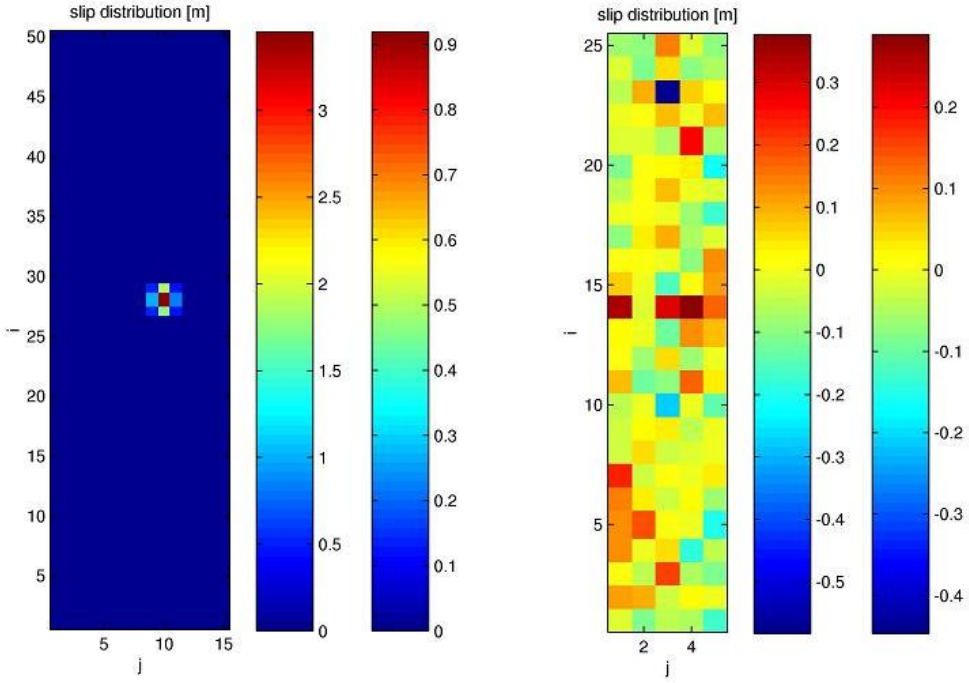


Figure A81: $M_W = 7.5$: target (left) and reconstructed, noiseless(right) slip distribution with original and normalised scale

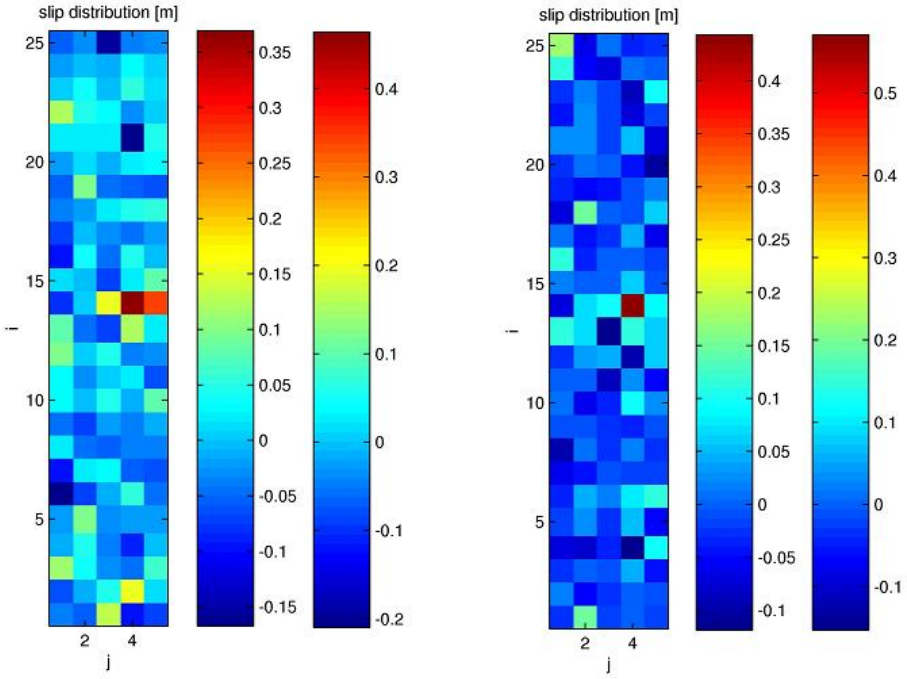


Figure A82: $M_W = 7.5$, noise level 1cm/3cm: non-stabilised (left) and stabilised (right) reconstruction of slip distribution with original and normalised scale

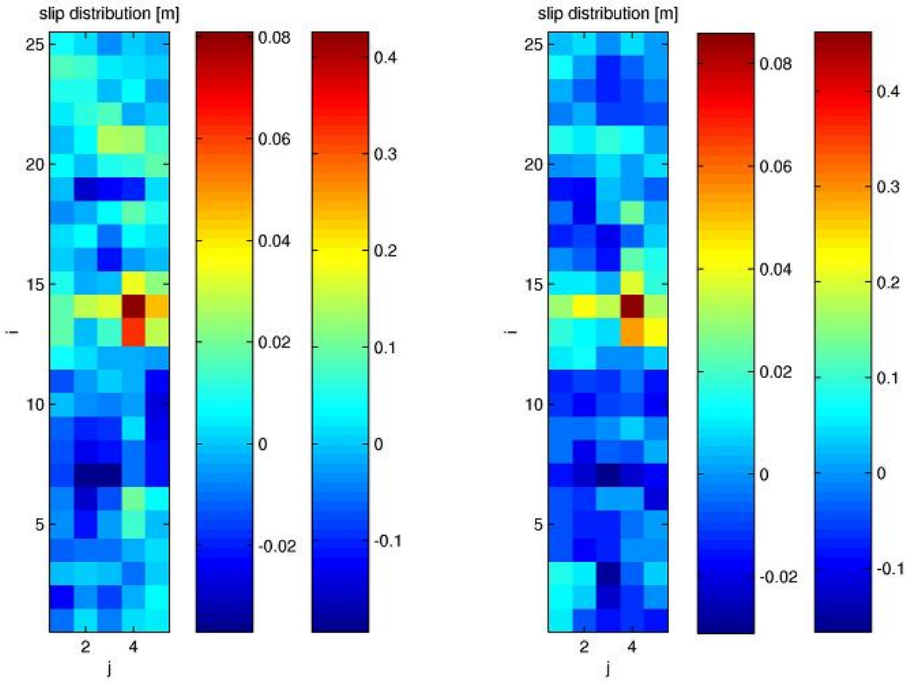


Figure A83: $M_W = 7.5$, noise level 5cm/10cm: non-stabilised (left) and stabilised (right) reconstruction of slip distribution with original and normalised scale

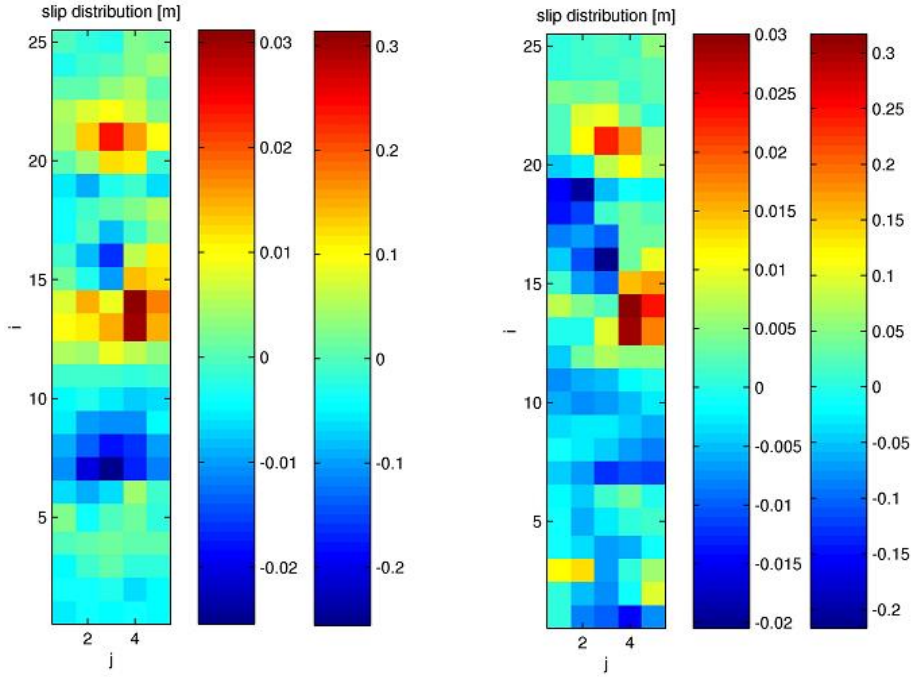


Figure A84: $M_W = 7.5$, noise level 10cm/20cm: non-stabilised (left) and stabilised (right) reconstruction of slip distribution with original and normalised scale

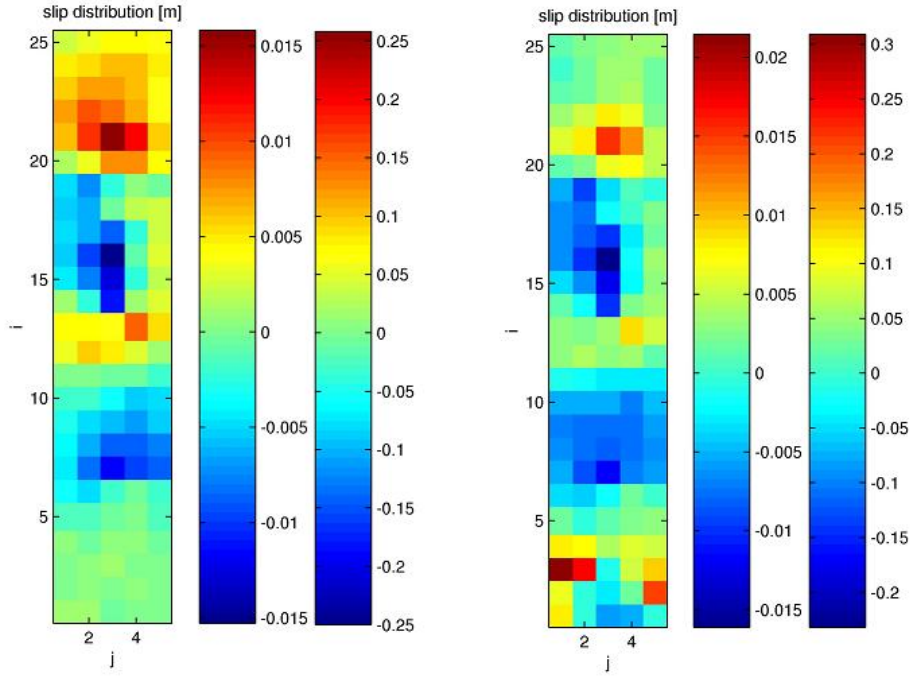


Figure A85: $M_W = 7.5$, noise level 20cm/40cm: non-stabilised (left) and stabilised (right) reconstruction of slip distribution with original and normalised scale

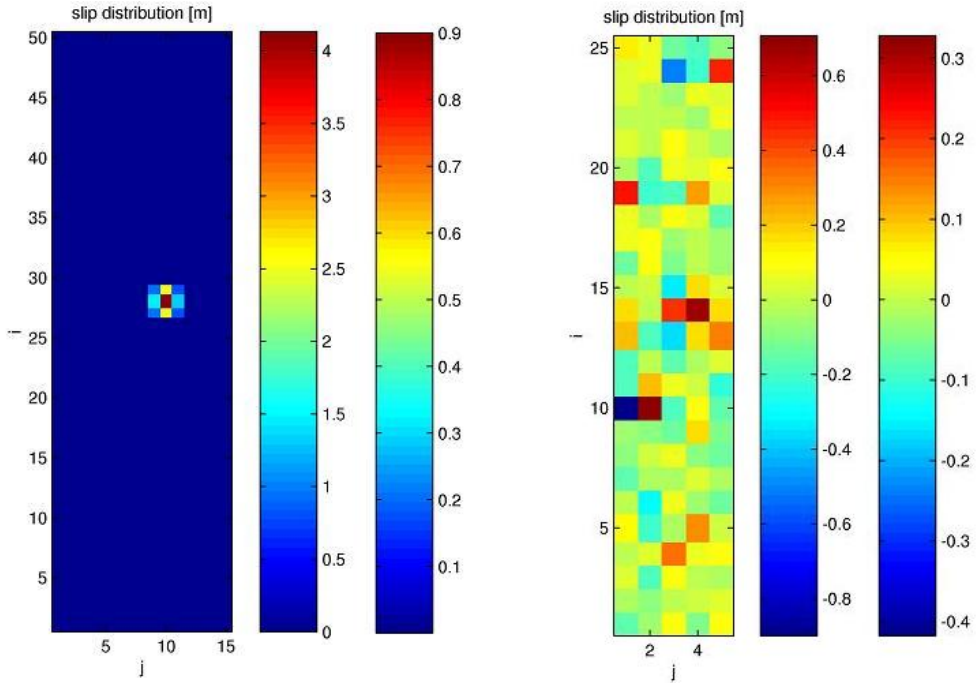


Figure A86: $M_W = 7.6$: target (left) and reconstructed, noiseless(right) slip distribution with original and normalised scale

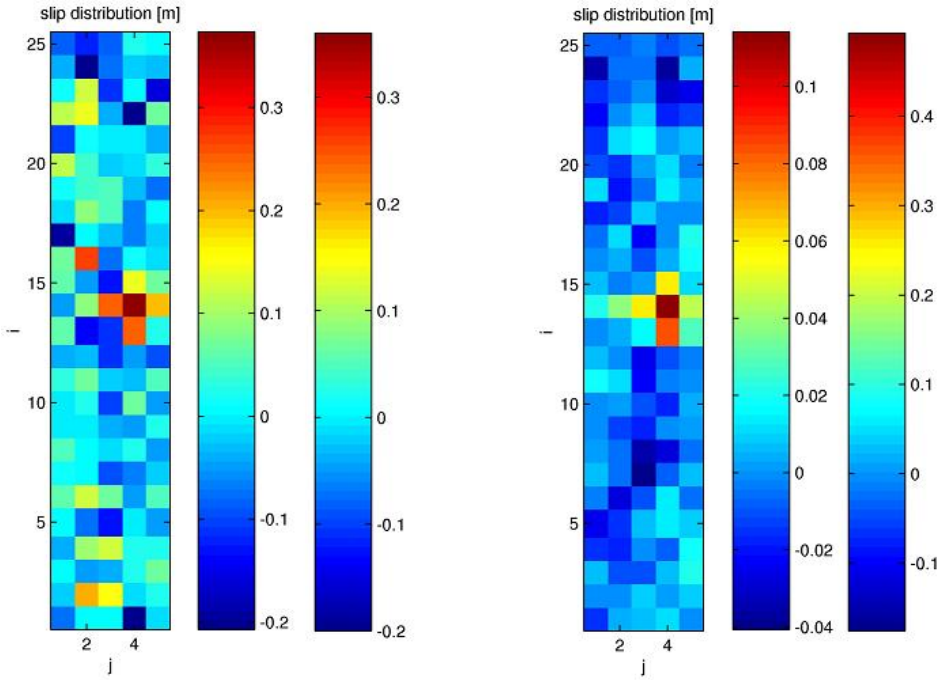


Figure A87: $M_W = 7.6$, noise levels: 1cm/3cm (left), 5cm/10cm (right): reconstruction of slip distribution with original and normalised scale

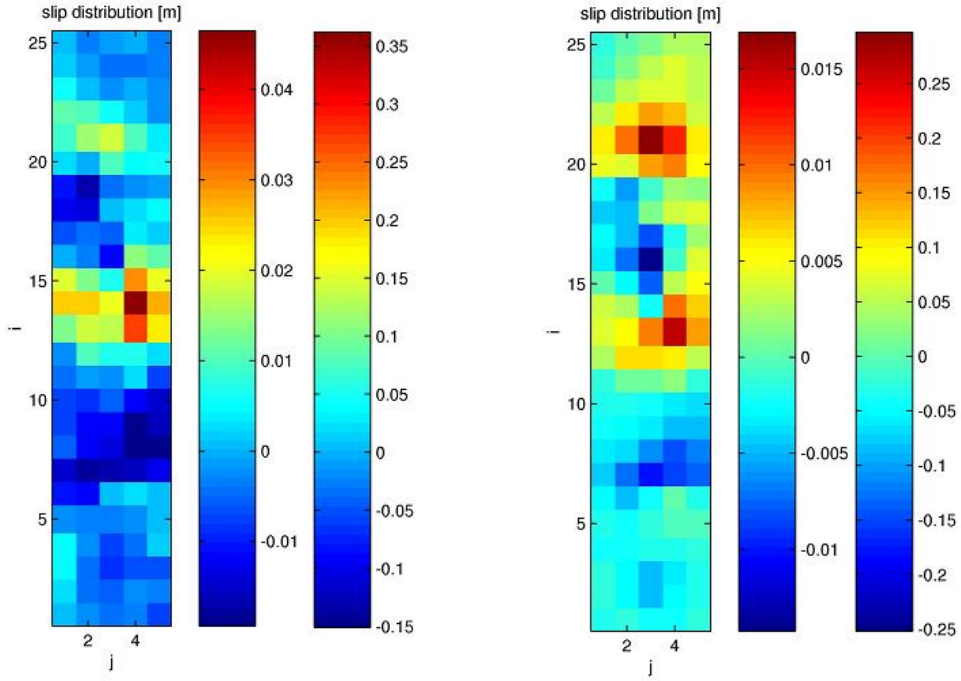


Figure A88: $M_W = 7.6$, noise levels: 10cm/20cm (left), 20cm/40cm (right): reconstruction of slip distribution with original and normalised scale

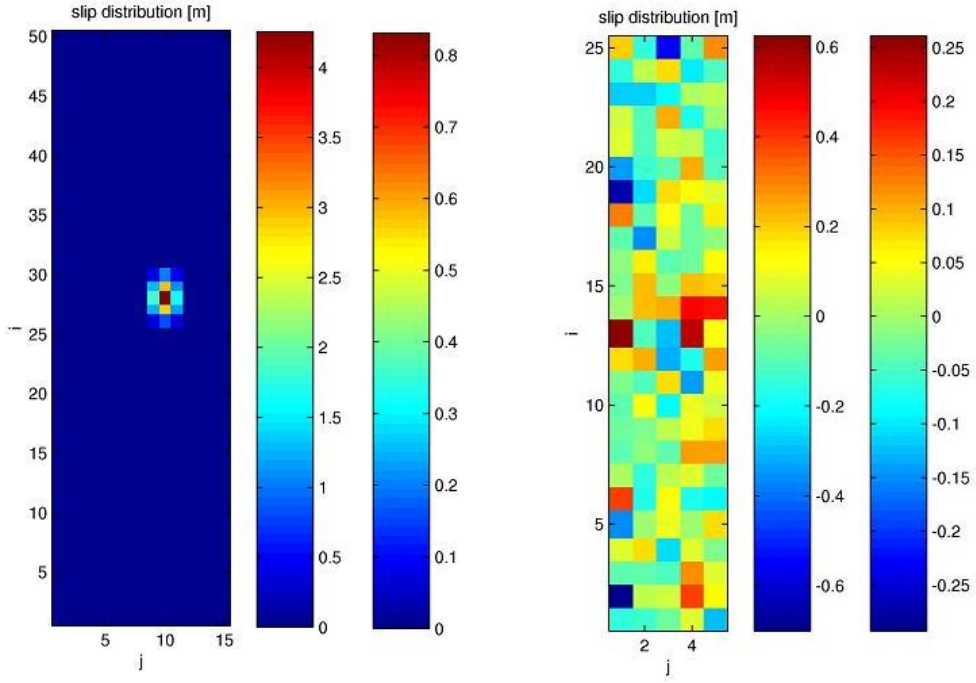


Figure A89: $M_W = 7.7$: target (left) and reconstructed, noiseless(right) slip distribution with original and normalised scale

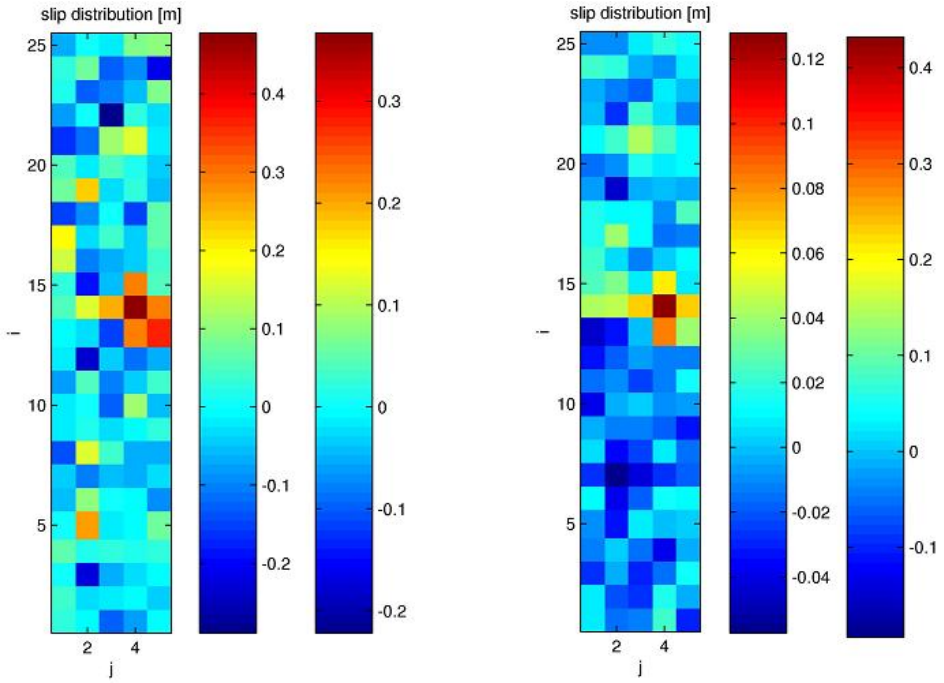


Figure A90: $M_W = 7.7$, noise levels: 1cm/3cm (left), 5cm/10cm (right): reconstruction of slip distribution with original and normalised scale

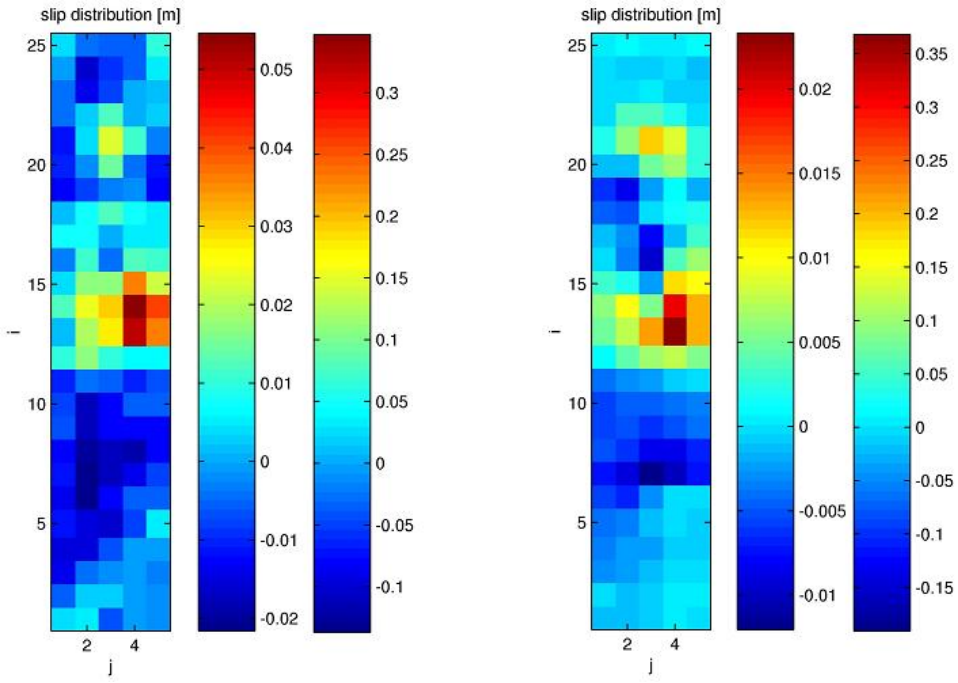


Figure A91: $M_W = 7.7$, noise levels: 10cm/20cm (left), 20cm/40cm (right): reconstruction of slip distribution with original and normalised scale

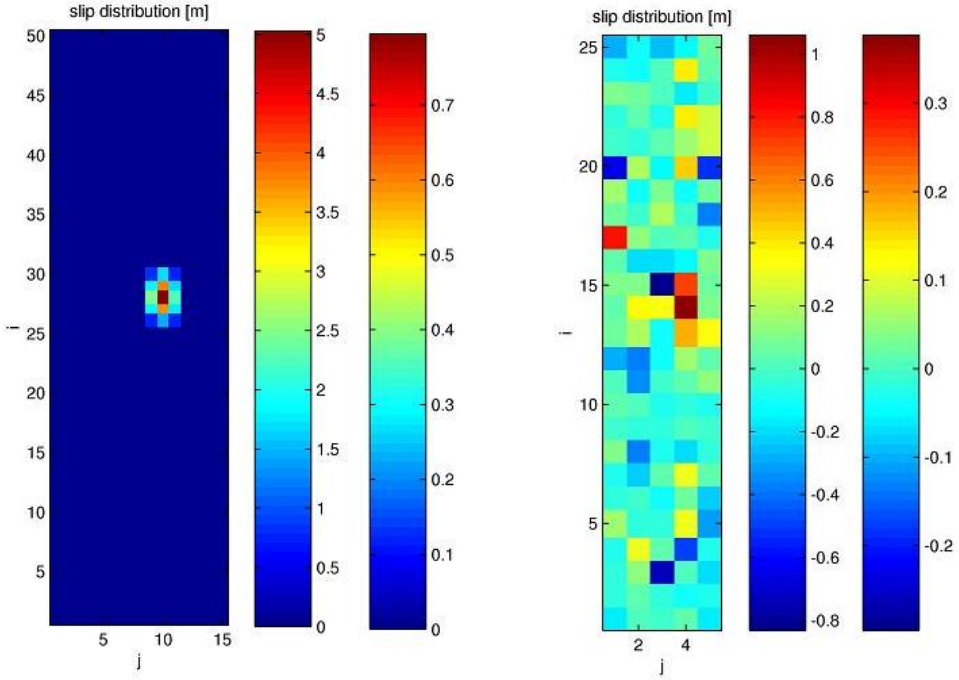


Figure A92: $M_W = 7.8$: target (left) and reconstructed, noiseless(right) slip distribution with original and normalised scale

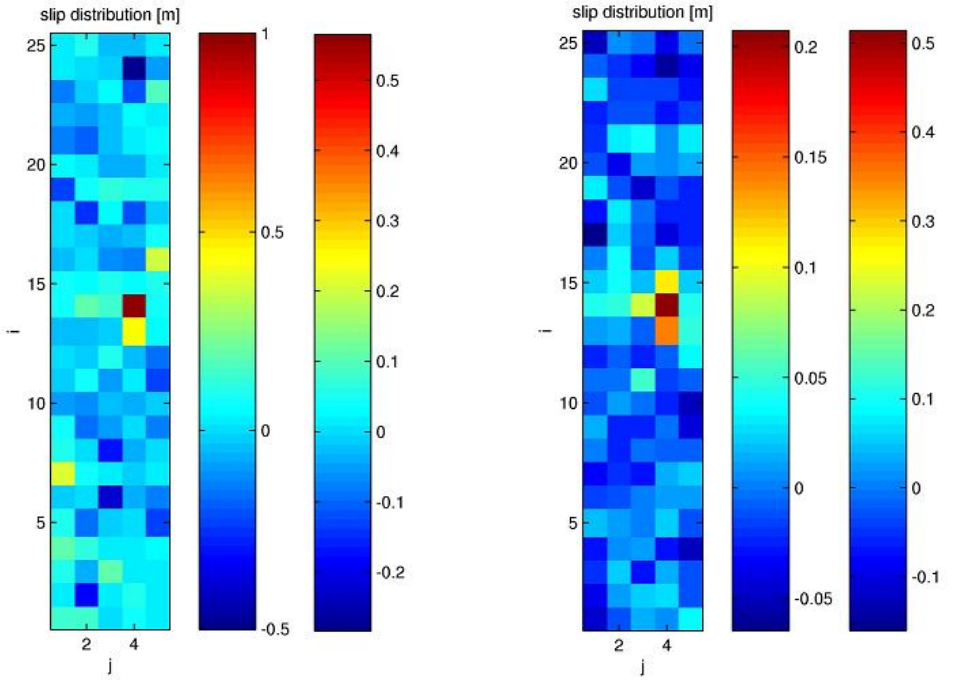


Figure A93: $M_W = 7.8$, noise levels: 1cm/3cm (left), 5cm/10cm (right): reconstruction of slip distribution with original and normalised scale

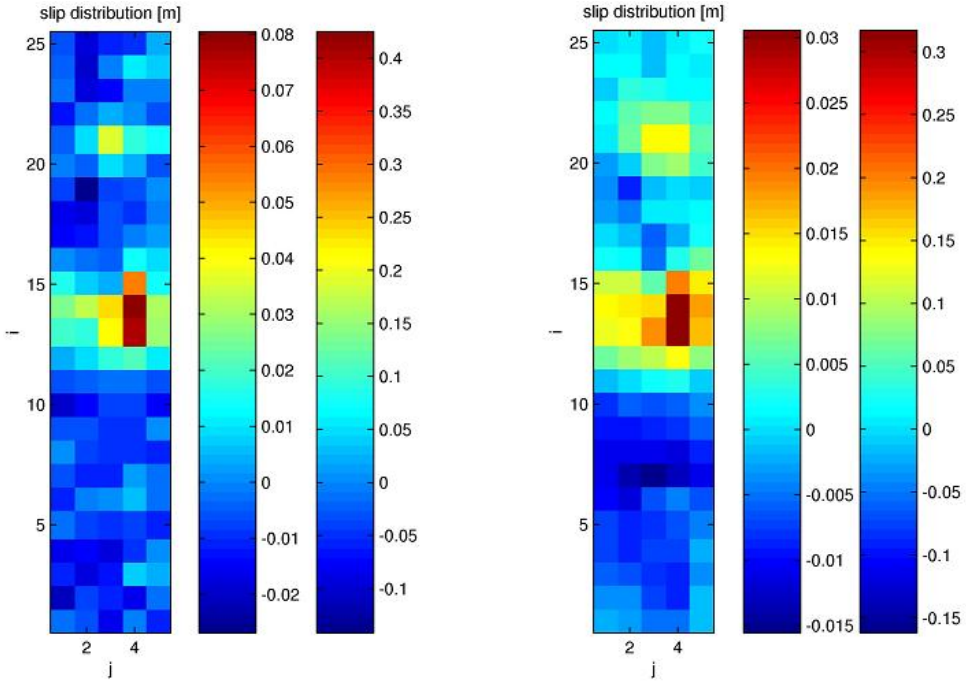


Figure A94: $M_W = 7.8$, noise levels: 10cm/20cm (left), 20cm/40cm (right): reconstruction of slip distribution with original and normalised scale

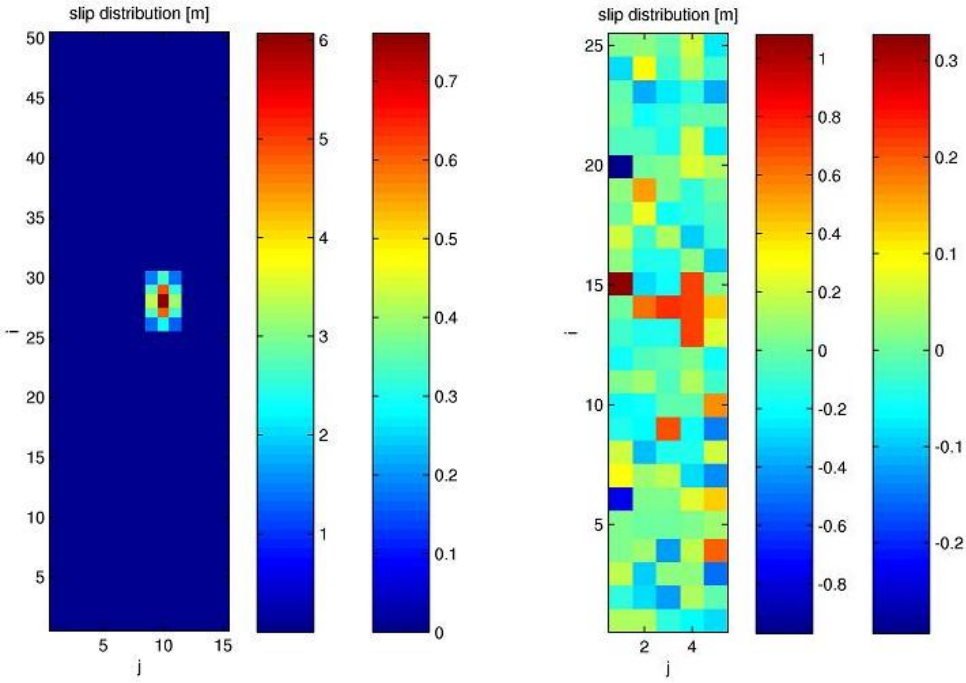


Figure A95: $M_W = 7.9$: target (left) and reconstructed, noiseless(right) slip distribution with original and normalised scale

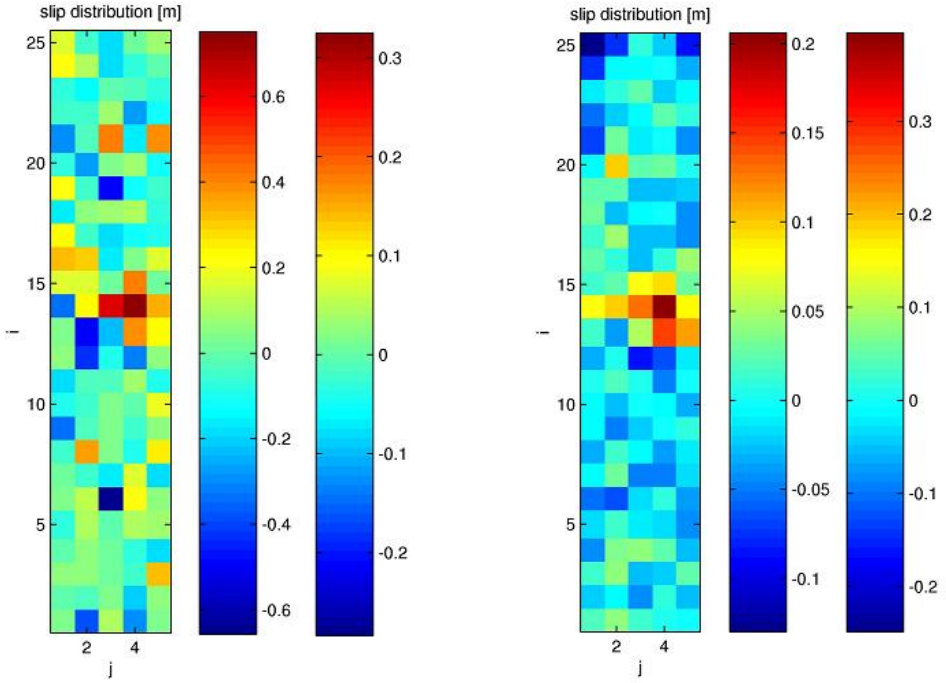


Figure A96: $M_W = 7.9$, noise levels: 1cm/3cm (left), 5cm/10cm (right): reconstruction of slip distribution with original and normalised scale

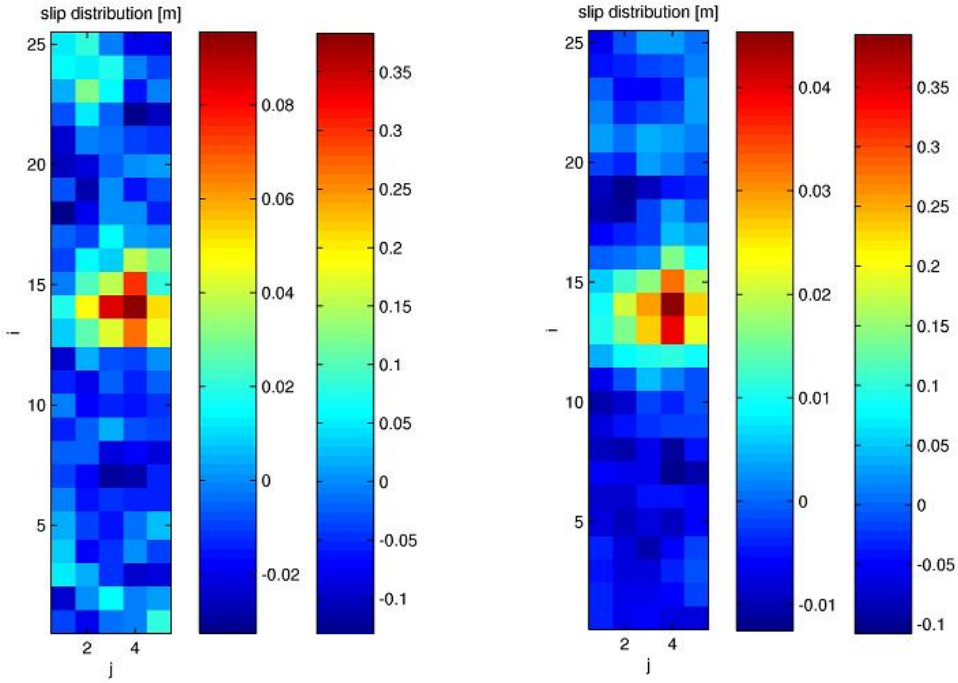


Figure A97: $M_W = 7.9$, noise levels: 10cm/20cm (left), 20cm/40cm (right): reconstruction of slip distribution with original and normalised scale

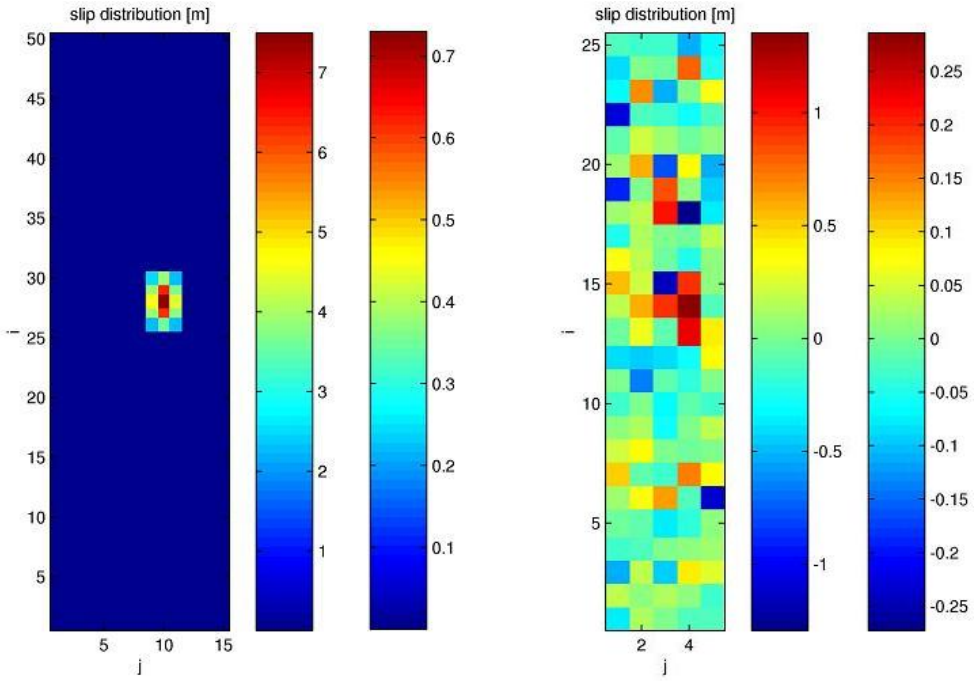


Figure A98: $M_W = 8.0$: target (left) and reconstructed, noiseless(right) slip distribution with original and normalised scale

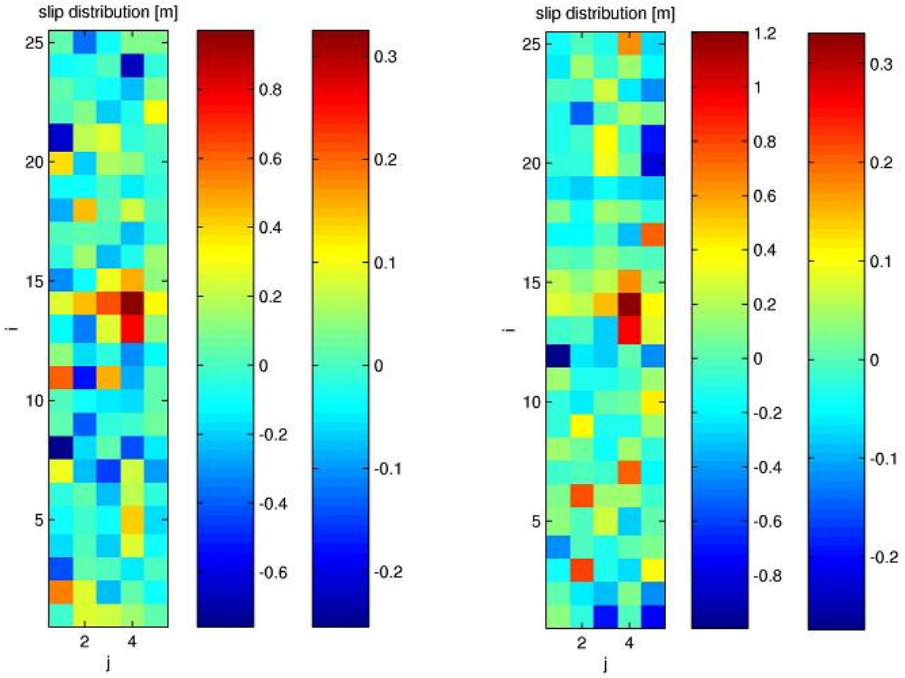


Figure A99: $M_W = 8.0$, noise level 1cm/3cm: non-stabilised (left) and stabilised (right) reconstruction of slip distribution with original and normalised scale

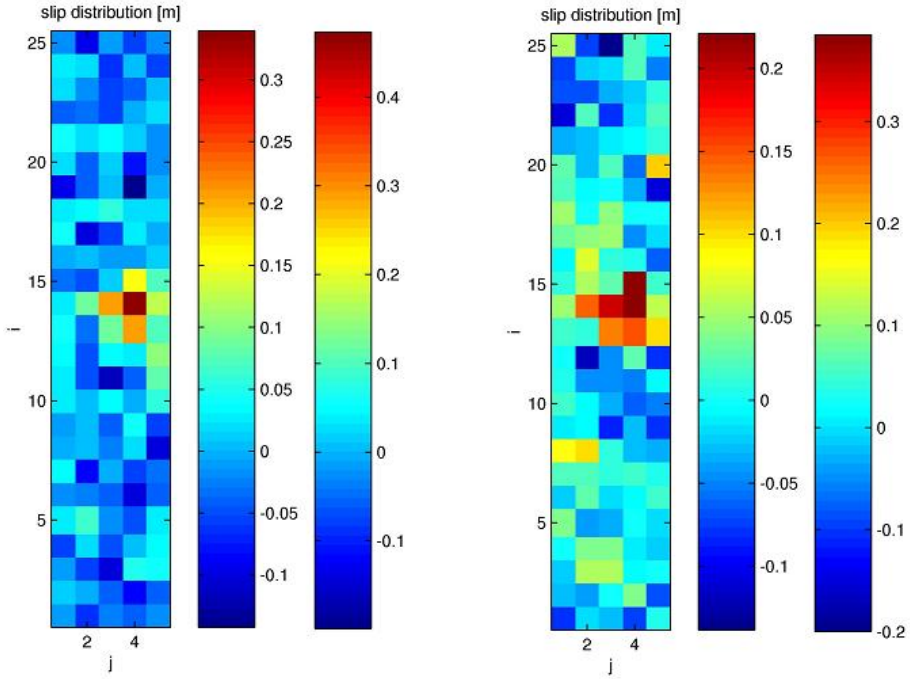


Figure A100: $M_W = 8.0$, noise level 5cm/10cm: non-stabilised (left) and stabilised (right) reconstruction of slip distribution with original and normalised scale

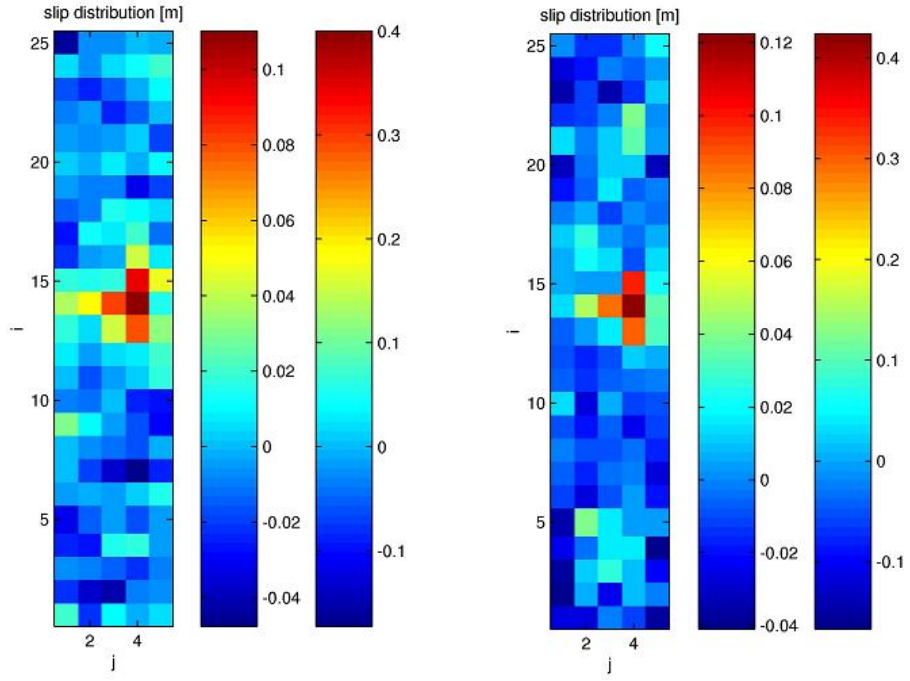


Figure A101: $M_W = 8.0$, noise level 10cm/20cm: non-stabilised (left) and stabilised (right) reconstruction of slip distribution with original and normalised scale

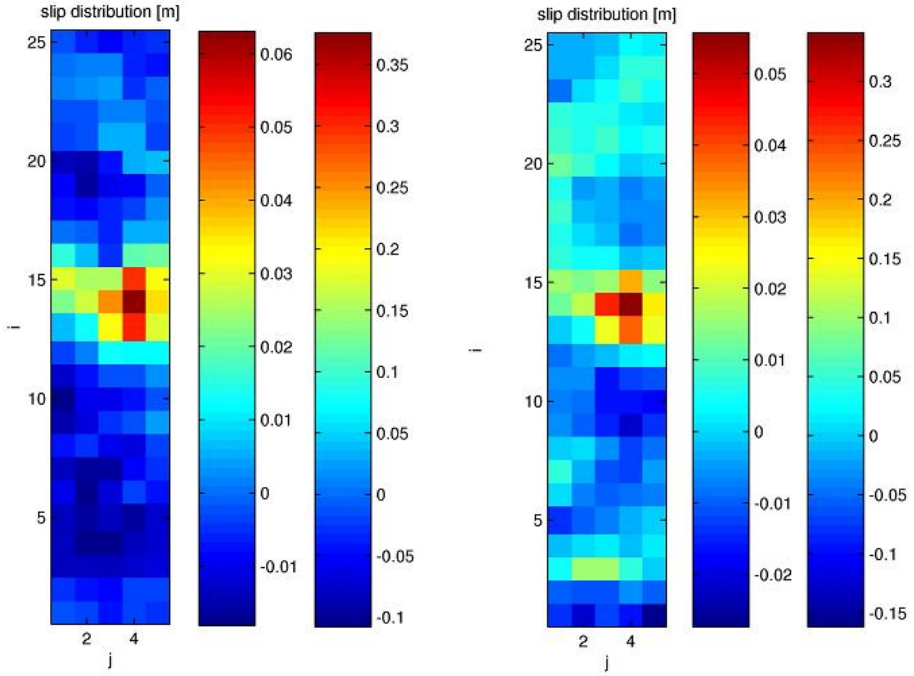


Figure A102: $M_W = 8.0$, noise level 20cm/40cm: non-stabilised (left) and stabilised (right) reconstruction of slip distribution with original and normalised scale

### A.1.3 Slip as graph

Normalised target ("slip") and reconstructed slip (noiseless = "slipopt", noise level 1cm/3cm = "slipopt_1_3", et cetera) can be found in following figures.

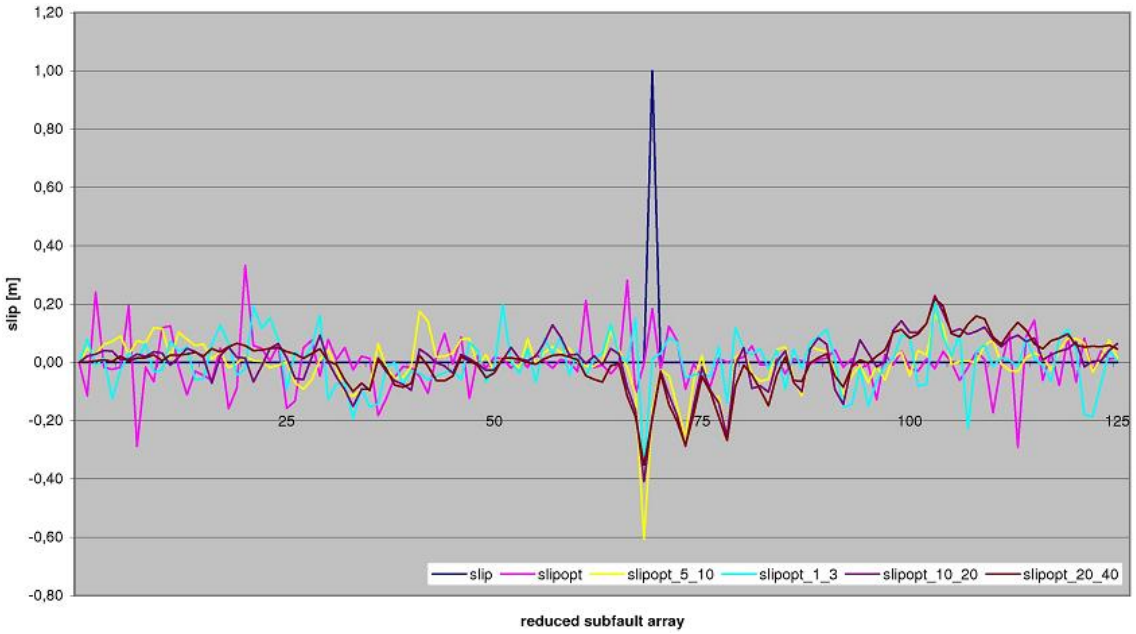


Figure A103: $M_W = 6.0$

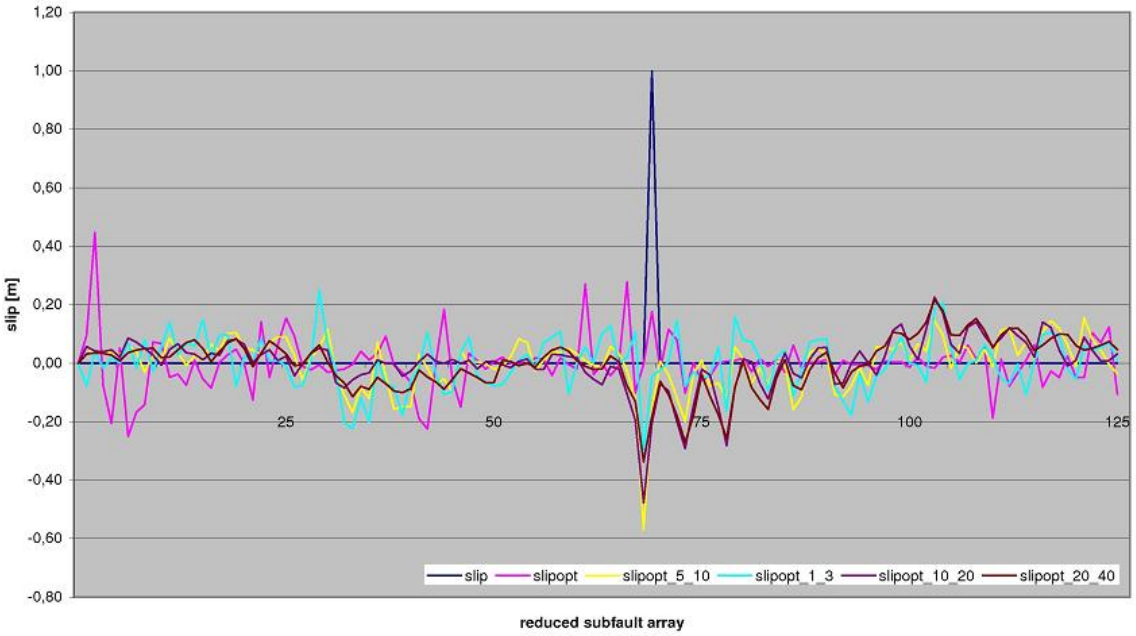


Figure A104: $M_W = 6.1$

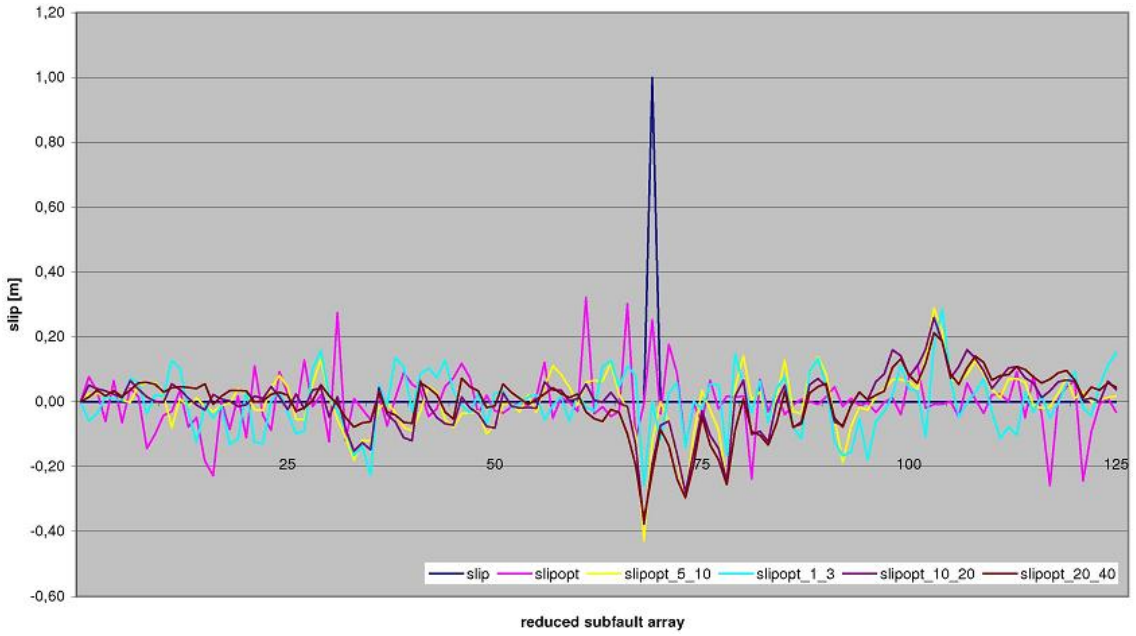


Figure A105: $M_W = 6.2$

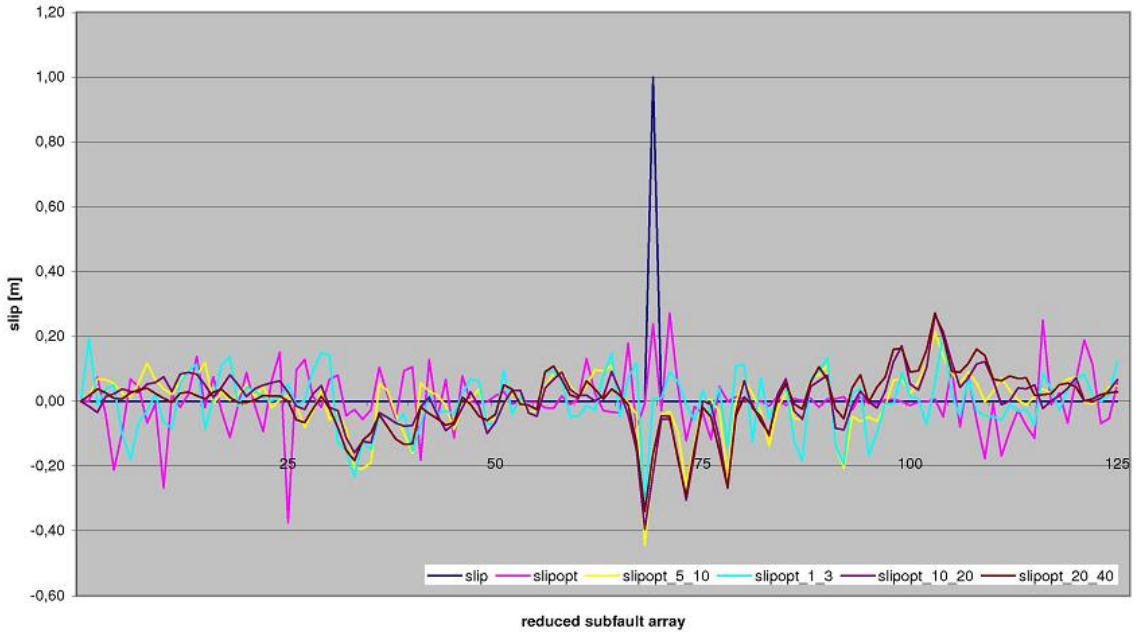


Figure A106: $M_W = 6.3$

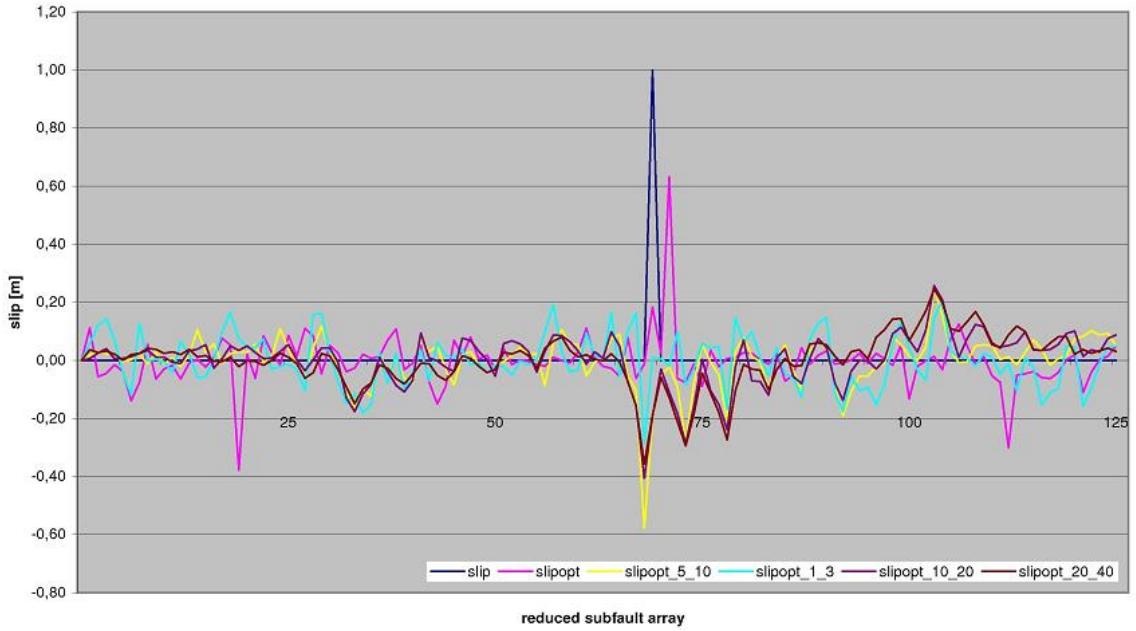


Figure A107: $M_W = 6.4$

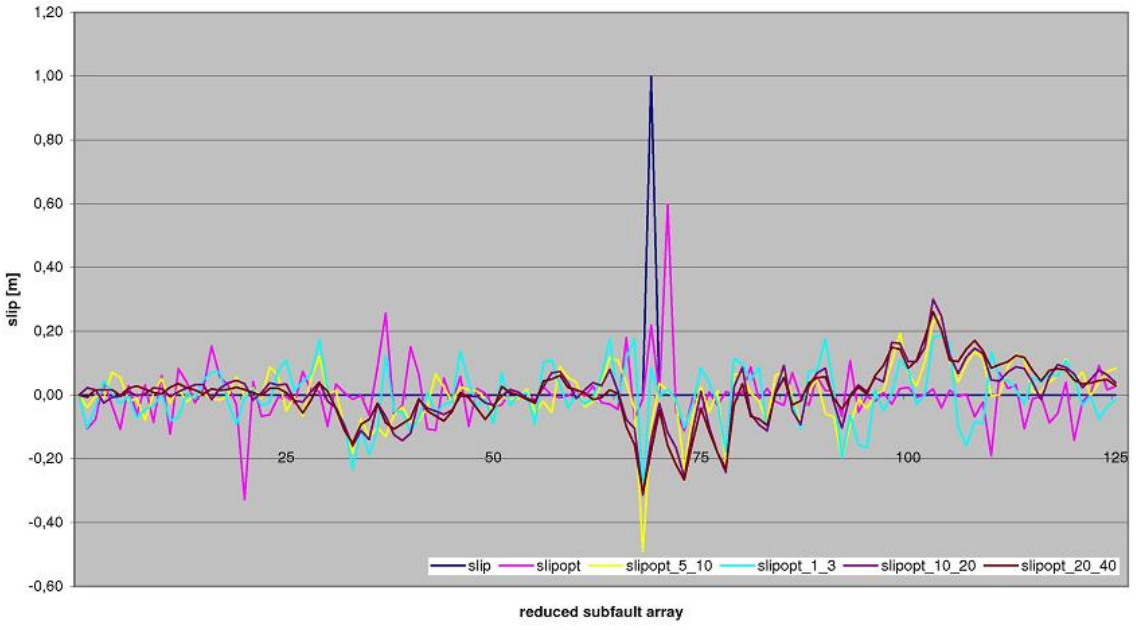


Figure A108: $M_W = 6.5$

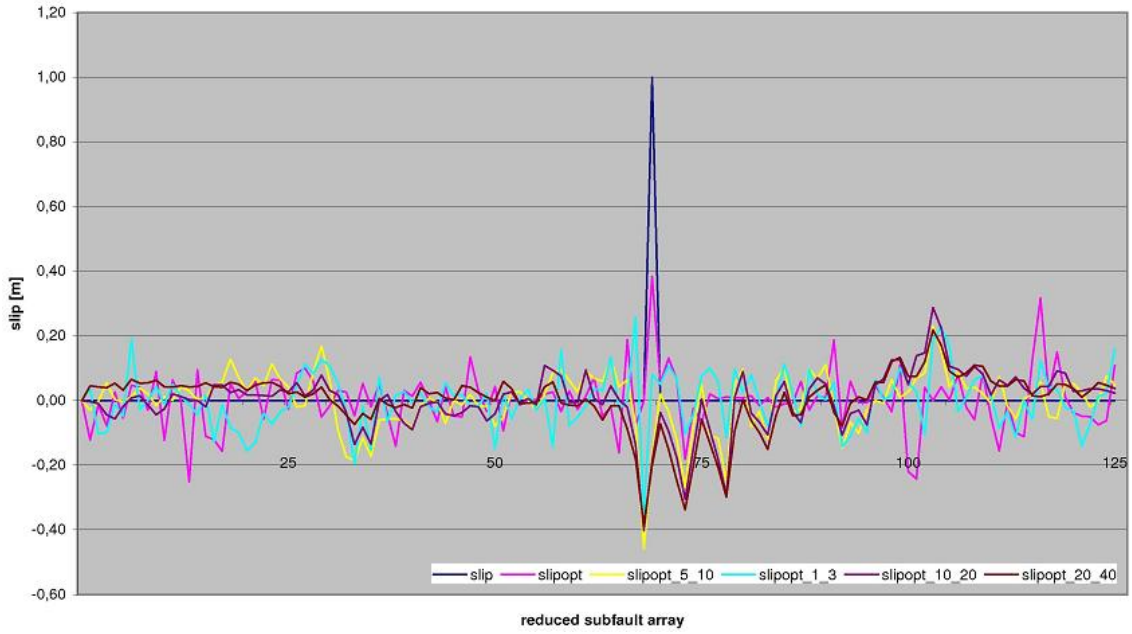


Figure A109: $M_W = 6.6$

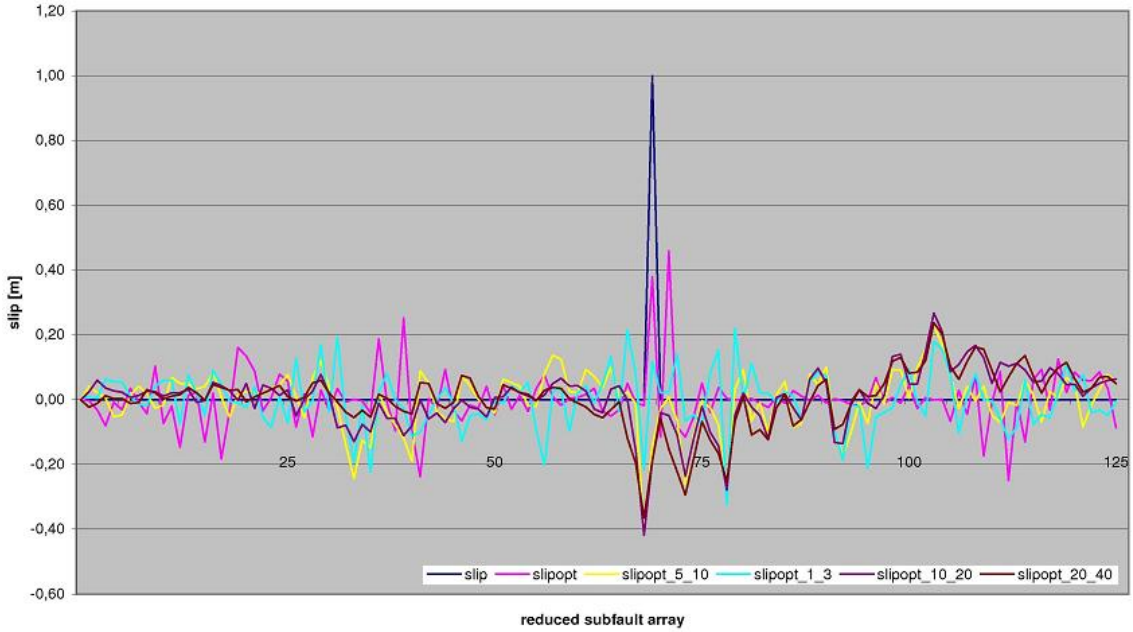


Figure A110: $M_W = 6.7$

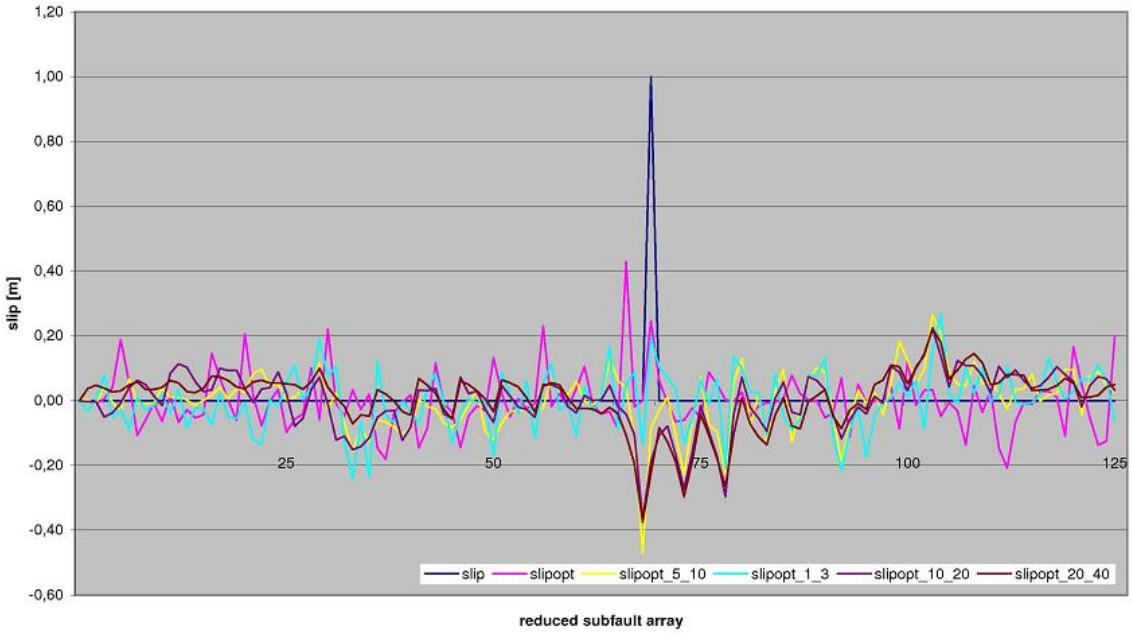


Figure A111: $M_W = 6.8$

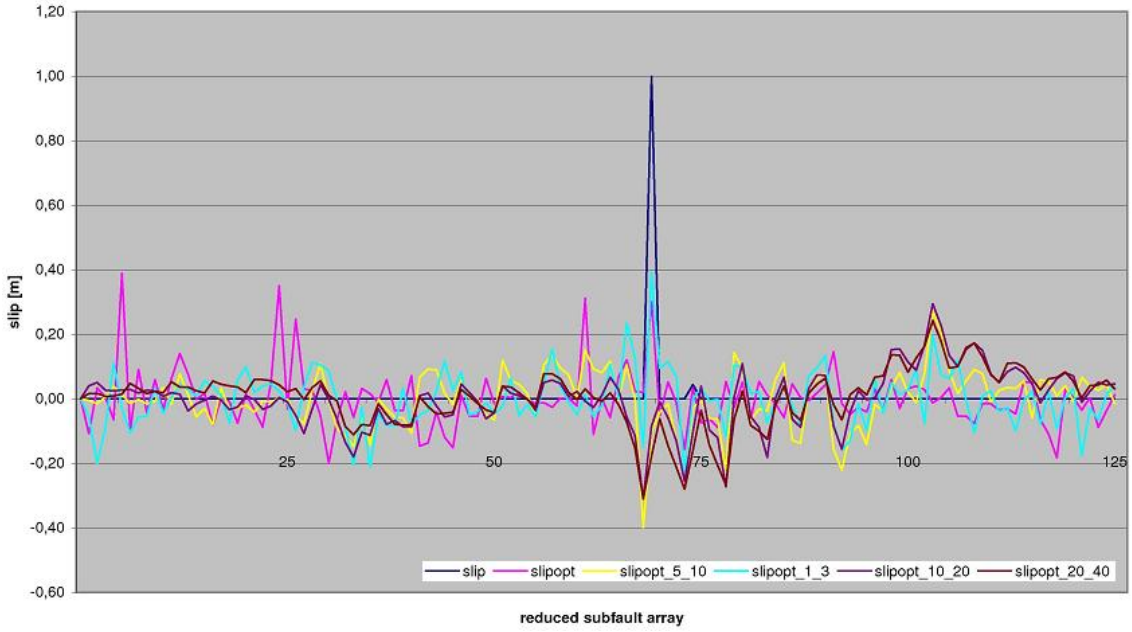


Figure A112: $M_W = 6.9$

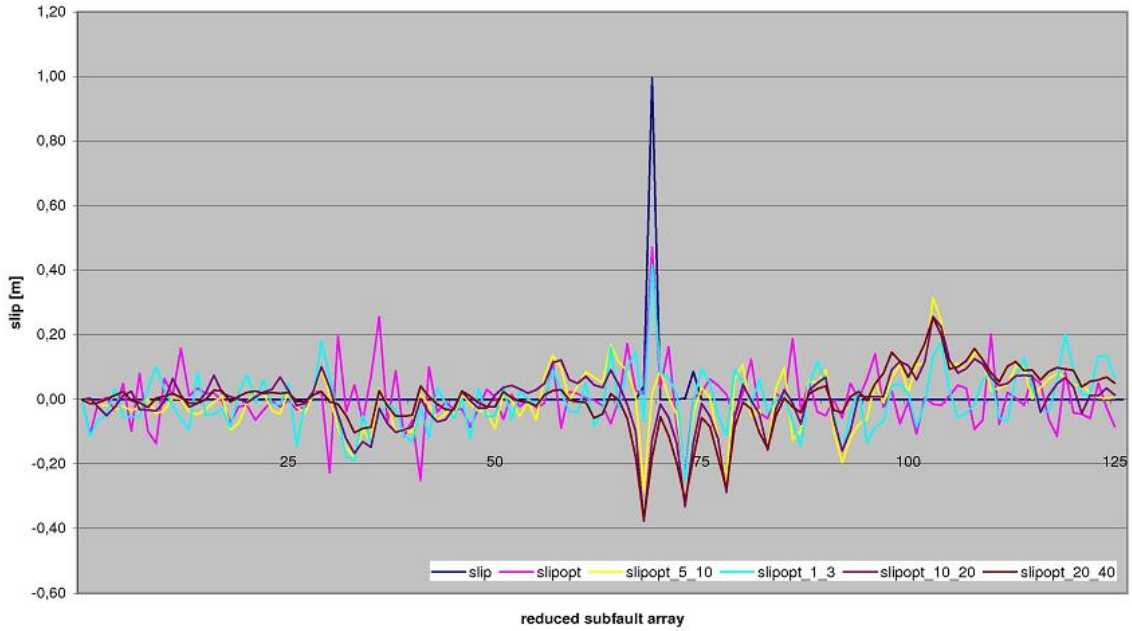


Figure A113: $M_W = 7.0$

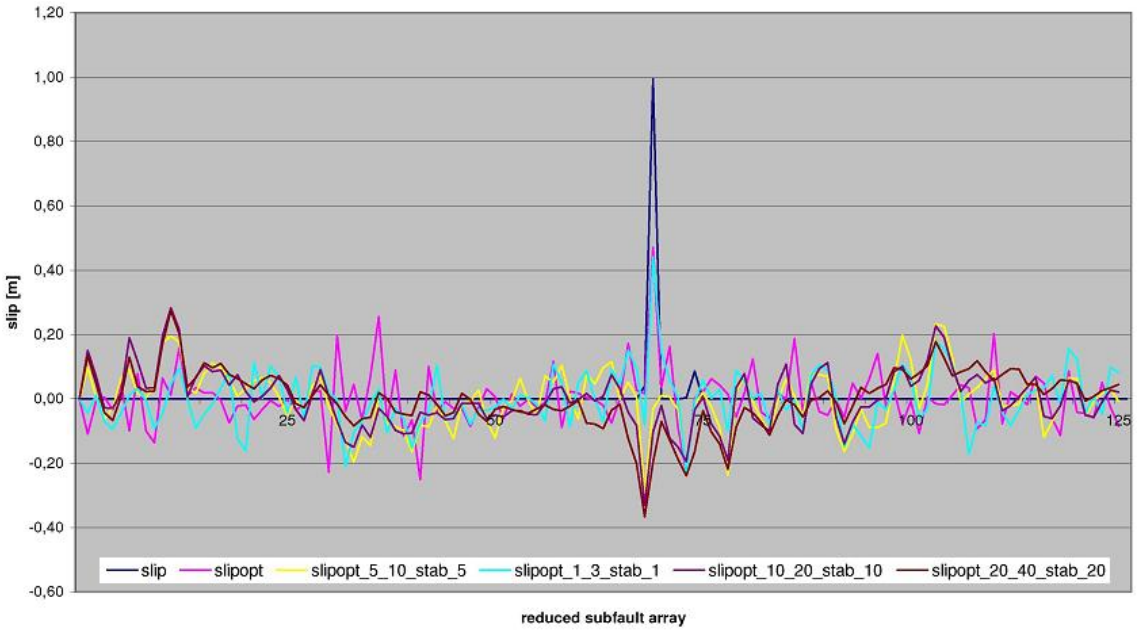


Figure A114: $M_W = 7.0$, stabilised

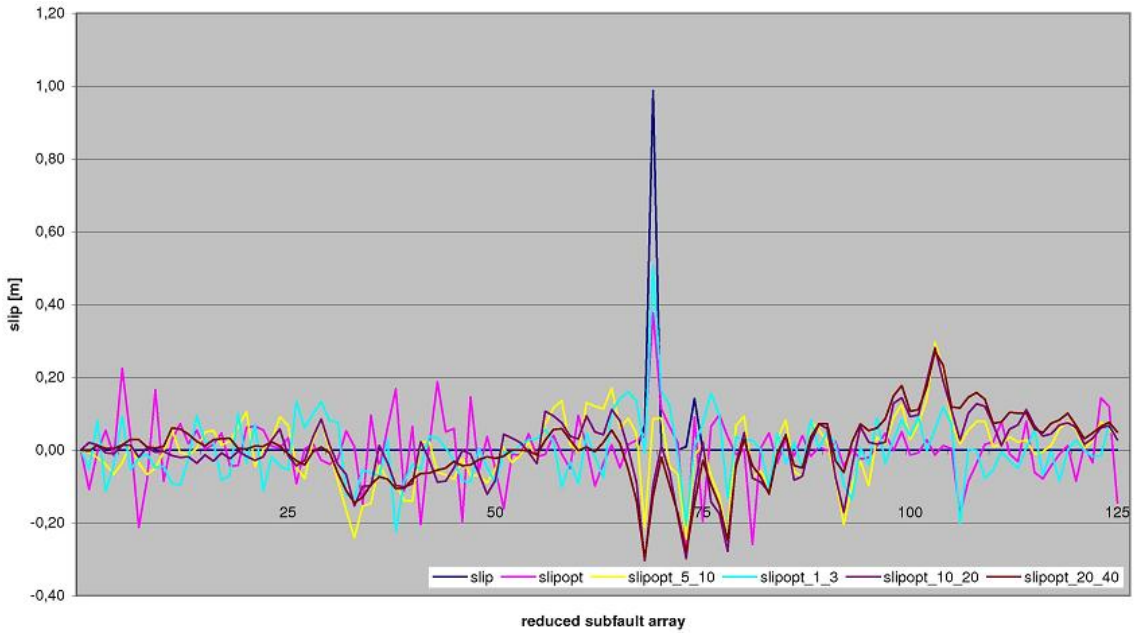


Figure A115: $M_W = 7.1$

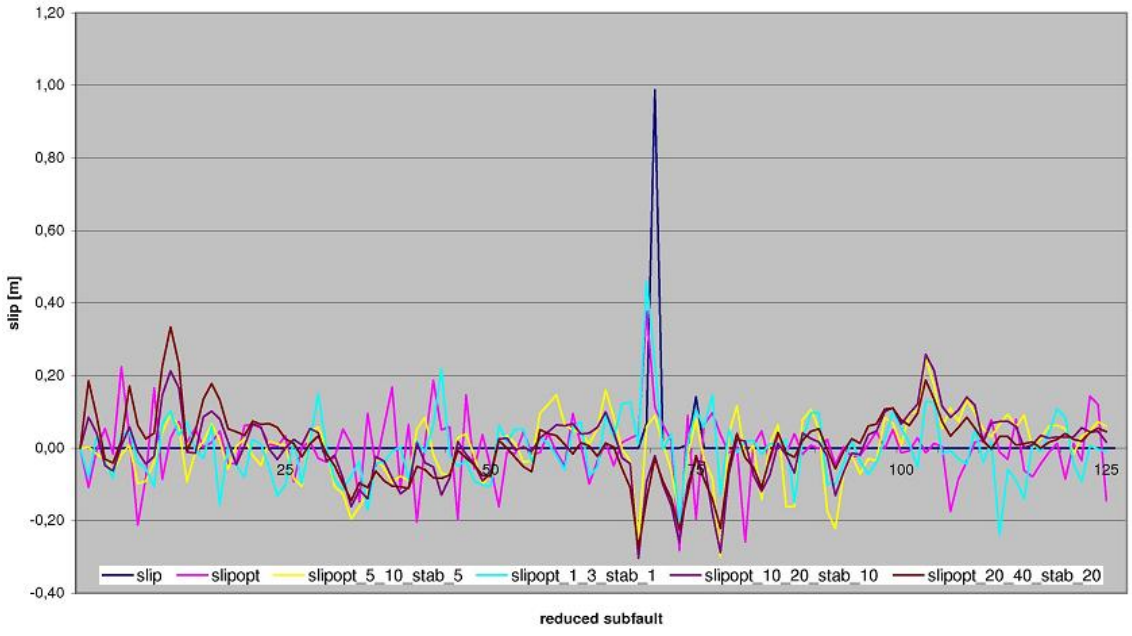


Figure A116: $M_W = 7.1$, stabilised

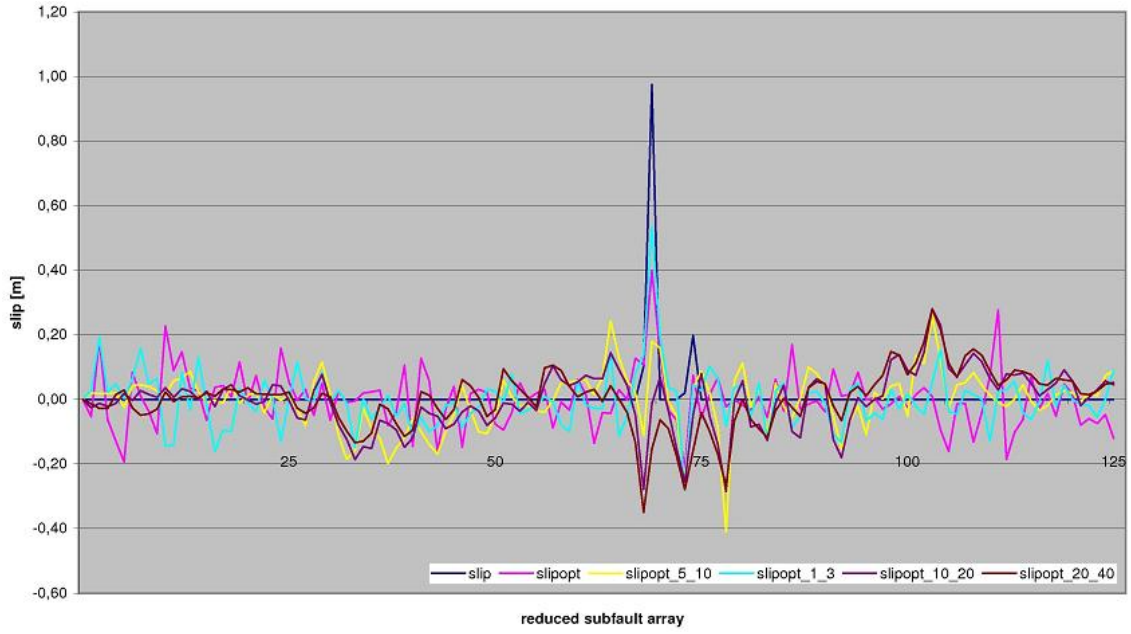


Figure A117: $M_W = 7.2$

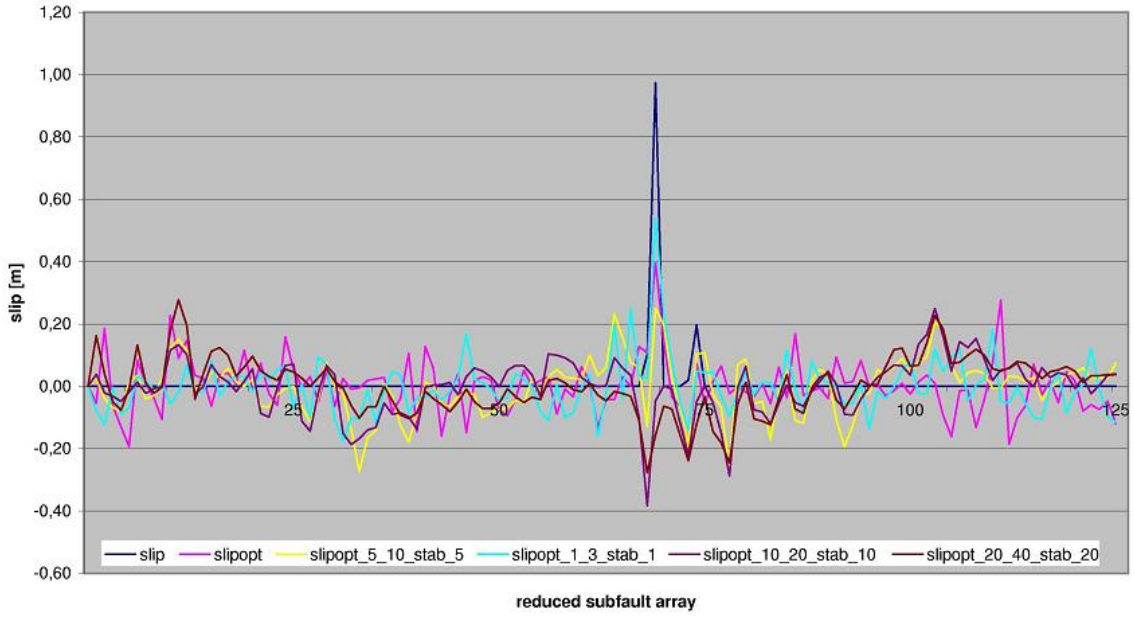


Figure A118: $M_W = 7.2$

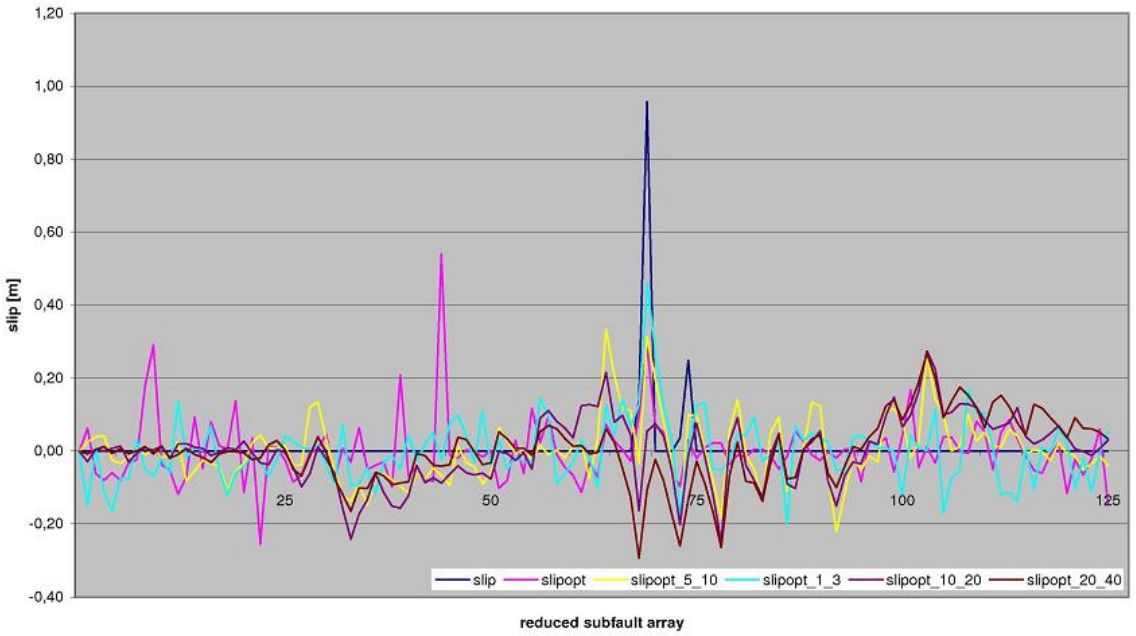


Figure A119: $M_W = 7.3$

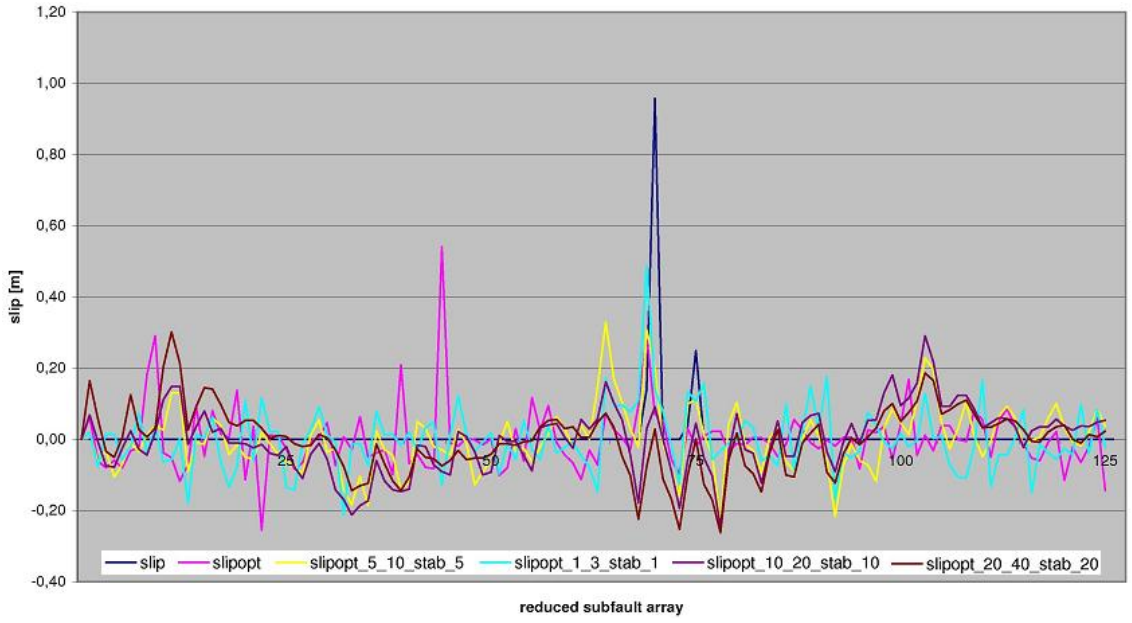


Figure A120: $M_W = 7.3$, stabilised

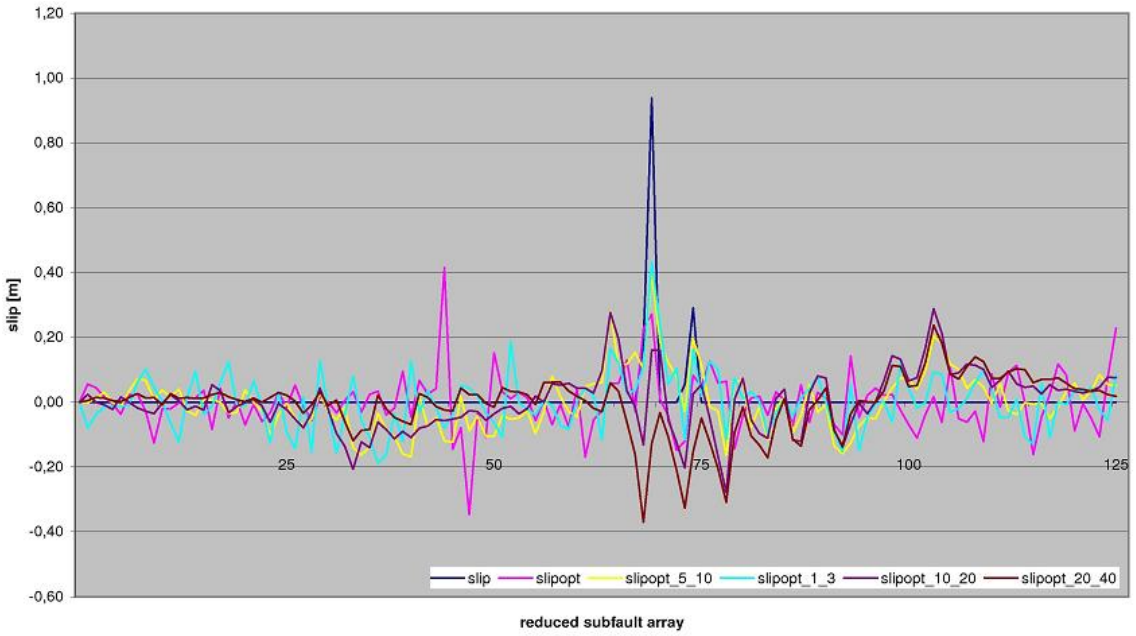


Figure A121: $M_W = 7.4$

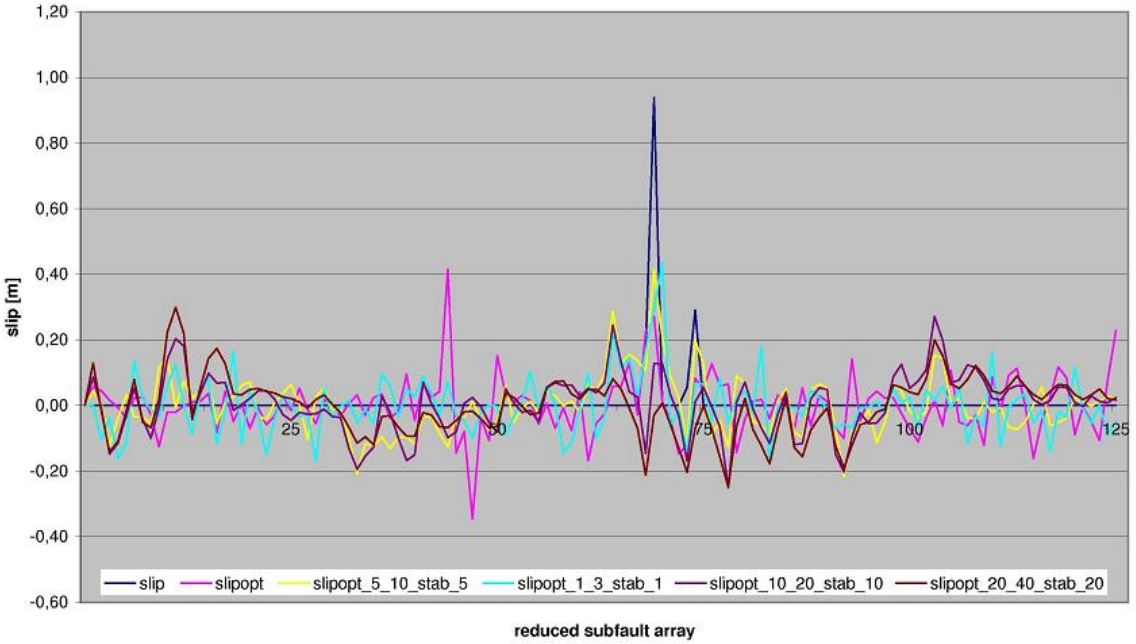


Figure A122: $M_W = 7.4$, stabilised

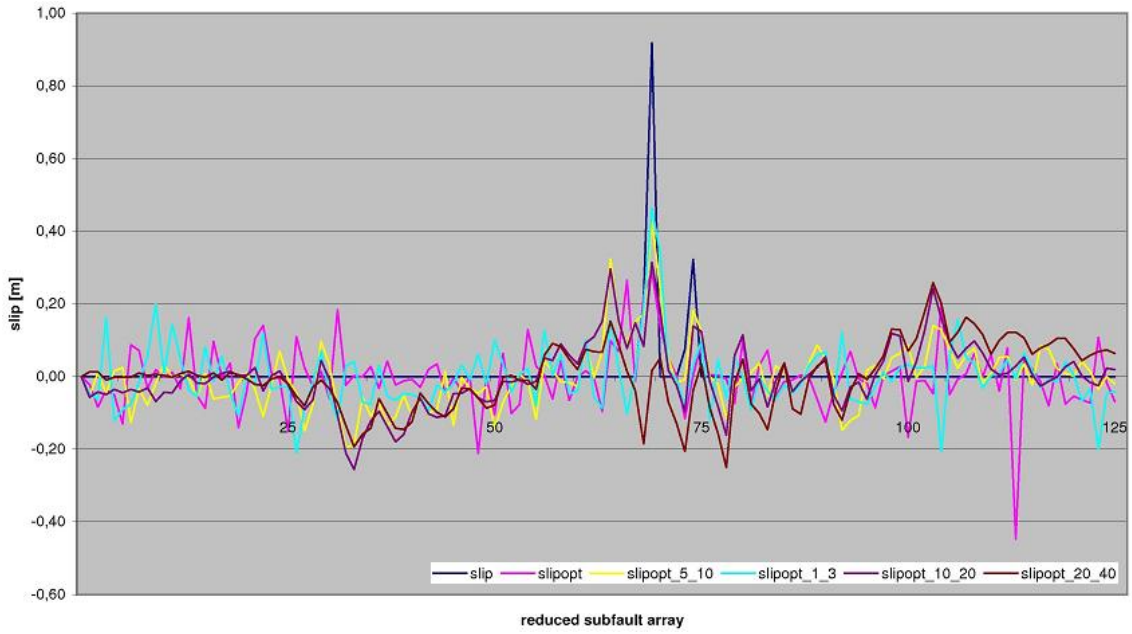


Figure A123: $M_W = 7.5$

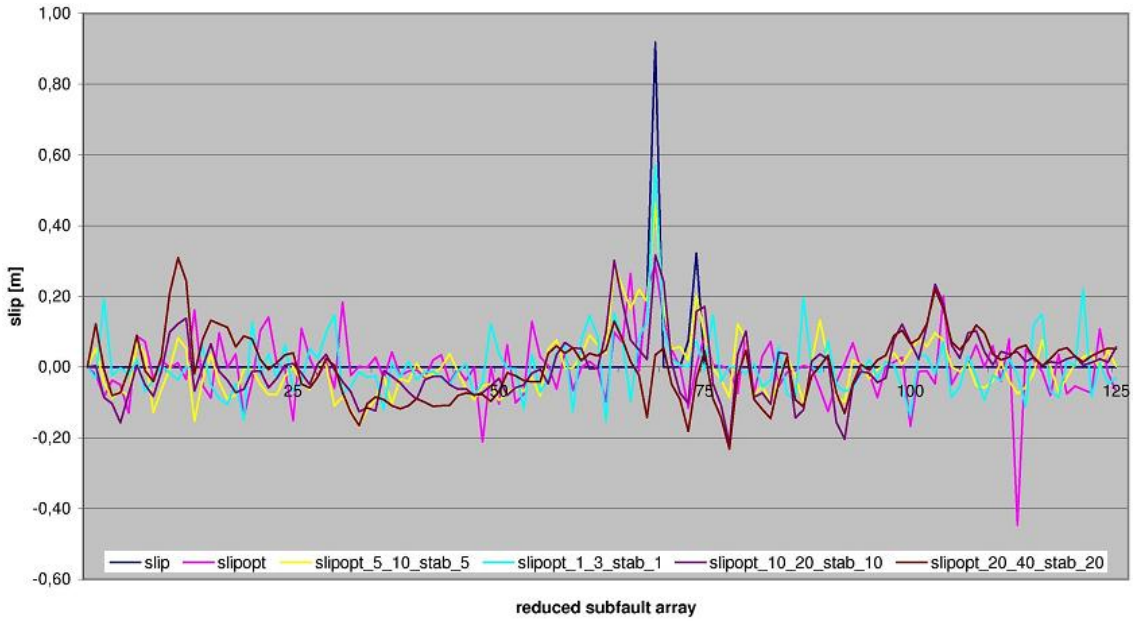


Figure A124: $M_W = 7.5$, stabilised

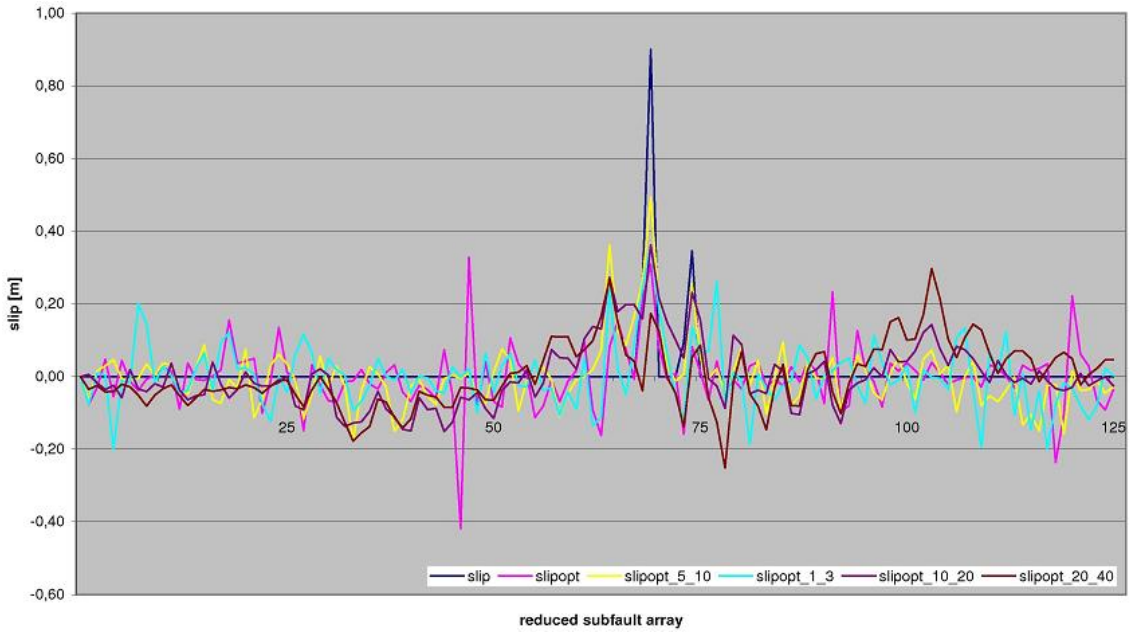


Figure A125: $M_W = 7.6$

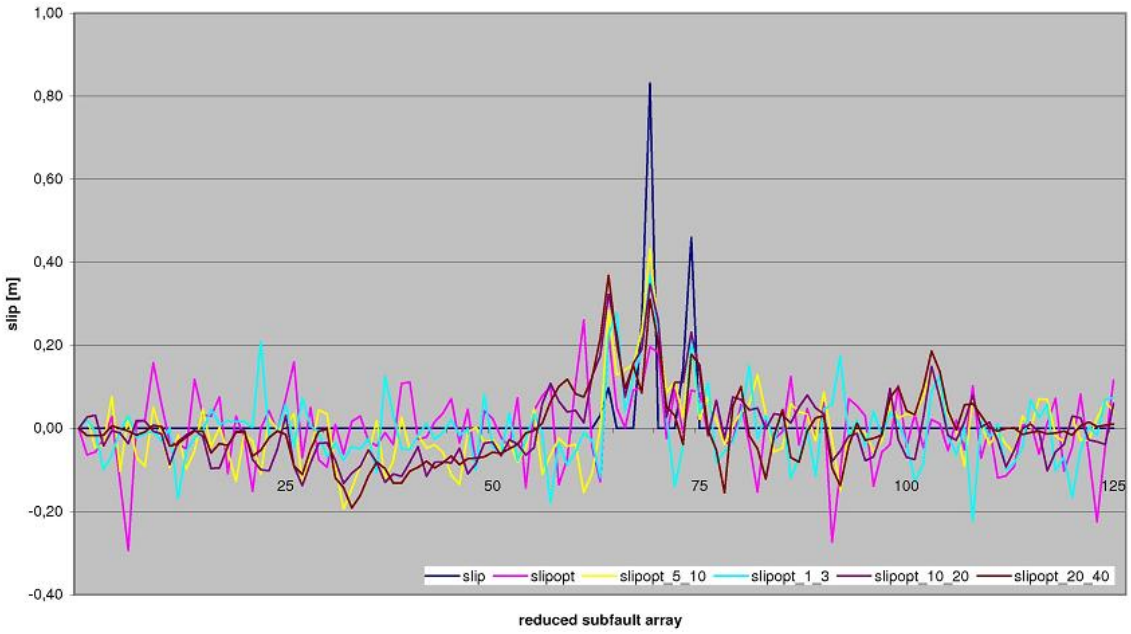


Figure A126: $M_W = 7.7$

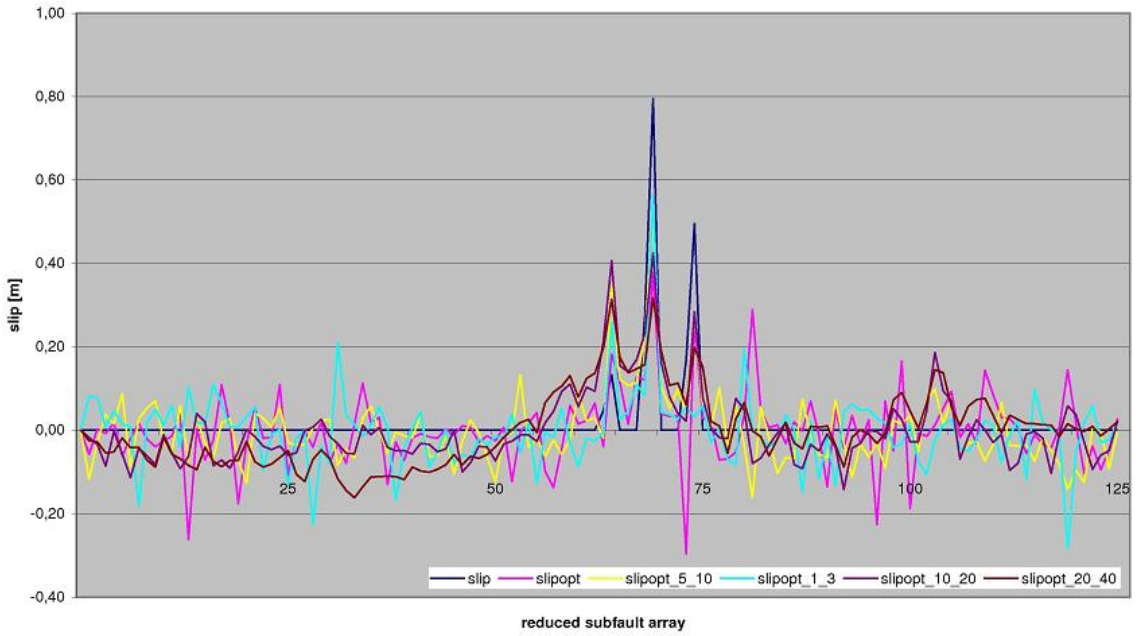


Figure A127: $M_W = 7.8$

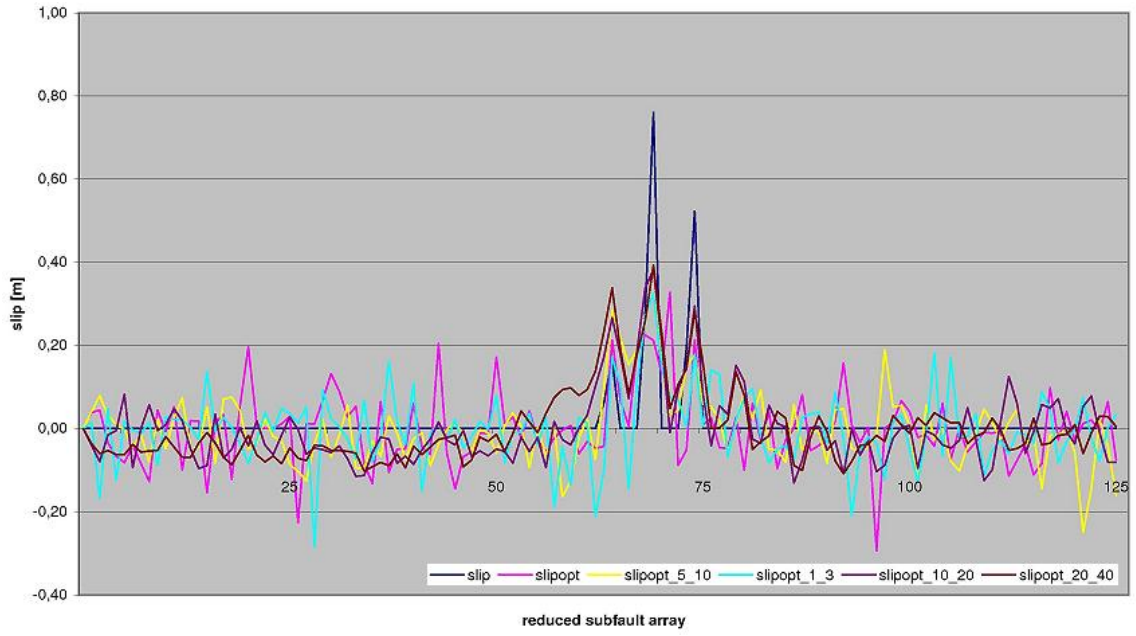


Figure A128: $M_W = 7.9$

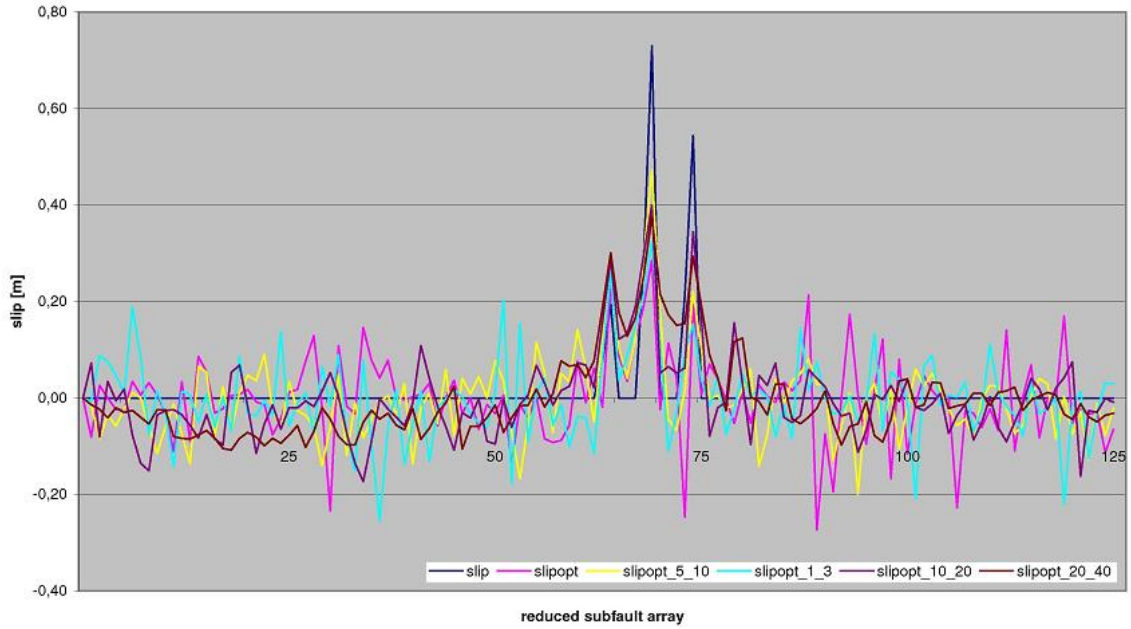


Figure A129: $M_W = 8.0$

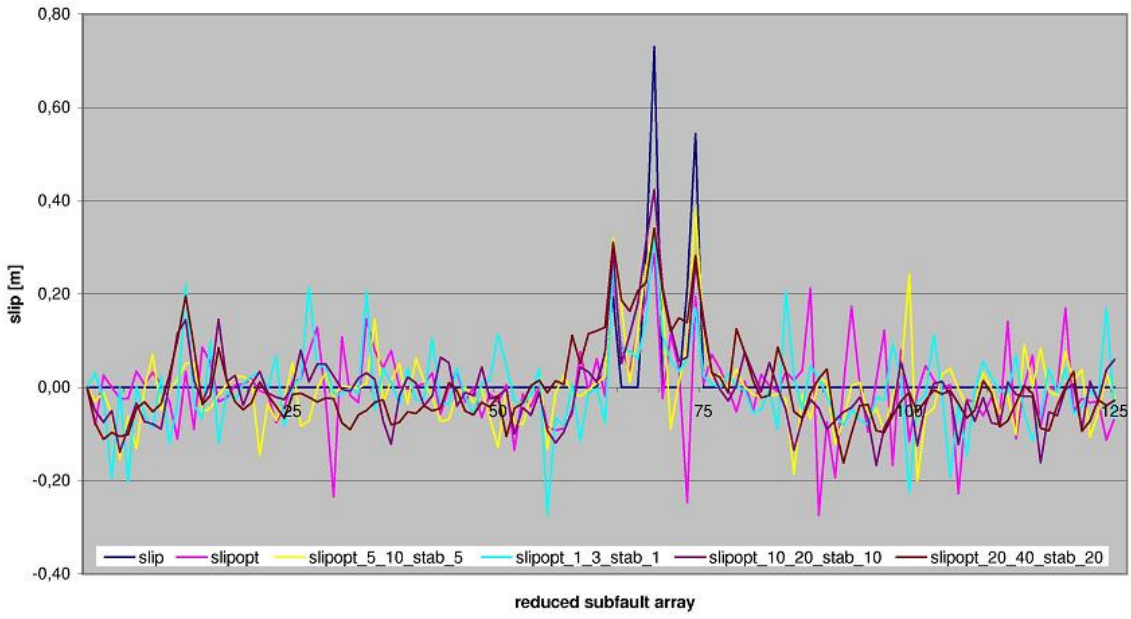


Figure A130: $M_W = 8.0$, stabilised

### A.1.4 Euclidean norm

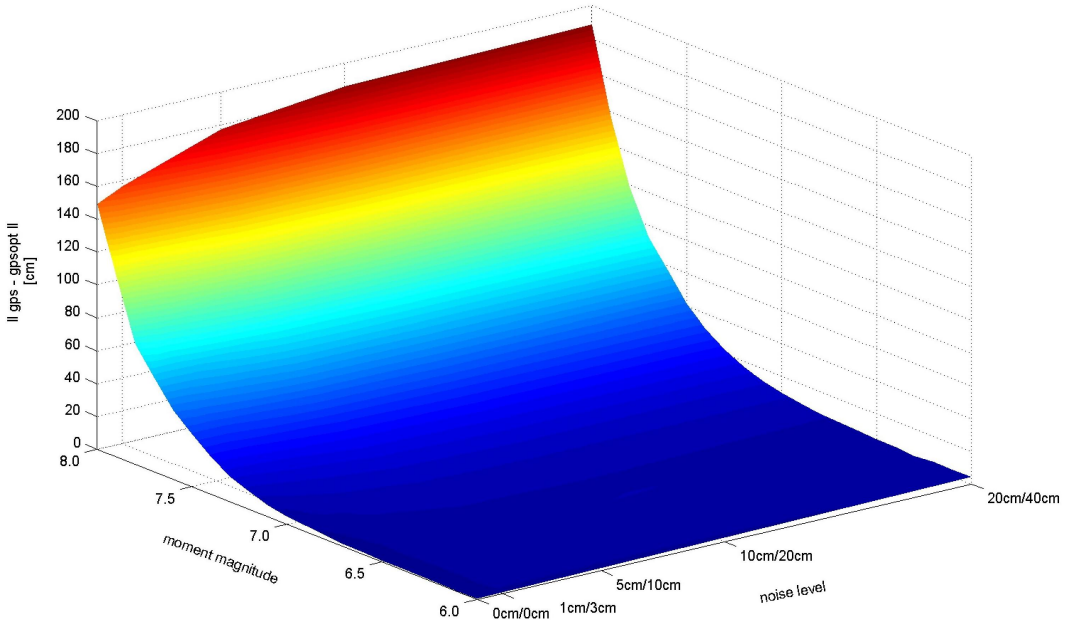


Figure A131: EUCLIDean norm of target ("gps") and actual ("gpsopt") GPS displacements concerning longitude, latitude and altitude for events of $6.0 \leq M_W \leq 8.0$

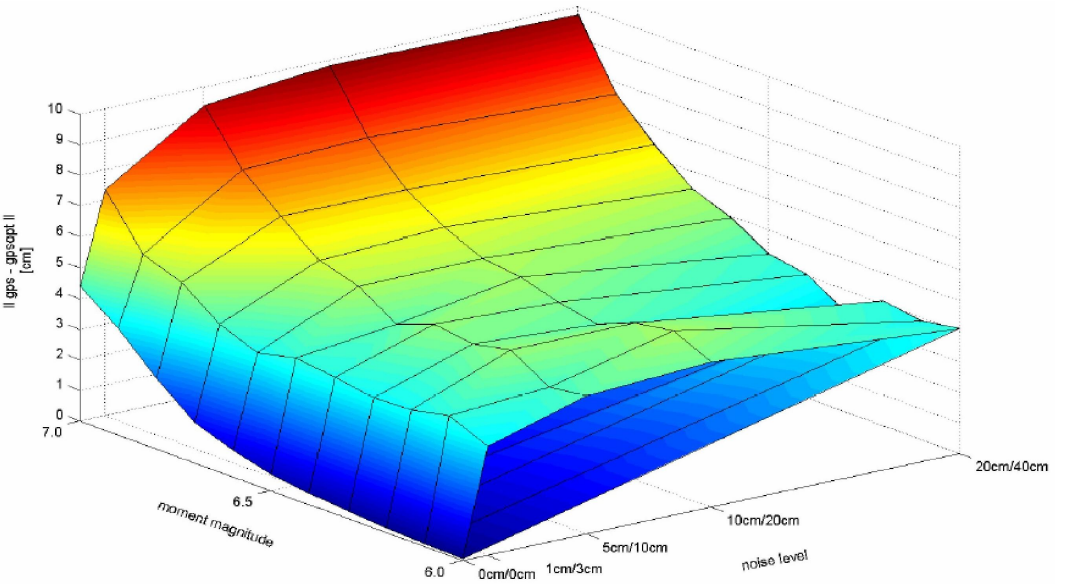


| | 6.0 | 6.1 | 6.2 | 6.3 | 6.4 | 6.5 | 6.6 | 6.7 | 6.8 | 6.9 | 7.0 |
|---|---|---|---|---|---|---|---|---|---|---|---|
| 0cm/0cm | 0,1 | 0,1 | 0,2 | 0,3 | 0,4 | 0,5 | 0,9 | 1,3 | 2,3 | 3,5 | 4,4 |
| 1cm/3cm | 3,6 | 4,1 | 3,9 | 3,8 | 4,0 | 4,2 | 3,9 | 4,4 | 5,3 | 5,7 | 7,4 |
| 5cm/10cm | 4,5 | 4,3 | 5,1 | 4,8 | 5,0 | 4,6 | 5,3 | 5,7 | 6,7 | 7,8 | 9,4 |
| 10cm/20cm | 4,7 | 5,3 | 5,1 | 4,6 | 4,9 | 5,2 | 5,4 | 5,9 | 6,7 | 7,9 | 9,8 |
| 20cm/40cm | 4,1 | 3,9 | 4,1 | 3,3 | 4,0 | 4,2 | 4,9 | 5,4 | 6,4 | 7,6 | 9,7 |

Figure A132: EUCLIDean norm of target ("gps") and actual ("gpsopt") GPS displacements concerning longitude, latitude and altitude for events of $6.0 \leq M_W \leq 7.0$

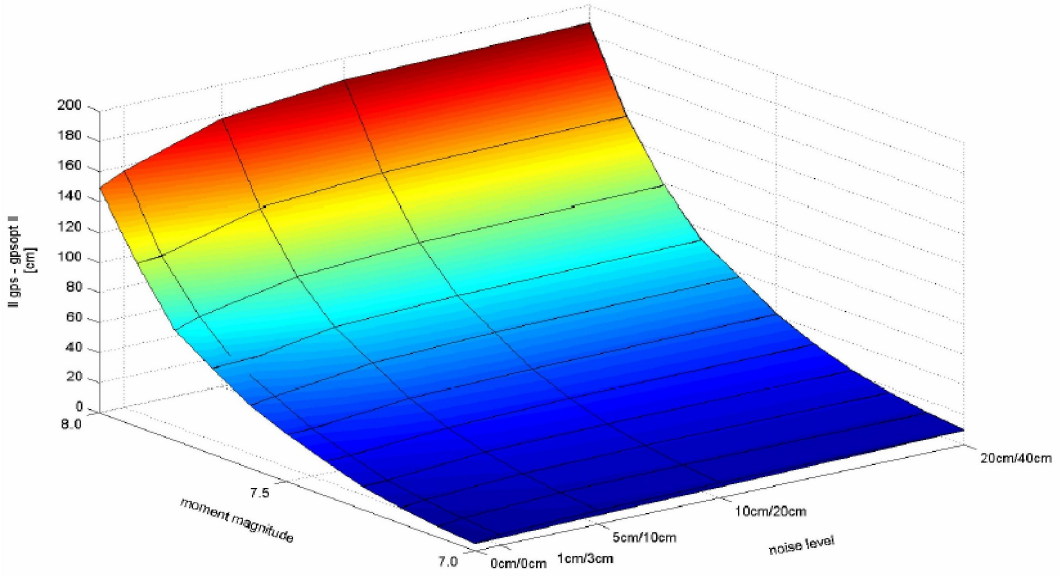


| | 7.0 | 7.1 | 7.2 | 7.3 | 7.4 | 7.5 | 7.6 | 7.7 | 7.8 | 7.9 | 8.0 |
|---|---|---|---|---|---|---|---|---|---|---|---|
| **0cm/0cm** | 4,4 | 6,6 | 10,3 | 15,0 | 22,6 | 31,5 | 41,6 | 57,1 | 73,1 | 108,7 | 149,1 |
| **1cm/3cm** | 7,4 | 8,9 | 11,7 | 15,9 | 23,2 | 31,7 | 44,1 | 56,1 | 78,8 | 110,0 | 156,7 |
| **5cm/10cm** | 9,4 | 12,0 | 15,4 | 20,3 | 27,4 | 37,9 | 52,4 | 67,2 | 91,4 | 127,7 | 177,5 |
| **10cm/20cm** | 9,8 | 12,7 | 16,3 | 21,6 | 29,4 | 39,8 | 54,9 | 70,2 | 96,3 | 132,8 | 185,9 |
| **20cm/40cm** | 9,7 | 12,4 | 16,5 | 22,2 | 30,5 | 41,3 | 56,9 | 72,2 | 98,7 | 136,0 | 188,3 |

Figure A133: EUCLIDean norm of target ("gps") and actual ("gpsopt") GPS displacements concerning longitude, latitude and altitude for events of $7.0 \leq M_W \leq 8.0$

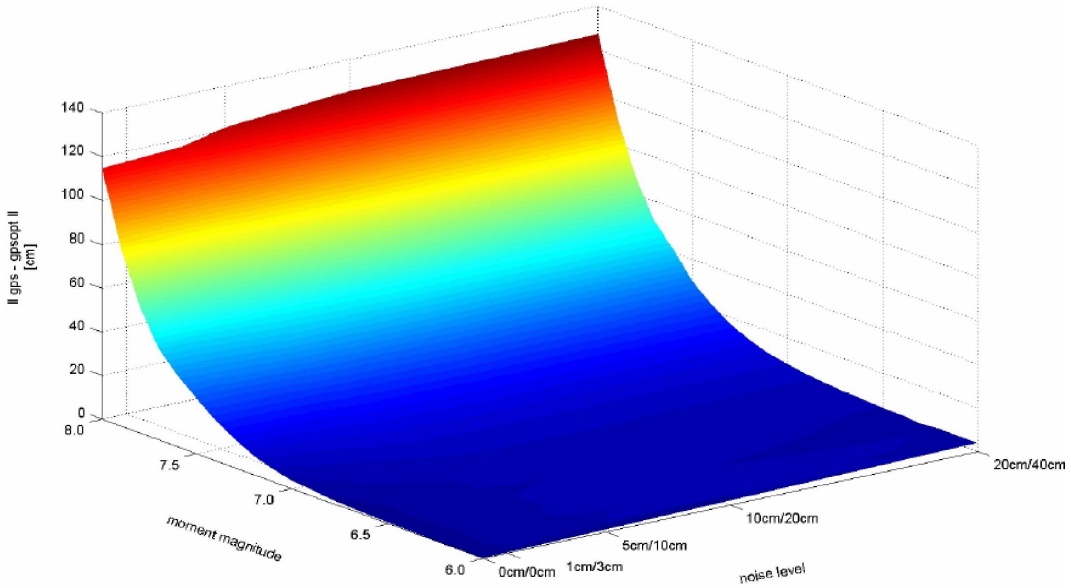


Figure A134: EUCLIDean norm of target ("gps") and actual ("gpsopt") GPS displacements concerning longitude and latitude for events of $6.0 \leq M_W \leq 8.0$

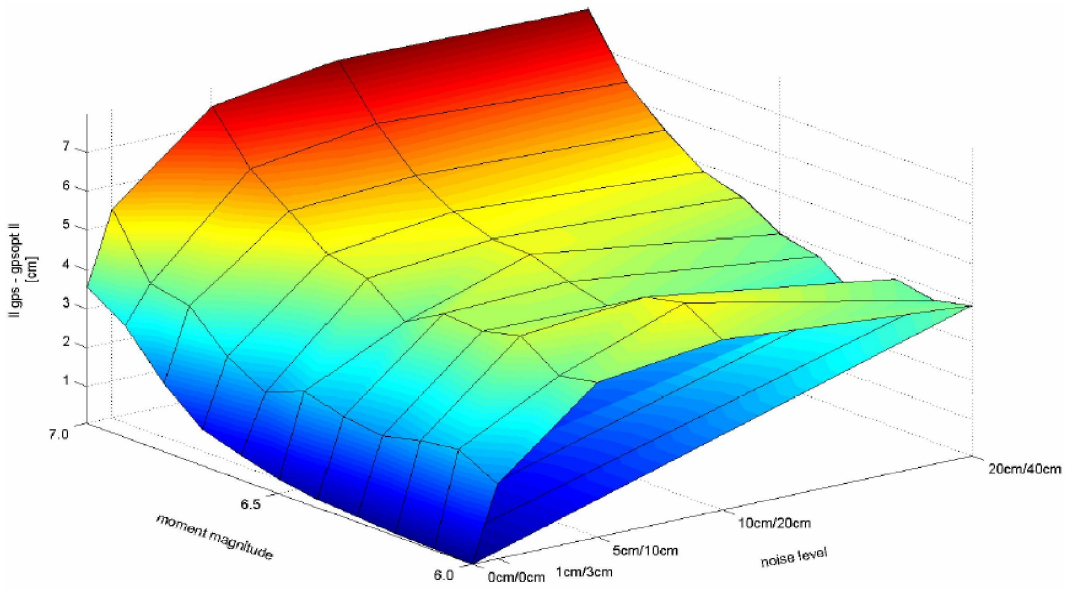


| | 6.0 | 6.1 | 6.2 | 6.3 | 6.4 | 6.5 | 6.6 | 6.7 | 6.8 | 6.9 | 7.0 |
|---|---|---|---|---|---|---|---|---|---|---|---|
| **0cm/0cm** | 0,1 | 0,1 | 0,1 | 0,2 | 0,3 | 0,4 | 0,7 | 1,0 | 1,8 | 2,9 | 3,6 |
| **1cm/3cm** | 2,0 | 2,5 | 2,4 | 2,1 | 2,3 | 2,6 | 2,2 | 2,7 | 3,7 | 3,9 | 5,4 |
| **5cm/10cm** | 4,0 | 3,8 | 4,5 | 4,3 | 4,4 | 3,8 | 4,5 | 4,8 | 5,5 | 6,2 | 7,5 |
| **10cm/20cm** | 4,4 | 5,0 | 4,8 | 4,2 | 4,5 | 4,8 | 4,8 | 5,2 | 5,7 | 6,7 | 8,0 |
| **20cm/40cm** | 3,9 | 3,7 | 3,9 | 3,0 | 3,8 | 3,9 | 4,5 | 4,8 | 5,5 | 6,4 | 7,9 |

Figure A135: EUCLIDean norm of target ("gps") and actual ("gpsopt") GPS displacements concerning longitude and latitude for events of $6.0 \leq M_W \leq 7.0$

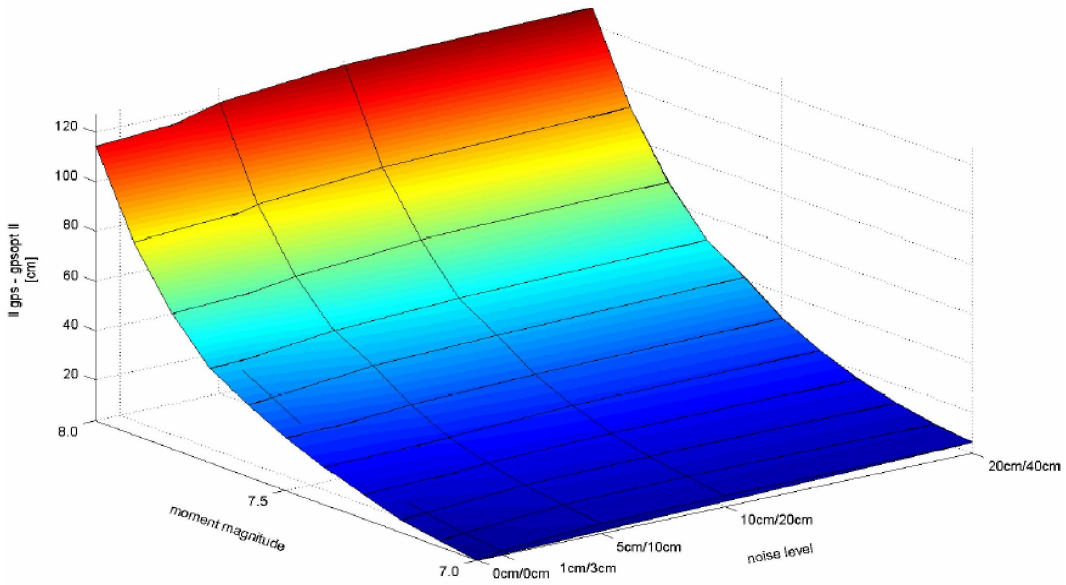


| | 7.0 | 7.1 | 7.2 | 7.3 | 7.4 | 7.5 | 7.6 | 7.7 | 7.8 | 7.9 | 8.0 |
|---|---|---|---|---|---|---|---|---|---|---|---|
| **0cm/0cm** | 3,6 | 5,8 | 8,4 | 13,3 | 18,6 | 24,9 | 32,6 | 41,7 | 58,3 | 81,3 | 114,5 |
| **1cm/3cm** | 5,4 | 6,6 | 9,4 | 12,1 | 17,3 | 24,5 | 33,4 | 41,7 | 56,7 | 75,5 | 110,9 |
| **5cm/10cm** | 7,5 | 9,5 | 11,8 | 15,1 | 20,0 | 27,5 | 37,7 | 46,1 | 62,4 | 85,6 | 121,1 |
| **10cm/20cm** | 8,0 | 10,1 | 12,6 | 16,1 | 21,8 | 28,9 | 39,1 | 48,5 | 66,3 | 89,8 | 125,6 |
| **20cm/40cm** | 7,9 | 9,7 | 12,6 | 16,7 | 22,6 | 30,0 | 41,0 | 50,2 | 67,8 | 92,5 | 127,2 |

Figure A136: EUCLIDean norm of target ("gps") and actual ("gpsopt") GPS displacements concerning longitude and latitude for events of $7.0 \leq M_W \leq 8.0$

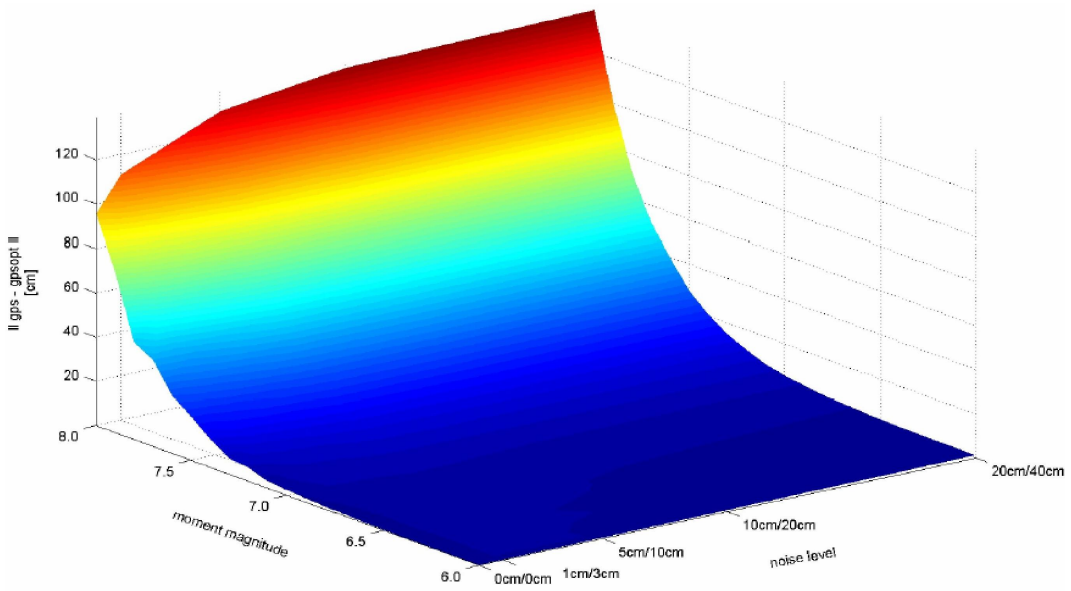


Figure A137: EUCLIDean norm of target ("gps") and actual ("gpsopt") GPS displacements concerning altitude for events of $6.0 \leq M_W \leq 8.0$

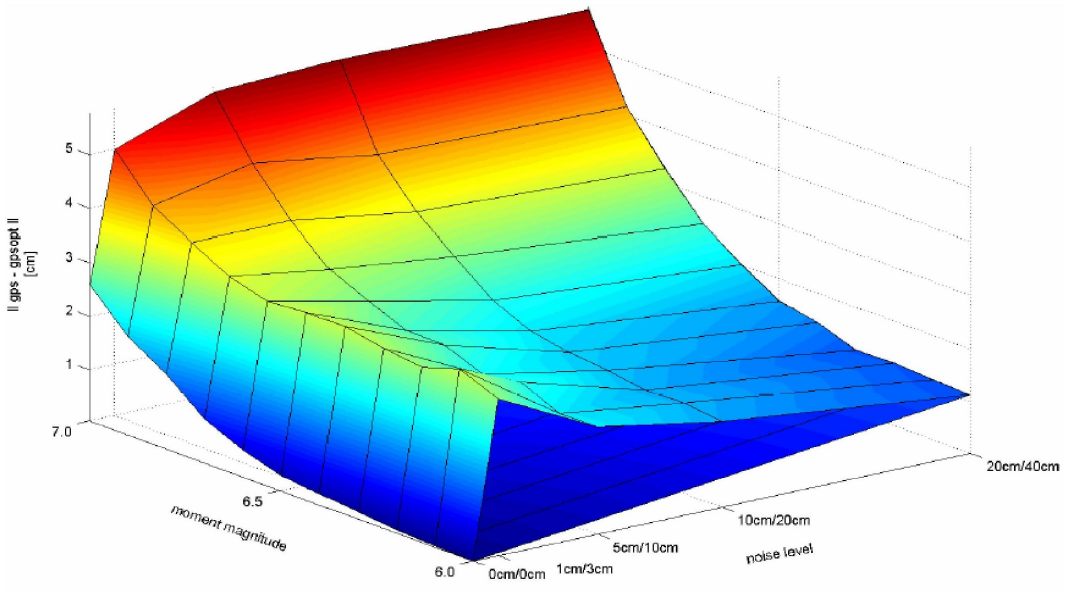


| | 6.0 | 6.1 | 6.2 | 6.3 | 6.4 | 6.5 | 6.6 | 6.7 | 6.8 | 6.9 | 7.0 |
|---|---|---|---|---|---|---|---|---|---|---|---|
| **0cm/0cm** | 0,1 | 0,1 | 0,1 | 0,2 | 0,3 | 0,3 | 0,6 | 0,9 | 1,4 | 1,9 | 2,6 |
| **1cm/3cm** | 3,0 | 3,3 | 3,0 | 3,1 | 3,3 | 3,3 | 3,2 | 3,4 | 3,8 | 4,2 | 5,0 |
| **5cm/10cm** | 2,1 | 2,0 | 2,4 | 2,2 | 2,5 | 2,5 | 2,8 | 3,2 | 3,8 | 4,6 | 5,7 |
| **10cm/20cm** | 1,7 | 1,7 | 1,7 | 1,8 | 1,9 | 2,0 | 2,3 | 2,9 | 3,5 | 4,3 | 5,8 |
| **20cm/40cm** | 1,1 | 1,2 | 1,2 | 1,2 | 1,4 | 1,6 | 2,0 | 2,5 | 3,3 | 4,1 | 5,7 |

Figure A138: EUCLIDean norm of target ("gps") and actual ("gpsopt") GPS displacements concerning altitude for events of $6.0 \leq M_W \leq 7.0$

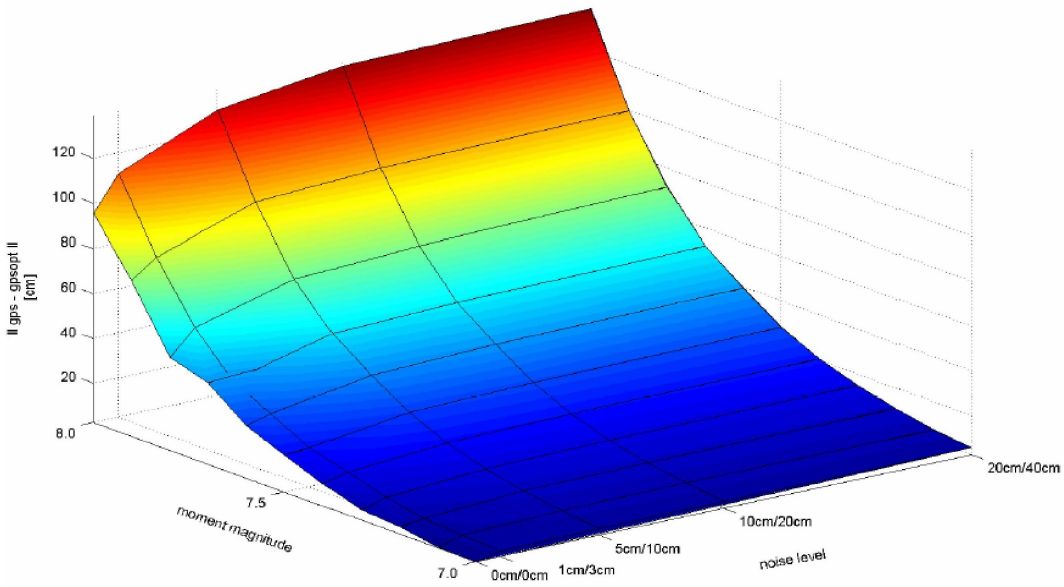


| | 7.0 | 7.1 | 7.2 | 7.3 | 7.4 | 7.5 | 7.6 | 7.7 | 7.8 | 7.9 | 8.0 |
|---|---|---|---|---|---|---|---|---|---|---|---|
| **0cm/0cm** | 2,6 | 3,1 | 6,0 | 7,1 | 12,8 | 19,3 | 25,8 | 39,0 | 44,1 | 72,2 | 95,5 |
| **1cm/3cm** | 5,0 | 5,9 | 7,0 | 10,4 | 15,4 | 20,1 | 28,8 | 37,5 | 54,8 | 80,0 | 110,8 |
| **5cm/10cm** | 5,7 | 7,4 | 9,9 | 13,5 | 18,7 | 26,1 | 36,4 | 48,8 | 66,8 | 94,8 | 129,7 |
| **10cm/20cm** | 5,8 | 7,6 | 10,4 | 14,3 | 19,8 | 27,5 | 38,5 | 50,7 | 69,8 | 97,9 | 137,1 |
| **20cm/40cm** | 5,7 | 7,6 | 10,7 | 14,7 | 20,6 | 28,4 | 39,5 | 51,9 | 71,8 | 99,6 | 138,8 |

Figure A139: EUCLIDean norm of target ("gps") and actual ("gpsopt") GPS displacements concerning altitude for events of $7.0 \leq M_W \leq 8.0$

## A.2 Figures - Using other inverse approaches

### A.2.1 Slip distributions at subfault array

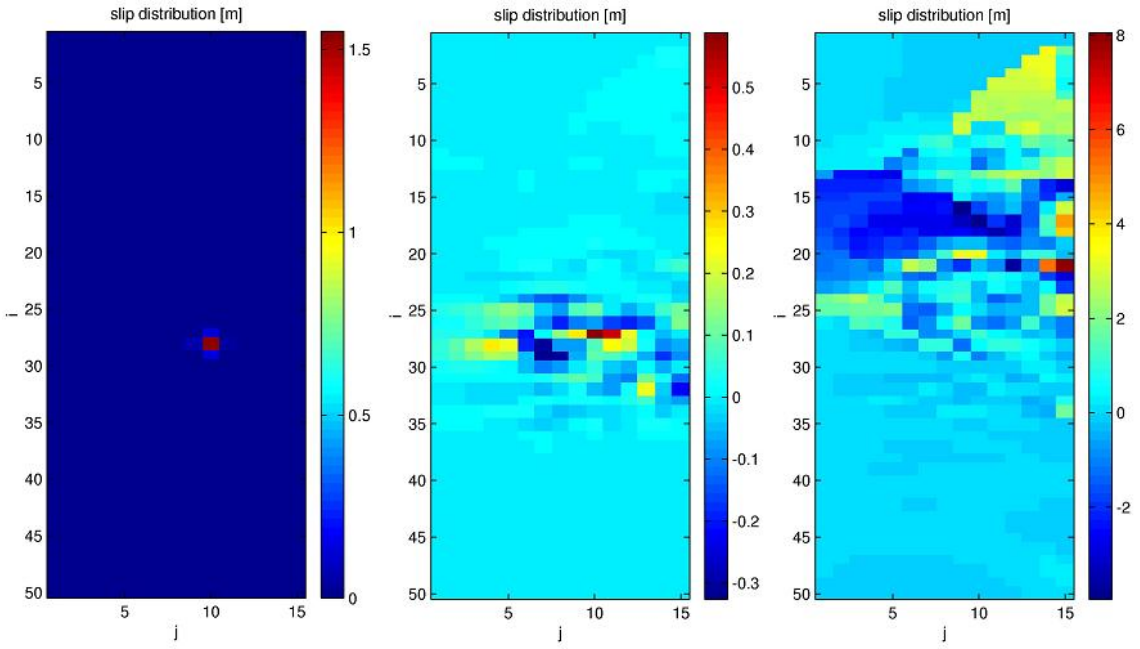


Figure A140: $M_W = 7.0$: QR decomposition of transposed system "QR_min": target slip (left), noiseless reconstruction (middle) and noisy reconstruction (right)

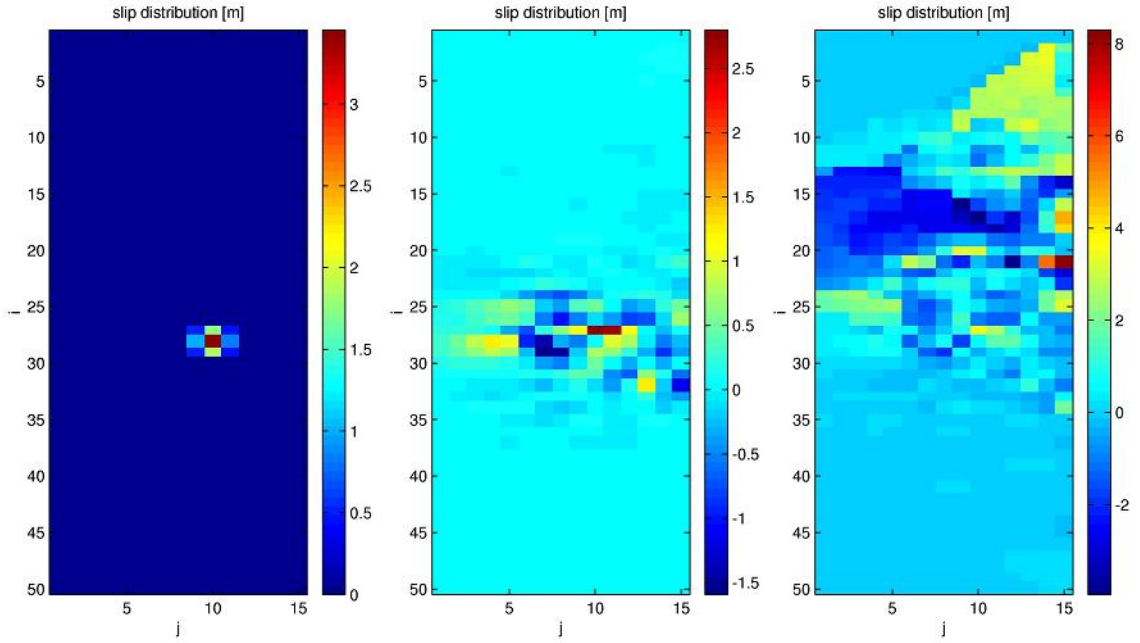


Figure A141: $M_W = 7.5$: QR decomposition of transposed system "QR_min": target slip (left), noiseless reconstruction (middle) and noisy reconstruction (right)

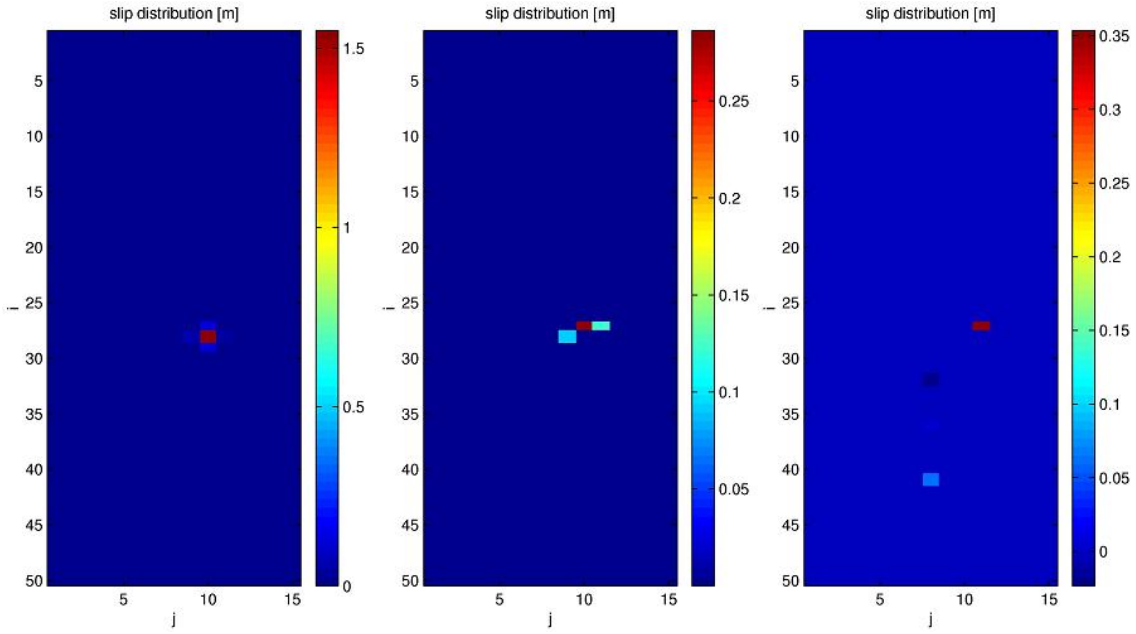


Figure A142: $M_W = 7.0$: iterative approach by surrogate functionals "sparse": target slip (left), noiseless reconstruction (middle) and noisy reconstruction (right)

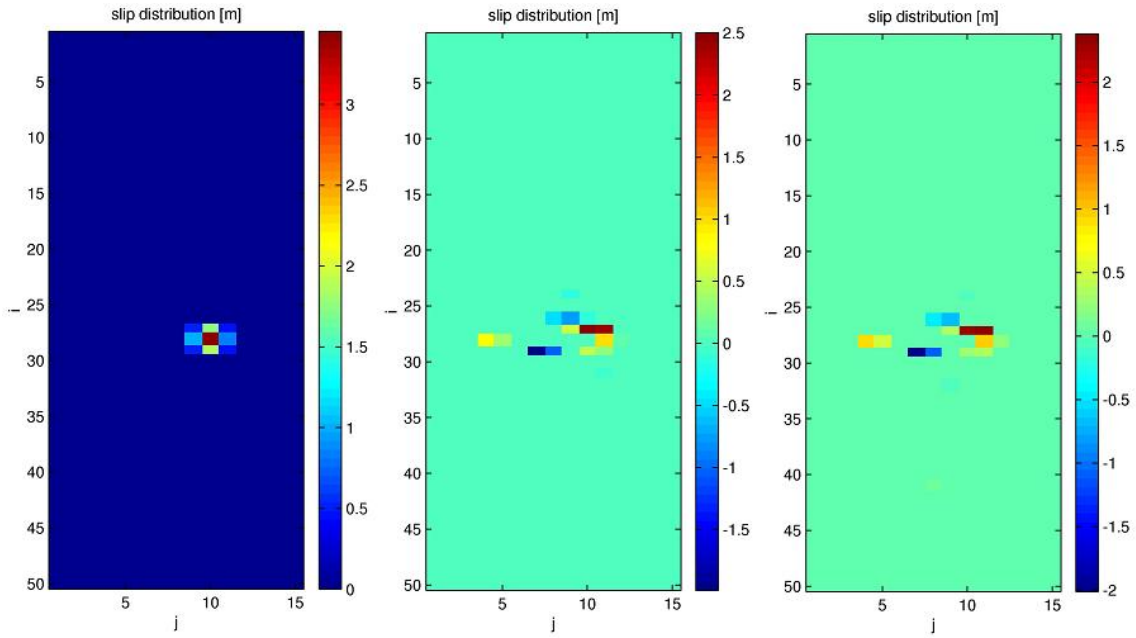


Figure A143: $M_W = 7.5$: iterative approach by surrogate functionals "sparse": target slip (left), noiseless reconstruction (middle) and noisy reconstruction (right)

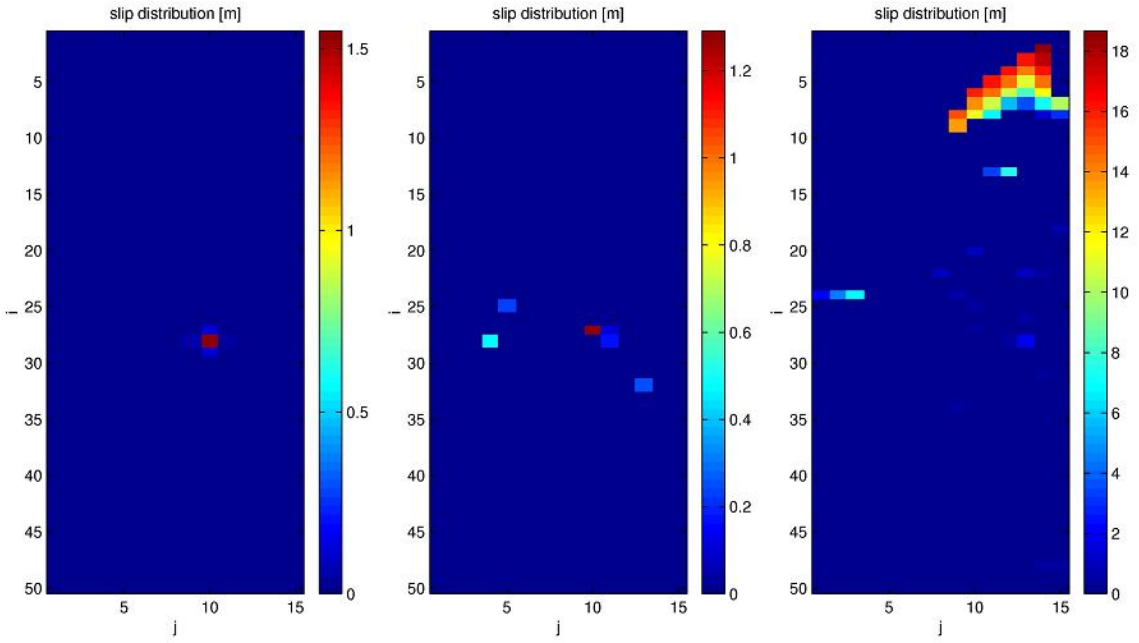


Figure A144: $M_W = 7.0$: QR decomposition of transposed system combined with iterative approach by surrogate functionals "QR_min_sparse": target slip (left), noiseless reconstruction (middle) and noisy reconstruction (right)

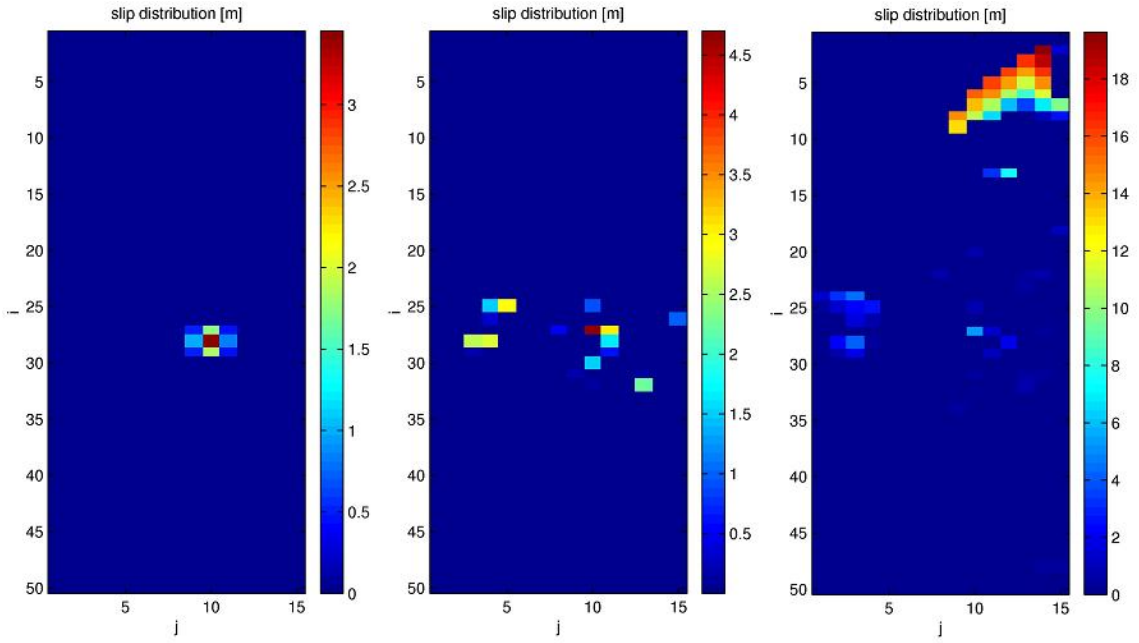


Figure A145: $M_W = 7.5$: QR decomposition of transposed system combined with iterative approach by surrogate functionals "QR_min_sparse": target slip (left), noiseless reconstruction (middle) and noisy reconstruction (right)

## A.3 Content of CD

The attached CD comprises three folders:

- "Thesis"
  - the entire thesis as a pdf-file
- "MATLAB files"
  - script files: cost_function.m, other_approaches.m
  - function files: addnoise.m, azi.m, azimuthsmoothness.m, chi2.m, costfunc.m, eff_thres.m, importdip.m, importgf.m, importgps.m, importgpscoord.m, importslip.m, importstrike.m, plot_array.m, reducegf.m, reduceslip.m, rms.m, showgps.m, showslip.m, slipsmoothness.m, soft_p.m
  - matrix: data.mat
- "RuptGen"
  - subfolder "Green's functions" that includes the GREEN's functions (gf.zip)
  - subfolder "matrix" that includes the propagation matrix (gf_SuGAr.mtx)
  - Patch Finder (PatchFinder.exe)
  - Rupture Generator (RuptGen1.exe)
  - RuptGen configuration file (ruptgen.cfg)
  - GPS stations input file (GPS-SuGAr.inp)
  - plate interface description file (pi15150.pi)

# Bibliography


[1] A. Babeyko. Rupture Generator v.1.1. unpublished manual 2007.

[2] A. Babeyko. WP 5100: Introducing the Rupture Generator. Technical report, Helmholtz Centre Potsdam, GFZ German Research Centre of Geosciences, 2008.

[3] A. Babeyko. WP 5100: modelling. Technical report, Helmholtz Centre Potsdam, GFZ German Research Centre of Geosciences, April 2008. (Internal) GITEWS Annual Meeting.

[4] A. Babeyko, A. Hoechner, and S. Sobolev. Modelling tsunami generation for local tsunami early warning in Indonesia. *Geophysical Research Abstracts*, 10, 2008. EGU2008-A-01523.

[5] P. Banerjee, F. Pollitz, and R. Bürgmann. The size and duration of the Sumatra-Andaman earthquake from far-field static offsets. *Science*, (308):1769–1772, 2005.

[6] G. Blewitt, C. Kreemer, W. Hammond, H.-P. Plag, S. Stein, and E. Okal. Rapid determination of earthquake magnitude using GPS for tsunami warning systems. *Geophysical Research Letter*, 33, 2006. L11309, doi: 10.1029/2006GL026145.

[7] H. Bock, G. Beutler, S. Schaer, T Springer, and M. Rothacher. Processing aspects related to permanent GPS arrays. *Earth Planets Space*, 52:657–662, 2000.

[8] Y. Bock, R. Nikolaidis, P. de Jonge, and M. Bevis. Instaneous geodetic positioning at medium distances with the Global Positioning System. *Journal of Geophysical Research*, 105:223–254, 2000.

[9] Y. Bock, L. Prawirodirdjo, and T. Melbourne. Detection of arbitrarily large dynamic ground motions with a dense high-rate GPS network. *Geophysical Research Letter*, 31, 2004. L06604, doi:10.1029/2003GL019150.

[10] M. Chlieh, J.-P. Avouac, V. Hjorleifsdottir, T.-R. Song, Chen Ji, K. Sieh, A. Sladen, H. Hebert, L. Prawirodirdjo, Y. Bock, and J. Galetzka. Coseismic slip and afterslip of the Great (mw 9.15) Sumatra-Andaman earthquake of 2004. *Bulletin of the Seismological Society of America*, 97(1A):152–173, January 2007. doi: 10.1785/0120050631.

[11] I. Daubechies, M. Defrise, and C. De Mol. An iterative thresholding algorithm for linear inverse problems with a sparsity constraint. *Communications on Pure and Applied Mathematics*, 57:1413–1541, November 2004. doi:10.1002/cpa.20042.

[12] P. Eakins. Faults and faulting, 1987.

[13] Alfred Wegener Institute for Polar and Marine Research (AWI). GITEWS - tsunami modellierung am AWI. Website, May 2008. `http://www.awi.de/de/forschung/wissenschaftliches_rechnen/forschungsthemen_wissenschaftliches_rechnen/tsunami_modellierung_am_awi/`.

[14] Alfred Wegener Institute for Polar and Marine Research (AWI). The model TsunAWI. Website, July 2008. `http://www.awi.de/de/forschung/wissenschaftliches_rechnen/forschungsthemen_wissenschaftliches_rechnen/tsunami_modellierung_am_awi/modell_tsunawi/`.

[15] Public Law Foundation GITEWS Project Management at the Helmholtz Centre Potsdam, GFZ German Research Centre for Geosciences. Press release, November 2008. `http://www.gitews.de/fileadmin/documents/content/press/GITEWS_operationell_de_nov-2008.pdf`.

[16] Public Law Foundation GITEWS Project Management at the Helmholtz Centre Potsdam, GFZ German Research Centre for Geosciences. German Indonesian Tsunami Early Warning System (GITEWS). Website, May 2008. `http://www.gitews.org`.

[17] G. Gramlich and W. Werner. *Numerische Mathematik mit Matlab*. dpunkt.verlag, 2000.

[18] O. Gudmundsson and M. Sambridge. A regionalized upper mantle (RUM) seismic model. *Journal of Geophysical Research*, (308):7121–7136, 1998.

[19] A. Hoechner, A. Babeyko, Brune S., and S. Sobolev. Slip distribution of recent Sunda Trench earthquakes: Reconciling 3D GPS inversions with seismological and ocean measurements. 2006. Abstract U53A-0034, American Geophysical Union Fall Meeting, San Francisco, USA.

[20] A. Hoechner, A. Babeyko, and S. Sobolev. Enhanced GPS inversion technique applied to the 2004 Sumatra earthquake and tsunami. *Geophysical Research Letter*, 35, April 2008. L08310, doi: 10.1029/2007GL033133.

[21] A. Hoechner, A. Babeyko, and S. Sobolev. GPS-based inversion: A sensitivity analysis and application to past and possible events. *Geophysical Research Abstracts*, 10, 2008. EGU2008-A-02680.

[22] B.L.N. Kennett and E.R. Engdahl. Traveltimes for global earthquake location and phase identification. *Geophysical Journal International*, 105:429–465, 1991.

[23] J. Lauterjung and E. Flueh. Sensornetze sollen ab 2008 eine Tsunamiwarnung spätestens zehn Minuten nach dem auslösenden Erdbeben ermöglichen. *Spektrum der Wissenschaft - Dossier*, 1/07:80–81, January 2007.

[24] W. Lee, H. Kanamori, P. Jennings, and C. Kisslinger. *International handbook of earthquake & engineering seismology.* Academic Press, 2002.

[25] A.K. Louis. *Inverse und schlecht gestellte Probleme.* B.G. Teubner, 1989.

[26] Maps.com. website, November 2008. `http://www.maps.com/ref_map.aspx?pid=12871`.

[27] The MathWorks Inc. *MATLAB Documentation*, 2000. version 6.

[28] F. Mundo. Banda Aceh before and after Sumatra-Andaman Tsunami 2004. Website, May 2008. `http://www.masternewmedia.org/images/before_after_tsunami_2004_500.jpg`.

[29] Federal Ministry of Education and Germany Research Berlin. Press release, November 2008. `http://www.gitews.de/fileadmin/documents/content/press/Pm1111-Tsunami-Fr__hwarnsystem.pdf`.

[30] Federal Ministry of Education and Germany Research Berlin. Tsunami - Wenn Wassermassen aus dem Gleichgewicht geraten. Website, May 2008. `http://www.bmbf.de/de/4840.php`.

[31] Helmholtz Centre Potsdam GFZ German Research Centre of Geosciences. The German contribution to the Tsunami Early Warning System for the Indonesian Ocean. Technical report, Helmholtz Centre Potsdam, GFZ German Research Centre of Geosciences, 2007.

[32] California Institute of Technology (Caltech). Caltech Tectonics Observatory IMS - SuGAr stations index. Website, July 2008. `http://tectonics-ims.caltech.edu/ims/net/1/sis/`.

[33] Y. Okada. Surface deformation due to shear and tensile faults in a half-space. *Bulletin of the Seismological Society of America*, 75(4):1135–1154, August 1985.

[34] Y. Okada. Internal deformation due to shear and tensile faults in a half-space. *Bulletin of the Seismological Society of America*, 82(2):1018–1040, April 1992.

[35] Scripps Orbit and Permanent Array Center (SOPAC). SuGAr RINEX data at SOPAC. Website, August 2008. `http://sopac.ucsd.edu/projects/sugar.html`.

[36] F. Pollitz, P. Banerjee, R. Bürgmann, M. Hashimoto, and N. Choosakul. Stress changes along thesunda trench following the 26 December 2004 Sumatra-Andaman and 28 March 2005 Nias earthquakes. *Geophysical Research Letter*, 33, March 2006. L06309, doi:10.1029/2005GL024558.

[37] A. Rieder. *Keine Probleme mit Inversen Problemen.* Vieweg, 2003.

[38] G. Seeber. *Satellite Geodesy.* Walter de Gruyther, 2nd edition, 2003.

[39] S. Sobolev, A. Babeyko, R. Wang, R. Galas, M. Rothacher, J. Lauterjung, D. Sein, Scröter J., and C. Subarya. Towards real-time tsunami amplitude prediction. *EOS, Transactions, American Geophysical Union*, 87(37):374, 378, September 2006.

[40] S. Sobolev, A. Babeyko, R. Wang, A. Hoechner, R. Galas, M. Rothacher, D. Sein, J. Schröter, J. Lauterjung, and C. Subarya. Tsunami early warning using GPS-shield arrays. *Journal of Geophysical Research*, (112), 2007. B08415, doi:10.1029/2006JB004640.

[41] AMS (American Meteorological Society). Green's function. Website, November 2008. `http://amsglossary.allenpress.com/glossary/browse?s=g&p=31`.

[42] G. Teschke. Multi-frame representations in linear inverse problems with mixed multi-constraints. *Applied and Computational Harmonic Analysis*, 22(37):43–60, January 2007. doi:10.1016/j.acha.2006.05.003.

[43] Pennsylvania USA The Pennsylvania State University, Department of Geosciences. Faults and faulting. Website, August 2008. `http://eqseis.geosc.psu.edu/~cammon/HTML/Classes/IntroQuakes/Notes/faults.html`.

[44] United States Geological Survey (USGS). Tectonic setting of the magnitude 9.0 earthquake that generated the tsunami. Website, May 2008. `http://soundwaves.usgs.gov/2005/01/tectonicLG.jpg`.

[45] R. Wang, F. Lorenzo Martin, and F. Roth. Computation of deformation inducted by earthquakes in a multi-layered elastic crust - FORTRAN programs EDGRN/EDCMP. *Computers & Geosciences*, (29):195–207, 2003.

[46] D. Wells and K. Coppersmith. New empirical relationships among magnitude, rupture length, rupture width, rupture area, and surface displacement. Bulletin, 1994.

[47] J. Werner. *Numerische Mathematik 1.* Vieweg, 2007.

[48] Wikipedia. 2004 Indian Ocean earthquake. Website, May 2008. `http://en.wikipedia.org/wiki/Indian_ocean_earthquake`.

[49] Wikipedia. Computermodell. Website, May 2008. `http://de.wikipedia.org/wiki/Computermodell`.

[50] Wikipedia. Curve fitting. Website, July 2008. `http://en.wikipedia.org/wiki/Curve_fitting`.

[51] Wikipedia. Downhill-Simplex-Verfahren. Website, November 2008. `http://de.wikipedia.org/wiki/Downhill-Simplex-Verfahren`.

[52] Wikipedia. Earthquake. Website, July 2008. `http://en.wikipedia.org/wiki/Earthquake`.

[53] Wikipedia. IASP91. Website, July 2008. `http://de.wikipedia.org/wiki/IASP91`.

[54] Wikipedia. Inverse problem. Website, November 2008. http://en.wikipedia.org/wiki/Inverse_problem.

[55] Wikipedia. Java Trench. Website, July 2008. http://en.wikipedia.org/wiki/Java_Trench.

[56] Wikipedia. Least squares. Website, July 2008. http://en.wikipedia.org/wiki/Least_squares.

[57] Wikipedia. Mathematical model. Website, May 2008. http://en.wikipedia.org/wiki/Mathematical_model.

[58] Wikipedia. Numerical analysis. Website, May 2008. http://en.wikipedia.org/wiki/Numerical_analysis.

[59] Wikipedia. Plate tectonics. Website, May 2008. http://en.wikipedia.org/wiki/Plate_tectonics.

[60] Wikipedia. Sunda Arc. Website, May 2008. http://en.wikipedia.org/wiki/Sunda_Arc.

[61] Wikipedia. Greensche Funktion. Website, July 2008. http://de.wikipedia.org/wiki/Greensche_Funktion.

[62] Wikipedia. Lagrange-Multiplikator. Website, November 2008. http://de.wikipedia.org/wiki/Lagrange-Multiplikator.

[63] Wikipedia. Tsunami. Website, May 2008. http://en.wikipedia.org/wiki/Tsunami.

[64] Wikipedia. Tsunami warning system. Website, May 2008. http://en.wikipedia.org/wiki/Tsunami_warning_system.

[65] Wikipedia. Well-posed problem. Website, November 2008. http://en.wikipedia.org/wiki/Well-posed_problem.